EXAMINING INHIBITION AND SUBSTRATE INTERACTION OF SPOIVFB, AN INTRAMEMBRANE METALLOPROTEASE OF *BACILLUS SUBTILIS*

By

Sandra D. Olenic

A DISSERTATION

Submitted to
Michigan State University
in partial fulfillment of the requirements
for the degree of

Cell and Molecular Biology—Doctor of Philosophy

2021

ABSTRACT

EXAMINING INHIBITION AND SUBTRATE INTERACTION OF SPOIVFB, AN INTRAMEMBRANE METALLOPROTEASE OF *BACILLUS SUBTILIS*

By

Sandra D. Olenic

Intramembrane proteases (IPs) regulate diverse signaling pathways in all three domains of life by cleaving membrane-associated substrates. Currently, there are four known IP families, including intramembrane metalloproteases (IMMPs), which contain characteristic HEXXH and NPDG motifs that coordinate a zinc ion at the active site. The study of IMMPs, including RseP (*Escherichia coli*) and SpoIVFB (*Bacillus subtilis*) have provided insights into potential mechanisms for substrate interaction and cleavage, which could guide efforts to develop inhibitors of IMMPs that regulate virulence in bacterial pathogens. Work described in this dissertation has advanced the knowledge of inhibition and substrate interaction of SpoIVFB, which cleaves Pro-σ^K during endosporulation. Improved methods are presented for heterologous production in *E. coli* of SpoIVFB, Pro-σ^K, and the inhibitory proteins BofA and SpoIVFA. Three conserved BofA residues (N48, N61, T64) in or near transmembrane segment (TMS) 2 are required for SpoIVFB inhibition. Cross-linking indicates that BofA TMS2 occupies the SpoIVFB active site region. Interestingly, BofA and SpoIVFA do not prevent interactions between portions of Pro-σ^K and SpoIVFB, so all four proteins can exist in a complex. A structural model of SpoIVFB with BofA and parts of SpoIVFA and Pro-σ^K was built using partial homology and constraints from cross-linking and co-evolutionary analyses. The model suggests that SpoIVFA stabilizes BofA in the SpoIVFB active site region and leads us to propose that BofA TMS2 sterically hinders access of the substrate. Our work has also advanced knowledge of interactions between Pro-σ^K and the broadly conserved SpoIVFB NPDG motif,

which is located in a predicted short loop that interrupts TMS4 and faces the active site. Three highly conserved residues (N129, P132, P135) of SpoIVFB were found to be important for substrate interactions and cleavage, and we propose that P135 is necessary to position D137 to act as a zinc ligand. More work is needed to fully understand how IMMPs interact with their substrates and whether the insights from BofA inhibition of SpoIVFB can be applied to other IMMPs. Outstanding questions and future directions related to these two projects are described.

This dissertation is dedicated to my parents, Bruce and Judy Olenic, and my partner, Andrew Barsom. Their support, guidance and love were essential during graduate school.

ACKNOWLEDGEMENTS

I would like to start by acknowledging Dr. Lee Kroos for his support during this work. His guidance and mentorship during my PhD have been invaluable. He not only trained me as a biochemist, but also served as a wonderful model for teaching and leadership. Next, I would like to thank the members of the Kroos lab, in particular: Dr. Daniel Parrell, Dr. Shreya Saha and Dr. Ý Hoàng during my time at Michigan State University. I am honored to have worked with such a fun, talented group of scientists. Finally, I would like to thank my friends and family. Their love and support during this time was incredible.

TABLE OF CONTENTS

LIST OF TABLES

LIST OF FIGURES

KEY TO ABBREVIATIONS

IP: Intramembrane protease

RIP: Regulated intramembrane proteolysis

IMMP: Intramembrane metalloprotease

TMS: Transmembrane segment

SPP: signal peptide peptidase

TFPP: Type 4 prepilin peptidase

PFP: Preflagellin peptidase

APP: amyloid precursor protein

cryo-EM: cryo-electron microscopy

PAL: P is Proline, A is Alanine and L is Leucine

ER: endoplasmic reticulum

EGF: epidermal growth factor

TGF: transforming growth factor

HEXXH: H is histidine, E is glutamate and X is any amino acid

NPDG: N is asparagine, P is proline, D is aspartate and G is glycine

S2P: Site-2 protease

SREBP: sterol-regulatory element-binding proteins

LDL: low density lipoprotein

S1P: Site-1 protease

PDZ: Post synaptic density protein (PSD95), Drosophila disc large tumor suppressor (Dlg1), and Zonula occludens-1 protein (ZO-1)

CBS: cystathionine-β-synthase

OMP: outer membrane protein

YXF: Y is tyrosine, X is any amino acid and F is phenylalanine

PhoA: alkaline phosphatase

LPS: lipopolysaccharides

GFP: green fluorescence protein

YFP: yellow fluorescence protein

Ppr1: PDZ-interacting protease regulator 1

Eep: enhanced expression of pheromone

MC: mother cell

FS: forespore

CHAPTER 1: Intramembrane Proteases

Introduction

Intramembrane proteases (IPs) are involved in cell signaling processes in all three domains of life. IPs contain a membrane-embedded active site, which is capable of cleaving a protein substrate within or near the membrane. The process of cleaving a transmembrane or membrane-associated substrate and releasing it to the cytosol is called regulated intramembrane proteolysis (RIP) [1]. Once freed from a membrane, cleaved substrates can control diverse signaling pathways, typically at the level of gene transcription [2]. There are four known IP families: aspartyl proteases like presenilin, serine proteases (also referred to as rhomboids), the glutamyl protease Rce1, and intramembrane metalloproteases (IMMPs) [2, 3].

Structures of IPs from Four Families Reveal That They Share Similarities. Crystal structures have been solved for representatives of all four IP families [3-8]. These structures show that IPs are composed of transmembrane segments (TMSs) that arrange to form channels open to solvent, bringing water molecules to the membrane embedded active site for hydrolysis of a substrate peptide bond (Figure 1.1).

Aspartyl proteases: In this family of IPs, the proposed mechanism employs an activated water molecule that is coordinated between two conserved aspartate residues, which enables water to perform a nucleophilic attack on the carbonyl carbon of the substrate [5, 9, 10] (Figure 1.2). Three members of this family will be discussed: presenilin, signal peptide peptidase (SPP) and FlaK.

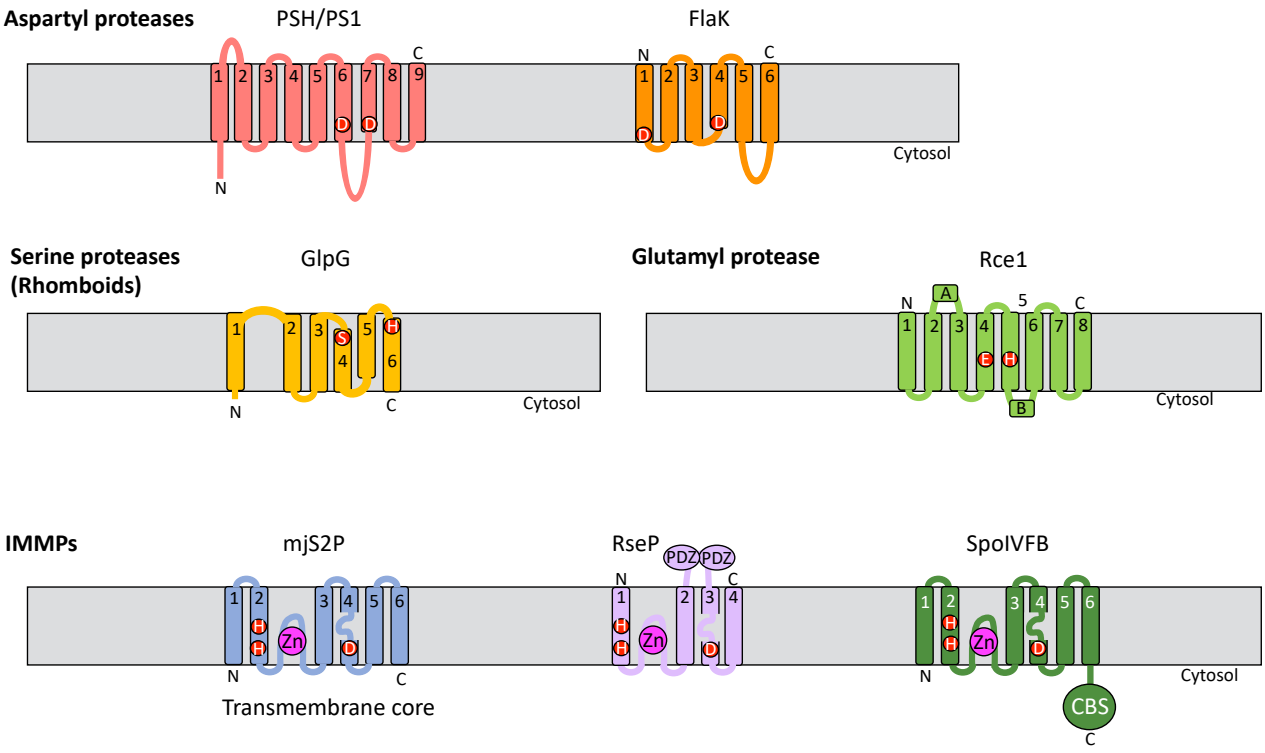

Figure 1.1 Structures of Intramembrane Proteases. There are four families of intramembrane proteases: aspartyl proteases, serine proteases, the glutamyl protease Rce1 and intramembrane metalloproteases (IMMPs). Structures have been solved for representatives of these families including PSH/PS1, FlaK, GlpG, Rce1 and mjS2P. Predicted structures are shown for RseP and SpoIVFB. Active site residues are highlighted in red. The TMSs are numbered numerically and the peripheral α-helices are numbered alphabetically.

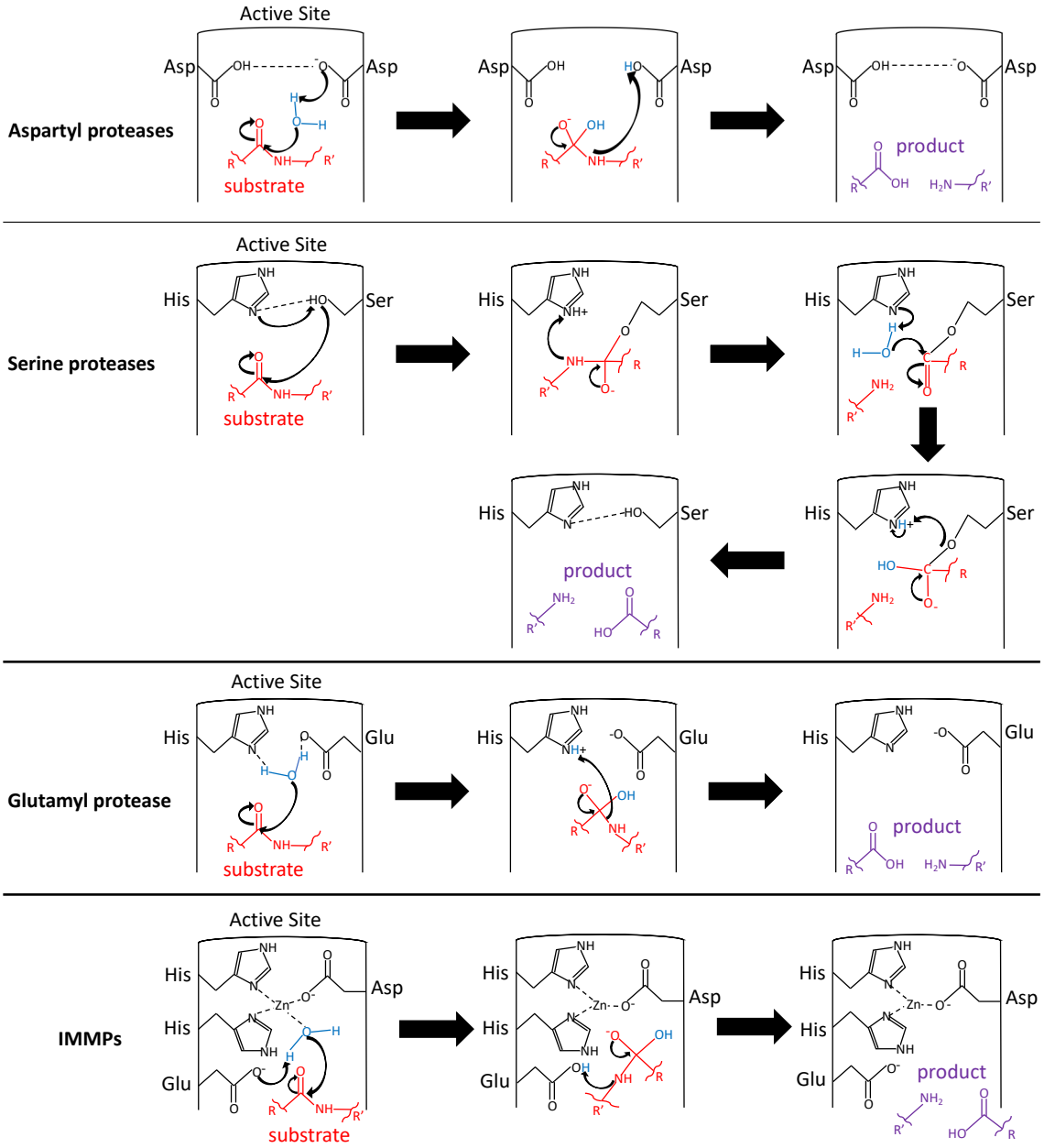

Figure 1.2 Proposed Mechanisms of Intramembrane Proteases. For aspartyl proteases, the proposed mechanism employs an activated water molecule (blue) that is coordinated between two conserved aspartate residues, which enables water to perform a nucleophilic attack on the carbonyl carbon of the substrate (red) to create cleaved product (purple). For serine proteases, the proposed mechanism employs a serine-histidine catalytic dyad that activates serine for a nucleophilic attack on the substrate to cleave the scissile peptide bond. In the glutamyl protease Rce1, the proposed mechanism uses an activated water molecule that is coordinated between histidine and glutamate residues, which enables water to perform a nucleophilic attack on the carbonyl carbon of the substrate. And for IMMPs, it has been proposed that aspartate and both histidine residues coordinate the zinc ion while the glutamate within the HEXXH motif is thought to activate a zinc-bound water molecule for peptide bond hydrolysis of the substrate.

The most extensively studied aspartyl IP is presenilin. Presenilin belongs to the catalytic component of γ-secretase [11-13], a multi-subunit protease complex (with PEN-2, APH-1 and nicastrin [14]) which cleaves two substrates: amyloid precursor protein (APP) and the Notch receptor [11-13]. Development of Alzheimer's disease is marked by cleavage of APP and the accumulation of a 42-residue amyloid-β peptide [15, 16]. Increased Notch cleavage by presenilin can impact cell signaling and lead to neurodevelopment defects, cancer and acne inversa [16-18]. Therefore, knowledge of presenilin regulation and substrate recognition can lead to advances in human health.

Currently, structures have been determined for the archaeal presenilin PSH and human presenilin PS1. The structure of PSH from *Methanoculleus marisnigri* JR1, was solved through X-ray crystallography [5]. PSH consists of nine α-helical TMSs (Figure 1.1), which contain a cavity facing the cytoplasm that exposes the catalytic residues (D162 and D220) on TMS6 and TMS7 to solvent. The structure shows that D162 and D220 are separated by a distance of 6.7 Å, suggesting that a conformational change induced by substrate binding could bring the catalytic residues in proximity to carry out proteolysis [5]. The structures of human γ-secretase, including the catalytic subunit PS1, have been solved using cryo-electron microscopy (cryo-EM) [19-21]. In these structures, PS1 exhibits a similar overall structure to PSH. The catalytic residues of PS1 (D257 and D385) located on TMS6 and TMS7, are a considerable distance (10.6 Å) from one another and share similar features with the PSH active site [5, 21], again suggesting that substrate binding may trigger alignment of these two residues.

Recently, structures of γ-secretase:substrate complexes have been solved, which show extensive interactions between inactive PS1 (D385A) and its substrates: Notch and APP [22, 23]. The cryo-EM structure of human γ-secretase complex and Notch fragment supports the previous

hypothesis that PS1 undergoes conformational change upon substrate binding/recognition. In this structure, the α-helical TMS of Notch fragment is surrounded by three TMSs of PS1 (TMS2, TMS3 and TMS5), and portions of PS1, including all of TMS2 and two loops between TMS1 and TMS2 and between TMS6 and TMS7, become more ordered with Notch substrate binding [22]. Additionally, an anti-parallel hybrid β-sheet is formed between Notch and two β-strands on the loop between TMS6 and TMS7, which unwinds the substrate α-helix and exposes the scissile peptide bond. The structure also shows that the Notch β-sheet is stabilized by a loop connecting TMS8 and TMS9 in PS1, containing the PAL motif (P433, A434, L435), which has been reported to play a role in substrate recognition [24]. Thus, formation of the hybrid β-sheet between PS1 and Notch is essential for substrate cleavage as it stabilizes binding and orients the scissile peptide bond towards the PS1 active site [22]. In contrast to Notch, the α-helical TMS of APP contains few bulky amino acids and no aromatic residues. However, the cryo-EM structure of γ-secretase:APP complex shows that the α-helical TMS of APP also traverses through a central pore of PS1 and forms a hybrid β-sheet in a similar manner to Notch substrate [23]. In this structure, APP interacts with both the loop between TMS6 and TMS7 and the PAL motif, which helps to position the scissile peptide bond in the PS1 active site. Although the global conformation of γ-secretase is unchanged when either Notch or APP are bound, structural differences are observed in the substrate binding regions of TMS2 and TMS3 in PS1, suggesting divergences in substrate recognition [23].

Another aspartyl IP is signal peptide peptidase (SPP), which is responsible for processing signal peptides from precursor proteins. No structure has been solved for SPP, but it does share sequence homology to presenilin [25-27]. Signal peptides are produced during the synthesis of secretory and membrane proteins. During translation, proteins targeted for secretion or the

plasma membrane are directed to the endoplasmic reticulum (ER) through a wide variety of N-terminal signal sequences [28]. After insertion into the ER, signal sequences can be cleaved from precursor proteins and further processed by SPP to generate signal peptide fragments [29]. In humans, SPP can cleave certain signal peptides in the ER to generate lymphocyte antigen-E epitopes, which are released from the ER membrane and transported to the cell surface [30]. SPP activity is also exploited by hepatitis C viral protein to release core protein, which constitutes the virion capsid, from the ER membrane [31]. Therefore, more knowledge on SPP structure and substrates may elucidate other functions of signal sequences in cell signaling pathways.

The final group of aspartyl IPs includes type 4 prepilin peptidase (TFPP) and preflagellin peptidase (PFP), which show no sequence homology to presenlins and SPP (Figure 1.1). Archaeal preflagellins and bacterial type-4 prepilins are cleaved in the membrane by either PFP or TFPP, respectively, before being secreted and incorporated into the mature flagellum or type-4 pilus [4, 32, 33]. The crystal structure of FlaK, a PFP from *Methanococcus meripaludis*, was solved [4]. FlaK contains six α-helical TMSs with catalytic residues (D18 and D79) located on the ends of TMS1 and TMS4, a short α-helix that does not protrude from the membrane, and 4 anti-parallel β-strands in the loop between TMS5 and TMS6 (Figure 1.1). The structure shows that D18 and D79 are separated by a distance of 12 Å, suggesting that FlaK changes conformation upon substrate binding [4], similar to that observed with presenilin [5, 21-23]. Analysis of the FlaK crystal structure shows similarities in the active site architecture with presenilin. In particular TMS1, TMS4 and TMS6 of FlaK are equivalent to TMS6, TMS7 and TMS9 in presenilin [4]. Currently, no structures for TFPPs have been solved, however

membrane topology analysis of Pibd, a TFPP from *Sulfolobus solfataricus*, suggests that it may have a similar structure to FlaK [34].

Serine proteases (Rhomboids): Serine IPs, also known as rhomboid proteases, are found in all three domains of life [35-37]. The characteristic feature of all rhomboid-like proteins is the conserved core of six α-helical TMSs, referred to as the rhomboid-fold, which can be extended by a seventh TMS added to the N- or C-terminus (Figure 1.1). The rhomboid fold contains a long loop between TMS1 and TMS2 and both catalytic serine and histidine residues are always located in TMS4 and TMS6, respectively [38]. It has been proposed that these proteases implement a serine-histidine catalytic dyad that activates the hydroxyl group side chain of serine for a nucleophilic attack on the substrate to cleave the scissile peptide bond [39, 40] (Figure 1.2). The following rhomboid proteins will be discussed below: Rhomboid-1, Pcp1/PARL, AarA, YqpG and GlpG.

The first rhomboid gene was discovered in a mutant screen of *Drosophila melanogaster,* where loss of *rhomboid-1* led to developmental defects in embryos [41]. Additional research has shown that Rhomboid-1 is an evolutionarily widespread serine protease that acts as a regulator of epidermal growth factor (EGF) signaling [42, 43]. During embryo development in *Drosophila*, the membrane embedded substrate of Rhomboid-1, Spitz, is transported from the ER membrane to the Golgi apparatus by the membrane protein Star [42-44]. Spitz is a homolog of mammalian transforming growth factor α (TGFα), which contains one TMS and an extracellular EGF domain [42, 43]. Once in the Golgi apparatus membrane, the TMS of Spitz is proteolytically cleaved by Rhomboid-1, and the EGF ligand is secreted from the cell, which mediates development and localization of wing veins in embryos [43, 45]. Currently, no structure has been solved of Rhomboid-1, but membrane topology predicts that this protease contains seven α-helical TMSs,

including the rhomboid fold with active site residues S217 and H281 plus an additional C-terminal TMS [42].

Another group of rhomboid proteases reside in the mitochondrial membrane. In *Saccharomyces cerevisiae*, the rhomboid protease Pcp1, also referred to as Rbd1, regulates mitochondrial membrane remodeling [46]. Cells lacking Pcp1 (Δ*pcp1*) display fragmented mitochondria, similar to deletions of the dynamin-related protein Mgm1p, which is the proposed substrate of Pcp1 [46, 47]. The mammalian mitochondrial rhomboid PARL is a homolog of Pcp1. PARL resides in the inner mitochondrial membrane and is thought to regulate cytochrome c release from the mitochondria during apoptosis by processing OPA1 [48, 49].

Rhomboid proteases are also found in archaea and bacteria. In the archaeon *Haloferax volcanii*, a rhomboid protease is involved in protein glycosylation of the S-layer [50, 51]. Additionally, several bacterial rhomboid proteases have been identified. In *Providencia stuartii*, the rhomboid protease AarA cleaves its substrate TatA, a component of the twin-arginine translocase protein secretion pathway, which mediates quorum-sensing in this pathogenic Gram-negative bacterium by an unknown mechanism [52]. In *Bacillus subtilis*, YqgP cleaves MgtE, a high-affinity magnesium transporter, and interacts with the membrane attached metalloprotease FtsH [53]. No structures have been solved for AarA and YqgP, but their predicted membrane topology suggests that these proteins are composed of seven α-helical TMSs [54].

Escherichia coli GlpG is the most extensively studied and structurally characterized rhomboid protease. Although it is a model rhomboid protease, its biological function is unknown. Crystal structures of GlpG show that it composed of six α-helical TMSs that form an aqueous active site cavity open to the extracellular side and a long membrane-embedded loop (denoted as loop 1) between TMS1 and TMS2, characteristic of the rhomboid fold [7, 8] (Figure

1.1). The central cavity contains the putative catalytic residues (S201 and H254) located on the ends of TMS4 and TMS6 respectively (Figure 1.1), and both structures support the hypothesis that a serine-histidine dyad is formed.

However, different mechanisms of substrate entry into the catalytic core of GlpG have been proposed. In the first published structure, the catalytic core was capped above by the short loop between TMS5 and TMS6 (denoted as loop 5) and laterally by loop 1 [7]. This led researchers to propose that the substrate laterally docks to the protease, substituting the loop 1 gate previously bound there. In contrast, the second published structure of GlpG shows a V-shaped cavity that is open to solvent with the loop 5 cap moved away and an observed conformational shift of TMS5 [8]. The researchers proposed that loop 5 regulates access of water molecules and the TMS5 shift provides access to entering substrate. Additional research examining variants in loop 1 and TMS5 of GlpG implicates TMS5 as the lateral substrate gate and suggests that loop 1 may serve an important structural role and not a dynamic gating function [55].

Because these structures raised questions concerning how the TMS of the substrate gains access to the rhomboid active site, additional work was done to co-crystalize GlpG with inhibitors. One is diisopropyl fluorophosphonate that inhibits via an irreversible mechanism. The crystal structures of GlpG in complex with this small molecule shows that the inhibitor displaces loop 5 from the active site but does not cause major lateral shifts in the TMSs [56, 57]. Crystal structures of GlpG with tetrapeptidyl-chloromethylketone (CMK) inhibitors, which bind in an irreversible substrate-like manner, show that the peptidyl portion of the inhibitor fills the active site cavity, wedged between loop 5 and loop3, the short loop between TMS3 and TMS4 [58]. In these GlpG:CMK structures, 4 protease subsites are revealed, which represent 4 distinct

grooves/cavities within the GlpG active site that potentially play roles in substrate binding or specificity. The S1 subsite is hydrophilic and merges into the previously defined "water retention site" [59], which suggests that the S1 site may play a crucial role in substrate binding, specificity and catalysis. Both subsites S2 and S3, located near the rim of the active site, are large and relatively insensitive to residue changes. The last subsite, S4, is a recessed hydrophobic patch facing the periplasmic solvent-exposed face of GlpG that is mainly composed of residues in loop 1, which led researchers to propose that loop 1 binds substrate [58]. In addition, alignment of the GlpG:CMK structure with the GlpG apoenzyme shows that the inhibitor displaces loop 5, but does not significantly move TMS5, again suggesting that major lateral movement of TMS5 is not required for substrate access. In order to elucidate the enzymatic mechanism of GlpG, researchers also determined the crystal structure of active GlpG in a membrane bicelle with peptide aldehyde inhibitors, which mimic substrate and act as reversible inhibitors [60]. In these structures, the peptidyl portion of the inhibitor formed multiple backbone interactions with loops 3 and 5 in GlpG, while the aldehyde carbon of the inhibitor was tetrahedral, mimicking the transition state with the active site residues H150, S201 and N154. During catalysis, the nucleophilic attack of the peptide carbonyl by serine generates a negatively charged oxygen, which needs to be stabilized for catalysis to proceed (Figure 1.2). This GlpG:inhibitor structure shows that the oxyanion is stabilized by side chain nitrogens of H150, N154 and the backbone nitrogen of S201, further elucidating the mechanism of proteolysis [60]. Recently, time-resolved crystallography structures of GlpG with an aldehyde inhibitor and a transmembrane peptide substrate in a bicelle membrane were solved [61]. Interestingly, these structures show that transmembrane substrate and inhibitor take different paths to the active site. These GlpG structures show movement of loop 5, TMS5 and the top of

TMS2 with substrate, but not with inhibitor [61]. Additionally, loop 5 in GlpG appears to clamp down on the substrate, restraining it into an approproate conformation for proteolysis.

The glutamyl protease Rce1: Rce1 is the founding member of the glutamyl IP family (Figure 1.1). The proposed mechanism of Rce1 proteolysis employs an activated water molecule that is coordinated between histidine and glutamate residues, which enables water to perform a nucleophilic attack on the carbonyl carbon of the substrate [3, 62] (Figure 1.2).

Rce1 is a prenyl endopeptidase which processes prenylated Ras protein and the precursor mating pheromone α-factor in the ER membrane of *S. cerevisiae* [63, 64]. Protein prenylation is defined as the covalent attachment of a lipid containing three (farnesyl) or four (geranylgeranyl) isoprene units to the thiol of a C-terminal cysteine residue [65]. Farneslyation of Ras protein in yeast and humans is necessary for proper membrane localization and activity [66]. Additionally, farensylation is required to convert the α-factor precursor into a mature mating pheromone [67, 68]. In prenylated proteins with a CAAX motif (C is cysteine, A is any aliphatic amino acid and X is any amino acid), like Ras and α-factor precursor, prenylation of cysteine is followed by proteolysis of three COOH-terminal residues (-AAX) by Rce1 [63]. Inactivation of Rce1 slows cell growth, causes Ras mislocalization from the plasma membrane, limits Ras-induced transformation of fibroblasts and can cause lethal dilated cardiomyopathy in mice [69, 70].

The structure was solved for *Mm*Rce1, an archaeal homolog of Rce1 from *Methanococcus maripaludis*, by X-ray crystallography [3]. *Mm*Rce1 consists of eight α-helical TMSs and two peripheral α-helices (Figure 1.1). The TMSs form a conical cavity facing the cytoplasm that exposes the catalytic residues (E140 and H173) on TMS4 and TMS5 to solvent, which is large enough to accommodate the prenalyated CAAX substrate for proteolysis. It has also been proposed that H227 and N231, positioned on TMS7 across from the catalytic dyad of

E140 and H173, may donate hydrogen bonds to stabilize the oxyanion state [3] (Figure 1.2). However, an Rce1:substrate complex structure is needed for confirmation.

Intramembrane metalloproteases: The final family of IPs include intramembrane metalloproteases (IMMPs), which activate transcription factors by RIP in all three domains of life [1, 2, 71]. IMMPs contain an HEXXH motif (H is histidine, E is glutamate and X is any amino acid), a characteristic of zinc metalloproteases, and a conserved aspartate residue within an NPDG motif (N is asparagine, P is proline, D is aspartate and G is glycine) [6, 71, 72] (Figure 1.1). It has been proposed that aspartate and both histidine residues coordinate the zinc ion within the membrane-embedded active site [1, 6, 73, 74]. During catalysis, the conserved glutamate within the HEXXH motif is thought to activate a zinc-bound water molecule for peptide bond hydrolysis of the substrate (Figure 1.2).

The first IMMP discovered was human Site-2 protease (S2P), which is required for proteolysis of sterol-regulatory element-binding proteins (SREBPs) at Site-2 [75]. When cells are depleted of cholesterol, SREBP precursor travels from the ER to the Golgi apparatus membrane [76, 77]. Once in the Golgi apparatus membrane, a two-step proteolytic process results in the release of the SREBP NH_2-terminal domain so that it can enter the nucleus and act as a transcription factor, activating genes encoding the low density lipoprotein (LDL) receptor and enzymes for cholesterol and fatty acid synthesis [78, 79]. The first proteolytic step involves a membrane bound serine protease which cleaves the luminal loop of SREBP at Site-1 [79-81]. After cleavage by the Site-1 protease (S1P), the covalent bond between the two TMSs of SREBP is broken, which then allows for the second proteolysis step by S2P [79, 82]. S2P cleaves TMS1 of the substrate, releasing the NH_2-terminal domain transcription factor into the cytosol [71, 82]. In addition to regulating cholesterol homeostasis, S2P also regulates the ER stress response by

cleaving a second substrate ATF6, which contains one TMS [83]. When unfolded proteins accumulate in the ER lumen, ATF6 moves from the ER membrane to the Golgi apparatus where it is first cleaved by S1P then by S2P, similar to SREBP [84-86]. Cleavage of ATF6 results in the liberation of the NH_2-terminal domain, allowing it to enter the nucleus to activate transcription of chaperones to facilitate protein folding in the ER [83]. Currently, no structure has been solved for the IMMP S2P, but it is predicted to contain 8 TMSs and an active site core between TMS4-6 with the HEXXH motif in TMS4 and the NPDG motif in TMS6 [71, 87, 88]. The S2P active site is predicted to be in a similar conformation to TMS2-4 in mjS2P (Figure 1.1) [6, 74].

The only IMMP crystal structure was solved for the transmembrane core of mjS2P, an S2P homolog from the archaeon *Methanocaldococcus jannaschii* [6]. mjS2P contains six α-helical TMSs, including an HEXXH motif in TMS2 and a conserved D148 within the NPDG motif in TMS4, which coordinate a zinc atom within the lipid bilayer approximately 14 angstroms from the membrane surface. The overall structure contains two features unique to IMMPs: 1) The N-terminal region contains two antiparallel β-strands which combine with a third strand, located in the long membrane re-entrant loop between TMS2 and TMS3; 2) TMS4 contains two separate α-helices, which are separated by a short nine-residue loop (Figure 1.1). Additionally, mjS2P shows 2 distinct conformations in the crystals [6]. In both conformations, the active site core, which is composed of TMS2, TMS3 and TMS4, is nearly identical in arrangement. By comparison, TMS1, TMS5 and TMS6 show different conformations in the two mjS2P molecules. One conformation exhibits a closed active site, in which TMSs surround the active site and block it from potential access by substrate. The open conformation shows

separation of TMS1 and TMS6 by 10-12 angstroms, which exposes the active site to substrate entry.

Classes of IMMPs. IMMPs belong to four broadly conserved families [74]. The most abundant and studied group includes IMMPs that contain PDZ domains (named from an acronym of the three proteins first discovered to share this feature: post synaptic density protein (PSD95), Drosophila disc large tumor suppressor (Dlg1), and zonula occludens-1 protein (ZO-1)). Examples of PDZ domain-containing IMMPs include S2P and RseP. PDZ domains mediate protein-protein interactions and are found in a wide variety of proteins involved in signaling, protein degradation, transport, and localization [89-91]. In IMMPs, PDZ domains are thought to aid substrate recognition [71, 90]. The next group of IMMPs contain CBS domains (named after the metabolic enzyme cystathionine-β-synthase). CBS domains regulate enzymatic activity in response to cellular energy status by binding adenosine-containing molecules and driving conformational changes [92-95]. Both mjS2P and SpoIVFB belong to this group of IMMPs. As noted previously, the mjS2P crystal structure was produced from a truncated protease variant, in which the CBS domain was removed from transmembrane core [6] (Figure 1.1). The two other IMMP families of are not well defined and contain uncharacterized regulatory domains [74].

RseP Is the Best Understood PDZ Domain-Containing IMMP. RseP (also referred to as YaeL in the literature) belongs to a proteolytic cascade in *E. coli* that responds to extracytoplasmic stress. This IMMP resides in the cytoplasmic membrane and contributes to activation of the transcription factor σ^E, the extracytoplasmic function sigma factor [96-98]. Activation of the σ^E pathway is thought to play a role in quality control of outer membrane

proteins (OMPs). When OMPs are misfolded, σ^E is activated by a proteolytic cascade. Many OMPs contain a C-terminal YXF motif (Y is tyrosine, X is any amino acid and F is phenylalanine), which is normally buried within a β-barrel structure but can become exposed when misfolded. This conserved YXF motif is directly recognized by the PDZ domain of DegS, an inner membrane protein with a periplasmic protease domain, triggering site-1 cleavage of the anti-σ factor RseA, which anchors σ^E to the inner membrane [99]. After the first proteolytic step removes the periplasmic region of RseA, RseP cleaves the TMS of RseA, releasing the soluble complex of RseA cytoplasmic domain and σ^E from the inner membrane of *E. coli* [98, 100]. The RseA cytoplasmic domain is then degraded by ClpXP proteases, which frees σ^E and allows it to regulate transcription of stress-responsive genes [101, 102]. Activation of σ^E is also regulated by the periplasmic protein RseB. RseB binds to the periplasmic domain of RseA to inhibit DegS cleavage *in vitro*, suggesting that RseB blocks the cleavage site [103, 104]. RseB inhibition appears to be released by lipopolysaccharides (LPS) allowing the subsequent DegS and RseP cleavage of RseA [105].

Predicted structure: The structure for RseP is not known. However, RseP contains four hydrophobic segments predicted to be α-helical TMSs. Experiments with alkaline phosphatase (PhoA) and green fluorescence protein (GFP) fusions show that RseP traverses the membrane four times with the N-terminal and C-terminal ends facing the periplasm [96, 106] (Figure 1.1). *phoA/gfp* fusions are a widely used method to analyze the topographical arrangement of membrane proteins as PhoA only folds into an enzymatically active conformation in the periplasm [107, 108] and GFP forms active enzyme in the cytoplasm but not in the periplasm [109]. The conserved HEXXH motif and NPDG motif are predicted to occupy TMS1 and TMS3, respectively. Additionally, the region between TMS1 and TMS2 contains a stretch of

hydrophobic residues, which may form a long membrane re-entrant loop. These results suggest that the core TMS1-3 of RseP could be similar to the active site core observed in TMS2-4 of mjS2P (Figure 1.1).

PDZ domains: RseP contains two cytoplasmic tandem PDZ domains that are proposed to act as a molecular sieve to exclude full-length RseA [110] (Figure 1.1). Tandem circularly permutated PDZ domains were predicted through sequence analysis and later were confirmed by solving their crystal structures [74, 111, 112]. The integrity of both PDZ domains is required for RseP suppression as substitutions and deletions enable RseP to cleave full-length RseA [100, 111]. Earlier studies predicted that the tandem PDZ domains may recognize a sequence of DegS-cleaved RseA [74, 100, 111, 112]. However, it appears that the RseP first discriminates substrates sterically by size-exclusion through their PDZ domains and then by interactions with three other RseP structural elements [110, 113-116].

Substrate recognition: Three RseP structural elements involved in substrate recognition and cleavage have been identified: the membrane reentrant loop, the short loop, and the PDZ carboxyl terminal region. Mutational analysis of the long loop, which forms a putative β-hairpin-like structure, provides evidence that it directly binds to substrate and induces an extended conformational change to substrate TMS in the proteolytic active site [113, 114]. The long loop also contains a conserved GFG motif (G43, F44, G45), which has been reported to play a role in substrate recognition [114]. In addition, mutational analysis of the short loop, which disrupts TMS3 and contains the conserved NPDG motif, suggests that this region in RseP directly binds to RseA [115]. The third structure, termed the PDZ carboxyl terminal region, contains a peripheral amphiphilic membrane helix that directly interacts with RseA, potentially

mediating substrate recognition and interactions between the protease domain and PDZ domains to support site-2 cleavage [116].

Inhibition: Batimastat, a hydroxamic acid derivative that mimics the peptide structure of natural substrates, was shown to inhibit RseP *in vivo* [117]. RseP inhibition led to the accumulation of misfolded OMPs in *E. coli*, which was expected since RseA cleavage was blocked, thus preventing activation of the σ^E transcription factor. Batimastat is a known inhibitor of eukaryotic matrix metalloproteases that coordinate the catalytic zinc ion [118, 119]. The inhibitor acts as a fourth zinc ligand, blocking the active site and preventing the activation of a water molecule, which is necessary for peptide bond hydrolysis of the substrate (Figure 1.2). Interestingly, two other peptidomimetic hydroxamic acids, ilomastat and miramastat, exhibited very little RseP inhibition, suggesting that batimastat is a selective inhibitor of RseP. Future work is needed to determine if batimastat is capable of inhibiting other IMMPs. A potential target for this investigation is the PDZ-containing IMMP RasP, the *B. subtilis* homolog of RseP which is predicted to share a similar structure [120].

IMMPs Play Important Roles in Pathogenic Bacteria. In bacteria, IMMPs play central roles in regulating or enhancing pathogenicity [121-123]. IMMPs that regulate virulence factors and mating signals in pathogenic bacteria will be discussed briefly below.

Rip1 (also referred to as Rv2869c): *Mycobacterium tuberculosis* contains the IMMP Rip1, which cleaves anti-σ factors for three extracytoplasmic function sigma factors: anti-σ^K factor RskA, anti-σ^L factor RslA and anti-σ^M factor RsmA [124]. Genetic analyses show that Δ*rip1* causes perturbation of expression of multiple lipid biosynthetic and catabolic genes and results in defects of the mycolic acids in the outer cell envelope [124, 125]. During infection,

Δ*rip1 M. tuberculosis* is significantly attenuated in comparison to wild type, which indicates that Rip1 plays a crucial role in virulence [125]. *phoA* and *lacZ* (which produces β-galactosidase) fusions show that Rip1 shares a similar membrane topology to RseP [126] (Figure 1.1). *phoA*/*lacZ* fusions are similar to the previous method described for *phoA/GFP* fusions, except that GFP is replaced by β-galactosidase, which is only catalytically active in the cytoplasm [127]. Because Rip1 can recognize multiple substrates, how does this protease achieve specificity in signaling? Researchers have identified a Rip1-PDZ interacting protein, Ppr1 (PDZ-interacting protease regulator 1), which acts as a substrate-specific adapter that holds Rip1 inactive and binds it to one of its substrates, RsmA [126]. After site-1 cleavage to remove the periplasmic domain of RsmA, Ppr1 facilitates Rip1 site-2 cleavage of RsmA. Further work is needed to elucidate the host signals that activate the Rip1 pathway, identity of site-1 protease and determine whether other adaptor proteins aid in the cleavage of RskA and RslA.

MucP: *Pseudomonas aeruginosa*, a Gram-negative pathogen that colonizes the lungs of cystic fibrosis patients, encodes the IMMP MucP, which regulates alginate biosynthesis. Alginate is an exopolysaccharide that contributes to mucoid morphology and biofilm formation, making the bacteria more adherent and better able to resist antibiotics and host immune system defenses [128]. During alginate biosynthesis, the site-1 protease AlgW cleaves the extracytoplasmic region of MucA, an anti-σ factor to AlgU [129]. After site-1 cleavage, MucP is free to cleave the TMS of MucA, releasing the complex of MucA cytoplasmic domain and AlgU from the membrane. The MucA cytoplasmic domain is then degraded by ClpXP proteases, freeing AlgU to activate the alginate biosynthesis operon [130, 131]. The AlgW/MucP pathway is very similar to the DegS/RseP in *E. coli*. However, more work is needed in order to determine how AlgW is activated.

YaeL: In the Gram-negative pathogen *Vibrio cholerae*, the IMMP YaeL regulates cholera toxin production by RIP of membrane bound transcription factor TcpP [132]. TcpP and ToxR are active transcriptional regulators of *toxT* when localized to the membrane. Production of ToxT results in transcription of cholera toxin *ctxAB* and the *tcp* operon, which includes the toxin-regulated pilus [133]. Thus, YaeL negatively regulates toxin expression by destabilizing the transcription factor TcpP. This leads to the question: why develop a system to negatively regulate virulence gene expression? *V. cholera* can exist in an aquatic environment outside of a human host. Therefore, virulence genes may need to be carefully regulated to be active only when the pathogen is inside a human host and not under other environmental conditions [133]. Further work is needed to understand this signaling pathway and the identity of the site-1 protease.

Eep: In the Gram-positive nosocomial pathogen *Enterococcus faecalis*, mating pheromone production is regulated by the IMMP Eep (named from the acronym for enhanced expression of pheromone) [134]. *E. faecalis* poses a potentially serious threat since antibiotic resistance is endemic, which is why the pheromone-regulated plasmid transfer system has been of interest. Plasmid-free recipient cells produce the sex pheromones cAD1, cPD1, and cCF10 by processing signal peptides [135-137]. Site-1 cleavage by the signal peptidase SPaseII frees the membrane embedded signal peptide from lipoprotein and allows for cleavage by Eep [123]. Eep site-2 cleavage releases the pheromone from the membrane, creating an extracellular diffusible signal that induces cell-to-cell plasmid transfer. In addition to pheromone production, Eep may also play an independent role in virulence. In a rabbit model of endocarditis, the *E. faecalis* strain lacking Eep (Δ*eep*) was severely attenuated and microscopic analysis showed abnormal

biofilms containing small cellular aggregates [138]. More work is needed in order to identify the Eep substrates that mediate the virulence phenotype.

SpoIVFB: A Model for CBS Domain-Containing IMMPs. The work described in this dissertation focuses on advancing knowledge about the IMMP SpoIVFB, which plays an essential role in endosporulation. When starved for nutrients (either carbon, nitrogen or phosphate), *B. subtilis* can undergo the process of endosporulation [139] (Figure 1.3). The starved cell will complete a round of DNA replication. During this stage, a polar septum will begin to form, creating a larger mother cell (MC) and smaller forespore (FS) compartment [140]. After the polar septum is formed, one copy of the bacterial chromosome is translocated into the FS. The MC then migrates around the FS during a process called engulfment, resulting in two membranes surrounding the FS (Figure 1.3). Modified peptidoglycan, which is less tightly crosslinked than the cell wall, forms a cortex in the intermembrane space between the inner and outer FS membrane [139]. Meanwhile, the MC produces coat proteins that assemble on the outer FS membrane to build a durable spore coat. After assembly is complete, the MC produces cell wall hydrolases to release the mature spore from the MC compartment [139] (Figure 1.3).

Endosporulation requires the FS and MC to follow distinct developmental programs that are coordinated by signaling the sequential activation of σ factors: σ^E, σ^F, σ^G and σ^K between the compartments [141, 142]. An example of this coordinated signaling is the activation of σ^K in the MC during the late stage of sporulation. This pathway has been termed the σ^K checkpoint [143]. σ^K directs RNA polymerase to transcribe genes whose products form the spore coat and lyse the

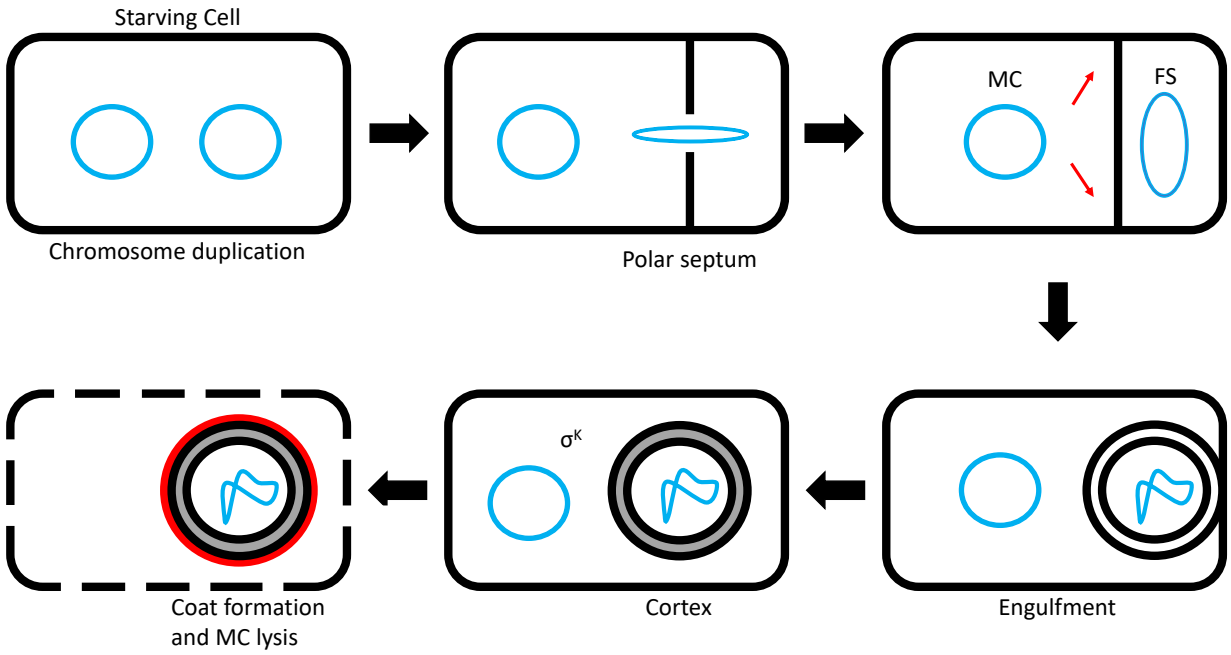

Figure 1.3 Endosporulation. During endosporulation in *B. subtilis*, a starving cell will duplicate its chromosome (blue). Then an asymmetrically-positioned septum divides the cell into MC and FS compartments. The septum then migrates, engulfing the FS. Cell wall-like material is synthesized between the two membranes surrounding the FS forming the cortex (gray). After signaling from the FS, SpoIVFB cleaves Pro-σ^K, releasing active σ^K into the MC. The spore coat (red), composed of proteins made in the MC, assembles on the surface of the FS. The process is complete when the MC lyses and releases a mature spore.

MC, releasing a mature spore [141, 144]. In order to produce viable mature spores, the timing of σ^K activation is tightly regulated [139, 143]. This late sporulation σ factor is synthesized as an inactive precursor, Pro-σ^K, which contains a 21-residue hydrophobic Pro-domain that associates with the outer FS membrane [139, 141, 145, 146]. When activated by signals from the FS, SpoIVFB will cleave the Pro-domain from Pro-σ^K and release active σ^K into the MC compartment (Figure 1.3).

Homology model: The N-terminal domain of SpoIVFB, comprised of six putative TMSs including an HEXXH metalloprotease motif in TMS2 and an NPDG motif in TMS4 [72, 147, 148] (Figure 1.1). Formation of a catalytic core similar to mjS2P [6] that coordinates a zinc ion and activates a water molecule for peptide bond hydrolysis enables SpoIVFB to cleave its membrane-associated substrate, Pro-σ^K [146, 149]. Disulfide cross-linking experiments show that the putative long membrane reentrant loop, located between TMS2 and TMS3, and the short loop within TMS4 face the active site and interact with substrate [150]. Additional chemical cross-linking experiments between SpoIVFB and Pro-σ^K provided constraints to build a homology model of the complex [151] that is based on the crystal structure of mjS2P [6]. Several biochemical assays indicate that SpoIVFB may form a tetramer. Gel filtration size chromatography, ion mobility-mass spectrometry analysis and stepwise photobleaching of SpoIVFB-eGFP suggest that a tetramer of SpoIVFB may interact with Pro-σ^K as a 4:2 complex [152]. However a structure of SpoIVFB is needed to determine if the stoichiometry and arrangement of the SpoIVFB tetrameric model is correct [151].

CBS domain: The C-terminal domain of SpoIVFB includes a cystathione-ß-synthase (CBS) domain [74], which resides in the mother cell compartment (Figure 1.1). CBS domains typically undergo conformational changes upon binding ligands to regulate protein activity [92,

95]. Because SpoIVFB activity *in vitro* depends on ATP, it was proposed that ATP binding to the CBS domain regulates SpoIVFB activity during sporulation in response to the energy level in the MC [149]. This notion has been challenged by two recent findings: 1) A SpoIVFB-YFP fusion protein lacking the CBS domain retains partial function [153]; 2) Chloramphenicol treatment of sporulating *B. subtilis* lowers ATP levels in the MC, but still allows for SpoIVFB to cleave Pro-σ^K [154].

Inhibition by BofA and SpoIVFA: Unlike other IMMPs, SpoIVFB is held inactive in the MC membrane by the inhibitory proteins BofA and SpoIVFA [72, 143, 155-158]. In *B. subtilis*, both BofA and SpoIVFA are necessary to prevent SpoIVFB cleavage of Pro-σ^K [143, 153, 156]. Previous studies have shown that SpoIVFA, SpoIVFB, and BofA form a stabilizing trimeric complex in *B. subtilis* and when expressed in *E. coli* [156, 159]. It is currently believed that BofA acts as the direct inhibitor of SpoIVFB [160], while SpoIVFA acts as a stabilizing scaffold [156, 161]. In Δ*spoIVFA* strains, BofA and SpoIVFB do not localize properly to the outer FS membrane during sporulation. Additionally, membrane topology assays involving *phoA*/*lacZ* fusions have predicted that the C-terminal ends of SpoIVFA and BofA are located in the intermembrane space surrounding the FS [148, 162]. Small truncations in either the C-terminal end of SpoIVFA or BofA relieve inhibition of SpoIVFB, allowing cleavage of Pro-σ^K in *B. subtilis* [157, 158, 162]. These findings have led researchers to propose that a C-terminal interaction between the inhibitory proteins holds BofA in a specific conformation, allowing for direct inhibition of SpoIVFB [163]. However, there is no direct evidence for this interaction. It is also currently unknown how BofA and SpoIVFA interact with SpoIVFB.

Signaling from the FS relieves BofA/SpoIVFA inhibition of SpoIVFB. Two serine proteases, SpoIVB (not to be confused with SpoIVFB) and CtpB, are synthesized under control

of σ^G in the FS and are secreted into the intermembrane space [159, 164-166]. SpoIVB and CtpB relieve SpoIVFB inhibition by cleaving the C-terminal ends of SpoIVFA and BofA [159, 163, 166, 167]. SpoIVB can cleave the C-terminal end of SpoIVFA at four positions, but will preferentially cleave the peptide bond between residues 154 and 155 [163, 166, 167]. CtpB then cleaves both the C-terminal end of SpoIVFA, between residues 131 and 132, and the C-terminal end of BofA [159, 166-168]. Only SpoIVB appears to be essential for spore formation, while CtpB may serve as a fine-tuning mechanism since Pro-σ^K processing was only delayed by about 1 hour in a *B. subtilis* strain lacking CtpB (Δ*ctpB*) [169]. Once inhibition is removed by these FS secreted proteases, SpoIVFB is free to cleave Pro-σ^K, releasing σ^K into the MC [72, 147, 149, 151, 152] (Figure 1.3).

Knowledge Gap That Work Described in This Dissertation Begins to Fill. IMMPs regulate gene expression in all three domains of life, including pathways that maintain human health and regulate bacterial pathogenesis. Thus, knowledge of IMMP interactions with substrates and inhibitors could inform rational design of therapeutics; however, structures of IMMP:substrate and IMMP:inhibitor complexes have not been reported. The work described in this dissertation uses experimental and modeling approaches to help elucidate the mechanism of inhibition and substrate interaction of SpoIVFB. I have engineered coexpression of proteins in *E. coli*, and performed *in vivo* assays of Pro-σ^K cleavage by SpoIVFB as well as disulfide cross-linking between BofA and SpoIVFB, which generated data to build structural models of SpoIVFB in complex with its inhibitors BofA and SpoIVFA. I have also explored the interaction between Pro-σ^K and the SpoIVFB short loop, which contains the conserved NPDG motif and interrupts TMS4. My studies provide insights into the mechanism of SpoIVFB inhibition and

the role of the SpoIVFB short loop in substrate interaction, which can guide efforts to modulate activity of other IMMPs.

REFERENCES

REFERENCES

1. Brown, M.S., et al., *Regulated intramembrane proteolysis: a control mechanism conserved from bacteria to humans.* Cell, 2000. **100**(4): p. 391-398.

2. Urban, S., *Mechanisms and cellular functions of intramembrane proteases.* Biochim. Biophys. Acta - Biomembr., 2013. **1828**: p. 2797-2800.

3. Manolaridis, I., et al., *Mechanism of farnesylated CAAX protein processing by the intramembrane protease Rce1.* Nature, 2013. **504**(7479): p. 301-305.

4. Hu, J., et al., *The crystal structure of GXGD membrane protease FlaK.* Nature, 2011. **475**(7357): p. 528-531.

5. Li, X., et al., *Structure of a presenilin family intramembrane aspartate protease.* Nature, 2013. **493**(7430): p. 56-61.

6. Feng, L., et al., *Structure of a site-2 protease family intramembrane metalloprotease.* Science, 2007. **318**(5856): p. 1608-1612.

7. Wang, Y., Y. Zhang, and Y. Ha, *Crystal structure of a rhomboid family intramembrane protease.* Nature, 2006. **444**(7116): p. 179-183.

8. Wu, Z., et al., *Structural analysis of a rhomboid family intramembrane protease reveals a gating mechanism for substrate entry.* Nat. Struct. Mol. Biol., 2006. **13**(12): p. 1084-1091.

9. Cooper, J.B., et al., *X-ray analyses of aspartic proteinases. II. Three-dimensional structure of the hexagonal crystal form of porcine pepsin at 2.3 A resolution.* J Mol Biol, 1990. **214**(1): p. 199-222.

10. Suguna, K., et al., *Binding of a reduced peptide inhibitor to the aspartic proteinase from Rhizopus chinensis: implications for a mechanism of action.* Proc Natl Acad Sci U S A, 1987. **84**(20): p. 7009-13.

11. De Strooper, B., et al., *Deficiency of presenilin-1 inhibits the normal cleavage of amyloid precursor protein.* Nature, 1998. **391**(6665): p. 387-90.

12. De Strooper, B., et al., *A presenilin-1-dependent gamma-secretase-like protease mediates release of Notch intracellular domain.* Nature, 1999. **398**(6727): p. 518-22.

13. Struhl, G. and I. Greenwald, *Presenilin is required for activity and nuclear access of Notch in Drosophila.* Nature, 1999. **398**(6727): p. 522-5.

14. De Strooper, B., *Aph-1, Pen-2, and Nicastrin with Presenilin generate an active gamma-Secretase complex.* Neuron, 2003. **38**(1): p. 9-12.

15. Selkoe, D.J. and M.S. Wolfe, *Presenilin: running with scissors in the membrane.* Cell, 2007. **131**(2): p. 215-21.

16. De Strooper, B., T. Iwatsubo, and M.S. Wolfe, *Presenilins and gamma-secretase: structure, function, and role in Alzheimer Disease.* Cold Spring Harb Perspect Med, 2012. **2**(1): p. a006304.

17. Weng, A.P., et al., *Activating mutations of NOTCH1 in human T cell acute lymphoblastic leukemia.* Science, 2004. **306**(5694): p. 269-71.

18. Wang, B., et al., *Gamma-secretase gene mutations in familial acne inversa.* Science, 2010. **330**(6007): p. 1065.

19. Lu, P., et al., *Three-dimensional structure of human gamma-secretase.* Nature, 2014. **512**(7513): p. 166-170.

20. Sun, L., et al., *Structural basis of human gamma-secretase assembly.* Proc Natl Acad Sci U S A, 2015. **112**(19): p. 6003-8.

21. Bai, X.C., et al., *An atomic structure of human gamma-secretase.* Nature, 2015. **525**(7568): p. 212-217.

22. Yang, G., et al., *Structural basis of Notch recognition by human gamma-secretase.* Nature, 2019. **565**(7738): p. 192-197.

23. Zhou, R., et al., *Recognition of the amyloid precursor protein by human gamma-secretase.* Science, 2019. **363**(6428).

24. Sato, C., et al., *The C-terminal PAL motif and transmembrane domain 9 of presenilin 1 are involved in the formation of the catalytic pore of the gamma-secretase.* J Neurosci, 2008. **28**(24): p. 6264-71.

25. Steiner, H., et al., *Glycine 384 is required for presenilin-1 function and is conserved in bacterial polytopic aspartyl proteases.* Nat Cell Biol, 2000. **2**(11): p. 848-51.

26. Weihofen, A., et al., *Release of signal peptide fragments into the cytosol requires cleavage in the transmembrane region by a protease activity that is specifically blocked by a novel cysteine protease inhibitor.* J Biol Chem, 2000. **275**(40): p. 30951-6.

27. Weihofen, A., et al., *Identification of signal peptide peptidase, a presenilin-type aspartic protease.* Science, 2002. **296**(5576): p. 2215-8.

28. Stroud, R.M. and P. Walter, *Signal sequence recognition and protein targeting.* Curr Opin Struct Biol, 1999. **9**(6): p. 754-9.

29. Martoglio, B. and B. Dobberstein, *Signal sequences: more than just greasy peptides.* Trends Cell Biol, 1998. **8**(10): p. 410-5.

30. Lemberg, M.K., et al., *Intramembrane proteolysis of signal peptides: an essential step in the generation of HLA-E epitopes.* J Immunol, 2001. **167**(11): p. 6441-6.

31. McLauchlan, J., et al., *Intramembrane proteolysis promotes trafficking of hepatitis C virus core protein to lipid droplets.* EMBO J, 2002. **21**(15): p. 3980-8.

32. Francetic, O., et al., *Signal recognition particle-dependent inner membrane targeting of the PulG Pseudopilin component of a type II secretion system.* J Bacteriol, 2007. **189**(5): p. 1783-93.

33. Bayley, D.P. and K.F. Jarrell, *Overexpression of Methanococcus voltae flagellin subunits in Escherichia coli and Pseudomonas aeruginosa: a source of archaeal preflagellin.* J Bacteriol, 1999. **181**(14): p. 4146-53.

34. Szabo, Z., S.V. Albers, and A.J. Driessen, *Active-site residues in the type IV prepilin peptidase homologue PibD from the archaeon Sulfolobus solfataricus.* J Bacteriol, 2006. **188**(4): p. 1437-43.

35. Gallio, M., et al., *A conserved mechanism for extracellular signaling in eukaryotes and prokaryotes.* Proc. Natl. Acad. Sci. USA, 2002. **99**(19): p. 12208-13.

36. Wasserman, J.D., S. Urban, and M. Freeman, *A family of rhomboid-like genes: Drosophila rhomboid-1 and roughoid/rhomboid-3 cooperate to activate EGF receptor signaling.* Genes Dev, 2000. **14**(13): p. 1651-63.

37. Koonin, E.V., et al., *The rhomboids: a nearly ubiquitous family of intramembrane serine proteases that probably evolved by multiple ancient horizontal gene transfers.* Genome Biol, 2003. **4**(3): p. R19.

38. Dusterhoft, S., U. Kunzel, and M. Freeman, *Rhomboid proteases in human disease: Mechanisms and future prospects.* Biochim Biophys Acta Mol Cell Res, 2017. **1864**(11 Pt B): p. 2200-2209.

39. Lemberg, M.K., et al., *Mechanism of intramembrane proteolysis investigated with purified rhomboid proteases.* EMBO J., 2005. **24**(3): p. 464-472.

40. Hedstrom, L., *Serine protease mechanism and specificity.* Chem Rev, 2002. **102**(12): p. 4501-24.

41. Wieschaus, E., C. Nusslein-Volhard, and G. Jurgens, *Mutations affecting the pattern of the larval cuticle inDrosophila melanogaster : III. Zygotic loci on the X-chromosome and fourth chromosome.* Wilehm Roux Arch Dev Biol, 1984. **193**(5): p. 296-307.

42. Urban, S., J.R. Lee, and M. Freeman, *Drosophila rhomboid-1 defines a family of putative intramembrane serine proteases.* Cell, 2001. **107**(2): p. 173-182.

43. Lee, J.R., et al., *Regulated intracellular ligand transport and proteolysis control EGF signal activation in Drosophila.* Cell, 2001. **107**(2): p. 161-171.

44. Rutledge, B.J., et al., *The Drosophila spitz gene encodes a putative EGF-like growth factor involved in dorsal-ventral axis formation and neurogenesis.* Genes Dev, 1992. **6**(8): p. 1503-17.

45. Sturtevant, M.A., et al., *The Drosophila rhomboid protein is concentrated in patches at the apical cell surface.* Dev Biol, 1996. **174**(2): p. 298-309.

46. McQuibban, G.A., S. Saurya, and M. Freeman, *Mitochondrial membrane remodelling regulated by a conserved rhomboid protease.* Nature, 2003. **423**(6939): p. 537-41.

47. Herlan, M., et al., *Processing of Mgm1 by the rhomboid-type protease Pcp1 is required for maintenance of mitochondrial morphology and of mitochondrial DNA.* J Biol Chem, 2003. **278**(30): p. 27781-8.

48. Cipolat, S., et al., *Mitochondrial rhomboid PARL regulates cytochrome c release during apoptosis via OPA1-dependent cristae remodeling.* Cell, 2006. **126**(1): p. 163-75.

49. Sik, A., et al., *Self-regulated cleavage of the mitochondrial intramembrane-cleaving protease PARL yields Pbeta, a nuclear-targeted peptide.* J Biol Chem, 2004. **279**(15): p. 15323-9.

50. Parente, J., et al., *A rhomboid protease gene deletion affects a novel oligosaccharide N-linked to the S-layer glycoprotein of Haloferax volcanii.* J Biol Chem, 2014. **289**(16): p. 11304-17.

51. Costa, M.I., et al., *Haloferax volcanii Proteome Response to Deletion of a Rhomboid Protease Gene.* J Proteome Res, 2018. **17**(3): p. 961-977.

52. Stevenson, L.G., et al., *Rhomboid protease AarA mediates quorum-sensing in Providencia stuartii by activating TatA of the twin-arginine translocase.* Proc Natl Acad Sci U S A, 2007. **104**(3): p. 1003-8.

53. Began, J., et al., *Rhomboid intramembrane protease YqgP licenses bacterial membrane protein quality control as adaptor of FtsH AAA protease.* EMBO J, 2020. **39**(10): p. e102935.

54. Strisovsky, K., H.J. Sharpe, and M. Freeman, *Sequence-specific intramembrane proteolysis: identification of a recognition motif in rhomboid substrates.* Mol. Cell, 2009. **36**(6): p. 1048-1059.

55. Baker, R.P., et al., *Enzymatic analysis of a rhomboid intramembrane protease implicates transmembrane helix 5 as the lateral substrate gate.* Proc. Natl. Acad. Sci. USA, 2007. **104**(20): p. 8257-8262.

56. Xue, Y. and Y. Ha, *Catalytic mechanism of rhomboid protease GlpG probed by 3,4-dichloroisocoumarin and diisopropyl fluorophosphonate.* J. Biol. Chem., 2012. **287**(5): p. 3099-3107.

57. Xue, Y. and Y. Ha, *Large lateral movement of transmembrane helix S5 is not required for substrate access to the active site of rhomboid intramembrane protease.* J Biol Chem, 2013. **288**(23): p. 16645-54.

58. Zoll, S., et al., *Substrate binding and specificity of rhomboid intramembrane protease revealed by substrate-peptide complex structures.* EMBO J., 2014. **33**(20): p. 2408-2421.

59. Zhou, Y., et al., *An internal water-retention site in the rhomboid intramembrane protease GlpG ensures catalytic efficiency.* Structure, 2012. **20**(7): p. 1255-1263.

60. Cho, S., S.W. Dickey, and S. Urban, *Crystal structures and inhibition kinetics reveal a two-stage catalytic mechanism with drug design implications for rhomboid proteolysis.* Mol. Cell, 2016. **61**(3): p. 329-340.

61. Cho, S., et al., *Ten catalytic snapshots of rhomboid intramembrane proteolysis from gate opening to peptide release.* Nat Struct Mol Biol, 2019. **26**(10): p. 910-918.

62. Hampton, S.E., T.M. Dore, and W.K. Schmidt, *Rce1: mechanism and inhibition.* Crit Rev Biochem Mol Biol, 2018. **53**(2): p. 157-174.

63. Boyartchuk, V.L., M.N. Ashby, and J. Rine, *Modulation of Ras and a-factor function by carboxyl-terminal proteolysis.* Science, 1997. **275**(5307): p. 1796-800.

64. Schmidt, W.K., et al., *Endoplasmic reticulum membrane localization of Rce1p and Ste24p, yeast proteases involved in carboxyl-terminal CAAX protein processing and amino-terminal a-factor cleavage.* Proc Natl Acad Sci U S A, 1998. **95**(19): p. 11175-80.

65. Clarke, S., *Protein isoprenylation and methylation at carboxyl-terminal cysteine residues.* Annu Rev Biochem, 1992. **61**: p. 355-86.

66. Hancock, J.F., K. Cadwallader, and C.J. Marshall, *Methylation and proteolysis are essential for efficient membrane binding of prenylated p21K-ras(B).* EMBO J, 1991. **10**(3): p. 641-6.

67. Schafer, W.R., et al., *Enzymatic coupling of cholesterol intermediates to a mating pheromone precursor and to the ras protein.* Science, 1990. **249**(4973): p. 1133-9.

68. Fujiyama, A., K. Matsumoto, and F. Tamanoi, *A novel yeast mutant defective in the processing of ras proteins: assessment of the effect of the mutation on processing steps.* EMBO J, 1987. **6**(1): p. 223-8.

69. Bergo, M.O., et al., *Absence of the CAAX endoprotease Rce1: effects on cell growth and transformation.* Mol Cell Biol, 2002. **22**(1): p. 171-81.

70. Bergo, M.O., et al., *On the physiological importance of endoproteolysis of CAAX proteins: heart-specific RCE1 knockout mice develop a lethal cardiomyopathy.* J Biol Chem, 2004. **279**(6): p. 4729-36.

71. Kroos, L. and Y. Akiyama, *Biochemical and structural insights into intramembrane metalloprotease mechanisms.* Biochim. Biophys. Acta - Biomembr., 2013. **1828**(12): p. 2873-2885.

72. Rudner, D., P. Fawcett, and R. Losick, *A family of membrane-embedded metalloproteases involved in regulated proteolysis of membrane-associated transcription factors.* Proc. Natl. Acad. Sci. USA, 1999. **96**: p. 14765-14770.

73. Lewis, A. and P. Thomas, *A novel clan of zinc metallopeptidases with possible intramembrane cleavage properties.* Protein Sci., 1999. **8**: p. 439-442.

74. Kinch, L.N., K. Ginalski, and N.V. Grishin, *Site-2 protease regulated intramembrane proteolysis: sequence homologs suggest an ancient signaling cascade.* Protein Sci., 2006. **15**(1): p. 84-93.

75. Rawson, R., et al., *Complementation cloning of SP2, a gene encoding a putative metalloprotease required for intramembrane cleavage of SREBPs.* Mol. Cell, 1997. **1**: p. 47-57.

76. Nohturfft, A., et al., *Sterols regulate cycling of SREBP cleavage-activating protein (SCAP) between endoplasmic reticulum and Golgi.* Proc. Natl. Acad. Sci. USA, 1999. **96**(20): p. 11235-11240.

77. DeBose-Boyd, R.A., et al., *Transport-dependent proteolysis of SREBP: relocation of site-1 protease from Golgi to ER obviates the need for SREBP transport to Golgi.* Cell, 1999. **99**(7): p. 703-12.

78. Brown, M.S. and J.L. Goldstein, *The SREBP pathway: regulation of cholesterol metabolism by proteolysis of a membrane-bound transcription factor.* Cell, 1997. **89**(3): p. 331-340.

79. Rawson, R.B., *The SREBP pathway--insights from Insigs and insects.* Nat. Rev. Mol. Cell Biol., 2003. **4**(8): p. 631-640.

80. Duncan, E.A., et al., *Cleavage site for sterol-regulated protease localized to a leu-Ser bond in the lumenal loop of sterol regulatory element-binding protein-2.* J Biol Chem, 1997. **272**(19): p. 12778-85.

81. Sakai, J., et al., *Molecular identification of the sterol-regulated luminal protease that cleaves SREBPs and controls lipid composition of animal cells.* Mol Cell, 1998. **2**(4): p. 505-14.

82. Sakai, J., et al., *Sterol-regulated release of SREBP-2 from cell membrane requires two sequential cleavages, one within a transmembrane domain.* Cell, 1996. **85**: p. 1037-1048.

83. Haze, K., et al., *Mammalian transcription factor ATF6 is synthesized as a transmembrane protein and activated by proteolysis in response to endoplasmic reticulum stress.* Mol Biol Cell, 1999. **10**(11): p. 3787-99.

84. Rawson, R.B., *The site-2 protease.* Biochim. Biophys. Acta - Biomembr., 2013. **1828**(12): p. 2801-2807.

85. Ye, J., et al., *ER stress induces cleavage of membrane-bound ATF6 by the same proteases that process SREBPs.* Mol. Cell, 2000. **6**(6): p. 1355-1364.

86. Chen, X., J. Shen, and R. Prywes, *The luminal domain of ATF6 senses endoplasmic reticulum (ER) stress and causes translocation of ATF6 from the ER to the Golgi.* J Biol Chem, 2002. **277**(15): p. 13045-52.

87. Ha, Y., *Structure and mechanism of intramembrane protease.* Semin. Cell Dev. Biol., 2009. **20**(2): p. 240-250.

88. Zelenski, N., et al., *Membrane topology of S2P, a protein required for intramembranous cleavage of sterol regulatory element-binding proteins.* J. Biol. Chem., 1999. **274**: p. 21973-21980.

89. Harris, B.Z. and W.A. Lim, *Mechanism and role of PDZ domains in signaling complex assembly.* J. Cell Sci., 2001. **114**(Pt 18): p. 3219-3231.

90. Jelen, F., et al., *PDZ domains - common players in the cell signaling.* Acta Biochim. Pol., 2003. **50**(4): p. 985-1017.

91. Ponting, C.P., et al., *PDZ domains: targeting signalling molecules to sub-membranous sites.* Bioessays, 1997. **19**(6): p. 469-479.

92. Baykov, A.A., H.K. Tuominen, and R. Lahti, *The CBS domain: a protein module with an emerging prominent role in regulation.* ACS Chem. Biol., 2011. **6**(11): p. 1156-1163.

93. Ereno-Orbea, J., I. Oyenarte, and L.A. Martinez-Cruz, *CBS domains: ligand binding sites and conformational variability.* Arch. Biochem. Biophys., 2013. **540**(1-2): p. 70-81.

94. Ignoul, S. and J. Eggermont, *CBS domains: structure, function, and pathology in human proteins.* Am. J. Physiol. Cell Physiol., 2005. **289**(6): p. C1369-C1378.

95. Scott, J.W., et al., *CBS domains form energy-sensing modules whose binding of adenosine ligands is disrupted by disease mutations.* J. Clin. Invest., 2004. **113**(2): p. 274-284.

96. Kanehara, K., Y. Akiyama, and K. Ito, *Characterization of the yaeL gene product and its S2P-protease motifs in Escherichia coli.* Gene, 2001. **281**(1-2): p. 71-79.

97. Kanehara, K., K. Ito, and Y. Akiyama, *YaeL (EcfE) activates the σ^E pathway of stress response through a site-2 cleavage of anti-σ^E, RseA.* Genes Dev., 2002. **16**(16): p. 2147-2155.

98. Alba, B.M., et al., *DegS and YaeL participate sequentially in the cleavage of RseA to activate the σ^E-dependent extracytoplasmic stress response.* Genes Dev., 2002. **16**(16): p. 2156-2168.

99. Walsh, N.P., et al., *OMP peptide signals initiate the envelope-stress response by activating DegS protease via relief of inhibition mediated by its PDZ domain.* Cell, 2003. **113**(1): p. 61-71.

100. Kanehara, K., K. Ito, and Y. Akiyama, *YaeL proteolysis of RseA is controlled by the PDZ domain of YaeL and a Gln-rich region of RseA.* EMBO J., 2003. **22**(23): p. 6389-6398.

101. Flynn, J.M., et al., *Proteomic discovery of cellular substrates of the ClpXP protease reveals five classes of ClpX-recognition signals.* Mol. Cell, 2003. **11**(3): p. 671-683.

102. Chaba, R., et al., *Design principles of the proteolytic cascade governing the σ^E-mediated envelope stress response in Escherichia coli: keys to graded, buffered, and rapid signal transduction.* Genes Dev., 2007. **21**(1): p. 124-136.

103. Cezairliyan, B.O. and R.T. Sauer, *Inhibition of regulated proteolysis by RseB.* Proc. Natl. Acad. Sci. USA, 2007. **104**(10): p. 3771-3776.

104. Kim, D.Y., et al., *Structural basis for the negative regulation of bacterial stress response by RseB.* Protein Sci., 2010. **19**(6): p. 1258-1263.

105. Lima, S., et al., *Dual molecular signals mediate the bacterial response to outer-membrane stress.* Science, 2013. **340**(6134): p. 837-41.

106. Drew, D., et al., *Rapid topology mapping of Escherichia coli inner-membrane proteins by prediction and PhoA/GFP fusion analysis.* Proc. Natl. Acad. Sci. USA, 2002. **99**(5): p. 2690-2695.

107. Akiyama, Y. and K. Ito, *Folding and assembly of bacterial alkaline phosphatase in vitro and in vivo.* J Biol Chem, 1993. **268**(11): p. 8146-50.

108. Derman, A.I. and J. Beckwith, *Escherichia coli alkaline phosphatase fails to acquire disulfide bonds when retained in the cytoplasm.* J Bacteriol, 1991. **173**(23): p. 7719-22.

109. Feilmeier, B.J., et al., *Green fluorescent protein functions as a reporter for protein localization in Escherichia coli.* J. Bacteriol., 2000. **182**(14): p. 4068-4076.

110. Hizukuri, Y., et al., *A structure-based model of substrate discrimination by a noncanonical PDZ tandem in the intramembrane-cleaving protease RseP.* Structure, 2014. **22**(2): p. 326-336.

111. Inaba, K., et al., *A pair of circularly permutated PDZ domains control RseP, the S2P family intramembrane protease of Escherichia coli.* J. Biol. Chem., 2008. **283**(50): p. 35042-35052.

112. Li, X., et al., *Cleavage of RseA by RseP requires a carboxyl-terminal hydrophobic amino acid following DegS cleavage.* Proc. Natl. Acad. Sci. USA, 2009. **106**(35): p. 14837-14842.

113. Akiyama, K., et al., *Roles of the membrane-reentrant beta-hairpin-like loop of RseP protease in selective substrate cleavage.* eLIFE, 2015. **4**: p. e08928

114. Akiyama, K., Y. Hizukuri, and Y. Akiyama, *Involvement of a conserved GFG motif region in substrate binding by RseP, an Escherichia coli S2P protease.* Mol. Microbiol., 2017. **Epub ahead of print**.

115. Koide, K., K. Ito, and Y. Akiyama, *Substrate recognition and binding by RseP, an Escherichia coli intramembrane protease.* J. Biol. Chem., 2008. **283**(15): p. 9562-9570.

116. Miyake, T., Y. Hizukuri, and Y. Akiyama, *Involvement of a Membrane-Bound Amphiphilic Helix in Substrate Discrimination and Binding by an Escherichia coli S2P Peptidase RseP.* Front Microbiol, 2020. **11**: p. 607381.

117. Konovalova, A., et al., *Inhibitor of intramembrane protease RseP blocks the sigma(E) response causing lethal accumulation of unfolded outer membrane proteins.* Proc Natl Acad Sci U S A, 2018. **115**(28): p. E6614-E6621.

118. Mosyak, L., et al., *Crystal structures of the two major aggrecan degrading enzymes, ADAMTS4 and ADAMTS5.* Protein Sci, 2008. **17**(1): p. 16-21.

119. Davies, B., et al., *A synthetic matrix metalloproteinase inhibitor decreases tumor burden and prolongs survival of mice bearing human ovarian carcinoma xenografts.* Cancer Res, 1993. **53**(9): p. 2087-91.

120. Parrell, D., et al., *Bacillus subtilis intramembrane protease RasP activity in Escherichia coli and in vitro.* J. Bacteriol., 2017. **199**: p. e00381-17.

121. Makinoshima, H. and M.S. Glickman, *Site-2 proteases in prokaryotes: regulated intramembrane proteolysis expands to microbial pathogenesis.* Microbes Infect., 2006. **8**(7): p. 1882-1888.

122. Urban, S., *Making the cut: central roles of intramembrane proteolysis in pathogenic microorganisms.* Nat. Rev. Microbiol., 2009. **7**: p. 411-423.

123. Schneider, J.S. and M.S. Glickman, *Function of site-2 proteases in bacteria and bacterial pathogens.* Biochim. Biophys. Acta - Biomembr., 2013. **1828**(12): p. 2808-2814.

124. Sklar, J.G., et al., *M. tuberculosis intramembrane protease Rip1 controls transcription through three anti-sigma factor substrates.* Mol. Microbiol., 2010. **77**(3): p. 605-617.

125. Makinoshima, H. and M.S. Glickman, *Regulation of Mycobacterium tuberculosis cell envelope composition and virulence by intramembrane proteolysis.* Nature, 2005. **436**(7049): p. 406-409.

126. Schneider, J.S., et al., *Site-2 protease substrate specificity and coupling in trans by a PDZ-substrate adapter protein.* Proc. Natl. Acad. Sci. USA, 2013. **110**(48): p. 19543-19548.

127. Gott, P. and W. Boos, *The transmembrane topology of the sn-glycerol-3-phosphate permease of Escherichia coli analysed by phoA and lacZ protein fusions.* Mol Microbiol, 1988. **2**(5): p. 655-63.

128. Ramsey, D.M. and D.J. Wozniak, *Understanding the control of Pseudomonas aeruginosa alginate synthesis and the prospects for management of chronic infections in cystic fibrosis.* Mol Microbiol, 2005. **56**(2): p. 309-22.

129. Qiu, D., et al., *Regulated proteolysis controls mucoid conversion in Pseudomonas aeruginosa.* Proc Natl Acad Sci U S A, 2007. **104**(19): p. 8107-12.

130. Qiu, D., et al., *ClpXP proteases positively regulate alginate overexpression and mucoid conversion in Pseudomonas aeruginosa.* Microbiology (Reading), 2008. **154**(Pt 7): p. 2119-2130.

131. Deretic, V., et al., *Conversion of Pseudomonas aeruginosa to mucoidy in cystic fibrosis: environmental stress and regulation of bacterial virulence by alternative sigma factors.* J Bacteriol, 1994. **176**(10): p. 2773-80.

132. Matson, J.S. and V.J. DiRita, *Degradation of the membrane-localized virulence activator TcpP by the YaeL protease in Vibrio cholerae.* Proc Natl Acad Sci U S A, 2005. **102**(45): p. 16403-8.

133. Matson, J.S., J.H. Withey, and V.J. DiRita, *Regulatory networks controlling Vibrio cholerae virulence gene expression.* Infect Immun, 2007. **75**(12): p. 5542-9.

134. An, F.Y., M.C. Sulavik, and D.B. Clewell, *Identification and characterization of a determinant (eep) on the Enterococcus faecalis chromosome that is involved in production of the peptide sex pheromone cAD1.* J. Bacteriol., 1999. **181**(19): p. 5915-5921.

135. Clewell, D.B., et al., *Enterococcal plasmid transfer: sex pheromones, transfer origins, relaxases, and the Staphylococcus aureus issue.* Plasmid, 2002. **48**(3): p. 193-201.

136. Chandler, J.R. and G.M. Dunny, *Enterococcal peptide sex pheromones: synthesis and control of biological activity.* Peptides, 2004. **25**(9): p. 1377-88.

137. An, F.Y. and D.B. Clewell, *Identification of the cAD1 sex pheromone precursor in Enterococcus faecalis.* J. Bacteriol., 2002. **184**(7): p. 1880-1887.

138. Frank, K.L., et al., *Use of recombinase-based in vivo expression technology to characterize Enterococcus faecalis gene expression during infection identifies in vivo-expressed antisense RNAs and implicates the protease Eep in pathogenesis.* Infect Immun, 2012. **80**(2): p. 539-49.

139. Kroos, L., *The Bacillus and Myxococcus developmental networks and their transcriptional regulators.* Annu. Rev. Genet., 2007. **41**: p. 13-39.

140. Tan, I.S. and K.S. Ramamurthi, *Spore formation in Bacillus subtilis.* Environ. Microbiol. Rep., 2014. **6**(3): p. 212-225.

141. Kroos, L., B. Kunkel, and R. Losick, *Switch protein alters specificity of RNA polymerase containing a compartment-specific sigma factor.* Science, 1989. **243**: p. 526-529.

142. Losick, R. and P. Stragier, *Crisscross regulation of cell-type-specific gene expression during development in B. subtilis.* Nature, 1992. **355**: p. 601-604.

143. Cutting, S., et al., *A forespore checkpoint for mother-cell gene expression during development in Bacillus subtilis.* Cell, 1990. **62**: p. 239-250.

144. Eichenberger, P., et al., *The program of gene transcription for a single differentiating cell type during sporulation in Bacillus subtilis.* PLoS Biol., 2004. **2**(10): p. e328.

145. Lu, S., R. Halberg, and L. Kroos, *Processing of the mother-cell s factor, σ^K, may depend on events occurring in the forespore during Bacillus subtilis development.* Proc. Natl. Acad. Sci. USA, 1990. **87**: p. 9722-9726.

146. Zhang, B., A. Hofmeister, and L. Kroos, *The pro-sequence of pro-σ^K promotes membrane association and inhibits RNA polymerase core binding.* J. Bacteriol., 1998. **180**: p. 2434-2441.

147. Yu, Y.-T.N. and L. Kroos, *Evidence that SpoIVFB is a novel type of membrane metalloprotease governing intercompartmental communication during Bacillus subtilis sporulation.* J. Bacteriol., 2000. **182**: p. 3305-3309.

148. Green, D. and S. Cutting, *Membrane topology of the Bacillus subtilis Pro-σ^K processing complex.* J. Bacteriol., 2000. **182**: p. 278-285.

149. Zhou, R., et al., *Intramembrane proteolytic cleavage of a membrane-tethered transcription factor by a metalloprotease depends on ATP.* Proc. Natl. Acad. Sci. USA, 2009. **106**: p. 16174-16179.

150. Zhang, Y., et al., *Residues in conserved loops of intramembrane metalloprotease SpoIVFB interact with residues near the cleavage site in Pro-σ^K.* J. Bacteriol., 2013. **195**(21): p. 4936-4946.

151. Halder, S., et al., *Interaction of intramembrane metalloprotease SpoIVFB with substrate Pro-σ^K.* Proc. Natl. Acad. Sci. USA, 2017. **114**: p. E10677-E10686.

152. Zhang, Y., et al., *Complex formed between intramembrane metalloprotease SpoIVFB and its substrate, Pro-σ^K.* J. Biol. Chem., 2016. **291**: p. 10347-10362.

153. Ramirez-Guadiana, F.H., et al., *Evidence that regulation of intramembrane proteolysis is mediated by substrate gating during sporulation in Bacillus subtilis.* PLoS Genet., 2018. **14**(11): p. e1007753.

154. Parrell, D. and L. Kroos, *Channels modestly impact compartment-specific ATP levels during Bacillus subtilis sporulation and a rise in the mother cell ATP level is not necessary for Pro-σ^K cleavage.* Mol. Microbiol., 2020. **in press**.

155. Resnekov, O. and R. Losick, *Negative regulation of the proteolytic activation of a developmental transcription factor in Bacillus subtilis.* Proc. Natl. Acad. Sci. USA, 1998. **95**: p. 3162-3167.

156. Rudner, D.Z. and R. Losick, *A sporulation membrane protein tethers the pro-σ^K processing enzyme to its inhibitor and dictates its subcellular localization.* Genes Dev., 2002. **16**(8): p. 1007-1018.

157. Cutting, S., S. Roels, and R. Losick, *Sporulation operon spoIVF and the characterization of mutations that uncouple mother-cell from forespore gene expression in Bacillus subtilis.* J. Mol. Biol., 1991. **221**: p. 1237-1256.

158. Ricca, E., S. Cutting, and R. Losick, *Characterization of bofA, a gene involved in intercompartmental regulation of pro-σ^K processing during sporulation in Bacillus subtilis.* J. Bacteriol., 1992. **174**: p. 3177-3184.

159. Zhou, R. and L. Kroos, *Serine proteases from two cell types target different components of a complex that governs regulated intramembrane proteolysis of pro-σ^K during Bacillus subtilis development.* Mol. Microbiol., 2005. **58**(3): p. 835-846.

160. Zhou, R. and L. Kroos, *BofA protein inhibits intramembrane proteolysis of pro-σ^K in an intercompartmental signaling pathway during Bacillus subtilis sporulation.* Proc. Natl. Acad. Sci. USA, 2004. **101**(17): p. 6385-6390.

161. Kroos, L., et al., *Forespore signaling is necessary for pro-σ^K processing during Bacillus subtilis sporulation despite the loss of SpoIVFA upon translational arrest.* J. Bacteriol., 2002. **184**(19): p. 5393-5401.

162. Varcamonti, M., et al., *Membrane topology analysis of the Bacillus subtilis BofA protein involved in pro-σ^K processing.* Microbiol., 1997. **143**(Pt 4): p. 1053-1058.

163. Dong, T.C. and S.M. Cutting, *SpoIVB-mediated cleavage of SpoIVFA could provide the intercellular signal to activate processing of Pro-σ^K in Bacillus subtilis.* Mol. Microbiol., 2003. **49**(5): p. 1425-1434.

164. Wakeley, P.R., et al., *Proteolysis of SpoIVB is a critical determinant in signalling of Pro-σ^K processing in Bacillus subtilis.* Mol. Microbiol., 2000. **36**(6): p. 1336-1348.

165. Cutting, S., et al., *Forespore-specific transcription of a gene in the signal transduction pathway that governs pro-σ^K processing in Bacillus subtilis.* Genes Dev., 1991. **5**: p. 456-466.

166. Campo, N. and D.Z. Rudner, *A branched pathway governing the activation of a developmental transcription factor by regulated intramembrane proteolysis.* Mol. Cell, 2006. **23**(1): p. 25-35.

167. Campo, N. and D.Z. Rudner, *SpoIVB and CtpB are both forespore signals in the activation of the sporulation transcription factor σ^K in Bacillus subtilis.* J. Bacteriol., 2007. **189**(16): p. 6021-6027.

168. Mastny, M., et al., *CtpB assembles a gated protease tunnel regulating cell-cell signaling during spore formation in Bacillus subtilis.* Cell, 2013. **155**(3): p. 647-658.

169. Pan, Q., R. Losick, and D.Z. Rudner, *A second PDZ-containing serine protease contributes to activation of the sporulation transcription factor σ^K in Bacillus subtilis.* J. Bacteriol., 2003. **185**(20): p. 6051-6056.

CHAPTER 2: Inhibitory proteins block substrate access to the membrane-embedded active site of *Bacillus subtilis* intramembrane protease SpoIVFB

We plan to submit this chapter for publication with the following citation:

Olenic S, Heo L, Feig M and Kroos L. Inhibitory proteins block substrate access to the membrane-embedded active site of *Bacillus subtilis* intramembrane protease SpoIVFB

I contributed significantly to the writing, editing and work in this manuscript, generating figures for cleavage assays, co-purifications and disulfide cross-linking. Drs. Lim Heo and Michael Feig performed coevolutionary analysis and modeling.

Abstract

Intramembrane proteases function in numerous signaling pathways that impact health, but how their membrane-embedded active sites interact with modulators is poorly understood. We examined inhibition of intramembrane metalloprotease SpoIVFB by proteins BofA and SpoIVFA. We found that BofA residues in and near a predicted transmembrane segment are required for SpoIVFB inhibition, and cross-linking experiments indicated that this transmembrane segment occupies the SpoIVFB active site region. BofA and SpoIVFA neither prevented SpoIVFB from interacting with substrate in co-purification assays nor interfered with cross-linking between the C-terminal regions of substrate and SpoIVFB. However, the inhibitory proteins did interfere with cross-linking between the SpoIVFB active site region and the substrate N-terminal Proregion, which is normally cleaved. We conclude that BofA and SpoIVFA block substrate access to the membrane-embedded active site of SpoIVFB. A structural model was built of SpoIVFB in complex with BofA and parts of SpoIVFA and substrate, using partial homology and constraints from cross-linking and co-evolutionary analyses. The model predicts that conserved BofA residues interact to stabilize a transmembrane segment and a membrane-embedded C-terminal region. SpoIVFA is predicted to bridge the BofA C-terminal region and SpoIVFB, forming a membrane-embedded inhibitory complex. Implications for design of intramembrane metalloprotease inhibitors are discussed.

Introduction

Intramembrane proteases (IPs) are membrane proteins containing a membrane-embedded active site. IPs cleave membrane-associated substrates within a transmembrane segment (TMS) or near the membrane surface in a process referred to as regulated intramembrane proteolysis (RIP) [1]. Released substrate fragments impact diverse signaling pathways in a wide variety of organisms [2]. There are four known IP families: intramembrane metalloproteases (IMMPs) like SpoIVFB, aspartyl proteases like presenilins, serine proteases (rhomboids), and the glutamyl protease Rce1 [2, 3]. Crystal structures have been solved for one or more IP in each family [3-8], revealing that TMSs arrange to form a channel that delivers water to the active site for hydrolysis of a substrate peptide bond. Structures have also been solved for rhomboid·peptide inhibitor complexes [9, 10] and for γ-secretase·substrate complexes [11, 12], which may guide the design of IP modulators as therapeutics or for other purposes.

IMMPs activate transcription factors via RIP in all three domains of life [1, 2]. In humans, S2P is involved in regulation of cholesterol homeostasis and responses to endoplasmic reticulum stress and viral infection [13, 14]. S2P homologs in plants and in the pathogenic fungus *Cryptococcus neoformans* play important roles in chloroplast development and virulence, respectively [15, 16]. In bacteria, IMMPs enhance pathogenicity, control stress responses and polar morphogenesis, produce mating signals, and clear signal peptides from the membrane [17-19]. In *Bacillus* and *Clostridium* species, SpoIVFB cleaves inactive Pro-σ^K to σ^K, which directs RNA polymerase to transcribe genes necessary for endospore formation [18, 20]. Endospores are dormant and are able to survive harsh environmental conditions [21], enhancing the persistence of pathogenic species [22, 23]. Knowledge of SpoIVFB interactions with its

inhibitory proteins, BofA and SpoIVFA [24-26], could lead to new strategies to manipulate endosporulation and other processes involving IMMPs in bacteria and eukaryotes.

During endospore formation, *B. subtilis* forms a polar septum that divides the mother cell (MC) and forespore (FS) compartments [27] (Figure S2.1). The MC engulfs the FS, surrounding it with a second membrane and pinching it off within the MC. SpoIVFB, BofA, and SpoIVFA form a complex in the outer FS membrane during engulfment [28-30]. BofA was implicated as the direct inhibitor of SpoIVFB [31], while SpoIVFA appeared to localize and stabilize the heterotrimer [30, 32]. Signaling from the FS relieves inhibition of SpoIVFB (Figure S2.1). Two proteases, SpoIVB and CtpB, are exported into the space between the two membranes surrounding the FS [33, 34]. SpoIVB cleaves the C-terminal end of SpoIVFA [35-38] and CtpB can cleave the C-terminal ends of both SpoIVFA and BofA [36, 37, 39]. Once inhibition is removed, SpoIVFB cleaves the N-terminal 21-residue Proregion from Pro-σ^K, releasing σ^K into the MC [40-42]. σ^K directs RNA polymerase to transcribe genes whose products form the spore coat and lyse the MC, releasing a mature spore [43, 44].

Cleavage of Pro-σ^K by SpoIVFB can be reproduced by expressing these proteins in *Escherichia coli* [31] (Figure 2.1A). Cleavage could be inhibited by additionally producing GFPΔ27BofA (a functional fusion protein lacking predicted TMS1 of BofA) and SpoIVFA [31, 39]. However, we found that the extent of cleavage inhibition was incomplete and variable. Here, we describe an improved cleavage inhibition assay. Using the assay and bioinformatics, we identified three conserved residues of BofA important for inhibition of SpoIVFB in *E. coli* and in sporulating *B. subtilis.* One of the residues, N48, is near the middle of BofA TMS2, close to the sole Cys residue of BofA, C46. We exploited C46 for disulfide cross-linking experiments that showed TMS2 of BofA can occupy the SpoIVFB active site region. These experiments

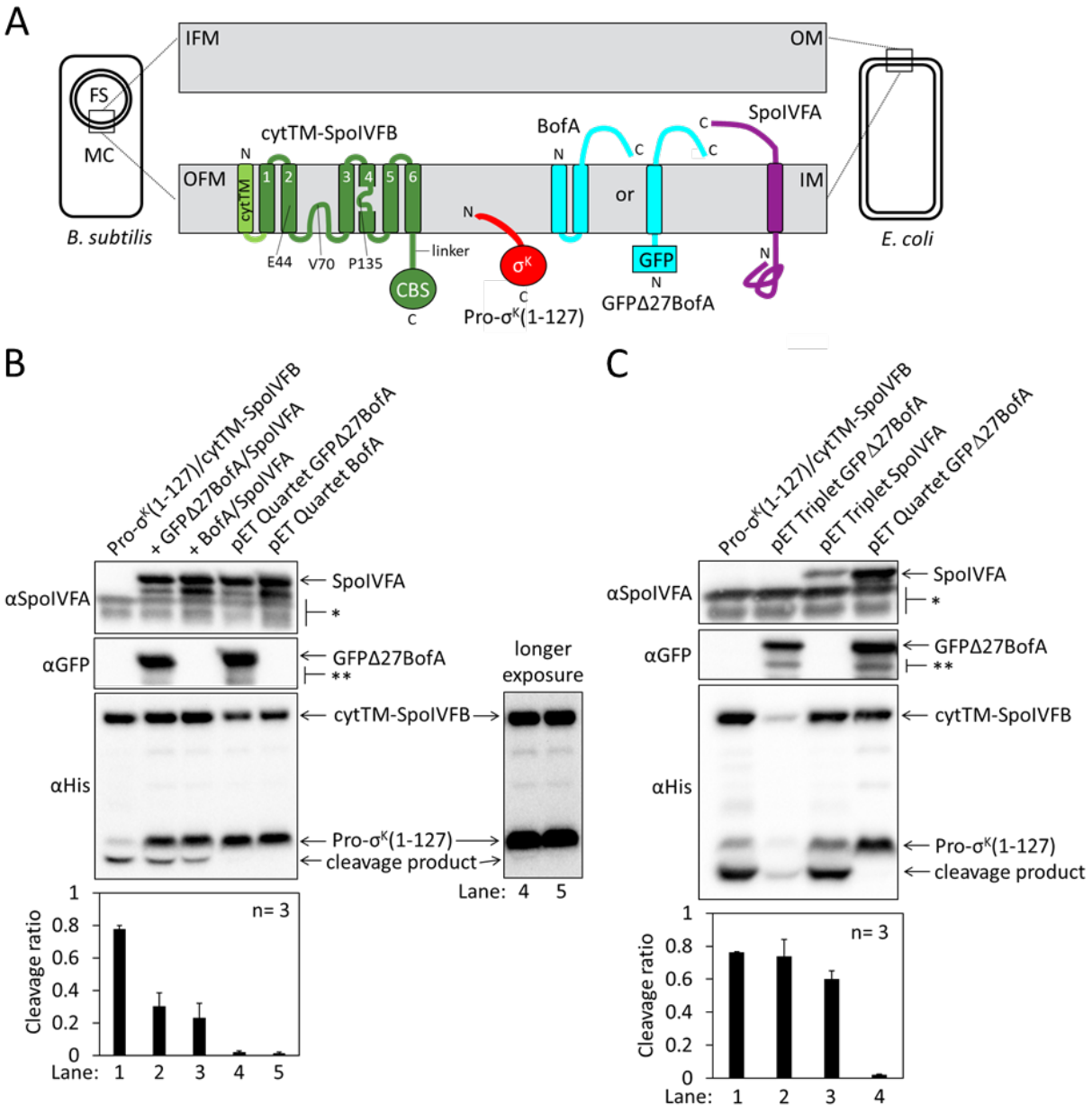

Figure 2.1 Inhibition of Pro-σ^K cleavage. (*A*) Diagram of SpoIVFB inhibition during *B. subtilis* endosporulation and upon heterologous expression in *E. coli*. During endosporulation (*Left*), SpoIVFB and its inhibitory proteins BofA and SpoIVFA are produced in the mother cell (MC) and localize to the outer forespore (FS) membrane (OFM). Pro-σ^K is also produced in the MC and associates with membranes. When these proteins are synthesized in *E. coli* (*Right*), they localize to the inner membrane (IM). The expanded view of the membranes (*Center*) shows a SpoIVFB variant with an extra N-terminal transmembrane segment (cytTM), and highlights several residues (E44, V70, P135) at or near the active site in the membrane domain, which is connected to the CBS domain by an interdomain linker. When produced in *E. coli*, cytTM-SpoIVFB cleaves Pro-σ^K(1-127), removing its N-terminal Proregion. Co-production of SpoIVFA and either full-length BofA or GFPΔ27BofA (lacking predicted TMS1) inhibits Pro-

Figure 2.1 (cont'd)
σ^K(1-127) cleavage. (*B*) Cleavage assays comparing inhibition by SpoIVFA and either GFPΔ27BofA or full-length BofA in *E. coli*. Pro-σ^K(1-127) and cytTM-SpoIVFB were produced alone (lane 1, pYZ2) or in combination with GFPΔ27BofA and SpoIVFA (lane 2, pYZ46) or full-length BofA and SpoIVFA (lane 3, pSO212). Alternatively, "pET Quartet" plasmids were used to produce Pro-σ^K(1-127), cytTM-SpoIVFB, SpoIVFA, and either GFPΔ27BofA (lane 4, pSO40) or full-length BofA (lane 5, pSO213). Samples collected after 2 h of IPTG induction were subjected to immunoblot analysis with SpoIVFA (*Top*), GFP (*Middle*), or penta-His antibodies (*Bottom*, 2 and 30 s exposures). The single star (*) indicates cross-reacting proteins below SpoIVFA and the double star (**) indicates breakdown species of GFPΔ27BofA. A breakdown species below SpoIVFA (not indicated) is observed in some experiments. The graph shows quantification of the cleavage ratio (cleavage product/[Pro-σ^K(1-127) + cleavage product]) for three biological replicates. Error bars, 1 standard deviation. (*C*) Cleavage assays comparing inhibition by either GFPΔ27BofA or SpoIVFA. pET Triplet plasmids were used to produce Pro-σ^K(1-127), cytTM-SpoIVFB, and either GFPΔ27BofA (lane 2, pSO64) or SpoIVFA (lane 3, pSO65). Samples were subjected to immunoblot analysis and quantification as in *B*.

relied on single-Cys variants of SpoIVFB created previously and used to cross-link residues predicted to be near the active site with residues near the cleavage site in single-Cys variants of Pro-σ^K [45]. We created additional single-Cys variants of SpoIVFB, Pro-σ^K, and BofA, as well as functional Cys-less SpoIVFA, and performed disulfide cross-linking experiments. We found that BofA and SpoIVFA interfere with cross-linking between the N-terminal Proregion of Pro-σ^K and the SpoIVFB active site region, indicating that the inhibitory proteins block substrate access to the IMMP active site. The results were used in combination with prior cross-linking studies [45, 46], partial homology, and evolutionary co-variation of amino acid residues, to constrain a structural model of SpoIVFB in complex with BofA and parts of SpoIVFA and Pro-σ^K. The model predicts that conserved residues in TMS2 and the C-terminal region of BofA interact, and that SpoIVFA bridges the BofA C-terminal region and SpoIVFB to form a membrane-embedded inhibitory complex.

Results

BofA and SpoIVFA Can Prevent Cleavage of Pro-σ^K by SpoIVFB in *E. coli*. To study RIP of Pro-σ^K, *E. coli* was engineered to synthesize variants of SpoIVFB and Pro-σ^K, and the two inhibitory proteins, BofA and SpoIVFA, in various combinations. The SpoIVFB variant cytTM-SpoIVFB-FLAG$_2$-His$_6$ (cytTM-SpoIVFB) (Figure 2.1A) contains cytTM [47], which improves accumulation [42]. The substrate variant Pro-σ^K(1-127)-His$_6$ [Pro-σ^K(1-127)] lacks the C-terminal half of Pro-σ^K, but can be cleaved by SpoIVFB and the cleavage product can easily be separated from Pro-σ^K(1-127) by SDS-PAGE [48] (Note: Pro-σ^K(1-126) was renamed Pro-σ^K(1-127) as explained in [46]). When Pro-σ^K(1-127) was produced with cytTM-SpoIVFB, cleavage was abundant (Figure 2.1B, lane 1), as shown previously [42]. To quantify cleavage,

we measured the abundance of cleavage product and divided that by the amount of Pro-σ^K(1-127) plus cleavage product, which resulted in a cleavage ratio of 0.78 $\pm$ 0.02. The additional production of GFPΔ27BofA and SpoIVFA from a second plasmid reduced the cleavage ratio to 0.3 $\pm$ 0.08, but cleavage product was visible (lane 2). A similar result was seen when full-length BofA (for which no antibody has been described) and SpoIVFA were produced from a second plasmid (lane 3). Since the second plasmid had the same replication origin as the plasmid used to produce Pro-σ^K(1-127) and cytTM-SpoIVFB (i.e., the two plasmids were "incompatible"), the copy number of the two plasmids may be unequal in some cells, despite using different selection markers to try to maintain both plasmids. Unequal copy numbers could result in Pro-σ^K(1-127) cleavage in cells producing too little of the inhibitory proteins. Therefore, we designed single plasmids to synthesize all four proteins, which we called "pET Quartet plasmids." When pET Quartets produced either GFPΔ27BofA (lane 4) or BofA (lane 5), inhibition improved, resulting in very little Pro-σ^K(1-127) cleavage. A longer exposure of the immunoblot revealed a faint cleavage product with pET Quartet GFPΔ27BofA, but not with pET Quartet BofA, indicating that full-length BofA inhibits cleavage slightly better than GFPΔ27BofA.

We tested whether both GFPΔ27BofA and SpoIVFA are required for cleavage inhibition by engineering "pET Triplet plasmids" to synthesize Pro-σ^K(1-127), cytTM-SpoIVFB, and either GFPΔ27BofA or SpoIVFA. With pET Triplet GFPΔ27BofA, cleavage of Pro-σ^K(1-127) was observed (ratio = 0.7 $\pm$ 0.1), but accumulation of cytTM-SpoIVFB, Pro-σ^K(1-127), and cleavage product was greatly diminished (Figure 2.1C, lane 2), suggesting that GFPΔ27BofA inhibits synthesis and/or enhances degradation of the other proteins when SpoIVFA is absent. With pET Triplet SpoIVFA (lane 3), the cleavage ratio (0.6 $\pm$ 0.05) and accumulation of cytTM-SpoIVB, Pro-σ^K(1-127), and cleavage product were similar to the control plasmid that synthesized only

cytTM-SpoIVFB and Pro-σ^K(1-127) (lane 1). We conclude that both GFPΔ27BofA and SpoIVFA are necessary to strongly inhibit Pro-σ^K(1-127) cleavage by cytTM-SpoIVB in *E. coli* (lane 4). Both inhibitory proteins are required to prevent cleavage of Pro-σ^K by SpoIVFB during *B. subtilis* sporulation [24, 30, 49].

Efficient relief of SpoIVFB inhibition by BofA and SpoIVFA during *B. subtilis* sporulation requires SpoIVB and CtpB (Figure S2.1), but SpoIVB alone can partially relieve inhibition [34, 36, 37, 39]. Likewise, SpoIVB partially relieved inhibition when produced in *E. coli* from "pET Quintet plasmids" (i.e., pET Quartet plus SpoIVB) (Supplemental Results and Figure S2.2). In the absence of SpoIVB, an F66A substitution in SpoIVFB-YFP can partially overcome inhibition by BofA and SpoIVFA during *B. subtilis* sporulation [49]. The F66A substitution in cytTM-SpoIVFB likewise partially overcame inhibition by GFPΔ27BofA and SpoIVFA when produced from pET Quartet in *E. coli* (Supplemental Results and Figure S2.3). Hence, the heterologous system mimics the endogenous pathway of *B. subtilis* in these respects. We next exploited the improved cleavage inhibition assay based on pET Quartet plasmids in *E. coli* to identify residues of BofA important for SpoIVFB inhibition.

Three Conserved Residues of BofA Are Important for Inhibition of SpoIVFB in *E. coli*. To identify residues of BofA that may play a role in SpoIVFB inhibition, an alignment of 70 BofA orthologs was made (Figure S2.4A). The majority of conserved residues reside in predicted TMS2 and the C-terminal region, which could explain why GFPΔ27BofA (lacking predicted TMS1) is a functional inhibitor [30, 31] (Figure 2.1B). Most endospore formers encode BofA, but about half lack a recognizable gene for SpoIVFA [20, 50]. A smaller alignment (Figure S2.4B) was made to see if additional residues are conserved in BofA orthologs

of species encoding SpoIVFA. In total, 17 residues of interest were conserved in BofA: 13 within TMS2 and the C-terminal region of the larger alignment, and 4 from the C-terminal region of the smaller alignment.

We substituted conserved residues in GFPΔ27BofA with alanine to investigate their roles. Since deletion of three residues from the C-terminal end of BofA caused a loss of function or stability in *B. subtilis* [26, 51], we also made Ala substitutions for F85 and I87 (as well as I86, which is conserved) in GFPΔ27BofA. Each GFPΔ27BofA variant was co-produced with Pro-σ^K(1-127), cytTM-SpoIVFB, and SpoIVFA from pET Quartet plasmids in *E. coli*, and the Pro-σ^K(1-127) cleavage ratio was quantified (Figure 2.2). Three GFPΔ27BofA variants, N48A, N61A, and T64A (lanes 4, 7 & 8), led to the greatest cleavage ratios, indicating that these substitutions strongly impaired inhibition of cytTM-SpoIVFB. However, less of the N61A and T64A variants accumulated than most of the other GFPΔ27BofA variants, and for all three variants, less SpoIVFA and cytTM-SpoIVFB accumulated, indicating that the variants reduce the synthesis and/or stability of proteins that normally form the SpoIVFB inhibition complex [24, 30, 31, 39, 49]. We reasoned that accumulation of the proteins may differ in *E. coli* and sporulating *B. subtilis*, so we examined the effects of GFPΔ27BofA N48A, N61A, and T64A variants during sporulation (see below).

Importantly, deletion of three residues from the C-terminal end of GFPΔ27BofA strongly impaired inhibition of cytTM-SpoIVFB in *E. coli* (Supplemental Results and Figure S2.5A), mimicking results obtained for the endogenous pathway of *B. subtilis* [26, 51]. We also used pET Quartet plasmids in *E. coli* to show that nine residues preceding predicted TMS2 of GFPΔ27BofA contribute to its inhibitory function (Supplemental Results and Figure S2.5B).

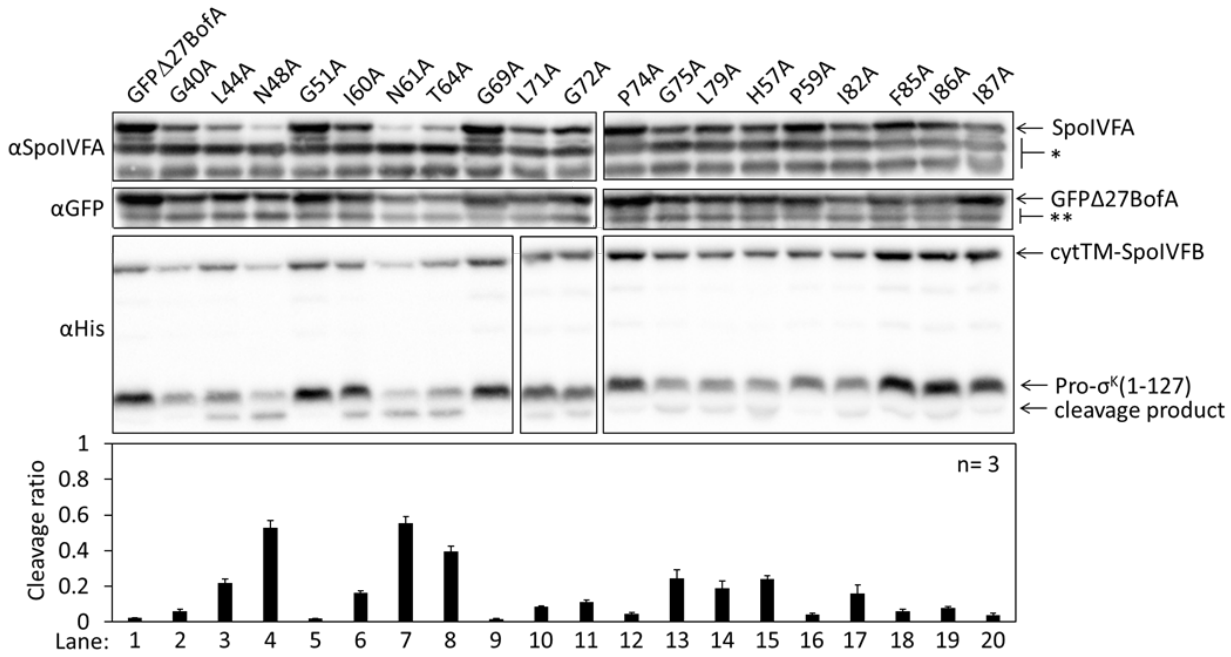

Figure 2.2 Effects of alanine substitutions in GFPΔ27BofA on inhibition of Pro-σ^K(1-127) cleavage in *E. coli.* pET Quartet plasmids were used to produce Pro-σ^K(1-127), cytTM-SpoIVFB, SpoIVFA, and GFPΔ27BofA (lane 1, pSO40) or Ala-substituted GFPΔ27BofA (lanes 2-20, pSO44-pSO58 and pSO60-pSO63). Samples collected after 2 h of IPTG induction were subjected to immunoblot analysis with SpoIVFA, GFP, and penta-His antibodies. Single (*) and double (**) stars are explained in the Figure 2.1B legend, as is the graph.

The Conserved Residues of BofA Are Important for SpoIVFB Inhibition during *B. subtilis* Sporulation. A *B. subtilis spoIVB165 bofA::erm* double mutant provides a genetic background to test the effects of Ala substitutions on BofA function during sporulation. The *spoIVB165* null mutation alone would block Pro-σ^K cleavage, but cleavage is restored in the *spoIVB165 bofA::erm* double mutant, and ectopic production of GFPΔ27BofA under control of an MC-specific promoter in the double mutant leads to inhibition of SpoIVFB [30, 31].

To test the effects of the three GFPΔ27BofA variants (N48A, N61A, and T64A) during sporulation, each was produced ectopically under control of the *bofA* promoter in the *spoIVB165 bofA::erm* double mutant background (Figure 2.3A). As a control, in wild-type *B. subtilis* strain PY79, BofA and SpoIVFA inhibited Pro-σ^K cleavage until between 4 and 5 h poststarvation (PS), and the levels of SpoIVFA and SpoIVFB decreased between 4 and 5 h PS (lanes 1 & 2). For the *spoIVB165* single mutant, very little Pro-σ^K cleavage was observed, as expected, and the SpoIVFA and SpoIVFB levels did not decrease at 5 h (lanes 3 & 4). For the *spoIVB165 bofA::erm* double mutant, inhibition of SpoIVFB was expected to be lost, and in agreement the Pro-σ^K cleavage ratio at 4 h (lane 5) was greater than for the wild-type strain at 4 h (lane 1) and similar to the ratios at 5 h (lanes 2 and 6). Very little SpoIVFA and SpoIVFB was detected (lanes 5 & 6), consistent with the need for BofA to stabilize these proteins [30]. As expected, ectopic production of GFPΔ27BofA in the double mutant inhibited SpoIVFB so that little Pro-σ^K cleavage was observed, and the SpoIVFA and SpoIVFB levels did not decrease at 5 h (lanes 7 & 8), similar to the *spoIVB165* single mutant (lanes 3 & 4). GFPΔ27BofA allowed a greater Pro-σ^K cleavage ratio at 5 h (lane 8) than BofA (lane 4), suggesting that full-length BofA is a slightly better inhibitor of SpoIVFB during *B. subtilis* sporulation, as observed in *E. coli* (Figure 2.1B, longer exposure).

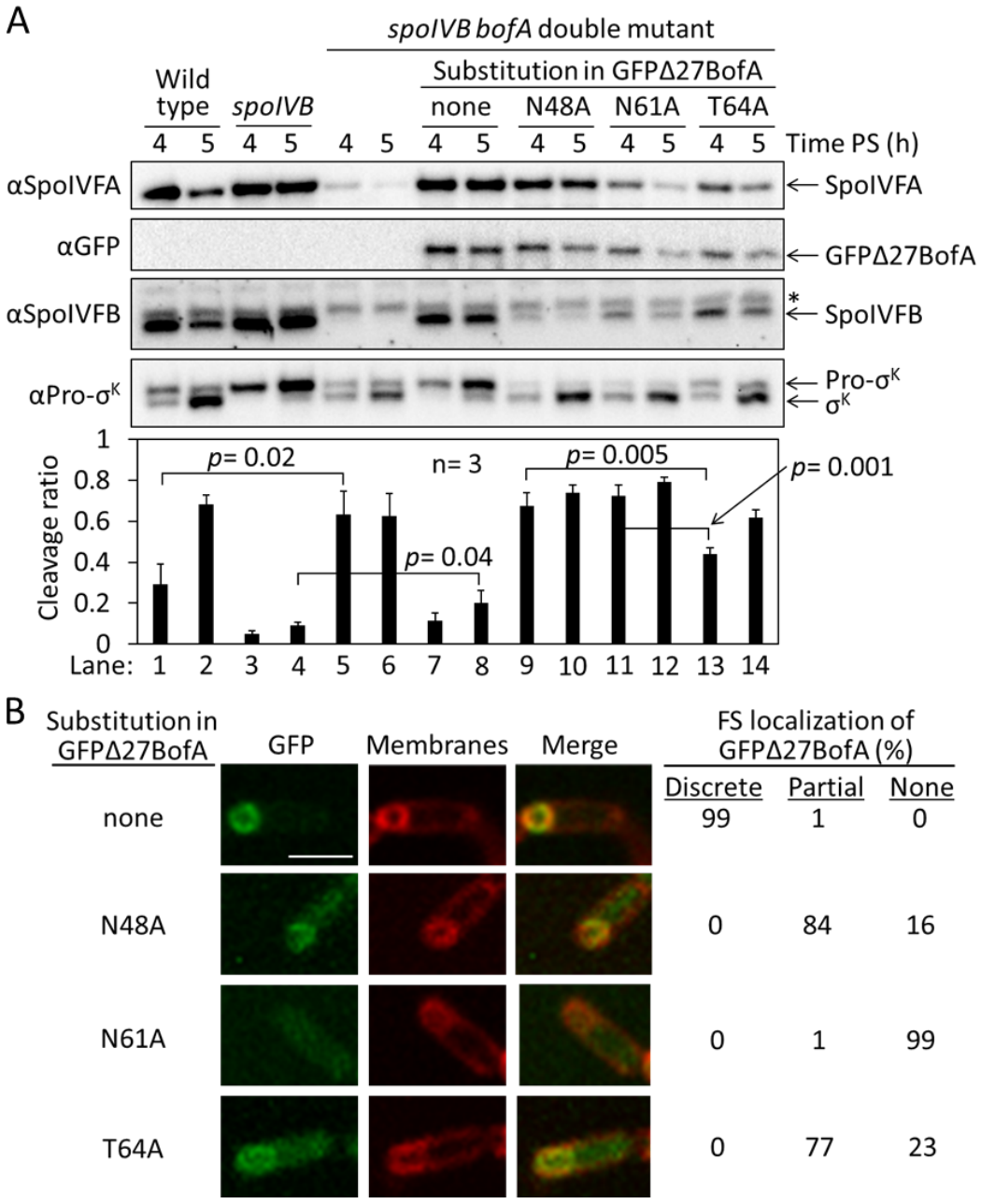

Figure 2.3 Effects of alanine substitutions in GFPΔ27BofA during *B. subtilis* sporulation. (*A*) Effects of GFPΔ27BofA variants (N48A, N61A, T64A) on Pro-σ^K cleavage. Wild-type strain PY79, a *spoIVB165* null mutant, a *spoIVB165 bofA::erm* double mutant, and the double mutant with P_{bofA}-*gfpΔ27bofA* integrated ectopically at *amyE* to express GFPΔ27BofA with no substitution (none) or the indicated Ala substitution, were starved to induce sporulation. Samples collected at 4 and 5 h poststarvation (PS) were subjected to immunoblot analysis with antibodies against SpoIVFA, GFP, SpoIVFB, and Pro-σ^K. The graph shows quantification of the cleavage ratio [cleavage product/(Pro-σ^K + cleavage product)] for three biological replicates. Error bars, 1 standard deviation. Student's two-tailed *t* tests were performed to compare certain

Figure 2.3 (cont'd)
cleavage ratios (*p* values). (*B*) Localization of GFPΔ27BofA and the three variants. Samples collected at 3 h PS were treated with FM 4-64 to stain membranes. Confocal microscopy images of fluorescence from GFPΔ27BofA, membranes, and merged images are shown for representative sporangia with discrete (no substitution in GFPΔ27BofA, designated "none"), partial (N48A and T64A), or no forespore (FS) localization (N61A). Scale bar, 1 μm. The percentage of sporangia (44-93 counted; non-sporulating cells were not counted) with each localization pattern is shown.

Strikingly, ectopic production of the GFPΔ27BofA N48A or N61A variant in the double mutant did not inhibit SpoIVFB, as Pro-σ^K was cleaved at 4 h (Figure 2.3A, lanes 9 & 11). The level of the N48A variant (lanes 9 & 10) was comparable with GFPΔ27BofA (lanes 7 & 8), but less of the N61A variant was observed, especially at 5 h (lanes 11 & 12). In comparison with the strain that produced GFPΔ27BofA, the SpoIVFA level was normal in the strain that produced the N48A variant, but less SpoIVFB was observed, and less of both SpoIVFA and SpoIVFB was observed in the strain producing the N61A variant. Production of the T64A variant in the double mutant (lanes 13 & 14) showed a pattern similar to the wild-type strain (lanes 1 & 2); Pro-σ^K cleavage increased between 4 and 5 h, and the levels of SpoIVFA and SpoIVFB decreased. The levels of all three proteins were slightly lower in the strain producing the T64A variant than in the wild-type strain. The level of the T64A variant was similar to the N48A and N61A variants at 4 h, yet the Pro-σ^K cleavage ratio was lower (lanes 9, 11 & 13), suggesting that the T64A variant inhibits SpoIVFB, although not as well as GFPΔ27BofA (lane 7). We conclude that the three conserved residues of BofA are important for SpoIVFB inhibition during sporulation.

Since GFPΔ27BofA co-localizes with SpoIVFA and SpoIVFB to the outer FS membrane during sporulation [28-30], we examined the ability of the GFPΔ27BofA variants to localize to the FS (Figure 2.3B). As a control, GFPΔ27BofA produced in the *spoIVB165 bofA::erm* double mutant localized discretely to the FS at 3 h PS. Strains producing the N48A and T64A variants showed GFP signal localized to the FS, but signal was also observed in the cytoplasm and possibly at the membrane of the MC, suggesting partial mislocalization. The strain producing the N61A variant appeared to have GFP signal dispersed evenly throughout the MC cytoplasm, suggesting a loss of FS localization. The fusion proteins were intact, suggesting the cytoplasmic signal was not attributable to breakdown (Figure S2.6). Inability of the N61A variant to localize

to the FS may explain the loss of SpoIVFB inhibition and the abundant cleavage of Pro-σ^K at 4 h (Figure 2.3A, lane 11). Importantly, the similar ability of the N48A and T64A variants to localize to the FS (Figure 2.3B) does not account for their differential effects on the level of SpoIVFB and its ability to cleave Pro-σ^K (Figure 2.3A). The strain producing GFPΔ27BofA N48A exhibited less SpoIVFB yet more Pro-σ^K cleavage at 4 h (lane 9) than the strain producing GFPΔ27BofA T64A (lane 13), so the N48A substitution more severely impairs the ability of GFPΔ27BofA to inhibit SpoIVFB.

BofA TMS2 Can Occupy the Active Site Region of SpoIVFB. N48 within TMS2 is conserved among BofA orthologs (Figure S2.4) and potentially in proximity to the active site of SpoIVFB. The SpoIVFB catalytic core formed by a zinc ion near E44 of the HELGH metalloprotease motif within TMS2 is predicted to be surrounded by five other TMSs in the membrane (Figure 2.1A and S2.7A). The model of the SpoIVFB membrane domain is based on the crystal structure of an archaeal homolog [6]. The model is supported by cross-linking studies of catalytically-inactive SpoIVFB E44Q in complex with Pro-σ^K(1-127), whose Proregion is predicted to occupy the SpoIVFB active site region [45, 46, 52]. If BofA TMS2 instead occupied the SpoIVFB active site region, it would likely inhibit Pro-σ^K cleavage.

To determine whether BofA TMS2 can occupy the SpoIVFB active site region, we performed disulfide cross-linking experiments that took advantage of the sole Cys residue of BofA, C46, located near N48 in TMS2. We created MBPΔ27BofA because MBP (unlike GFP) contains no Cys residues. As a negative control, we replaced C46 with Ser to obtain Cys-less MBPΔ27BofA C46S. We also created Cys-less SpoIVFA C77L C82L, which cannot form disulfide cross-links. Cys-less SpoIVFA and either MBPΔ27BofA or Cys-less MBPΔ27BofA

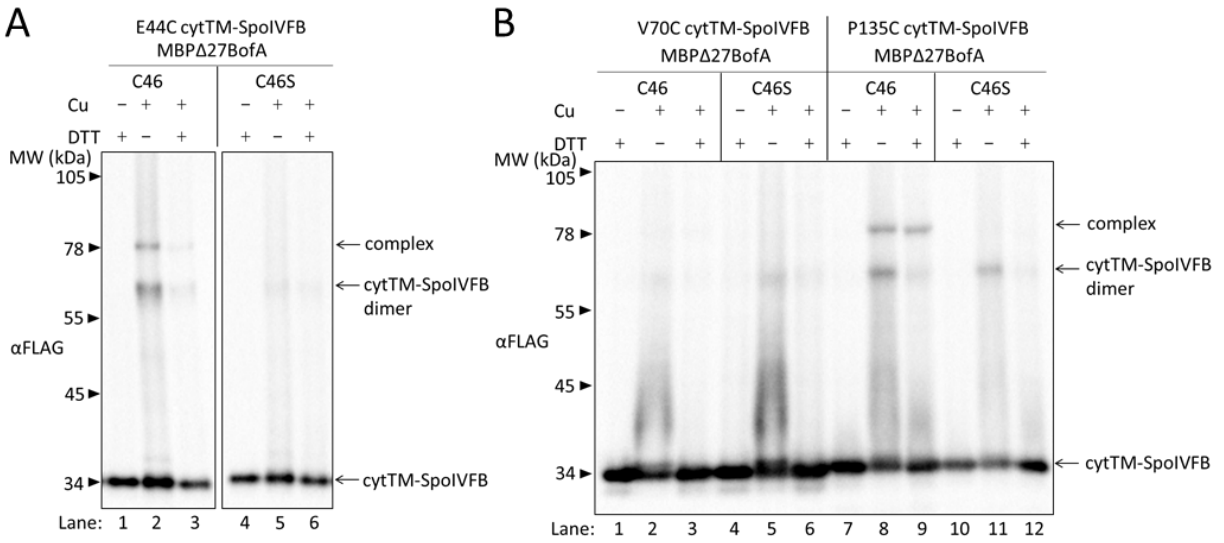

Figure 2.4 MBPΔ27BofA TMS2 is near the cytTM-SpoIVFB active site. (*A*) Disulfide cross-linking of single-Cys E44C cytTM-SpoIVFB to MBPΔ27BofA C46. pET Quartet plasmids were used to produce single-Cys E44C cytTM-SpoIVFB in combination with MBPΔ27BofA C46 (pSO91) or Cys-less MBPΔ27BofA C46S as a negative control (pSO110), and Cys-less variants of SpoIVFA and Pro-σ^K(1-127) in *E. coli*. Samples collected after 2 h of IPTG induction were treated with Cu^{2+}(phenanthroline)$_3$ (Cu +) for 60 min or with 2-phenanthroline (Cu –) as a control. Samples were treated with TCA to precipitate proteins and resuspended in sample buffer with DTT (+) or without (–) and subjected to immunoblot analysis with FLAG antibodies to visualize cytTM-SpoIVFB monomer, dimer, and complex with MBPΔ27BofA. (*B*) Disulfide cross-linking of single-Cys V70C or P135C cytTM-SpoIVFB E44Q variants to MBPΔ27BofA C46. pET Quartet plasmids were used to produce single-Cys V70C or P135C cytTM-SpoIVFB E44Q variants in combination with MBPΔ27BofA (pSO92, pSO93) or Cys-less MBPΔ27BofA C46S as a negative control (pSO111, pSO112), and Cys-less variants of SpoIVFA and Pro-σ^K(1-127) in *E. coli*. Samples collected after 2 h of IPTG induction were treated and subjected to immunoblot analysis as in *A*. A representative result from at least two biological replicates is shown in *A* and *B*.

were functional when produced from a pET Quartet plasmid, since Pro-σ^K(1-127) cleavage by cytTM-SpoIVFB was inhibited in *E. coli* (Figure S2.8). For the disulfide cross-linking experiments, we used Cys-less Pro-σ^K(1-127) C110S and single-Cys variants of cytTM-SpoIVFB created previously [45].

To test whether BofA TMS2 C46 could be cross-linked to a Cys located at the SpoIVFB active site, MBPΔ27BofA C46 and single-Cys E44C cytTM-SpoIVFB were co-produced with Cys-less variants of SpoIVFA and Pro-σ^K(1-127) from a pET Quartet plasmid in *E. coli*. Cells were treated with the oxidant Cu^{2+}(phenanthroline)$_3$ to promote disulfide bond formation. For MBPΔ27BofA C46 (Figure 2.4A, lane 2), but not the Cys-less C46S negative control (lane 5), treatment with oxidant caused formation of a species of the expected size for a cross-linked complex with single-Cys E44C cytTM-SpoIVFB, which was detected by immunoblotting with anti-FLAG antibodies. Treatment with the reducing agent DTT greatly diminished the abundance of the apparent complex, consistent with cross-link reversal (lane 3). A species of the expected size for a cross-linked dimer of single-Cys E44C cytTM-SpoIVFB was also observed. Formation of the apparent dimer varies (see below), as reported previously [45]. As expected, anti-MBP antibodies detected the presumptive cross-linked complex of MBPΔ27BofA C46 with single-Cys E44C cytTM-SpoIVFB, albeit weakly, and the negative control with E44Q rather than E44C failed to form the complex (Figure S2.9, lanes 2 & 5). Since the signal for the complex was stronger with anti-FLAG antibodies (Figure 2.4A), we used those antibodies in the cross-linking experiments reported below.

In addition to E44 of SpoIVFB, V70 in a predicted membrane-reentrant loop and P135 in a predicted short loop interrupting TMS4 (Figure 2.1A and S2.7A) were shown to be in proximity to the Proregion of Pro-σ^K(1-127) [45]. Therefore, we tested whether MBPΔ27BofA

C46 could be cross-linked to single-Cys V70C or P135C cytTM-SpoIVFB E44Q variants. We included the inactivating E44Q substitution since the V70C and P135C variants (unlike the E44C variant) could cleave Cys-less Pro-σ^K(1-127) [45], even though Cys-less SpoIVFA and either MBPΔ27BofA or Cys-less MBPΔ27BofA were expected to almost completely inhibit cleavage (Figure S2.8). MBPΔ27BofA C46 formed a complex with the P135C variant, but not with the V70C variant (Figure 2.4B, lanes 2 & 8). As expected, Cys-less MBPΔ27BofA C46S failed to form a complex with either variant (lanes 5 & 11). Full-length BofA C46 also formed a complex of the expected (smaller) size with the E44C and P135C variants, but not with the V70C variant (Figure S2.10, lanes 2, 14, & 8). As expected, Cys-less BofA C46S failed to form a complex with any of the variants (lanes 5, 11, & 17). Our cross-linking results show that BofA TMS2 can occupy the active site region of SpoIVFB, placing BofA C46 in proximity to SpoIVFB E44 and P135, but not V70.

Based on our cross-linking results, we modeled BofA TMS2 in the SpoIVFB active site region, and tested predictions of the model using additional disulfide cross-linking experiments (Supplemental Results and Figure S2.11). The results confirmed predictions of the initial model and suggested a preferred orientation of BofA TMS2 in the SpoIVFB active site region, which led to a refined model (Figure S2.7B).

BofA and SpoIVFA Do Not Prevent Pro-σ^K(1-127) from Interacting with SpoIVFB. Since our cross-linking results show that BofA TMS2 can occupy the SpoIVFB active site region, we tested whether BofA and SpoIVFA prevent Pro-σ^K(1-127) from interacting with SpoIVFB in *E. coli*. Using a catalytically-inactive E44C cytTM-SpoIVFB variant containing the $FLAG_2$ epitope tag but lacking His_6, co-produced Pro-σ^K(1-127), SpoIVFA, and GFPΔ27BofA

co-purified with the cytTM-SpoIVFB variant in pull-down assays with anti-FLAG antibody beads (Figure 2.5). All four proteins were seen in the bound sample (lane 4), indicating that GFPΔ27BofA and SpoIVFA did not completely prevent Pro-σ^K(1-127) from interacting with the cytTM-SpoIVFB variant. However, only the cytTM-SpoIVFB variant was detected when the bound sample was diluted tenfold (lane 3) to match the input sample concentration (lane 1), and portions of the other three proteins were observed in the unbound sample (lane 2). The results indicate inefficient co-purification and/or recovery from the beads. A negative control with the cytTM-SpoIVFB variant lacking the $FLAG_2$ epitope tag showed no Pro-σ^K(1-127) in the bound sample, but small amounts of GFPΔ27BofA and SpoIVFA were detected (lane 8), indicative of weak, nonspecific binding to the beads.

We also performed pull-down assays with cobalt resin, which binds to the His_6 tag on Pro-σ^K(1-127), and we performed both types of pull-down assays (i.e., anti-FLAG antibody beads and cobalt resin) when full-length BofA rather than GFPΔ27BofA was co-produced with the other three proteins (Supplemental Results and Figure S2.12). Neither BofA nor GFPΔ27BofA when co-produced with SpoIVFA prevented Pro-σ^K(1-127) from interacting with the cytTM-SpoIVFB variant. However, GFPΔ27BofA and SpoIVFA reduced co-purification of full-length Pro-σ^K-His_6 with the cytTM-SpoIVFB variant in both types of pull-down assays (Supplemental Results and Figure S2.13), as compared with Pro-σ^K(1-127) (Figure 2.5 and S2.12A), suggesting that the C-terminal half of Pro-σ^K affects complex formation (Supplemental Discussion). As expected, GFPΔ27BofA and SpoIVFA strongly inhibited cytTM-SpoIVFB cleavage of full-length Pro-σ^K-His_6 (Figure S2.14), similar to the inhibition of Pro-σ^K(1-127) cleavage we observed (Figure 2.1B, lane 4). To further investigate the strong inhibition of

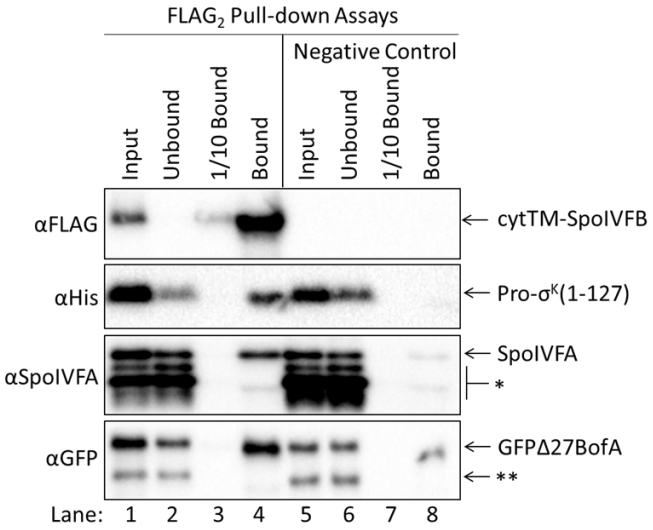

Figure 2.5 GFPΔ27BofA and SpoIVFA do not prevent Pro-σ^K(1-127) from co-purifying with SpoIVFB. pET Quartet plasmids were used to produce a catalytically-inactive E44C cytTM-SpoIVFB variant containing $FLAG_2$ but lacking His_6 (pSO73), or a variant also lacking $FLAG_2$ as a negative control (pSO149), in combination with Pro-σ^K(1-127), GFPΔ27BofA, and SpoIVFA in *E. coli*. Samples collected after 2 h of IPTG induction were subjected to co-immunoprecipitation with anti-FLAG antibody beads. Input, unbound, 1/10 bound (diluted to match input), and (undiluted) bound samples were subjected to immunoblot analysis with FLAG, penta-His, SpoIVFA, and GFP antibodies. The single star (*) indicates cross-reacting proteins below SpoIVFA and the double star (**) indicates a cross-reacting protein or breakdown species of GFPΔ27BofA that fail to co-purify. A representative result from two biological replicates is shown.

cleavage despite the presence of substrate in the pulled-down protein complexes, we next examined the effects of full-length BofA or MBPΔ27BofA co-produced with SpoIVFA on the interaction of Pro-σ^K(1-127) with cytTM-SpoIVFB using disulfide cross-linking approaches.

Full-length BofA and SpoIVFA Interfere with Cross-Linking between the Proregion of Pro-σ^K(1-127) and the SpoIVFB Active Site Region, and MBPΔ27BofA in Combination with SpoIVFA Is Less Effective at Interfering with Some of the Cross-links. SpoIVFB cleaves Pro-σ^K [43] and Pro-σ^K(1-127) [31] between residues S21 and Y22. In disulfide cross-linking experiments, Cys substitutions for several residues near the cleavage site of otherwise Cys-less Pro-σ^K(1-127) formed a cross-linked complex with single-Cys (E44C, V70C, P135C) cytTM-SpoIVFB variants [45]. The complex was most abundant with the E44C and V70C variants, so we compared these interactions in the presence or absence of Cys-less inhibitory proteins.

To examine proximity between single-Cys E44C cytTM-SpoIVFB and the Proregion, we first co-produced single-Cys (F18C, V20C, S21C, K24C) Pro-σ^K(1-127) variants in the absence of inhibitory proteins and measured time-dependent cross-linking. We quantified the cross-linking by measuring the abundance of the complex and dividing that by the total amount of the cytTM-SpoIVFB variant monomer, dimer, and complex. The ratio over time was plotted with a best-fit trend line. Single-Cys E44C cytTM-SpoIVFB formed abundant complex with single-Cys V20C and K24C Pro-σ^K(1-127) variants, and the amount of complex increased over time, but with the F18C and S21C variants much less complex formed, only slightly more than with the Cys-less Pro-σ^K(1-127) negative control (Figure 2.6A and S2.15A). Figure 2.6B shows a representative immunoblot (60-min oxidant treatment).

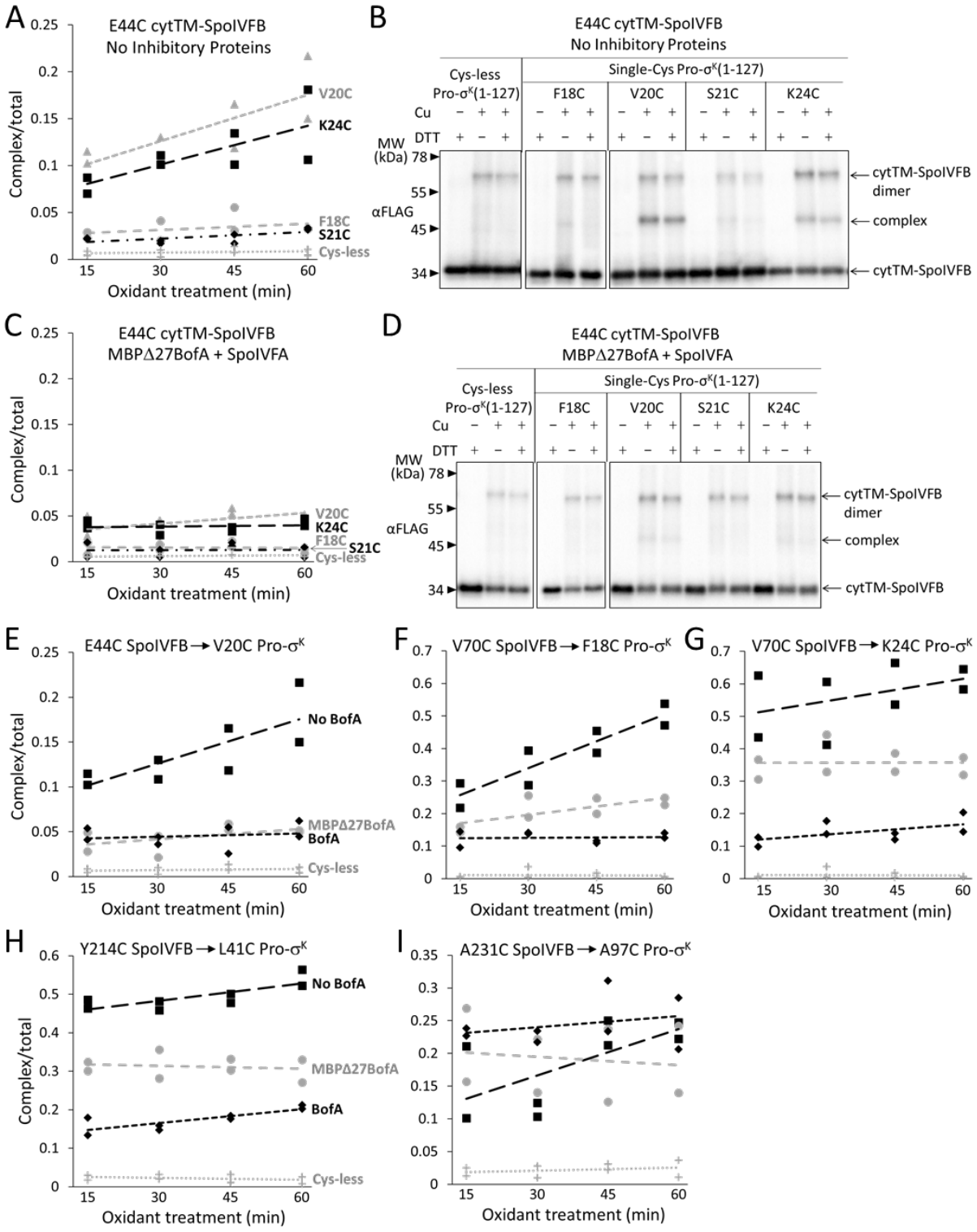

Figure 2.6 Effects of inhibitory proteins on cross-linking between cytTM-SpoIVFB and Pro-σ^K(1-127). (*A*) Quantification of disulfide cross-linking between single-Cys E44C cytTM-

Figure 2.6 (cont'd)
SpoIVFB and single-Cys Pro-σ^K(1-127) variants in the absence of inhibitory proteins. pET Duet plasmids were used to produce single-Cys E44C cytTM-SpoIVFB in combination with single-Cys F18C (pSO167), V20C (pSO169), S21C (pSO170), or K24C (pSO128) Pro-σ^K(1-127), or with Cys-less Pro-σ^K(1-127) (pSO79) as a negative control, in *E. coli*. Samples collected after 2 h of IPTG induction were treated with Cu^{2+}(phenanthroline)$_3$ (oxidant; Cu + in *B*) for 15, 30, 45, or 60 min or with 2-phenanthroline (Cu – in *B*) as a control. Samples were treated with TCA to precipitate proteins and resuspended in sample buffer with DTT (+ in *B*) or without (– in *B*) and subjected to immunoblot analysis with FLAG antibodies to visualize the cytTM-SpoIVFB monomer, dimer, and complex with Pro-σ^K(1-127) (Figure S2.15A). Abundance of the complex was divided by the total amount of cytTM-SpoIVFB monomer, dimer, and complex. The ratio over time was plotted (n=2) with a best-fit trend line. (*B*) Representative immunoblots of 60-min samples from the experiment described in *A*. (*C*) Quantification of cross-linking between single-Cys E44C cytTM-SpoIVFB and single-Cys Pro-σ^K(1-127) variants in the presence of Cys-less variants of MBPΔ27BofA and SpoIVFA. pET Quartet plasmids were used to produce single-Cys E44C cytTM-SpoIVFB in combination with single-Cys F18C (pSO163), V20C (pSO165), S21C (pSO166), or K24C (pSO131) Pro-σ^K(1-127), or with Cys-less Pro-σ^K(1-127) (pSO110) as a negative control, and Cys-less variants of MBPΔ27BofA and SpoIVFA in *E. coli*. Samples collected after 2 h of IPTG induction were treated and subjected to immunoblot analysis as in *A* (Figure S2.15B). (*D*) Representative immunoblots of 60-min samples from the experiment described in *C*. (*E*) Quantification of cross-linking between single-Cys E44C cytTM-SpoIVFB and single-Cys V20C Pro-σ^K(1-127) in the absence or presence of inhibitory proteins. Data from *A* (No BofA), *C* (MBPΔ27BofA), and Figure S2.16A (full-length BofA) are plotted along with Cys-less Pro-σ^K(1-127) as a negative control. (*F* and *G*) Quantification of cross-linking between single-Cys V70C cytTM-SpoIVFB E44Q and single-Cys F18C or K24C Pro-σ^K(1-127) variants in the absence or presence of inhibitory proteins. Data from Figure S2.17 are plotted using symbols and lines as in *E*. (*H* and *I*) Quantification of cross-linking between single-Cys Y214C or A231C cytTM-SpoIVFB E44Q and single-Cys L41C or A97C Pro-σ^K(1-127) in the absence or presence of inhibitory proteins. Data from Figure S2.20 are plotted using symbols and lines as in *E*.

Co-production of Cys-less inhibitory proteins greatly reduced complex formation between single-Cys E44C cytTM-SpoIVFB and the V20C and K24C Pro-σ^K(1-127) variants. When Cys-less MBPΔ27BofA and SpoIVFA were co-produced, much less complex formed and its abundance did not increase over time (Figure 2.6C and S2.15B). The decrease in abundance of the complex is most evident comparing representative immunoblots (60-min oxidant treatment) with (Figure 2.6D) or without (Figure 2.6B) co-produced inhibitory proteins. When Cys-less full-length BofA and SpoIVFA were co-produced, similar decreases in abundance of the complex were observed (Figure S2.16). Figure 2.6E shows a comparison of the cross-linking time courses with and without inhibitory proteins for single-Cys E44C cytTM-SpoIVFB with single-Cys V20C Pro-σ^K(1-127). The effects of Cys-less MBPΔ27BofA and Cys-less full-length BofA were indistinguishable. Similar results were observed with single-Cys K24C Pro-σ^K(1-127) (compare Figure 2.6C and S2.16B). We conclude that MBPΔ27BofA (lacking TMS1) is as effective as full-length BofA at interfering with cross-linking between the Proregion of Pro-σ^K and single-Cys E44C cytTM-SpoIVFB. These results likely explain why BofA TMS1 is dispensable for most of the inhibitory function of BofA [30, 31] (Figs. 2.1B and 2.3A). SpoIVFB E44 normally activates a water molecule to hydrolyze the bond between S21 and Y22 of Pro-σ^K. Interfering with this interaction is expected to inhibit cleavage.

We next examined proximity between V70 of SpoIVFB and the Proregion of Pro-σ^K(1-127). V70 is located in a predicted long and potentially flexible membrane-reentrant loop in the SpoIVFB active site region (Figure 2.1A and S2.7A), perhaps explaining why single-Cys V70C cytTM-SpoIVFB E44Q formed abundant cross-linked complex with both the F18C and K24C Pro-σ^K(1-127) variants in the absence of inhibitory proteins [45] (Figure 2.6 F and G; Figure S2.17 A and B). With co-production of Cys-less variants of MBPΔ27BofA and SpoIVFA, a

lower relative amount of complex was measured, which did not increase over time (Figure 2.6 F and G; Figure S2.17 C and D), but the impact on complex formation was not as great as when Cys-less variants of full-length BofA and SpoIVFA were co-produced (Figure 2.6 F and G; Figure S2.17 E and F). Full-length BofA and SpoIVFA also caused four novel species to be observed, including with the Cys-less Pro-σ^K(1-127) negative control (Figure S2.17G), perhaps due to cross-linking of the V70C cytTM-SpoIVFB variant to *E. coli* proteins (i.e., BofA may cause the SpoIVFB membrane-reentrant loop to be exposed). In any case, full-length BofA hindered cross-linking more than MBPΔ27BofA (lacking TMS1) (Figure 2.6 F and G), suggesting that both TMSs of BofA interfere with the normal interaction between the membrane-reentrant loop of SpoIVFB and the Proregion of Pro-σ^K.

Since full-length BofA also inhibited cleavage of Pro-σ^K(1-127) in *E. coli* (Figure 2.1B) and Pro-σ^K in *B. subtilis* (Figure 2.3A) slightly more than GFPΔ27BofA (lacking TMS1), we compared time-dependent cross-linking of BofA and MBPΔ27BofA to single-Cys cytTM-SpoIVFB variants. The results suggest that full-length BofA C46 forms slightly more complex with single-Cys E44C cytTM-SpoIVFB and single-Cys P135C cytTM-SpoIVFB E44Q over time, whereas the abundance of complex did not increase over time in the case of MBPΔ27BofA C46 (Figure S2.18). Hence, BofA TMS1 may slightly enhance TMS2 occupancy in the active site region of SpoIVFB.

BofA and SpoIVFA Interfere with Cross-Linking between Pro-σ^K(1-127) and the SpoIVFB Interdomain Linker, but Not with Cross-Linking between Pro-σ^K(1-127) and the SpoIVFB CBS Domain. To further examine the effects of the inhibitory proteins on the interaction of Pro-σ^K(1-127) with SpoIVFB, we identified additional residues that formed

disulfide cross-linked complexes. A model of catalytically-inactive SpoIVFB E44Q in complex with Pro-σ^K(1-127) [46] predicts interactions between the C-terminal part of SpoIVFB and parts of Pro-σ^K(1-127). The C-terminal part of SpoIVFB includes a 26-residue interdomain linker and a CBS domain (Figure 2.1A and S2.7A). For both the linker and the CBS domain, we used the model to predict residues of SpoIVFB in proximity to residues of Pro-σ^K(1-127). We tested the predictions by co-producing single-Cys variants of the two proteins and performing disulfide cross-linking experiments. We discovered that a single-Cys Y214C linker variant of cytTM-SpoIVFB E44Q formed abundant complex with single-Cys L41C Pro-σ^K(1-127), and a single-Cys A231C CBS domain variant of cytTM-SpoIVFB E44Q formed complex with single-Cys A97C Pro-σ^K(1-127) (Figure S2.19 A and B). We showed that the Cys substitutions do not impair cytTM-SpoIVFB activity or Pro-σ^K(1-127) susceptibility to cleavage (Figure S2.19C). Finally, we measured time-dependent cross-linking in the presence or absence of Cys-less inhibitory proteins.

Interestingly, formation of cross-linked complex between the Y214C linker variant of cytTM-SpoIVFB and single-Cys L41C Pro-σ^K(1-127) was hindered more by Cys-less full-length BofA than by Cys-less MBPΔ27BofA, when co-produced with Cys-less SpoIVFA (Figure 2.6H and S2.20A). The pattern is similar to that observed for the V70C membrane-reentrant loop variant of cytTM-SpoIVFB and single-Cys F18C or K24C Pro-σ^K(1-127) (Figure 2.6 F and G). The similar pattern suggests that in both cases BofA TMS2 partially interferes with the interaction and BofA TMS1 augments the interference.

Strikingly, co-production of Cys-less inhibitory proteins had little or no effect on formation of cross-linked complex between the A231C CBS domain variant of cytTM-SpoIVFB and single-Cys A97C Pro-σ^K(1-127) (Figure 2.6I and S2.20B). These results suggest that neither

full-length BofA nor MBPΔ27BofA, when co-produced with SpoIVFA, prevent Pro-σ^K(1-127) from interacting with the CBS domain of SpoIVFB in *E. coli*, consistent with our finding that inhibitory proteins did not completely prevent co-purification of SpoIVFB and Pro-σ^K(1-127) (Figure 2.5 and S2.12).

Model of SpoIVFB in Complex with BofA, Parts of SpoIVFA and Pro-σ^K. Models were generated using a similar protocol as described previously [46], but including additional constraints reflecting experimental cross-linking data reported herein, as well as newly predicted intra- and inter-chain contacts based on co-evolutionary couplings. Two final models were generated: 1) Full-length SpoIVFB modeled as a tetramer, with part of one Pro-σ^K molecule (residues 1-114), referred to as 'fb.sigk'; 2) Full-length SpoIVFB, again modeled as a tetramer, with one molecule each of full-length BofA and parts of Pro-σ^K (residues 38-114) and SpoIVFA (residues 65-111), referred to as 'fb.sigk.bofa.fa'. The omitted residues of Pro-σ^K and SpoIVFA could not be placed with sufficient confidence. The first model is described in Supplemental Methods and Figure S2.21.

Relevant features of the second model are illustrated in Figure 2.7 (only one molecule of SpoIVFB is shown). The first side view shows SpoIVFB with BofA TMS2 and the C-terminal part of Pro-σ^K(1-127) (Figure 2.7A). The membrane domain of SpoIVFB (green) interacts with BofA TMS2 (cyan) while the interdomain linker and CBS domain of SpoIVFB interact with the modeled portion of Pro-σ^K(1-127) (red). The enlarged view of the SpoIVFB active site region shows BofA TMS2 surrounded by SpoIVFB (TMSs labeled 1-6). The top view of the membrane domain emphasizes proximity between BofA TMS2, SpoIVFB TMSs 2-4, and the zinc ion (magenta) involved in catalysis. The second side view shows SpoIVFB with full-length BofA

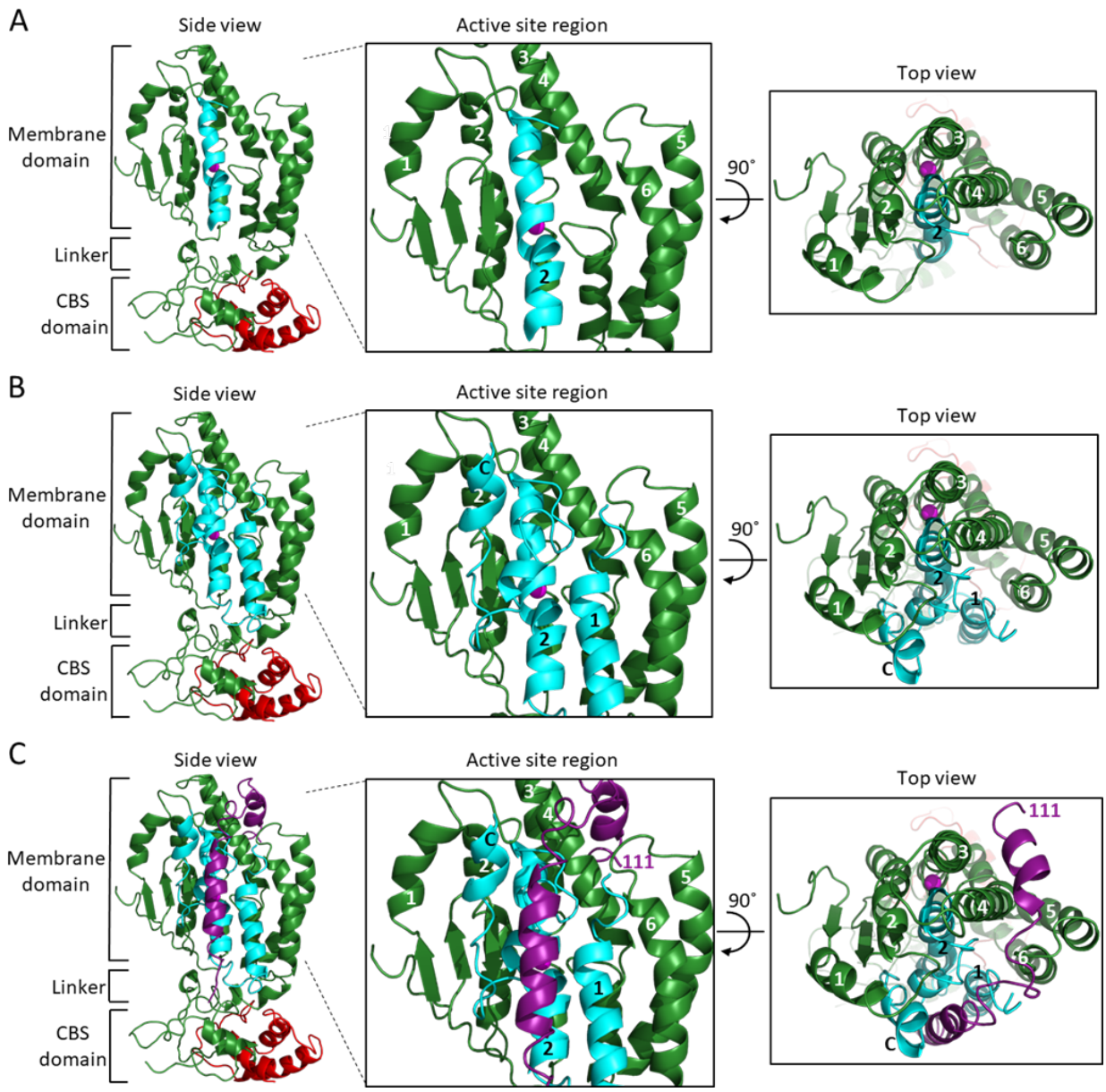

Figure 2.7 Model of SpoIVFB monomer with BofA and parts of SpoIVFA and Pro-σ^K. (*A*) Model of SpoIVFB, BofA TMS2, and the C-terminal part of Pro-σ^K(1-127). At *Left*, a side view of the complex, showing the six TMSs of the SpoIVFB membrane domain with the active site zinc ion (magenta), the interdomain linker, and the CBS domain (green), BofA TMS2 (cyan), and Pro-σ^K(38-114) (red). In the enlarged view of the active site region (*Center*), TMSs 1– 6 of SpoIVFB and TMS2 of BofA are numbered. At *Right*, a top view is shown. (*B*) Model of SpoIVFB with full-length BofA and Pro-σ^K(38-114). Predicted TMSs 1 and 2 of BofA are numbered and its C-terminal region is labeled "C" near the C-terminus in the views shown in the *Center* and at *Right*. (*C*) Model of SpoIVFB with full-length BofA, SpoIVFA(65-111) (purple, residue 111 is numbered), and Pro-σ^K(38-114).

and the C-terminal part of Pro-σ^K(1-127) (Figure 2.7B). Our model predicts that BofA contains 2 TMSs and a membrane-embedded C-terminal region (labeled C near the C-terminus in the enlarged view of the SpoIVFB active site region) that forms two short α-helices connected by a turn. The enlarged and top views show that BofA interacts extensively with SpoIVFB and occupies its active site region, which would sterically hinder access of the Proregion of Pro-σ^K. Figure 2.7C shows the addition of the modeled portion of SpoIVFA (purple), which is predicted by co-evolutionary couplings to contact the BofA C-terminal region and SpoIVFB TMS4. Hence, the model predicts that SpoIVFA stabilizes the interaction of BofA with SpoIVFB. Since GFPΔ27BofA has the C-terminal region predicted to interact with SpoIVFA, the interaction of GFPΔ27BofA with SpoIVFB is likewise predicted to be stabilized by SpoIVFA, which may explain the dependence of SpoIVFB inhibition on both GFPΔ27BofA and SpoIVFA (Figure 2.1C), and why GFPΔ27BofA inhibits substrate cleavage (Figure 2.1B and 2.3A) and MBPΔ27BofA occupies the SpoIVFB active site region (Figure S2.18) nearly as well as full-length BofA.

Discussion

Our results provide evidence that BofA occupies the active site region of SpoIVFB. BofA residue C46 near the middle of TMS2 formed disulfide cross-links with SpoIVFB variants containing a single-Cys at (E44C) or near (P135C) its active site. BofA variants containing a single-Cys near the ends of TMS2 formed cross-links with single-Cys SpoIVFB variants that suggest BofA TMS2 adopts a preferred orientation in the SpoIVFB active site region. N48 within BofA TMS2 and both N61 and T64 near its C-terminal end are highly conserved among BofA orthologs. We showed that these residues are important for SpoIVFB inhibition during *B.*

subtilis sporulation and upon heterologous expression in *E. coli*. Structural modeling based on partial homology and constraints from cross-linking and co-evolutionary analyses predicts that BofA N48 and T64 interact, and that nearby N61 may also interact to stabilize the BofA structure. SpoIVFA is also important for SpoIVFB inhibition and the model predicts that SpoIVFA bridges the BofA C-terminal region and SpoIVFB to form a membrane-embedded inhibitory complex (Figure 2.7C). We found that BofA and SpoIVFA interfere with cross-linking between the Pro-σ^K N-terminal region and the SpoIVFB active site region, supporting a steric hindrance mechanism of SpoIVFB inhibition. BofA TMS1 enhanced interference with some cross-links between Pro-σ^K and SpoIVFB, and slightly enhanced inhibition of SpoIVFB, suggesting that BofA TMS1 enhances steric hindrance of substrate access to the enzyme active site. Our findings have implications for the design of IMMP inhibitors.

Conserved Residues May Stabilize BofA in a Membrane-Embedded Inhibitory Complex with SpoIVFA that Sterically Hinders Substrate Access to the SpoIVFB Active Site. BofA, SpoIVFA, and SpoIVFB form a heterotrimeric membrane complex that improves accumulation of each protein likely by inhibiting proteolytic degradation [30]. Ala substitutions for N48, N61, and T64 in GFPΔ27BofA reduced its level as well as the levels of SpoIVFA and SpoIVFB, both upon heterologous expression in *E. coli* (Figure 2.2) and during *B. subtilis* sporulation (Figure 2.3A), suggesting that assembly of the inhibitory complex was impaired. In agreement, the Ala substitutions caused partial or complete mislocalization of GFPΔ27BofA during sporulation (Figure 2.3B), which normally relies on SpoIVFA [30]. Impaired assembly of the inhibitory complex can explain the observed cleavage of Pro-σ^K(1-127) in *E. coli* (Figure 2.2) and premature cleavage of Pro-σ^K in sporulating *B. subtilis* (Figure 2.3A).

Our structural model predicts proximity within BofA between the N48 side chain and a loop that includes N61 and T64. In particular, the T64 side chain is oriented toward the N48 side chain in the model, predicting an interaction. The N61 side chain points away from the N48 and T64 side chains in the model, but the orientation of the N61 side chain is uncertain given the predicted loop structure, so an interaction with the side chains of N48 and/or T64 remains possible. Alternatively, the three conserved residues may contact other residues within BofA, based on co-evolutionary couplings, to stabilize the BofA structure and promote interactions with SpoIVFA and SpoIVFB. For example, disulfide cross-linking supports proximity between BofA L62 and V63 (in the predicted loop that includes N61 and T64) and SpoIVFB M30, which is located in a predicted short loop between TMS1 and TMS2 (Figure S2.11). Our model satisfies restraints based on this observed cross-linking, as well as many other experimental cross-linking results [45, 46]. The model also predicts numerous interactions between BofA, SpoIVFA, and SpoIVFB that remain to be tested, which will be facilitated by approaches described herein. Of note, the model predicts that BofA C-terminal residues 85 to 87 interact with SpoIVFA and SpoIVFB, and that BofA residues 28 to 36 preceding predicted TMS2 interact with SpoIVFA (Figure 2.7C), which may explain the effects of deleting or changing those BofA residues, including loss of SpoIVFB inhibition resulting in Pro-σ^K(1-127) cleavage and reduced levels of SpoIVFA and SpoIVFB in *E. coli* (Supplemental Results and Figure S2.5). The predicted interactions can be tested further by disulfide cross-linking.

BofA and SpoIVFA interfere with cross-linking between the Pro-σ^K N-terminal region and the SpoIVFB active site region, supporting a steric hindrance mechanism of SpoIVFB inhibition. Many latent zymogens likewise use a prosegment or prodomain to sterically hinder substrate access to their active site [53]. Many metalloprotease zymogens in addition use a

ligand switch mechanism of inhibition and activation. Inhibition involves an amino acid side chain of a residue in the prosegment acting as a metal ligand to prevent catalysis. Activation requires replacement of the side chain metal ligand with a water molecule necessary for substrate peptide bond hydrolysis. BofA residue C46 near the middle of TMS2 is well-positioned in our model to act as a zinc ligand, but C46 is not conserved among BofA orthologs (Figure S2.4). Therefore, we favor a simple steric hindrance mechanism of SpoIVFB inhibition. During sporulation, SpoIVFB would be activated when SpoIVB cleaves the C-terminal end of SpoIVFA [35-38] and CtpB cleaves the C-terminal ends of both SpoIVFA and BofA [36, 37, 39] (Figure S2.1). These cleavages result in a conformational change in the inhibition complex [36], which we propose allows the Proregion of Pro-σ^K to be positioned in the active site for cleavage. After cleavage, the conformational change may also aid in release of the product, σ^K.

BofA TMS1 Appears to Enhance Inhibition of SpoIVFB Slightly by Partially Interfering with Its Interaction with Pro-σ^K. Full-length BofA inhibited cleavage of Pro-σ^K(1-127) in *E. coli* (Figure 2.1B) and Pro-σ^K in *B. subtilis* (Figure 2.3A) slightly more than GFPΔ27BofA. The most likely explanation for the difference, based on our results, is that TMS1 of BofA sterically hinders some interactions between the Pro-σ^K N-terminal region and SpoIVFB more than BofA variants lacking TMS1 (such as GFPΔ27BofA and MBPΔ27BofA). The interactions hindered more by full-length BofA included cross-links between the Pro-σ^K Proregion (F18C and K24C) and the SpoIVFB membrane-reentrant loop (V70C) (Figure 2.6F and G), which may bind to the Proregion and present it to the SpoIVFB active site for cleavage [46] based on a study of the homologous membrane-reentrant loop of *E. coli* RseP [54]. Our model predicts that both TMSs of BofA, as well as its C-terminal region, occupy the active site

region of SpoIVFB (Figure 2.7B), which would sterically hinder interactions between the SpoIVFB membrane-reentrant loop and the Pro-σ^K Proregion.

Full-length BofA also hindered cross-links between Pro-σ^K L41C and the SpoIVFB interdomain linker (Y214C) more than MBPΔ27BofA (Figure 2.6H). The interdomain linker has been proposed to allow coordination between ATP binding by the CBS domain and Pro-σ^K cleavage by the membrane domain [46]. Thus, BofA TMS1 may interfere with coordination between the domains of SpoIVFB by inhibiting movement of the linker, in addition to hindering linker interaction with the Pro-σ^K N-terminal region.

Design of IMMP Inhibitors. Our findings reveal concepts that may inform efforts to design selective inhibitors of IMMPs. BofA TMS2 appears to block the SpoIVFB active site (Figure 2.7A), similar to the prosegment of many latent zymogens [53]. Like BofA, some prosegments can act in *trans*, an observation that has led to the demonstration of prodomains as selective inhibitors of A Disintegrin And Metalloproteinase (ADAM) family enzymes [55, 56]. Selectivity relies on the extensive interaction surface between the prodomain and the enzyme, including features specific to the pair, which can boost efficacy and diminish off-target effects in therapeutic strategies [57]. A peptide encompassing residues 48 to 64 of BofA may inhibit SpoIVFB, but our model also predicts extensive interactions between the BofA C-terminal region (residues 65 to 87) and SpoIVFB (Figure 2.7B), so a longer BofA peptide, perhaps flexibly linked to SpoIVFA residues 96 to 109, which are also predicted to interact with SpoIVFB (Figure 2.7C), may exhibit improved inhibition and selectivity. Since cleavage of Pro-σ^K(1-127) by cytTM-SpoIVFB has been reconstituted *in vitro* [42], it will be possible to test peptides for inhibition. Structure determination of SpoIVFB in complex with an inhibitory

peptide, GFPΔ27BofA, or full-length BofA is an important goal to facilitate design of IMMP inhibitors. In particular, it may inform efforts to design inhibitors of SpoIVFB orthologs in *Bacillus* and *Clostridium* species, many of which cause disease or provide benefits, and persist by forming endospores [58]. Such efforts could lead to new strategies to control endosporulation.

Our findings also suggest that BofA TMS1 interferes with interactions between the Pro-σ^K N-terminal region and SpoIVFB. Therefore, a cyclic peptide inhibitor may prove to be more effective than a linear one. The desirable characteristics of cyclic peptides as therapeutics, and new methods of producing and screening cyclic peptide libraries, make this an attractive possibility [59, 60].

The inhibitor design concepts discussed above could apply equally well to IMMPs that normally use one or more PDZ domains to exclude substrate from their active site region. *E. coli* RseP appears to use two PDZ domains to block access of substrate RseA [61-63]. Cleavage of the RseA periplasmic domain by DegS (referred to as site-1 cleavage) [64-66] is proposed to allow entry of the RseA TMS into the RseP active site region for site-2 cleavage [67]. Recently, batimastat, a hydroxamic acid derivative that mimics the peptide structure of natural substrates, was shown to selectively inhibit RseP *in vivo* [68]. Two other peptidomimetic hydroxamic acids, ilomastat and miramastat, exhibited very little RseP inhibition. A lack of selectivity has been a problem in efforts toward using peptidomimetic hydroxamic acids as matrix metalloprotease inhibitors for treatment of cancer, arthritis, and other diseases [57, 69, 70]. The hydroxamic acid group of these compounds strongly coordinates the catalytic zinc ion, and the peptidomimetic portions have not provided enough specificity to prevent off-target effects. Even so, the side effects may not preclude using hydroxamic acid-based peptidomimetics to treat bacterial

infections topically, and systemically if administered briefly. Perhaps weaker zinc ligands based on amino acid side chains would reduce side effects. A cyclic peptidomimetic with a zinc ligand could presumably block access of the RseA TMS to the RseP active site, or substrate access to the active site of other IMMPs. Other small-molecule matrix metalloprotease inhibitors that have already been developed [69] should be screened for activity against bacteria and fungi with IMMPs known to be involved in pathogenesis [16-19].

Materials and Methods

Plasmids, Primers, and Strains. Plasmids used in this study are described in Table S2.1. Primers used in plasmid construction are listed in Table S2.2. Plasmids were cloned in *E. coli* strain DH5α [71]. Relevant parts of plasmids were verified by DNA sequencing with primers listed in Table S2.3. *B. subtilis* strains used in this study are described in Table S2.4.

Pro-σ^K(1-127) Cleavage in *E. coli*. Strain BL21(DE3) (Novagen) was used to produce proteins in *E. coli*. Two plasmids with different antibiotic resistance genes were cotransformed [31] or a single plasmid was transformed, with selection on Luria-Bertani (LB) agar supplemented with kanamycin sulfate (50 μg/mL) and/or ampicillin (100 μg/mL). Transformants (4-5 colonies) were grown in LB medium with 50 μg/mL kanamycin sulfate and/or 200 μg/mL ampicillin at 37°C with shaking (200 rpm). Typically, overnight culture (200 μL) was transferred to 10 mL of LB medium with antibiotics, cultures were grown at 37°C with shaking (250 rpm) to an optical density of 60-80 Klett units, and isopropyl β-D-thiogalactopyranoside (IPTG) (0.5 mM) was added to induce protein production for 2 h. For transformants with either pET Quintet or full-length Pro-σ^K-His_6, overnight growth was avoided.

Transformants were transferred directly to 10 mL of LB medium with antibiotic, and cultures were grown and induced as described above. Equivalent amounts of cells (based on optical density in Klett units) were collected (12,000 × *g* for 1 min) and extracts were prepared [31], then subjected to immunoblot analysis (Supplemental Methods).

BofA Sequence Analysis. Orthologs of *B. subtilis bofA*, which are present in the genomes of most endospore-forming bacteria [20], were collected from the NCBI and Uniprot databases. The protein sequences of BofA orthologs were aligned using the T-Coffee multiple sequence alignment package [72]. Residues identical in at least 70% of the sequences were considered conserved.

***B. subtilis* Sporulation and GFPΔBofA Localization.** GFPΔ27BofA or its variants were expressed under control of the *bofA* promoter (P_{bofA}) after ectopic chromosomal integration. Plasmids bearing P_{bofA}-*gfpΔ27bofA* or its variant, bordered by regions of homology to *B. subtilis amyE*, were transformed into strain ZR264. Transformants with a gene replacement at *amyE* were selected on LB agar with spectinomycin sulfate (100 μg/mL) and identified by loss of amylase activity [73]. Sporulation was induced by growing cells in the absence of antibiotics followed by the resuspension of cells in SM medium [73]. At indicated times PS, samples (50 μL) were centrifuged (12,000 × *g* for 1 min), supernatants were removed, and cell pellets were stored at -80°C. Whole-cell extracts were prepared as described for *E. coli* [31], except samples were incubated at 50°C for 3 min instead of boiling for 3 min [46], and proteins were subjected to immunoblot analysis (Supplemental Methods).

To image GFPΔ27BofA localization, samples collected at 3 h PS were examined by fluorescence microscopy using an Olympus FluoView FV-1000 filter-based confocal microscope. GFPΔ27BofA (ex/em ~488/507 nm) was excited using a 458 nM argon laser and fluorescence was captured using a BA465-495 nm band pass filter. The lipophilic dye FM 4-64 (1 μg/mL) (AAT Bioquest) was used to stain membranes. FM 4-64 (ex/em ~515/640 nm) was excited using a 515 nm argon laser and fluorescence was captured using a BA560IF band pass filter [74].

Disulfide Cross-Linking. A method described previously [75] was used with slight modifications [45]. Briefly, as described above for Pro-σ^K(1-127) cleavage, *E. coli* BL21(DE3) was transformed with a plasmid, grown in LB (10 mL), induced with IPTG, and equivalent amounts of cells were collected. Cells were subjected to disulfide cross-linking, then lysed and proteins were precipitated by addition of trichloroacetic acid (5%), and proteins were subjected to immunoblot analysis (Supplemental Methods).

Co-Immunoprecipitation ($FLAG_2$ Pull-Down Assays). *E. coli* BL21(DE3) was transformed with a plasmid, grown in LB (1 L), and induced with IPTG as described above. The culture was split, cells were harvested, and cell pellets were stored at -80°C. Cell lysates were prepared as described [52], except that each cell pellet was resuspended in 20 mL of lysis buffer containing 50 mM Tris-HCl pH 7.1 rather than PBS. Cell lysates were centrifuged (15,000 × *g* for 15 min at 4 °C) to sediment cell debris and protein inclusion bodies. The supernatant was treated with 1% *n*-dodecyl-β-D-maltoside (DDM) (Anatrace) for 1 h at 4 °C to solubilize membrane proteins, then centrifuged at 150,000 × *g* for 1 h at 4 °C. The supernatant was

designated the input sample and 1 mL was mixed with 50 uL anti-DYKDDDDK magnetic agarose (Pierce) that had been equilibrated with buffer (50 mM Tris-HCl pH 7.1, 0.1% DDM, 5 mM 2-mercaptoethanol, 10% glycerol) and the mixture was rotated for 1 h at 25°C. The magnetic agarose was removed with a DynaMag-2 magnet (Invitrogen) and the supernatant was saved (unbound sample). The magnetic agarose was washed three times by gently vortexing with 500 μL wash buffer (50 mM Tris-HCl pH 7.1, 150 mM NaCl, 10% glycerol, 0.1% DDM), then washed once with 500 μL water. The magnetic agarose was mixed with 50 μL of 2× sample buffer (50 mM Tris·HCl pH 6.8, 4% SDS, 20% glycerol, 200 mM DTT 0.03% bromophenol blue) and boiled for 3 min (bound sample). A portion of the bound sample was diluted tenfold (1/10 bound sample) with 1× sample buffer to match the concentration of the input sample. Samples were subjected to immunoblot analysis (Supplemental Methods).

Colbalt Affinity Purification (His_6 Pull-Down Assays). Input sample (15 mL) prepared as described above was mixed with imidazole (5 mM) and 0.5 mL of Talon superflow metal affinity resin (Clontech) that had been equilibrated with buffer (as above for magnetic agarose). The mixture was rotated for 1 h at 4°C. The cobalt resin was sedimented by centrifugation at 708 × *g* for 2 min at 4 °C and the supernatant was saved (unbound sample). The resin was washed three times with 5 mL wash buffer (as above plus 5 mM imidazole), each time rotating the mixture for 10 min at 4 °C and sedimenting resin as above. The resin was mixed with 0.5 mL 2× sample buffer and boiled for 3 min (bound sample). A portion of the bound sample was diluted fifteenfold (1/15 bound sample) with 1× sample buffer to match the concentration of the input sample. Samples were subjected to immunoblot analysis (Supplemental Methods).

Modeling of Complexes Containing SpoIVFB, BofA, and Parts of SpoIVFA and Pro-σ^K. The modeling proceeded through stages where initial monomeric models were assembled step-by-step into multimeric complexes guided primarily by the restraints from cross-linking experiments and predicted contacts from co-evolutionary coupling analysis. More specifically, a SpoIVFB monomer was first assembled from the membrane and CBS domains. Two monomers were combined into a dimer and the dimer was assembled into a plausible tetramer. Part of one molecule of Pro-σ^K (residues 1-114) was subsequently added, which resulted in 'fb.sigk'. The 'fb.sigk.bofa.fa' model was developed by starting from 'fb.sigk', truncating the Pro-σ^K N-terminus (residues 1-37), and subsequently adding first BofA and finally SpoIVFA (residues 65-111). See Supplemental Methods for additional description of the modeling.

Acknowledgments. We thank Daniel Parrell for assistance with fluorescence microscopy, Jon Kaguni for helpful comments on the manuscript, and David Rudner, Simon Cutting, Ruanbao Zhou, and Yang Zhang for plasmids. This research was supported by National Institutes of Health Grants R01 GM43585 (to L.K.) and R35 GM126948 (to M.F.), and by Michigan State University AgBioResearch.

APPENDIX

Results

SpoIVB Partially Relieves Inhibition of SpoIVFB by BofA and SpoIVFA in *E. coli.*

To determine whether SpoIVFB inhibition could be relieved by SpoIVB in *E. coli*, "pET Quintet plasmids" were engineered to produce Pro-σ^K(1-127), cytTM-SpoIVFB, GFPΔ27BofA or full-length BofA, SpoIVFA, and SpoIVB or inactive SpoIVB S378A in various combinations. With pET Quintet plasmids that produced active SpoIVB and either GFPΔ27BofA or BofA (Figure S2.2, lanes 2 & 4), the Pro-σ^K(1-127) cleavage ratios were greater than with corresponding pET Quintet plasmids that produced inactive SpoIVB S378A (lanes 3 & 5). When *spoIVB* was expressed under the same T7 promoter as inhibitory proteins (i.e., *gfpΔ27bofA/spoIVFA* or *bofA/spoIVFA*), accumulation of GFPΔ27BofA and SpoIVFA was consistently less (lanes 2-5) compared to pET Quartet (lane 1), which exhibited a very low cleavage ratio, as expected. To try to increase protein production, we attempted to engineer pET Quintet plasmids with *spoIVB* under control of an additional T7 promoter. Samples with *spoIVB S378A* under control of an additional T7 promoter (T7-SpoIVB S378A) (lanes 6 & 7) accumulated more SpoIVB S378A (compared with lanes 3 & 5), and more GFPΔ27BofA and SpoIVFA (similar to that observed for pET Quartet in lane 1), and exhibited a very low cleavage ratio (similar to lane 1). Attempts at engineering pET Quintet plasmids to express active *spoIVB* from an additional T7 promoter were unsuccessful. Cell lysis occurred in overnight cultures of strains containing such plasmids, suggesting that T7-SpoIVB is toxic to *E. coli*.

An F66A Substitution in SpoIVFB Partially Overcomes Inhibition by GFPΔ27BofA and SpoIVFA in *E. coli.*

The phenylalanine residue at position 66 of SpoIVFB was predicted to help stabilize a closed conformation that would prevent Pro-σ^K access to the active site, and

BofA and SpoIVFA were envisioned to further stabilize SpoIVFB in a closed conformation [49]. SpoIVB-dependent cleavage of SpoIVFA would presumably favor an open conformation of SpoIVFB capable of cleaving Pro-σ^K. In the absence of SpoIVB, it was found that an F66A substitution in SpoIVFB-YFP allowed Pro-σ^K cleavage during *B. subtilis* sporulation, albeit with reduced efficiency [49]. To test whether SpoIVFB inhibition could be relieved by the F66A substitution in *E. coli*, a pET Quartet plasmid was engineered to produce cytTM-SpoIVFB F66A, Pro-σ^K(1-127), GFPΔ27BofA, and SpoIVFA. The Pro-σ^K(1-127) cleavage ratio (Figure S2.3, lane 1) was greater than when cytTM-SpoIVFB was produced from a pET Quartet plasmid as a control (lane 2), but not as great as in the absence of inhibitory proteins (Figure 2.1B, lane 1). We conclude that cytTM-SpoIVFB F66A partially overcomes inhibition by GFPΔ27BofA and SpoIVFA in *E. coli*.

BofA C-terminal Residues and Residues Preceding Predicted TMS2 Contribute to Inhibition of SpoIVFB in *E. coli*. Single-Ala substitutions for each of the last three residues of GFPΔ27BofA had little effect in Pro-σ^K(1-127) cleavage assays (Figure 2.2, lanes 18, 19 & 20). Since a deletion of those three residues from BofA caused a loss of function or stability in *B. subtilis* [26, 51], a triple-Ala substitution was made for the last three residues of GFPΔ27BofA in pET Quartet. The triple-Ala variant increased the cleavage ratio (Figure S2.5A, lane 6), as did a variant lacking the three residues (lane 2). Both variants accumulated normally, but less SpoIVFA accumulated compared to the controls. These results show that residues near the C-terminal end of GFPΔ27BofA affect the synthesis and/or stability of SpoIVFA, and inhibition of cytTM-SpoIVFB in *E. coli*.

GFPΔ27BofA lacks TMS1 and all but nine residues preceding predicted TMS2 [30]. A pET Quartet plasmid with GFPΔ36BofA, which additionally lacks the nine residues, allowed some cleavage of Pro-σ^K(1-127) in *E. coli* (Figure S2.5B, lane 2). Since all four proteins accumulated well, the nine residues appeared to contribute to the inhibitory function of GFPΔ27BofA. Replacement of the nine residues with a glycine/serine linker decreased the cleavage ratio (lane 3), suggesting that moving the GFP tag away from the membrane partially restored inhibitory function. We conclude that the nine residues preceding predicted TMS2 of GFPΔ27BofA contribute to its inhibitory function.

Preferred Orientation of BofA TMS2 in the SpoIVFB Active Site Region. We modeled BofA TMS2 in the SpoIVFB active site region based on our initial cross-linking results (Figure 2.4). The initial model predicted proximity between residues at or near the ends of BofA TMS2 and residues of SpoIVFB (Figure S2.11A). We tested the predictions using disulfide cross-linking experiments. Since cytTM-SpoIVFB with Cys substitutions for residues of interest cleaved Pro-σ^K(1-127) (Figure S2.11B, lanes 2-6), we included the inactivating E44Q substitution in the single-Cys cytTM-SpoIVFB variants created for cross-linking. GFPΔ27BofA with Cys substitutions for residues of interest inhibited Pro-σ^K(1-127) cleavage by cytTM-SpoIVFB, although the G40C and H57C substitutions caused partial loss of inhibition, and the G40C substitution resulted in less accumulation of all four proteins (Figure S2.11B, lanes 8-13). Ala substitutions at these positions had similar effects (Figure 2.2, lanes 2 & 15). Single-Cys MBPΔ27BofA C46S variants were also created as negative controls for cross-linking. In agreement with the model, I56C and H57C MBPΔ27BofA variants formed a cross-linked complex with A32C and Q181C cytTM-SpoIVFB variants, respectively, (Figure S2.11C, lanes 4

& 13). The I56C MBPΔ27BofA variant formed very little complex with the L33C cytTM-SpoIVFB variant (lane 10), suggesting that a preferred orientation of BofA TMS2 places I56C farther from L33C than from A32C in TMS2 of SpoIVFB. Similarly, comparison of complex formation by G40C and A41C MBPΔ27BofA variants with the V86C cytTM-SpoIVFB variant (lanes 7 & 16) suggested that a preferred orientation of BofA TMS2 places G40C farther than A41C from V86C near the C-terminal end of SpoIVFB TMS3. Likewise, L62C and V63C MBPΔ27BofA variants formed a cross-linked complex with the M30C cytTM-SpoIVFB variant (Figure S2.11C, lanes 19 & 22), suggesting a loop near the C-terminal end of BofA TMS2 is in proximity to a loop between SpoIVFB TMS1 and TMS2, as predicted by our initial model (Fig, S2.11A, right). The additional cross-linking results were used to derive additional constraints for modeling, which led to the refined model shown in Figure S2.7B.

BofA and SpoIVFA Do Not Prevent Pro-σ^K(1-127) from Interacting with SpoIVFB in *E. coli*. Pro-σ^K(1-127), SpoIVFA, and GFPΔ27BofA co-purified with a catalytically-inactive E44C cytTM-SpoIVFB variant containing $FLAG_2$ but lacking His_6, in pull-down assays with anti-FLAG antibody beads (Figure 2.5), indicating that GFPΔ27BofA and SpoIVFA did not completely prevent Pro-σ^K(1-127) from interacting with the cytTM-SpoIVFB variant. Therefore, the cytTM-SpoIVFB variant, GFPΔ27BofA, and SpoIVFA were predicted to co-purify with Pro-σ^K(1-127) (which contains His_6) in pull-down assays with cobalt resin. Indeed, all four proteins were seen in the bound sample (Figure S2.12A, lane 7). Only Pro-σ^K(1-127) and the cytTM-SpoIVFB variant were detected in the diluted bound sample (lane 6). Most of the cytTM-SpoIVFB variant, GFPΔ27BofA, and SpoIVFA were observed in the unbound sample (lane 2), indicating inefficient co-purification. A negative control with a Pro-σ^K(1-127) variant

lacking the His_6 tag showed none of the Pro-σ^K(1-127) variant or GFPΔ27BofA in the bound sample, but a small amount of the cytTM-SpoIVFB variant and considerable SpoIVFA were detected (lane 14), indicative of nonspecific binding to the resin. In the case of SpoIVFA, nonspecific binding rather than co-purification with Pro-σ^K(1-127) appears to account for most of the signal in lane 7. A putative SpoIVFA breakdown species (indicated by ***) exhibited a similar pattern of abundance in samples as intact SpoIVFA.

Pull-down assays were likewise performed with co-produced full-length BofA rather than GFPΔ27BofA. Importantly, BofA and SpoIVFA did not completely prevent Pro-σ^K(1-127) from interacting with the cytTM-SpoIVFB variant in pull-down assays with anti-FLAG antibody beads (Figure S2.12B, lane 7) or with cobalt resin (Figure S2.12C, lane 7). We note that co-production of BofA decreased the accumulation of Pro-σ^K(1-127) in the input samples (lane 1 in each panel) compared to co-production of GFPΔ27BofA (lane 1 in Figure 2.5 and Figure S2.12A). We also note that SpoIVFA failed to co-purify with the cytTM-SpoIVFB variant when BofA was co-produced (Figure S12B, lane 7), in contrast to the result when GFPΔ27BofA was co-produced (Figure 2.5, lane 4). Perhaps BofA decreased Pro-σ^K(1-127) accumulation and SpoIVFA co-purification more than GFPΔ27BofA because TMS1 in full-length BofA hinders the interaction between Pro-σ^K(1-127) and the cytTM-SpoIVFB variant, making Pro-σ^K(1-127) more susceptible to degradation, which may impair SpoIVFA co-purification. In any case, neither BofA nor GFPΔ27BofA when co-produced with SpoIVFA prevented Pro-σ^K(1-127) from interacting with SpoIVFB based on our pull-down assays.

GFPΔ27BofA and SpoIVFA Do Not Prevent Full-Length Pro-σ^K from Interacting with SpoIVFB in *E. coli*, but Co-purification Is Reduced in Comparison with Pro-σ^K(1-

127). We considered the possibility that full-length Pro-σ^K (242 residues) would behave differently than Pro-σ^K(1-127) in pull-down assays, because BofA and SpoIVFA appeared to prevent Pro-σ^K from interacting with SpoIVFB during *B. subtilis* sporulation unless SpoIVB was present to initiate relief of SpoIVFB inhibition [49]. Therefore, we tested whether Pro-σ^K-His_6 co-purifies with the cytTM-SpoIVFB variant containing $FLAG_2$ but lacking His_6, when co-produced with GFPΔ27BofA and SpoIVFA in *E. coli.* We found that GFPΔ27BofA and SpoIVFA did not completely prevent Pro-σ^K-His_6 from interacting with the cytTM-SpoIVFB variant in pull-down assays with anti-FLAG antibody beads (Figure S2.13A, lane 7) or with cobalt resin (Figure S2.13B, lane 7). However, co-purification was reduced in comparison with Pro-σ^K(1-127) in similar experiments (Figs. 2.5 and S2.12A). These results suggest that the C-terminal half of full-length Pro-σ^K affects complex formation. In agreement, when Pro-σ^K-His_6 was co-produced rather than Pro-σ^K(1-127), less SpoIVFA and more GFPΔ27BofA co-purified with the cytTM-SpoIVFB variant (compare Figs. S2.13A and 2.5), and less of both inhibitory proteins co-purified with Pro-σ^K-His_6 (compare Figs. S2.13B and S2.12A).

GFPΔ27BofA and SpoIVFA Strongly Inhibit Cleavage of Full-Length Pro-σ^K by SpoIVFB in *E. coli*. To test whether GFPΔ27BofA and SpoIVFA inhibit cleavage of full-length Pro-σ^K by SpoIVFB, similar to the results observed for Pro-σ^K(1-127) (Figure 2.1B, lane 4), plasmids were engineered to produce Pro-σ^K-His_6 and cytTM-SpoIVFB with or without GFPΔ27BofA and SpoIVFA in *E. coli*. When Pro-σ^K-His_6 and cytTM-SpoIVFB were produced, cleavage occurred (Figure S2.14, lane 1), although not as abundantly as for Pro-σ^K(1-127) (Figure 2.1B, lane 1). When GFPΔ27BofA and SpoIVFA were produced with Pro-σ^K-His_6 and cytTM-SpoIVFB, the cleavage ratio was very low (Figure 2.14, lane 2), similar to that observed

for Pro-σ^K(1-127) (Figure 2.1B, lane 4), so we conclude that GFPΔ27BofA and SpoIVFA strongly inhibit cleavage of full-length Pro-σ^K.

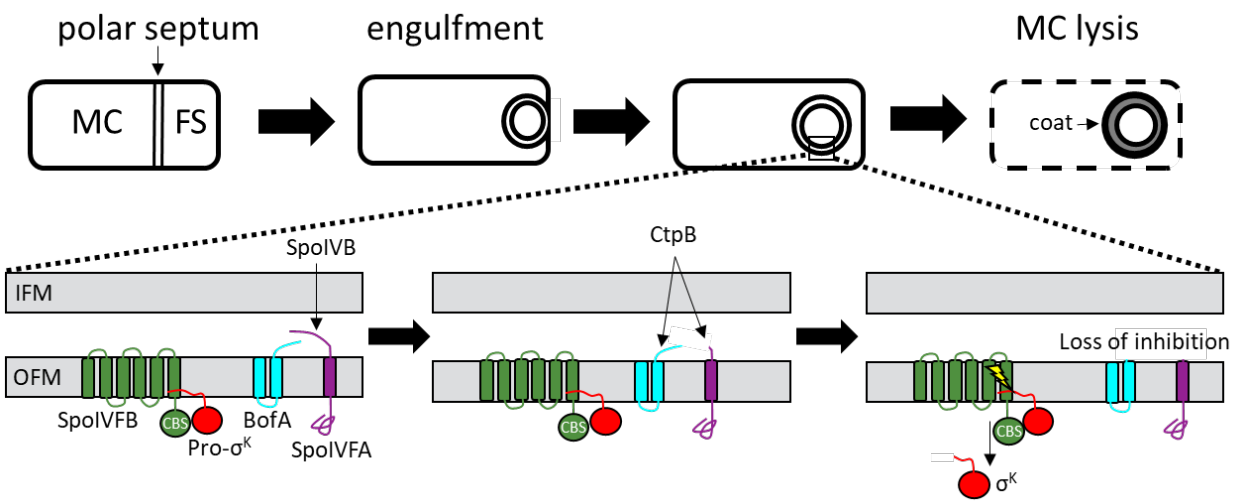

Figure S2.1 Morphological changes during endosporulation and RIP of Pro-σ^K in *B. subtilis*. Upon starvation, a polar septum forms that divides the cell into MC (MC) and FS (FS) compartments (*Top*). The MC engulfs the FS, resulting in two membranes surrounding the FS. After engulfment, a proteolytic cascade leads to RIP of Pro-σ^K, releasing σ^K into the MC where it directs RNA polymerase to transcribe genes whose products form the spore coat and cause MC lysis. The proteolytic cascade begins with SpoIVB, which is exported from the FS into the intermembrane space between the inner FS membrane (IFM) and outer FS membrane (OFM) (*Bottom*). SpoIVB cleaves the C-terminal region of SpoIVFA. A second protease, CtpB, is also exported from the FS, and further cleaves the C-terminal region of SpoIVFA, and can cleave the C-terminal end of BofA. Inhibition of SpoIVFB is lost, allowing it to cleave Pro-σ^K (lightning bolt), releasing σ^K into the MC.

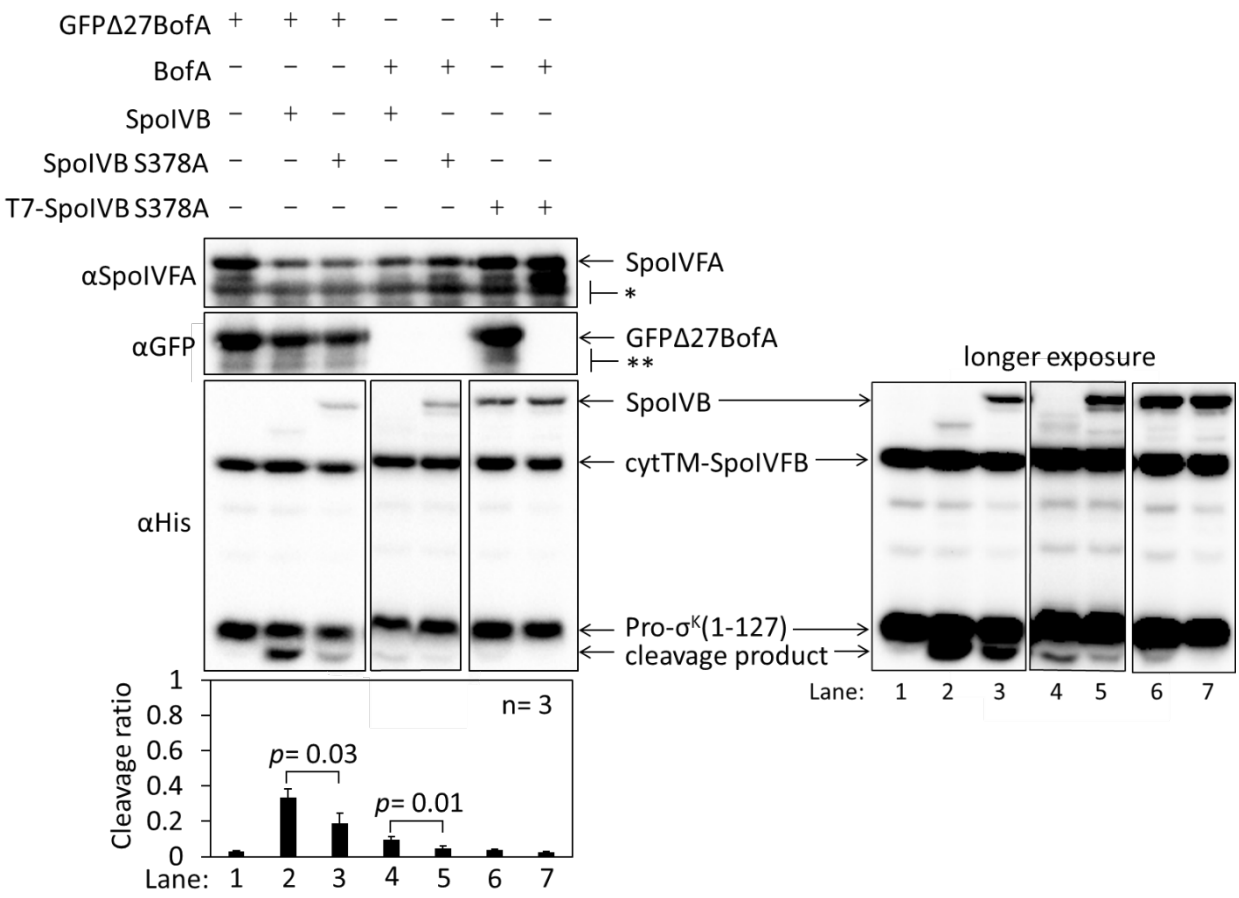

Figure S2.2 Cleavage assays examining the effects of SpoIVB production on BofA and SpoIVFA inhibition of SpoIVFB. pET Quintet plasmids were used to produce Pro-σ^K(1-127), cytTM-SpoIVFB, SpoIVFA, GFPΔ27BofA or full-length BofA, and SpoIVB or SpoIVB S378A from pSO240, pSO241 and pSO251-pSO254 in *E. coli*. Samples collected after 2 h of IPTG induction were subjected to immunoblot analysis with SpoIVFA (*Top*), GFP (*Middle*), or penta-His antibodies with a 3 sec exposure (*Bottom left*) or a 30 sec exposure (*Bottom right*). The single star (*) indicates cross-reacting proteins below SpoIVFA and the double star (**) indicates breakdown species of GFPΔ27BofA. A breakdown species below SpoIVFA (not indicated) is observed in some samples. The graph shows quantification of the cleavage ratio (cleavage product/[Pro-σ^K(1-127) + cleavage product]) for n=3 biological replicates with error bars indicating 1 standard deviation. Student's two-tailed *t* tests were performed to compare certain cleavage ratios (*p* values are indicated).

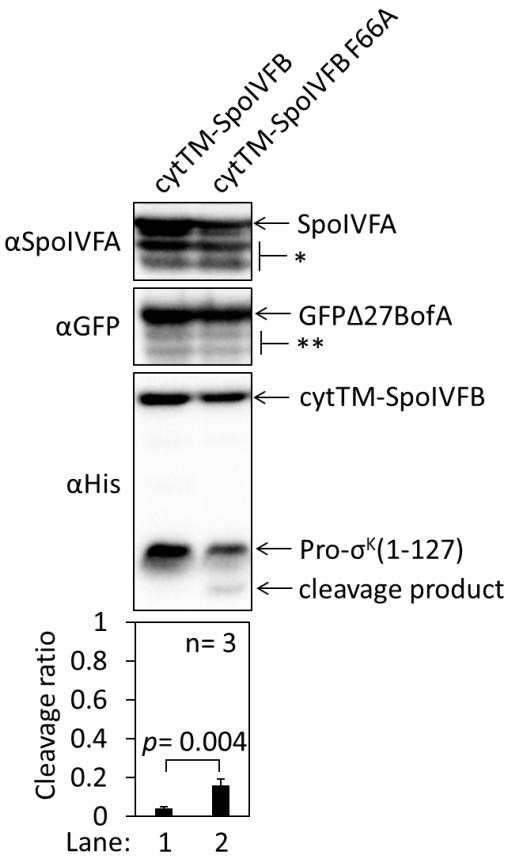

Figure S2.3 An F66A substitution in cytTM-SpoIVFB partially overcomes inhibition by GFPΔ27BofA and SpoIVFA in *E. coli*. pET Quartet plasmids were used to produce Pro-σ^K(1-127), SpoIVFA, GFPΔ27BofA, and cytTM-SpoIVFB from pSO40 as a control (lane 1) or cytTM-SpoIVFB F66A from pSO193 (lane 2). Samples collected after 2 h of IPTG induction were subjected to immunoblot analysis with SpoIVFA, GFP, or penta-His antibodies as indicated. The single star (*) indicates cross-reacting proteins below SpoIVFA and the double star (**) indicates breakdown species of GFPΔ27BofA. A breakdown species below SpoIVFA (not indicated) is observed in some samples. The graph shows quantification of the cleavage ratio (cleavage product/[Pro-σ^K(1-127) + cleavage product]) for n=3 biological replicates with error bars indicating 1 standard deviation. A Student's two-tailed *t* test was performed to compare the cleavage ratios (*p* value is indicated).

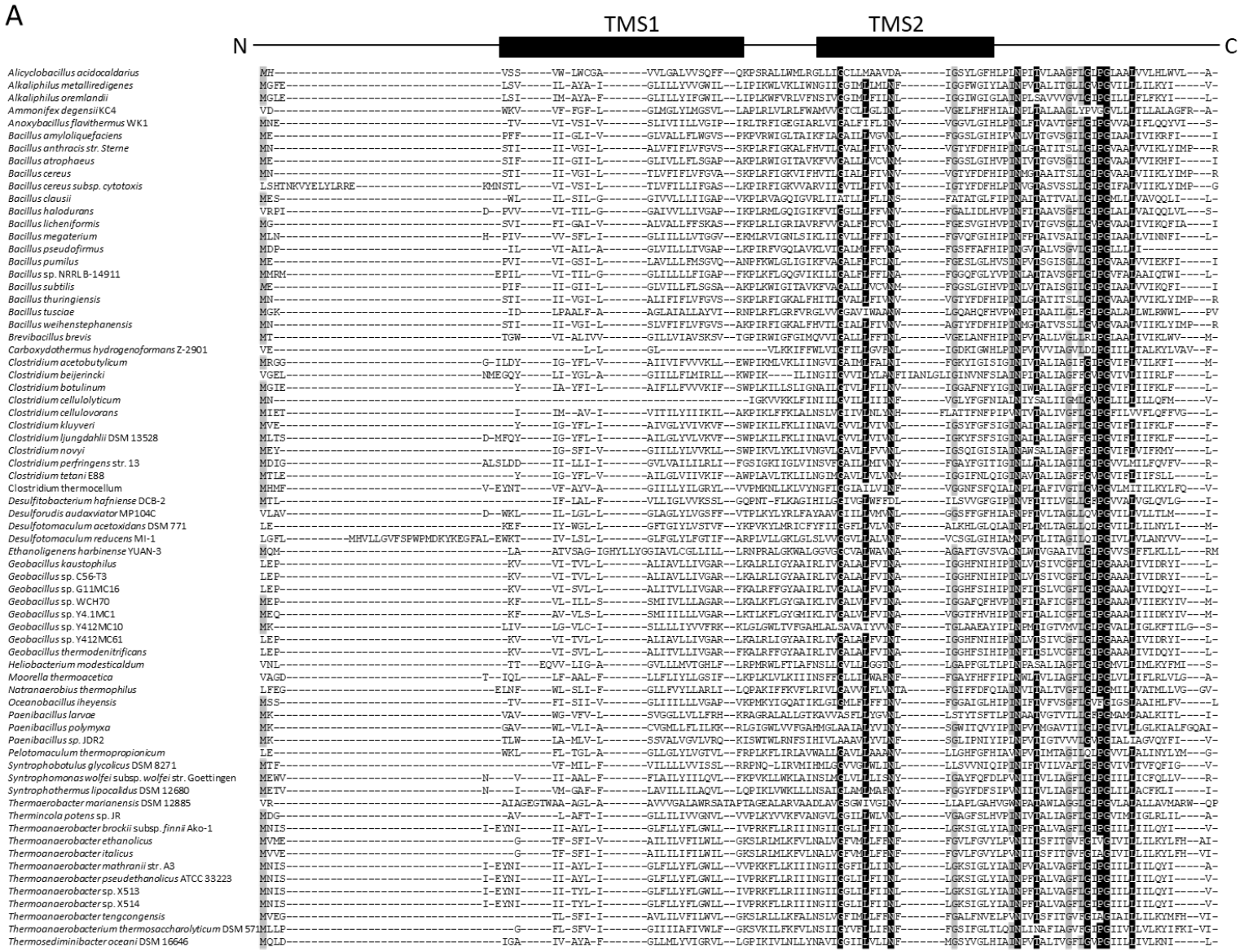

Figure S2.4 Sequence alignments of BofA orthologs to determine conserved residues. (*A*) Sequence alignment of *B. subtilis* BofA with 69 orthologs. Five residues (gray: M1, G51, I60, G69, L71) are at least 70% conserved and nine residues (black: G40, L44, N48,

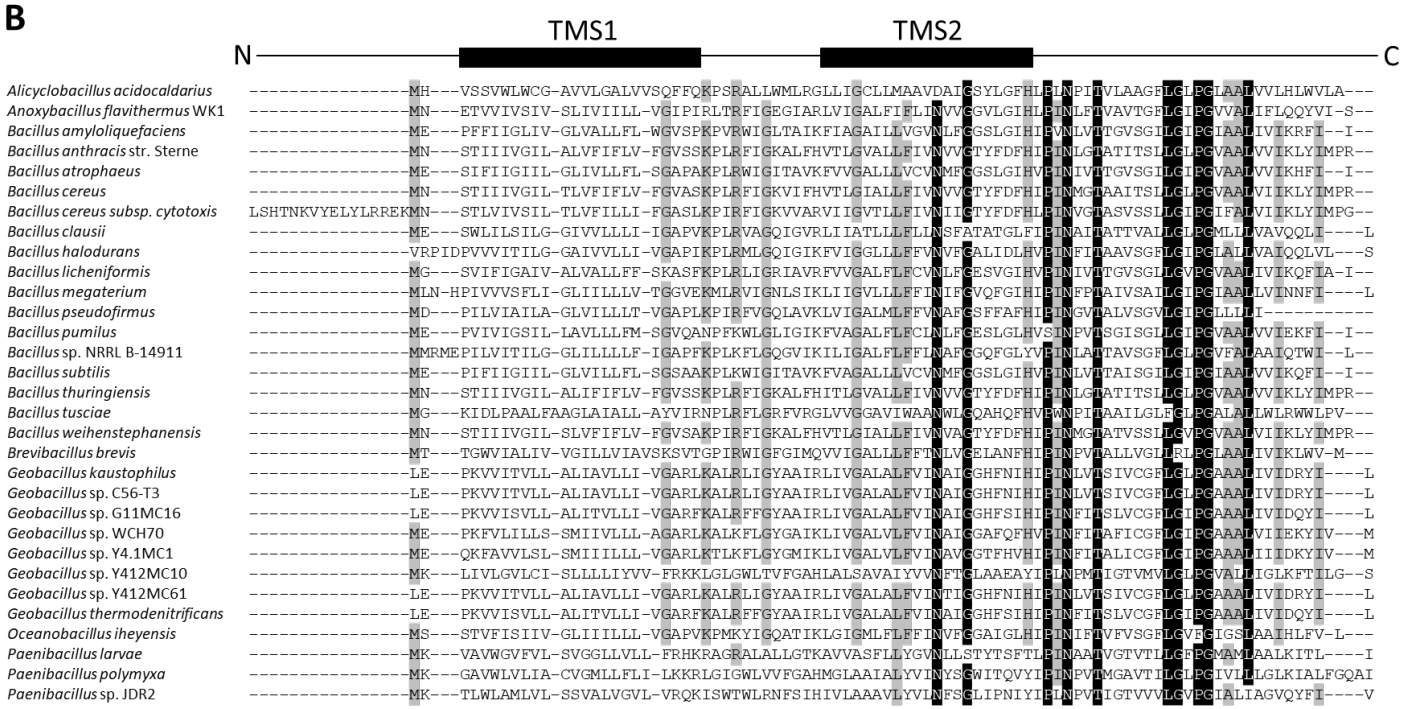

Figure S2.4 (cont'd)
N61, T64, G72, P74, G75, L79) are at least 90% conserved, all within transmembrane segment 2 (TMS2) and the C-terminal end, except M1. (*B*) Sequence alignment of *B. subtilis* BofA with 30 orthologs that contain *spoIVFA* in their genome. In comparison to *A*, 4 additional residues in the C-terminal end are conserved (H57, I82, and I86 are at least 70% conserved, and P59 is at least 90% conserved). A77 and A78 are also at least 70% conserved, but ineligible for Ala substitutions.

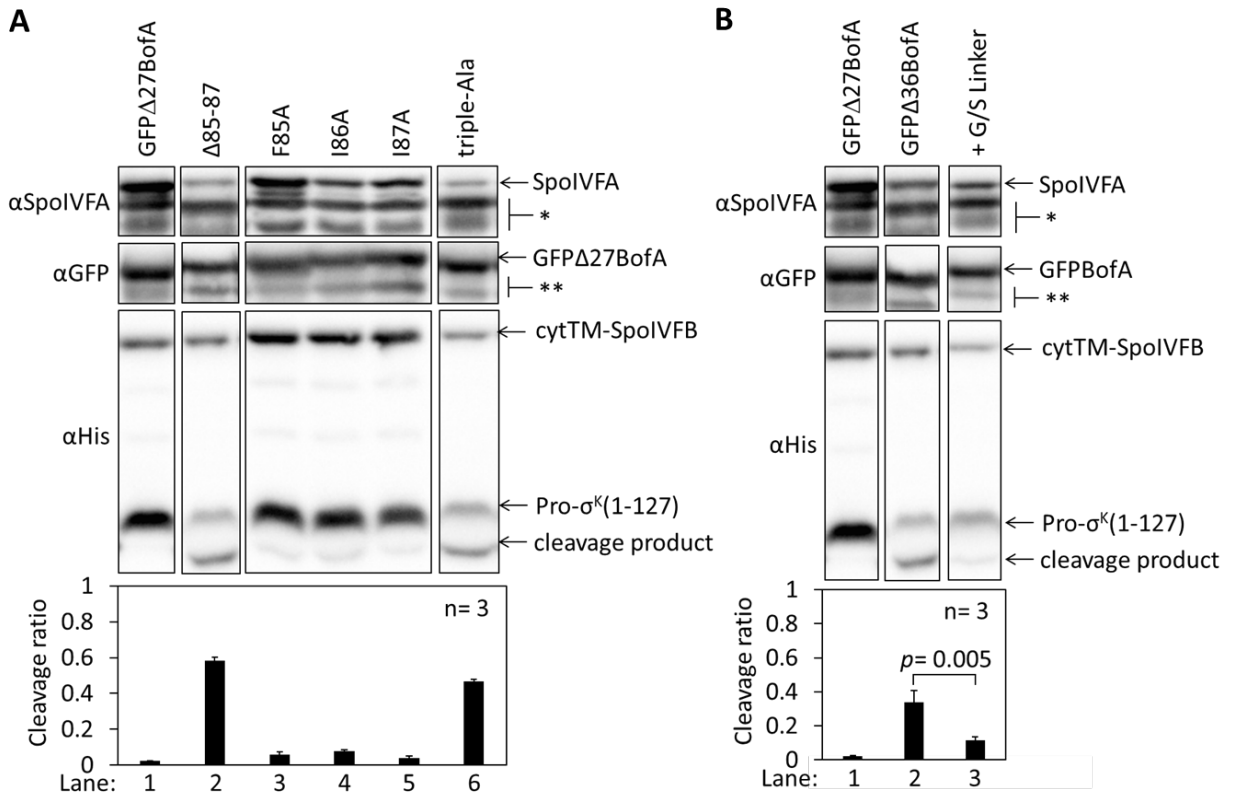

Figure S2.5 Effects of BofA C-terminal residues and residues preceding predicted TMS2 on SpoIVFB inhibition in *E. coli.* (*A*) Cleavage assays examining the effects of a GFPΔ27BofA truncation and a triple-Ala substitution for the last three residues of GFPΔ27BofA. pET Quartet plasmids were used to produce Pro-σ^K(1-127), cytTM-SpoIVFB, SpoIVFA, and GFPΔ27BofA from pSO40 as a control (lane 1), GFPΔ27BofA lacking the last three residues (Δ85-87) from pSO43 (lane 2), or GFPΔ27BofA with a triple-Ala substitution for the last three residues from pSO67. Samples collected after 2 h of IPTG induction were subjected to immunoblot analysis with SpoIVFA, GFP, or penta-His antibodies as indicated. The single star (*) indicates cross-reacting proteins below SpoIVFA and the double star (**) indicates breakdown species of GFPΔ27BofA. A breakdown species below SpoIVFA (not indicated) is observed in some samples. The graph shows quantification of the cleavage ratio (cleavage product/[Pro-σ^K(1-127) + cleavage product]) for n=3 biological replicates with error bars indicating 1 standard deviation. For comparison, lanes 3-5 show data from Figure 2.2 for single-Ala substitutions in GFPΔ27BofA. (*B*) Cleavage assays comparing inhibition by GFPΔ36BofA without or with a nine-residue glycine/serine (G/S) linker. pET Quartet plasmids were used to produce Pro-σ^K(1-127), cytTM-SpoIVFB, SpoIVFA, and GFPΔ27BofA from pSO40 as a control (lane 1, same data as in *A*), GFPΔ36BofA from pSO42 (lane 2), or GFPΔ36BofA with a nine-residue G/S linker added between GFP and Δ36BofA, from pSO69 (lane 3). Samples were subjected to immunoblot analysis and quantification as in *A*. Samples containing GFPΔ36BofA have a greater cleavage ratio than samples containing GFPΔ36BofA with a nine-residue G/S linker, based on a Student's two-tailed *t* test (*p* value is indicated).

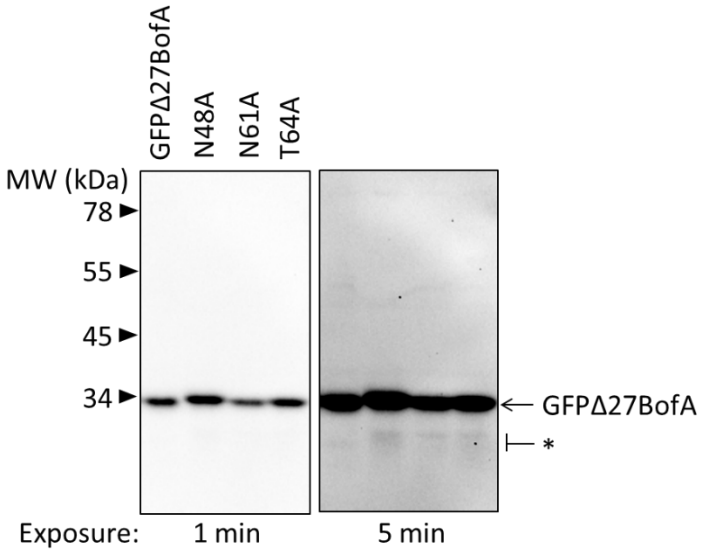

Figure S2.6 GFPΔ27BofA variants are intact during *B. subtilis* sporulation. A *spoIVB165 bofA::erm* double mutant with P_{bofA}-*gfpΔ27bofA* or the indicated mutant version integrated ectopically at *amyE*, were starved to induce sporulation. Samples collected at 3 h poststarvation were subjected to immunoblot analysis with antibodies against GFP. The star (*) indicates very small amounts of potential breakdown species of GFPΔ27BofA and the variants detectable in the long exposure.

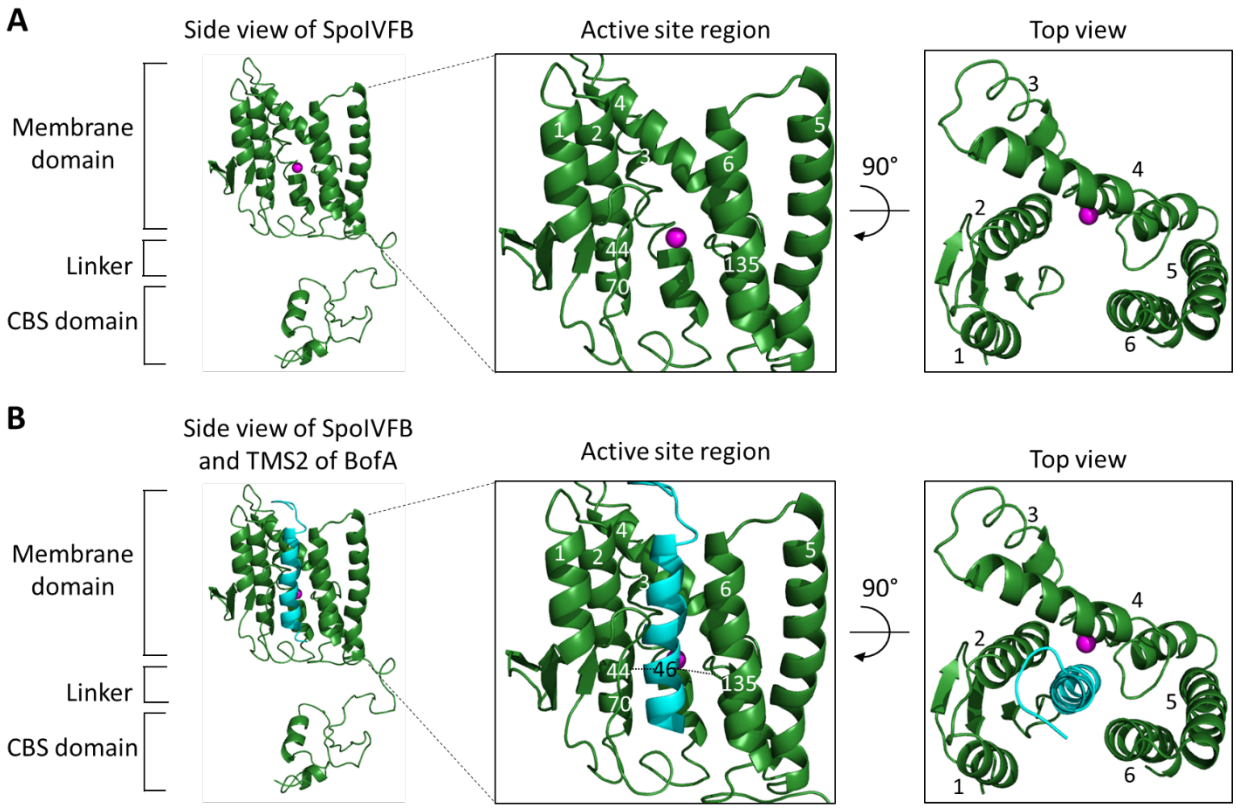

Figure S2.7 Models of SpoIVFB and BofA TMS2. (*A*) Model of SpoIVFB. At *Left*, a side view of a SpoIVFB monomer. The model shows the six TMSs of the SpoIVFB membrane domain, the zinc ion (magenta) involved in catalysis, the interdomain linker, and the CBS domain. In the enlarged view of the active site region (*Center*), TMSs 1– 6 and residues 44, 70, and 135 of SpoIVFB are labeled. At *Right*, a top view is shown. (*B*) Model of SpoIVFB with BofA TMS2. Labeling is as in *A* and BofA TMS2 (cyan) is modeled in the SpoIVFB active site region. The enlarged view of the active site region depicts experimentally observed disulfide cross-links (dashed lines) between BofA C46 and both E44C (in TMS2) and P135C (in a short loop in TMS4) of single-Cys cytTM-SpoIVFB variants.

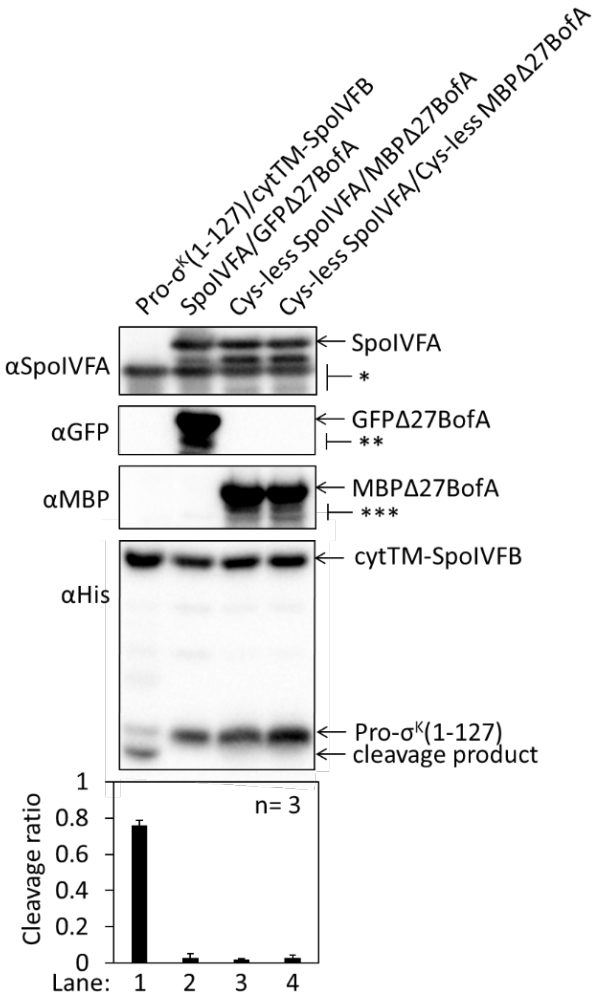

Figure S2.8 Cys-less variants of SpoIVFA and MBPΔ27BofA inhibit cleavage of Pro-σ^K(1-127) by cytTM-SpoIVFB in *E. coli*. Pro-σ^K(1-127) and cytTM-SpoIVFB were produced from pYZ2 as a control (lane 1), or pET Quartet plasmids were used to produce Pro-σ^K(1-127), cytTM-SpoIVFB, and either SpoIVFA and GFPΔ27BofA from pSO40 as another control (lane 2), Cys-less SpoIVFA and MBPΔ27BofA from pSO90 (lane 3), or Cys-less SpoIVFA and Cys-less MBPΔ27BofA from pSO97 (lane 4). Samples collected after 2 h of IPTG induction were subjected to immunoblot analysis with SpoIVFA, GFP, or penta-His antibodies as indicated. The single star (*) indicates cross-reacting proteins below SpoIVFA. The double (**) and triple (***) star indicate breakdown species of GFPΔ27BofA and MBPΔ27BofA, respectively. A breakdown species below SpoIVFA (not indicated) is observed in some samples. The graph shows quantification of the cleavage ratio (cleavage product/[Pro-σ^K(1-127) + cleavage product]) for n=3 biological replicates with error bars indicating 1 standard deviation.

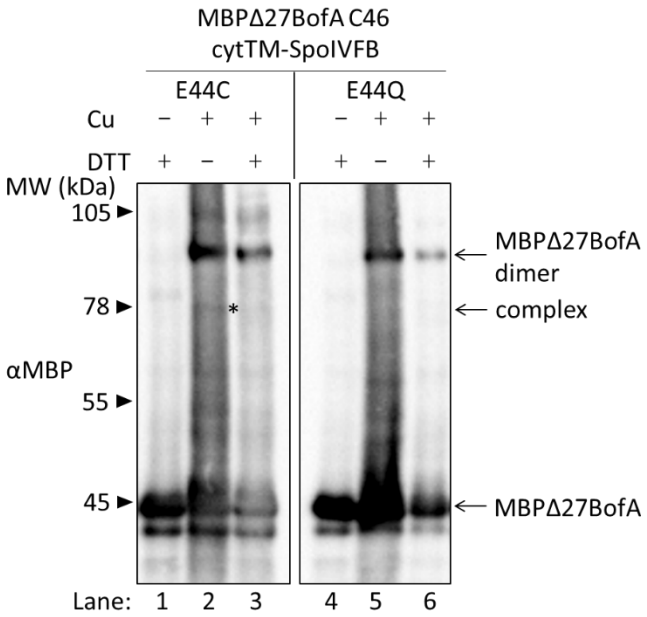

Figure S2.9 BofA TMS2 is in proximity to the active site of SpoIVFB. Disulfide cross-linking of single-Cys E44C cytTM-SpoIVFB to MBPΔ27BofA C46. pET Quartet plasmids were used to produce single-Cys E44C cytTM-SpoIVFB (pSO91) or Cys-less cytTM-SpoIVFB E44Q as a negative control (pSO94) in combination with MBPΔ27BofA, and Cys-less variants of SpoIVFA and Pro-σ^K(1-127) in *E. coli*. Samples collected after 2 h of IPTG induction were treated with Cu^{2+}(phenanthroline)$_3$ (Cu +) for 60 min or with 2-phenanthroline (Cu –) as a control. Samples were treated with TCA to precipitate proteins and resuspended in sample buffer with DTT (+) or without (–) and subjected to immunoblot analysis with MBP antibodies to visualize MBPΔ27BofA monomer, dimer, and complex with cytTM-SpoIVFB. A representative result from at least two biological replicates is shown. The star indicates the complex in lane 2.

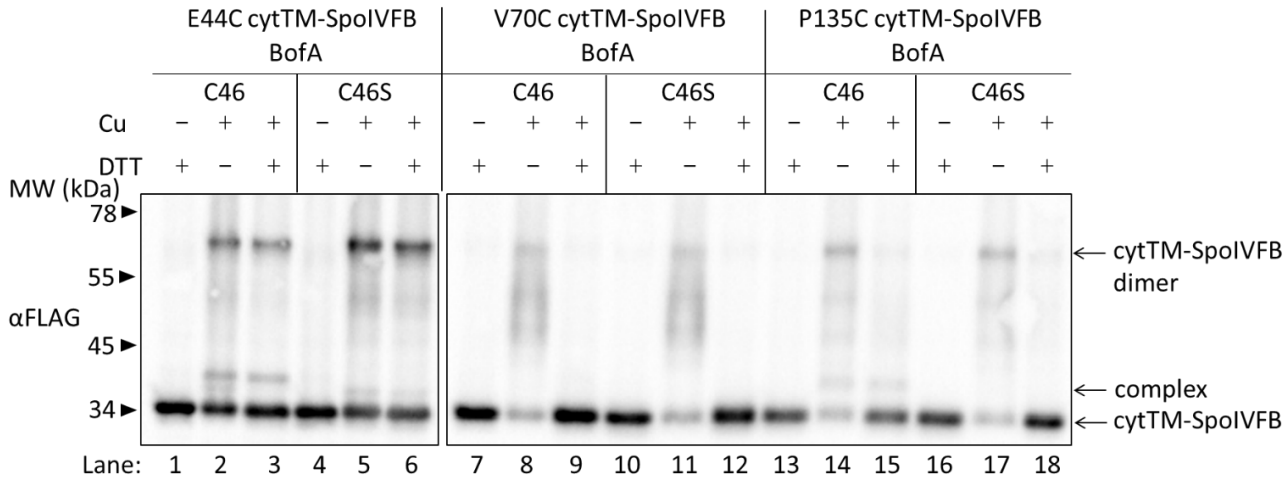

Figure S2.10 Full-length BofA is in proximity to the active site of SpoIVFB. Disulfide cross-linking of single-Cys cytTM-SpoIVFB variants to BofA C46. pET Quartet plasmids (pSO226-pSO231) were used to produce single-Cys E44C cytTM-SpoIVFB, or single-Cys V70C or P135C cytTM-SpoIVFB E44Q variants, in combination with BofA or BofA C46S, and Cys-less variants of SpoIVFA and Pro-σ^K(1-127) in *E. coli*. Samples collected after 2 h of IPTG induction were treated with Cu^{2+}(phenanthroline)$_3$ (Cu +) for 60 min or with 2-phenanthroline (Cu –) as a control. Samples were treated with TCA to precipitate proteins and resuspended in sample buffer with DTT (+) or without (–) and subjected to immunoblot analysis with FLAG antibodies to visualize cytTM-SpoIVFB monomer, dimer, and complex with full-length BofA. A representative result from at least two biological replicates is shown.

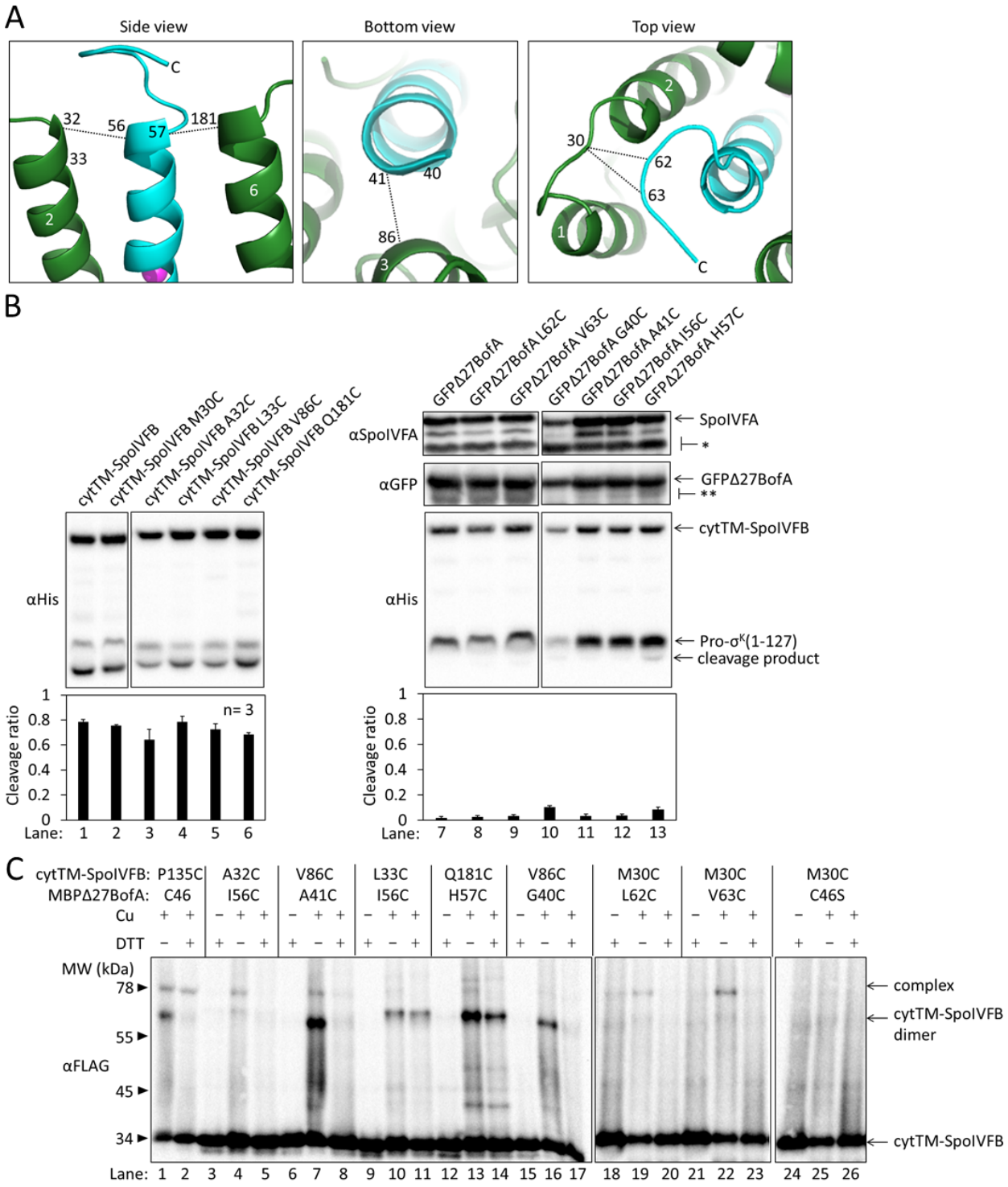

Figure S2.11 BofA TMS2 can occupy the active site region of SpoIVFB. (*A*) Enlarged view of an initial model of SpoIVFB and BofA TMS2. At *Left*, the side view of SpoIVFB TMS2 and TMS6 (green) is shown with the zinc ion (magenta) involved in catalysis and BofA TMS2 (cyan). This view depicts experimentally observed disulfide cross-links (dashed lines) between BofA I56C and SpoIVFB A32C, and between BofA H57C and SpoIVFB Q181C. In the bottom view (*Center*), BofA TMS2 is shown with SpoIVFB TMS3. The dashed line indicates a cross-

Figure S2.11 (cont'd)
link between BofA A41C and SpoIVFB V86C that was observed. At *Right*, the top view of the model is shown. The dashed lines indicate observed cross-links between SpoIVFB residue M30C (located in the loop connecting TMS1 and TMS2) and BofA L62C and V63C (in a loop near the C-terminal end of TMS2). (*B*) Cleavage assays examining the effects of Cys substitutions in cytTM-SpoIVFB or GFPΔ27BofA. pET Duet plasmids were used to produce Pro-σ^K(1-127) in combination with cytTM-SpoIVFB from pYZ2 as a control (lane 1) or with the indicated Cys-substituted cytTM-SpoIVFB from pSO141 or pSO256-pSO259 in *E. coli* (*Left*). pET Quartet plasmids were used to produce Pro-σ^K(1-127), cytTM-SpoIVFB, and SpoIVFA in combination with GFPΔ27BofA from pSO40 as a control (lane 7) or with the indicated Cys-substituted GFPΔ27BofA from pSO142, pSO143, or pSO260-pSO263 in *E. coli* (*Right*). Samples collected after 2 h of IPTG induction were subjected to immunoblot analysis with SpoIVFA, GFP, and/or penta-His antibodies as indicated. The single star (*) indicates cross-reacting proteins below SpoIVFA and the double star (**) indicates breakdown species of GFPΔ27BofA. A breakdown species below SpoIVFA (not indicated) is observed in some samples. The graphs show quantification of the cleavage ratio (cleavage product/[Pro-σ^K(1-127) + cleavage product]) for n=3 biological replicates with error bars indicating 1 standard deviation. (*C*) Disulfide cross-linking of single-Cys cytTM-SpoIVFB variants to single-Cys MBPΔ27BofA variants. pET Quartet plasmids (pSO93 as a control in lanes 1 & 2, pSO144, pSO147, pSO148, pSO186-pSO190) were used to produce single-Cys cytTM-SpoIVFB E44Q variants in combination with single-Cys MBPΔ27BofA variants, and Cys-less variants of SpoIVFA and Pro-σ^K(1-127) in *E. coli*. Samples collected after 2 h of IPTG induction were treated with Cu^{2+}(phenanthroline)$_3$ (Cu +) for 60 min or with 2-phenanthroline (Cu –) as a control. Samples were treated with TCA to precipitate proteins and resuspended in sample buffer with DTT (+) or without (–) and subjected to immunoblot analysis with FLAG antibodies to visualize cytTM-SpoIVFB monomer, dimer, and complex with MBPΔ27BofA. A representative result from two biological replicates is shown.

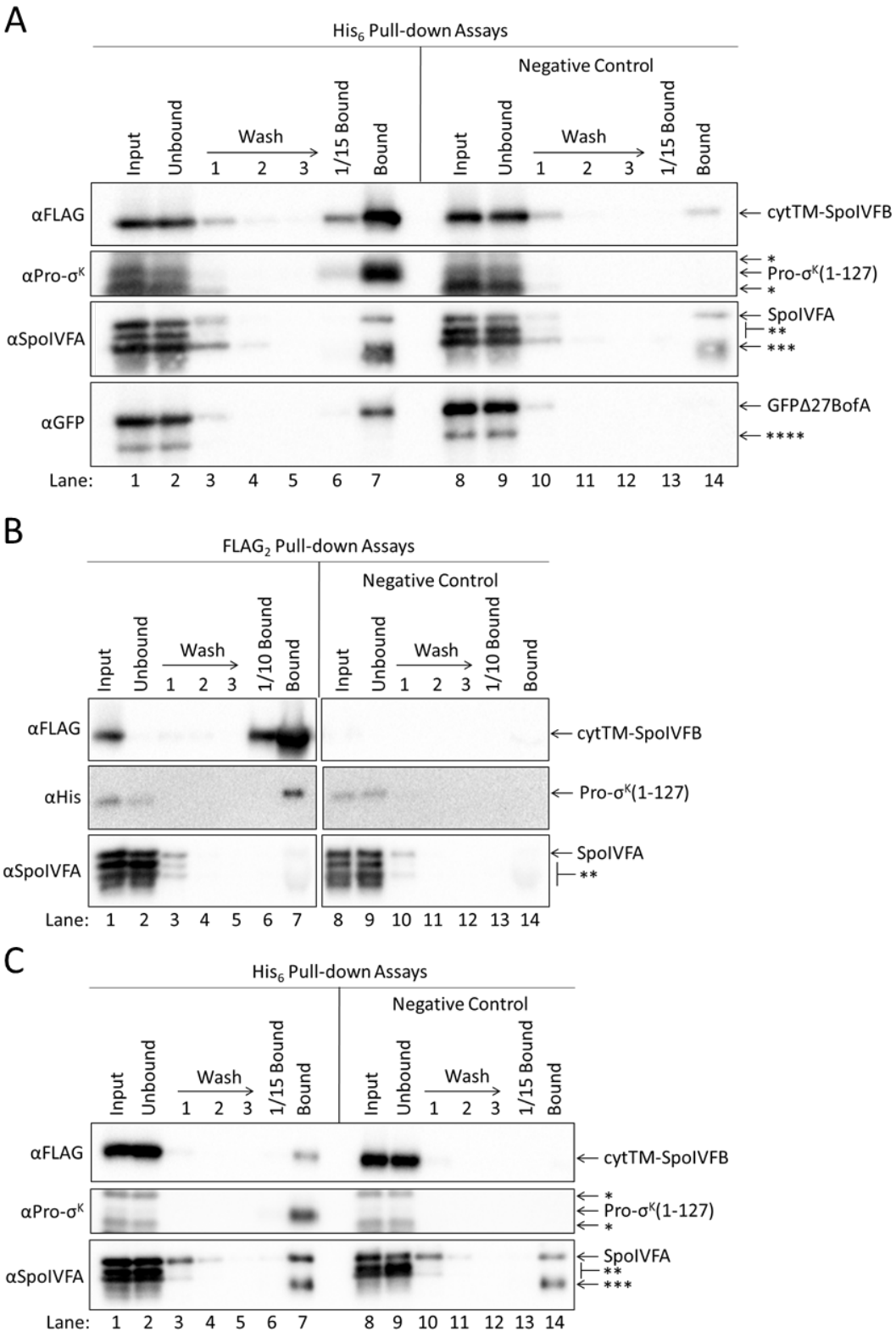

Figure S2.12 Neither GFPΔ27BofA nor native BofA when co-produced with SpoIVFA prevent Pro-σ^K(1-127) from interacting with SpoIVFB. (*A*) GFPΔ27BofA and SpoIVFA do not prevent SpoIVFB from co-purifying with Pro-σ^K(1-127). pET Quartet plasmids were used to

Figure S2.12 (cont'd)
produce Pro-σ^K(1-127) (pSO73), or a variant lacking His_6 as a negative control (pSO82), in combination with a catalytically-inactive E44C cytTM-SpoIVFB variant containing $FLAG_2$ but lacking His_6, GFPΔ27BofA, and SpoIVFA in *E. coli*. Samples collected after 2 h of IPTG induction were subjected to co-purification with cobalt resin. Input, unbound, wash, 1/15 bound (diluted to match input), and (undiluted) bound samples were subjected to immunoblot analysis with FLAG, Pro-σ^K, SpoIVFA, and GFP antibodies as indicated. The single star (*) indicates cross-reacting proteins above and below Pro-σ^K(1-127) that fail to co-purify. The double star (**) indicates cross-reacting proteins below SpoIVFA that fail to co-purify. The triple star (***) indicates a putative breakdown species of SpoIVFA that appears to co-purify, but also binds non-specifically. The quadruple star (****) indicates a cross-reacting protein or breakdown species of GFPΔ27BofA that fails to co-purify. (*B*) Native BofA and SpoIVFA do not prevent Pro-σ^K(1-127) from co-purifying with SpoIVFB. pET Quartet plasmids were used to produce a catalytically-inactive E44C cytTM-SpoIVFB variant containing $FLAG_2$ but lacking His_6 (pSO215), or a variant lacking $FLAG_2$ as a negative control (pSO217), in combination with Pro-σ^K(1-127), native BofA, and SpoIVFA in *E. coli*. Samples collected after 2 h of IPTG induction were subjected to co-immunoprecipitation with anti-FLAG antibody beads. Input, unbound, wash, 1/10 bound (diluted to match input), and (undiluted) bound samples were subjected to immunoblot analysis with FLAG, penta-His, and SpoIVFA antibodies as indicated. Stars indicate proteins as in *A*. (*C*) Native BofA and SpoIVFA do not prevent SpoIVFB from co-purifying with Pro-σ^K(1-127). pET Quartet plasmids were used to produce Pro-σ^K(1-127) (pSO215), or a variant lacking His_6 as a negative control (pSO216), in combination with a catalytically-inactive E44C cytTM-SpoIVFB variant containing $FLAG_2$ but lacking His_6, native BofA, and SpoIVFA in *E. coli*. Samples collected after 2 h of IPTG induction were subjected to co-purification with cobalt resin. Input, unbound, wash, 1/15 bound (diluted to match input), and (undiluted) bound samples were subjected to immunoblot analysis with FLAG, Pro-σ^K, and SpoIVFA antibodies as indicated. Stars indicate proteins as in *A*. A representative result from two biological replicates is shown in each panel.

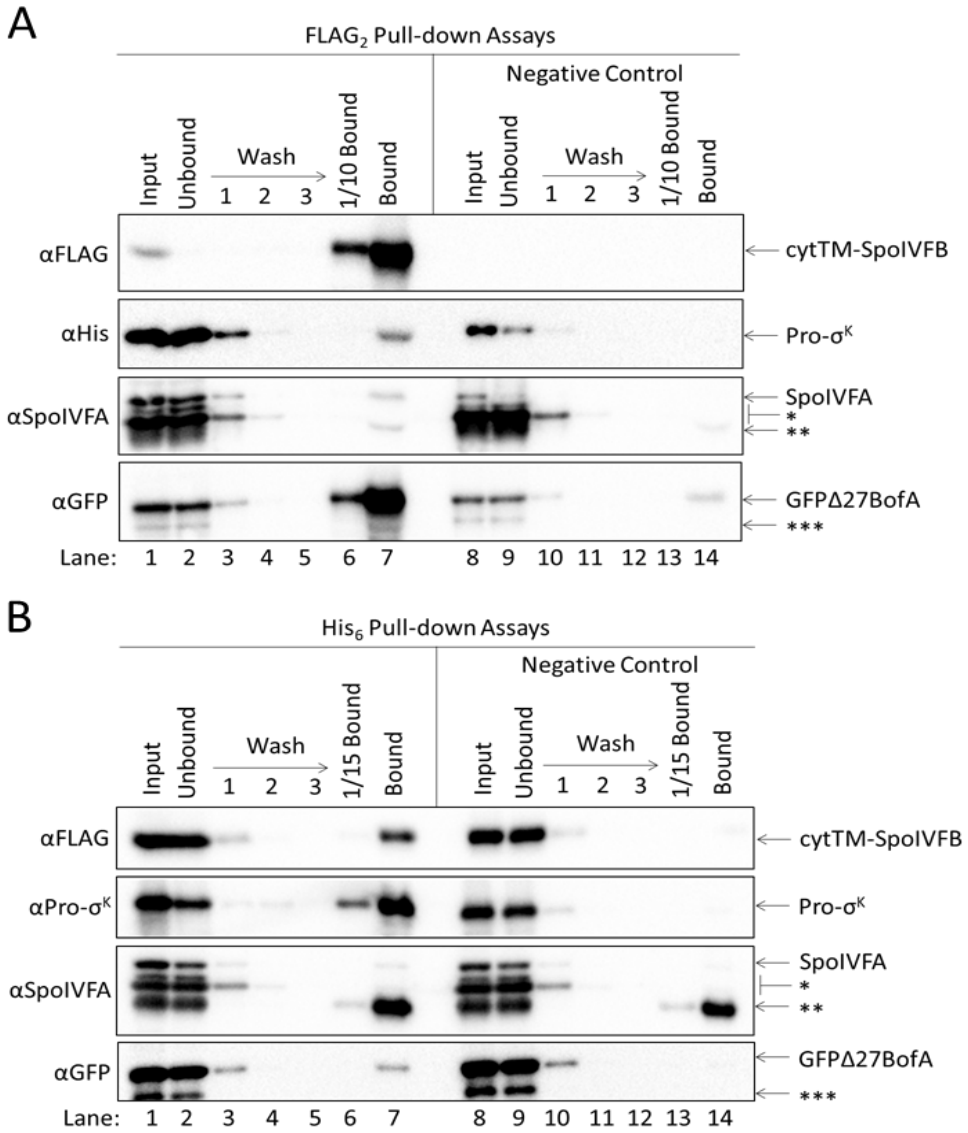

Figure S2.13 GFPΔ27BofA and SpoIVFA do not prevent full-length Pro-σ^K from interacting with SpoIVFB. (*A*) GFPΔ27BofA and SpoIVFA do not prevent Pro-σ^K from co-purifying with SpoIVFB. pET Quartet plasmids were used to produce a catalytically-inactive E44C cytTM-SpoIVFB variant containing $FLAG_2$ but lacking His_6 (pSO211), or a variant lacking $FLAG_2$ as a negative control (pSO221), in combination with Pro-σ^K-His_6, GFPΔ27BofA, and SpoIVFA in *E. coli*. Samples collected after 2 h of IPTG induction were subjected to co-immunoprecipitation with anti-FLAG antibody beads. Input, unbound, wash, 1/10 bound (diluted to match input), and (undiluted) bound samples were subjected to immunoblot analysis with FLAG, penta-His, SpoIVFA, and GFP antibodies as indicated. The single star (*) indicates cross-reacting proteins below SpoIVFA that fail to co-purify. The double star (**) indicates a putative breakdown species of SpoIVFA that appears to co-purify, but also binds non-specifically. The triple star (***) indicates a cross-reacting protein or breakdown species of GFPΔ27BofA that fails to co-purify. (*B*) GFPΔ27BofA and SpoIVFA do not prevent SpoIVFB from co-purifying with Pro- σ^K. pET Quartet plasmids were used to produce Pro-σ^K-His_6

Figure S2.13 (cont'd)
(pSO211), or a variant lacking His_6 as a negative control (pSO220), in combination with a catalytically-inactive E44C cytTM-SpoIVFB variant containing $FLAG_2$ but lacking His_6, GFPΔ27BofA, and SpoIVFA in *E. coli*. Samples collected after 2 h of IPTG induction were subjected to co-purification with cobalt resin. Input, unbound, wash, 1/15 bound (diluted to match input), and (undiluted) bound samples were subjected to immunoblot analysis with FLAG, Pro-σ^K, SpoIVFA, and GFP antibodies as indicated. Stars indicate proteins as in *A*. A representative result from two biological replicates is shown in each panel.

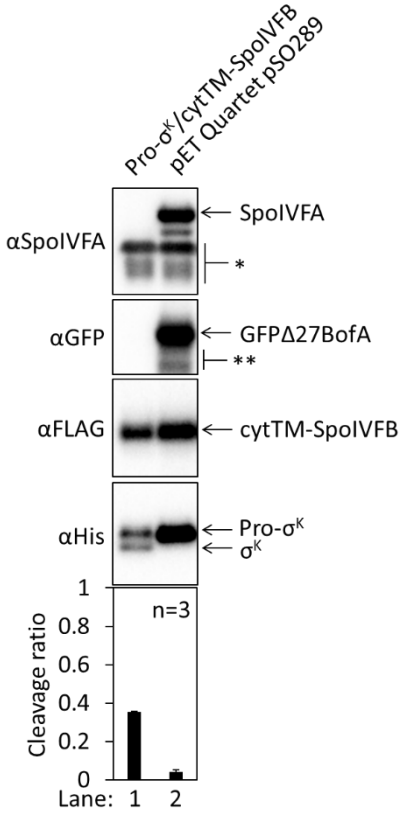

Figure S2.14 GFPΔ27BofA and SpoIVFA strongly inhibit cleavage of full-length Pro-σ^K by SpoIVFB. Pro-σ^K and cytTM-SpoIVFB were produced from pSO290 as a control (lane 1), or pET Quartet plasmid pSO289 was used to produce Pro-σ^K, cytTM-SpoIVFB, SpoIVFA, and GFPΔ27BofA (lane 2). Samples collected after 2 h of IPTG induction were subjected to immunoblot analysis with SpoIVFA, GFP, or penta-His antibodies as indicated. The single star (*) indicates cross-reacting proteins below SpoIVFA and the double star (**) indicates breakdown species of GFPΔ27BofA. A breakdown species below SpoIVFA (not indicated) is observed. The graph shows quantification of the cleavage ratio (σ^K/[Pro-σ^K + σ^K]) for n=3 biological replicates with error bars indicating 1 standard deviation.

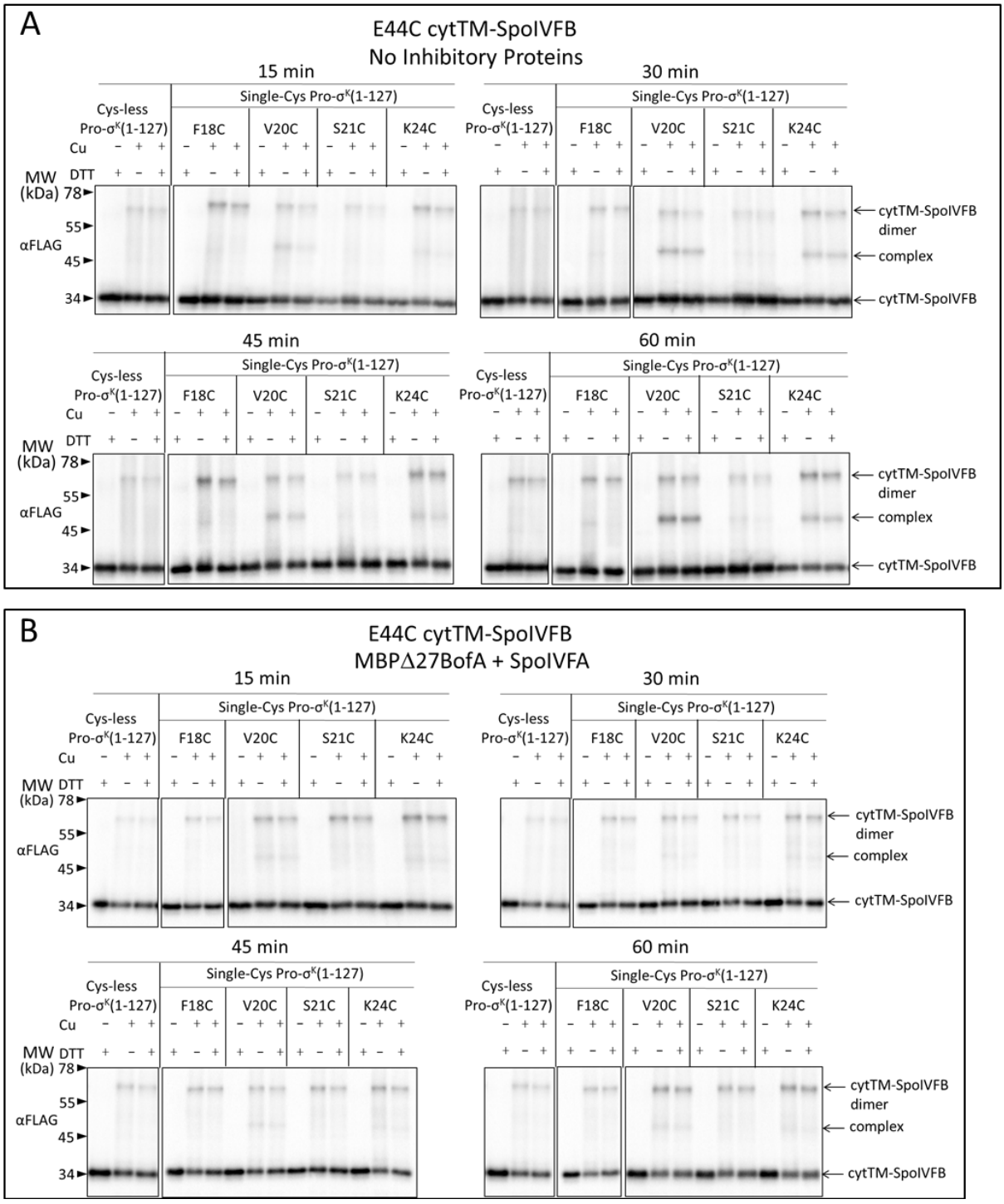

Figure S2.15 Effects of MBPΔ27BofA on disulfide cross-linking between the active site region of cytTM-SpoIVFB and the Proregion of Pro-σ^K(1-127). (*A*) Time course of cross-linking between single-Cys E44C cytTM-SpoIVFB and single-Cys Pro-σ^K(1-127) variants in the absence of inhibitory proteins. See the Figure 2.6A legend for explanation of the experiment. (*B*) Time course of cross-linking between single-Cys E44C cytTM-SpoIVFB and single-Cys Pro-σ^K(1-127) variants in the presence of Cys-less variants of MBPΔ27BofA and SpoIVFA. See

Figure S2.15 (cont'd)
the Figure 2.6C legend for explanation of the experiment. Representative results from two biological replicates are shown in *A* and *B*.

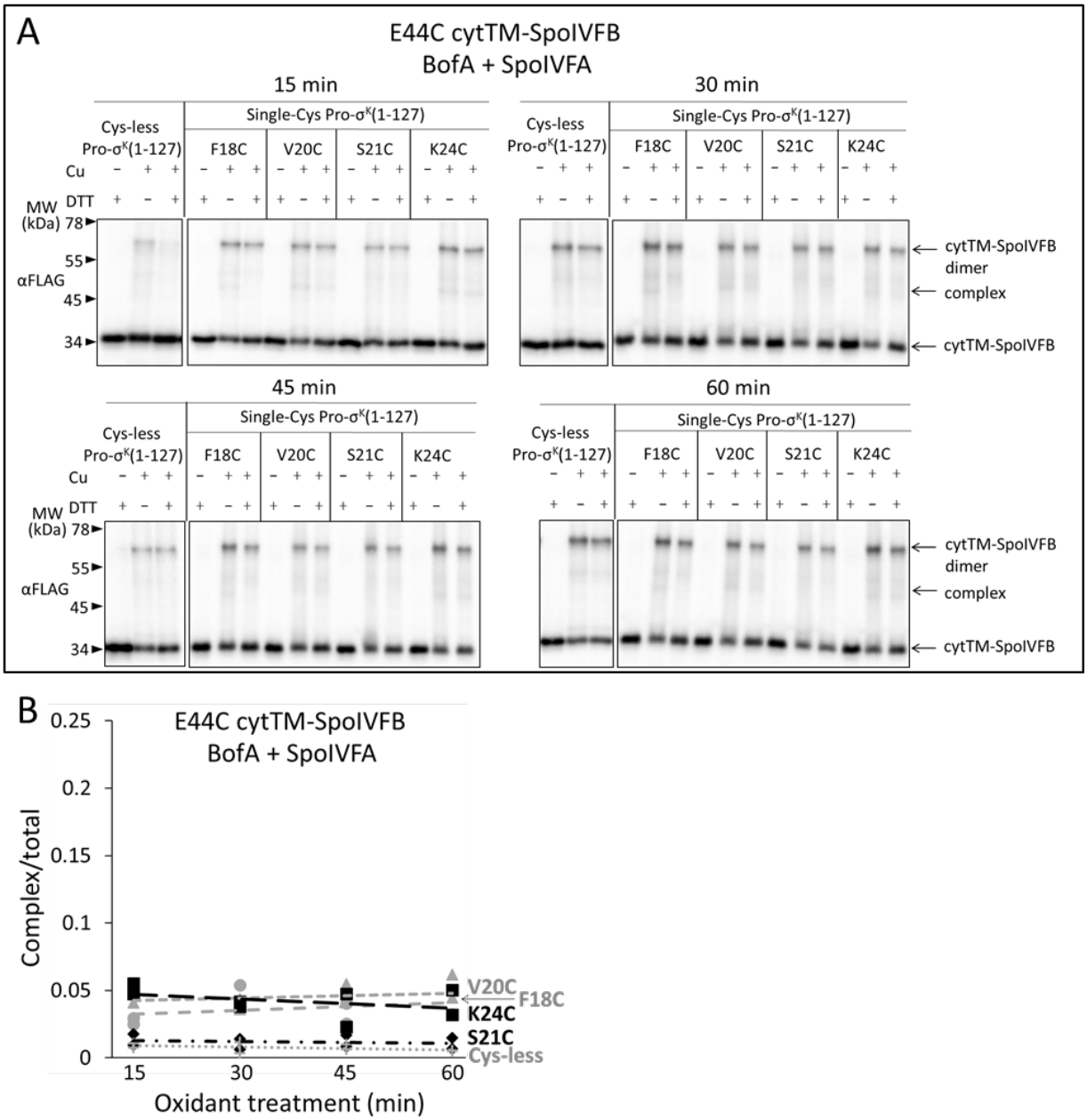

Figure S2.16 Effects of full-length BofA on disulfide cross-linking between the active site region of cytTM-SpoIVFB and the Proregion of Pro-σ^K(1-127). (*A*) Time course of cross-linking between single-Cys E44C cytTM-SpoIVFB and single-Cys Pro-σ^K(1-127) variants in the presence of Cys-less variants of BofA and SpoIVFA. pET Quartet plasmids were used to produce single-Cys E44C cytTM-SpoIVFB in combination with single-Cys Pro-σ^K(1-127) F18C (pSO238), V20C (pSO234), S21C (pSO235), or K24C (pSO239), or with Cys-less Pro-σ^K(1-127) (pSO229) as a negative control, and Cys-less variants of BofA and SpoIVFA in *E. coli*. Samples collected after 2 h of IPTG induction were treated and subjected to immunoblot analysis as explained in the Figure 2.6A legend. Representative results from two biological replicates are shown. (*B*) Quantification of cross-linking. Abundance of the complex was divided by the total amount of cytTM-SpoIVFB monomer, dimer, and complex. The ratio over time was plotted (n=2) with a best-fit trend line.

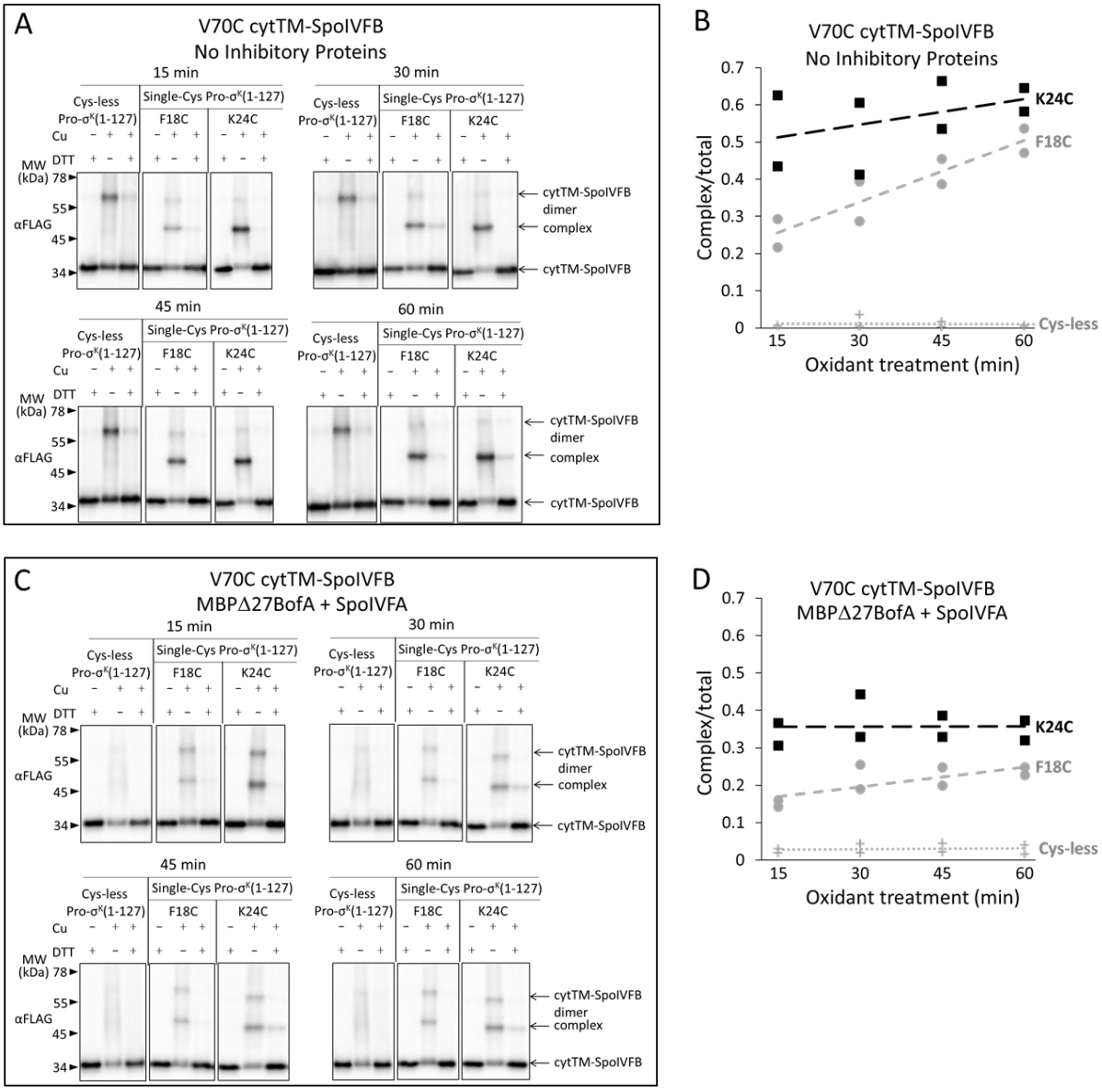

Figure S2.17 Effects of BofA on disulfide cross-linking between the membrane-reentrant loop of cytTM-SpoIVFB and the Proregion of Pro-σ^K(1-127). (*A*) Timecourse of disulfide cross-linking between the single-Cys V70C cytTM-SpoIVFB E44Q and single-Cys Pro-σ^K(1-127) variants in the absence of inhibitory proteins. pET Duet plasmids were used to produce single-Cys V70C cytTM-SpoIVFB E44Q in combination with single-Cys F18C (pSO168) or K24C (pSO134) Pro-σ^K(1-127), or with Cys-less Pro-σ^K(1-127) (pSO136) as a negative control, in *E. coli*. Samples collected after 2 h of IPTG induction were treated and subjected to immunoblot analysis as explained in the Figure 2.6A legend. Representative results from two biological replicates are shown. (*B*) Quantification of cross-linking for the experiment described in *A*. Signal intensity of the complex was divided by the total intensity of the monomer, dimer, and complex. The ratio over time was plotted (n=2) with a best-fit trend line. (*C*) Timecourse of disulfide cross-linking between single-Cys V70C cytTM-SpoIVFB E44Q and single-Cys Pro-

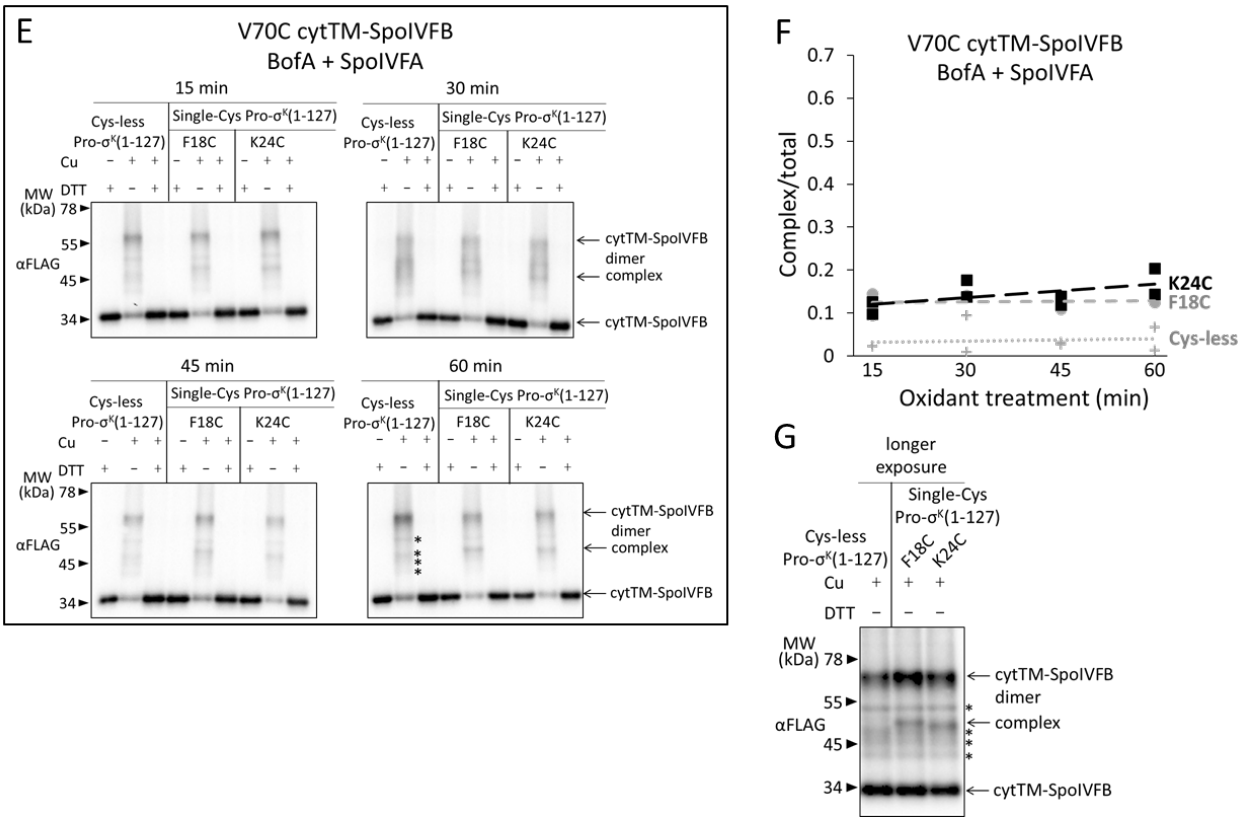

Figure S2.17 (cont'd)
σ^K(1-127) variants in the presence of Cys-less variants of MBPΔ27BofA and SpoIVFA. pET Quartet plasmids were used to produce single-Cys V70C cytTM-SpoIVFB E44Q in combination with single-Cys F18C (pSO164) or K24C (pSO132) Pro-σ^K(1-127), or with Cys-less Pro-σ^K(1-127) (pSO111) as a negative control, and Cys-less variants of MBPΔ27BofA and SpoIVFA in *E. coli*. Samples collected after 2 h of IPTG induction were treated and subjected to immunoblot analysis as explained in the Figure 2.6A legend. Representative results from two biological replicates are shown. (*D*) Quantification of cross-linking for the experiment described in *C*. Quantification was performed as described in *B*. (*E*) Timecourse of disulfide cross-linking between single-Cys V70C cytTM-SpoIVFB E44Q and single-Cys Pro-σ^K(1-127) variants in the presence of Cys-less variants of BofA and SpoIVFA. pET Quartet plasmids were used to produce the single-Cys V70C cytTM-SpoIVFB E44Q in combination with single-Cys F18C (pSO236) or K24C (pSO237) Pro-σ^K(1-127), or with Cys-less Pro-σ^K(1-127) (pSO230) as a negative control, and Cys-less variants of BofA and SpoIVFA in *E. coli*. Samples collected after 2 h of IPTG induction were treated and subjected to immunoblot analysis as explained in the Figure 2.6A legend. Representative results from two biological replicates are shown. (*F*) Quantification of cross-linking for the experiment described in *E*. Quantification was performed as described in *B*. (*G*) Immunoblot of 60-min samples (Cu +) from the experiment described in *E* with a longer exposure (30 sec). Stars (*) indicate four novel species.

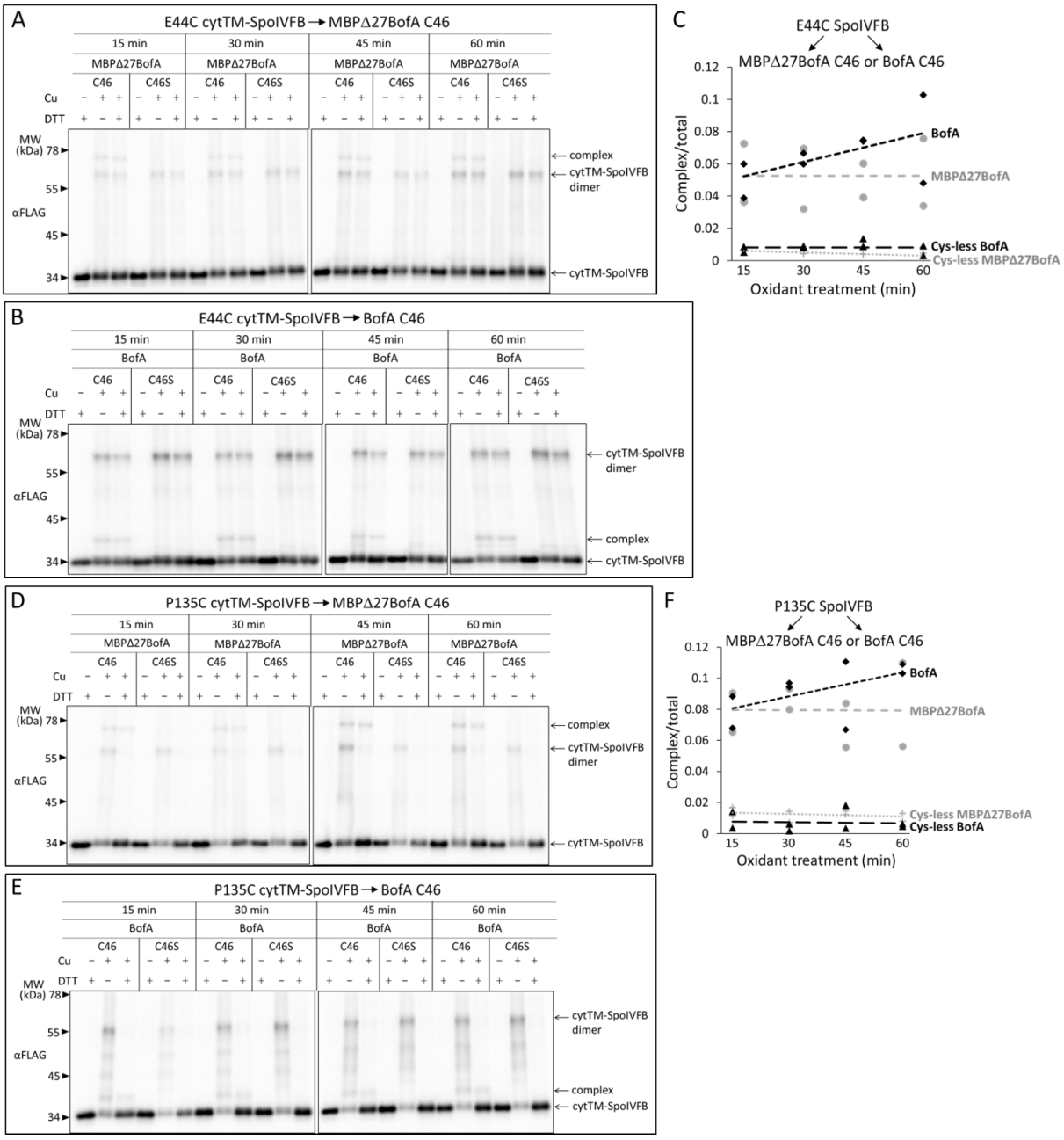

Figure S2.18 Disulfide cross-linking between the active site region of cytTM-SpoIVFB and MBPΔ27BofA or full-length BofA. (*A* and *B*) Time courses of cross-linking between single-Cys E44C cytTM-SpoIVFB and MBPΔ27BofA C46 or full-length BofA C46. pET Quartet plasmids were used to produce single-Cys E44C cytTM-SpoIVFB in combination with MBPΔ27BofA C46 (pSO91) or BofA C46 (pSO226), or with Cys-less MBPΔ27BofA C46S (pSO110) or BofA C46S (pSO229) variants as negative controls, and Cys-less variants of Pro-σ^K(1-127) and SpoIVFA in *E. coli*. Samples collected after 2 h of IPTG induction were treated and subjected to immunoblot analysis as explained in the Figure 2.6A legend. Representative results from two biological replicates are shown. (*C*) Quantification of cross-linking for the experiments described in *A* and *B*. Abundance of the complex was divided by the total amount

Figure S2.18 (cont'd)
of cytTM-SpoIVFB monomer, dimer, and complex. The ratio over time was plotted (n=2) with a best-fit trend line. (*D* and *E*) Time courses of cross-linking between single-Cys P135C cytTM-SpoIVFB and MBPΔ27BofA C46 or full-length BofA C46. pET Quartet plasmids were used to produce single-Cys P135C cytTM-SpoIVFB in combination with MBPΔ27BofA C46 (pSO93) or BofA C46 (pSO228), or with Cys-less MBPΔ27BofA C46S (pSO112) or (BofA C46S (pSO231) variants as negative controls, and Cys-less variants of Pro-σ^K(1-127) and SpoIVFA in *E. coli*. Samples collected after 2 h of IPTG induction were treated and subjected to immunoblot analysis as explained in the Figure 2.6A legend. Representative results from two biological replicates are shown. (*F*) Quantification of cross-linking for the experiments described in *D* and *E*. Quantification was performed as described in *C*.

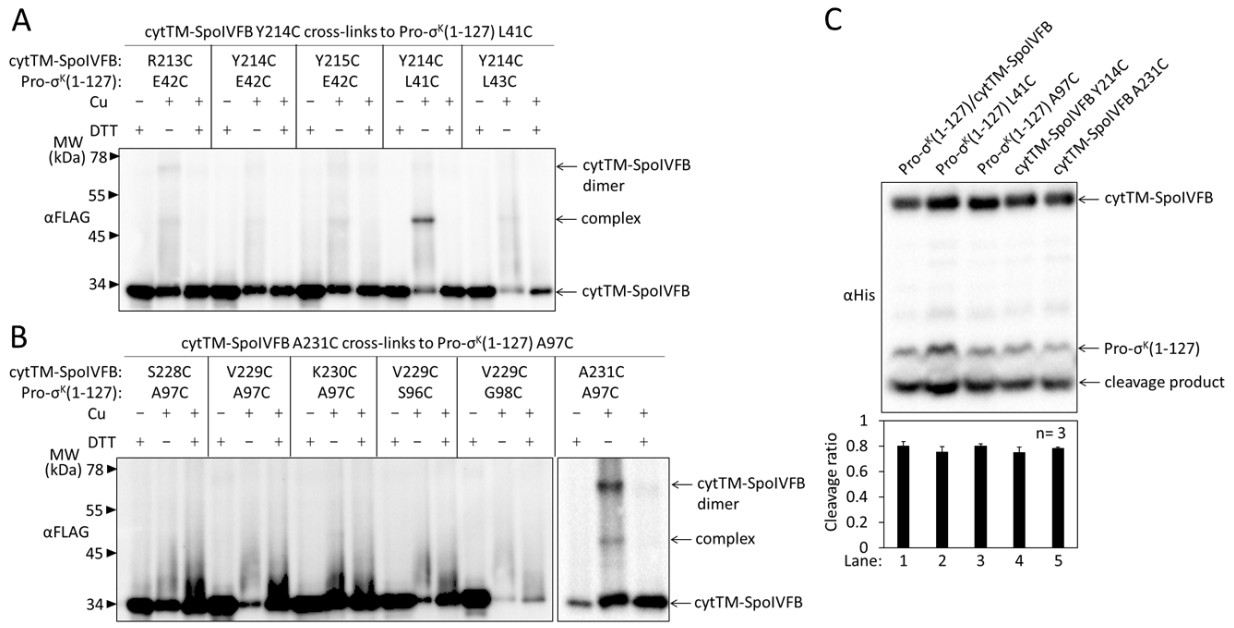

Figure S2.19 Disulfide cross-linking between the interdomain linker or CBS domain of cytTM-SpoIVFB and Pro-σ^K(1-127). (*A*) Cross-linking between single-Cys cytTM-SpoIVFB variants with Cys located in the interdomain linker and single-Cys Pro-σ^K(1-127) variants. pET Duet plasmids (pSO117- pSO121) were used to produce single-Cys R213C, Y214C, or Y215C cytTM-SpoIVFB E44Q variants in combination with single-Cys L41C, E42C, or L43C Pro-σ^K(1-127) variants in *E. coli*. Samples collected after 2 h of IPTG induction were treated with Cu^{2+}(phenanthroline)$_3$ (oxidant; Cu +) for 60 min or with 2-phenanthroline (Cu –) as a control. Samples were treated with TCA to precipitate proteins and resuspended in sample buffer with DTT (+) or without (–) and subjected to immunoblot analysis with FLAG antibodies to visualize cytTM-SpoIVFB monomer, dimer, and complex with Pro-σ^K(1-127). (*B*) Cross-linking between single-Cys cytTM-SpoIVFB variants with Cys located in the CBS domain and single-Cys Pro-σ^K(1-127) variants. pET Duet plasmids (pSO122- pSO126, pSO130) were used to produce single-Cys S228C, V229C, K230C or A231C cytTM-SpoIVFB E44Q variants in combination with single-Cys S96C, A97C, or G98C Pro-σ^K(1-127) variants in *E. coli*. Samples collected after 2 h of IPTG induction were treated and subjected to immunoblot analysis as in *A*. Representative results from two biological replicates are shown in *A* and *B*. (*C*) Cleavage assays examining the effects of Cys substitutions in cytTM-SpoIVFB or Pro-σ^K(1-127). pET Duet plasmids were used to produce Pro-σ^K(1-127) and cytTM-SpoIVFB from pYZ2 as a control (lane 1), cytTM-SpoIVFB and the indicated Cys-substituted Pro-σ^K(1-127) from pSO157 or pSO158 (lanes 2 & 3), or Pro-σ^K(1-127) and the indicated Cys-substituted cytTM-SpoIVFB from pSO159 or pSO160 (lanes 4 & 5) of in *E. coli*. Samples collected after 2 h of IPTG induction were subjected to immunoblot analysis with penta-His antibodies. The graph shows quantification of the cleavage ratio (cleavage product/[Pro-σ^K(1-127) + cleavage product]) for n=3 biological replicates with error bars indicating 1 standard deviation.

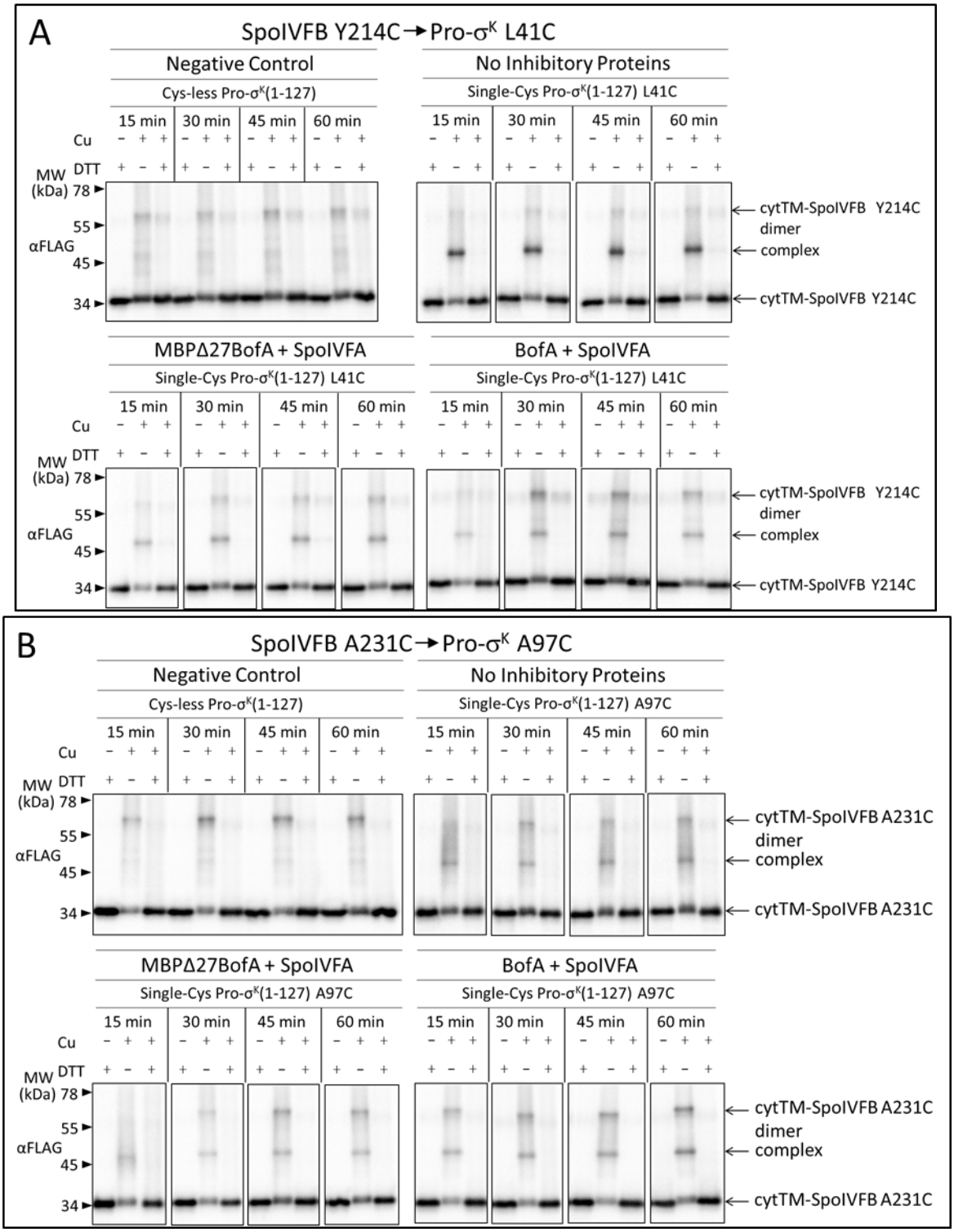

Figure S2.20 Effects of BofA on disulfide cross-linking between the interdomain linker or CBS domain of cytTM-SpoIVFB and Pro-σ^K(1-127). (*A*) Time course of cross-linking between the single-Cys Y214C linker variant of cytTM-SpoIVFB E44Q and single-Cys L41C

Figure S2.20 (cont'd)
Pro-σ^K(1-127) in the absence or presence of inhibitory proteins. pET Duet plasmids were used to produce single-Cys Y214C cytTM-SpoIVFB E44Q in combination with single-Cys L41C Pro-σ^K(1-127) from pSO120 in the absence of inhibitory proteins (No BofA) or with Cys-less Pro-σ^K(1-127) from pSO114 as a negative control, in *E. coli*. pET Quartet plasmids were used to produce single-Cys Y214C cytTM-SpoIVFB E44Q, single-Cys L41C Pro-σ^K(1-127), and Cys-less SpoIVFA in combination with Cys-less MBPΔ27BofA from pSO127 (MBPΔ27BofA) or with Cys-less full-length BofA from pSO245 (BofA) in *E. coli*. Samples collected after 2 h of IPTG induction were treated and subjected to immunoblot analysis as explained in the Figure 2.6A legend. Representative results from two biological replicates are shown. (*B*) Time course of cross-linking between the single-Cys A231C CBS domain variant of cytTM-SpoIVFB E44Q and single-Cys A97C Pro-σ^K(1-127) in the absence or presence of inhibitory proteins. pET Duet plasmids were used to produce single-Cys A231C cytTM-SpoIVFB E44Q in combination with single-Cys Pro-σ^K(1-127) A97C from pSO130 in the absence of inhibitory proteins (No BofA) or with Cys-less Pro-σ^K(1-127) from pSO255 as a negative control, in *E. coli*. pET Quartet plasmids were used to produce single-Cys A231C cytTM-SpoIVFB E44Q, single-Cys A97C Pro-σ^K(1-127), and Cys-less SpoIVFA in combination with Cys-less MBPΔ27BofA from pSO133 (MBPΔ27BofA) or with Cys-less full-length BofA from pSO246 (BofA) in *E. coli*. Samples collected after 2 h of IPTG induction were treated and subjected to immunoblot analysis as in *A*. Representative results from two biological replicates are shown.

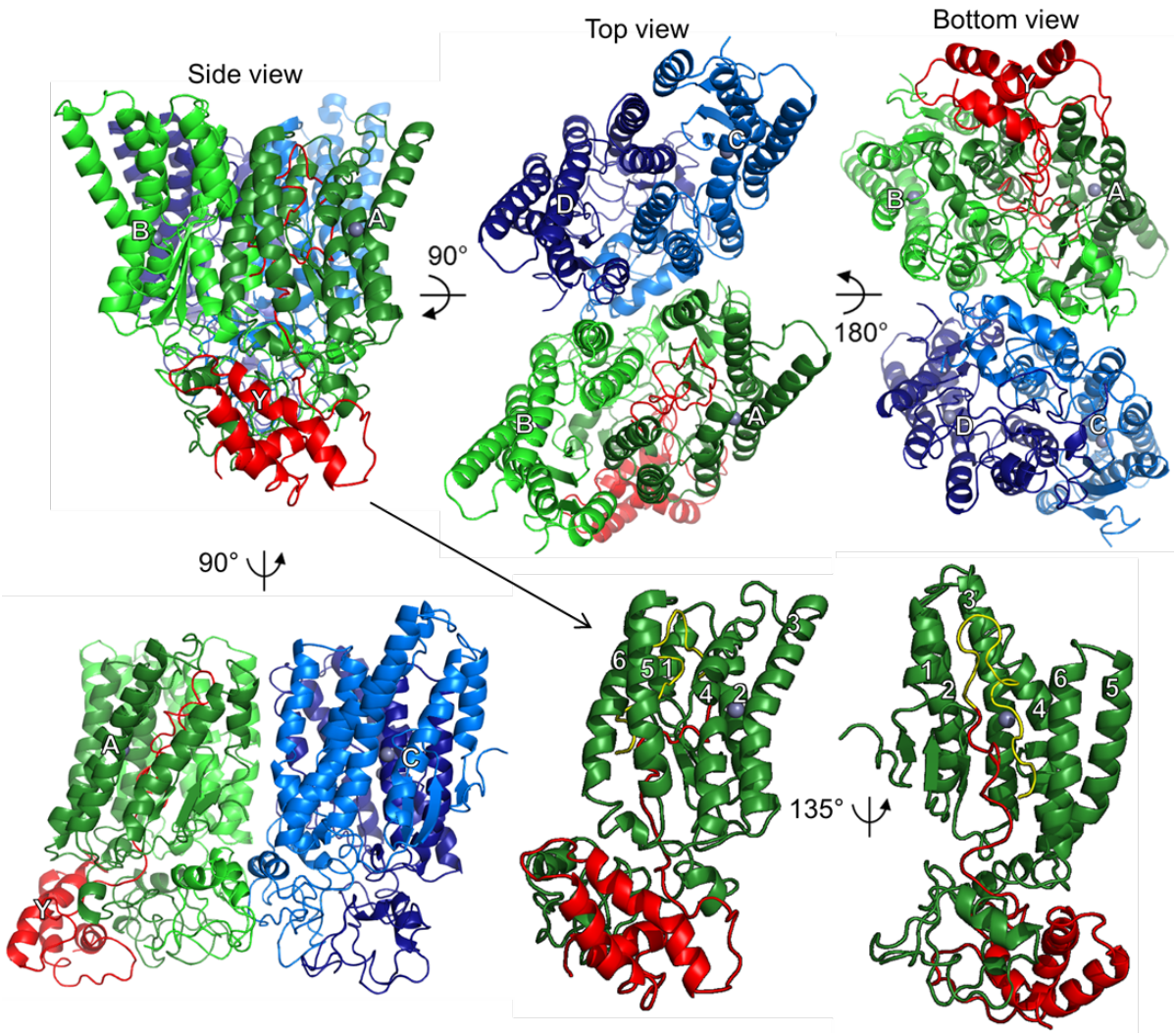

Figure S2.21. Model of SpoIVFB tetramer with part of one Pro-σ^K molecule. At *Upper Left*, a side view shows the SpoIVFB membrane domains at the top and the CBS domains at the bottom, facing the A (dark green) and B chains (light green), whose CBS domains primarily provide the dimerization interface. The SpoIVFB A chain also interacts with the Pro-σ^K Y chain (residues 1-114) (red). The top view (*Center*) reveals the SpoIVFB C (light blue) and D (dark blue) chains, whose CBS domains dimerize. The bottom view (*Upper Right*) emphasizes the CBS domains, as well as the interface between the A/B and C/D dimers, formed primarily by the CBS domains of the B and C chains. At *Lower Left*, a side view facing the A and C chains also shows the interface between the A/B and C/D dimers of the SpoIVFB tetramer. Each SpoIVFB chain is labeled near its zinc ion (gray), which is hidden in some views. At *Lower Center*, a side view of the SpoIVFB A chain monomer (TMSs 1-6 labeled) interacting with the Pro-σ^K Y chain (Proregion residues 1-21 yellow and σ^K residues 22-114 red), in the same orientation as at *Upper Left* (hence the arrow), but with the other SpoIVFB chains hidden. At *Lower Right*, a side view into the active site region of the SpoIVFB A chain emphasizes proximity between the zinc ion and the cleavage site in the Pro-σ^K Y chain (between residues 21 and 22).

Discussion

BofA and SpoIVFA May Prevent Pro-σ^K from Interacting with SpoIVFB Prior to Activation during Sporulation. Stable association of Pro-σ^K with SpoIVFB depended on SpoIVB during *B. subtilis* sporulation, presumably to cleave SpoIVFA and thus initiate relief of SpoIVFB inhibition [49]. In the absence of SpoIVB, Pro-σ^K did not co-immunoprecipitate with SpoIVFB(E44Q)-GFP using anti-GFP antibody resin and Pro-σ^K-CFP did not co-localize with SpoIVFB(E44Q)-YFP to the outer FS membrane using fluorescence microscopy. These results suggest that SpoIVFA and BofA prevent Pro-σ^K from interacting with SpoIVFB prior to activation, although it is possible that the SpoIVFB variants used in the experiments differ from wild-type SpoIVFB in their interaction with Pro-σ^K.

Our experiments employed cytTM-SpoIVFB variants and heterologous expression in growing *E. coli.* Neither GFPΔ27BofA nor full-length BofA when co-produced with SpoIVFA prevented co-purification of Pro-σ^K(1-127) and a cytTM-SpoIVFB variant in pull-down assays (Figs. 2.5 and S2.12) or interfered with disulfide cross-linking between the C-terminal regions of single-Cys Pro-σ^K(1-127) and cytTM-SpoIVFB variants (Figs. 2.6I and S2.20B). These results show that BofA and SpoIVFA do not prevent Pro-σ^K(1-127) from interacting with cytTM-SpoIVFB variants when the proteins are produced in *E. coli.* Neither did GFPΔ27BofA and SpoIVFA prevent full-length Pro-σ^K from interacting with a cytTM-SpoIVFB variant in *E. coli* (Figure S2.13), although the interaction appeared to be weakened by the presence of the C-terminal half of Pro-sigK (compare Figs. 2.5, S2.12A, and S2.13). Perhaps co-production of full-length BofA (rather than GFPΔ27BofA) and SpoIVFA would completely prevent Pro-σ^K from interacting with the cytTM-SpoIVFB variant in *E. coli.* It is worth noting that GFPΔ27BofA appeared to interact more strongly with the cytTM-SpoIVFB variant when Pro-σ^K

was co-produced (Figure S2.13A) than when Pro-σ^K(1-127) co-produced (Figure 2.5), as if the weaker interaction of full-length Pro-σ^K with the cytTM-SpoIVFB variant allowed GFPΔ27BofA instead to interact with the cytTM-SpoIVFB variant. This observation is consistent with competition between GFPΔ27BofA and Pro-σ^K for occupancy of the SpoIVFB active site region.

Despite the presence of substrate in pulled-down complexes when proteins were co-produced in *E. coli*, cleavage of both Pro-σ^K(1-127) (Figure 2.1B) and full-length Pro-σ^K (Figure S2.14) was strongly inhibited. Our cross-linking and modeling show how BofA and SpoIVFA interfere with access of the Pro-σ^K Proregion to the SpoIVFB active site region, yet allow interaction of the Pro-σ^K(1-127) C-terminal part with the SpoIVFB CBS domain (Figure 2.6 and 2.7). Whether BofA and SpoIVFA completely prevent full-length Pro-σ^K from interacting with wild-type SpoIVFB prior to activation during sporulation is an open question.

Materials and Methods

Immunoblot Analysis. Samples were subjected to immunoblot analysis as described [32]. Briefly, proteins were separated by SDS-PAGE using 14% Prosieve (Lonza) polyacrylamide gels and electroblotted to Immobilon-P membranes (Millipore). Protein migration was monitored using SeeBlue Plus2 Prestained Standard (Invitrogen) and blots were blocked with 5% nonfat dry milk (Meijer) in TBST (20 mM Tris-HCl pH 7.5, 0.5 M NaCl, 0.1% Tween 20) for 1 h at 25°C with shaking. Blots were probed with antibodies against His_6 (penta-His Qiagen catalog #34460; 1:10,000), $FLAG_2$ (Sigma catalog #A8592; 1:10,000), GFP [32] (1:10,000), MBP (NEB catalog #E8030S; 1:10,000), SpoIVFA [32] (1:3,000), Pro-σ^K [76] (1:3,000), and/or SpoIVFB [41, 46] (1:5,000) diluted in TBST with 2% milk, overnight at 4°C with shaking. Since the GFP, MBP, SpoIVFA, Pro-σ^K, and SpoIVFB antibodies were not HRP-

conjugated, they were detected with goat anti-rabbit-HRP antibody (Bio-Rad catalog #170-6515; 1:10,000) diluted in TBST with 2% milk, 1 h at 25°C with shaking. Signals were generated using the Western Lightning Plus ECL reagent (PerkinElmer) and detected using a ChemiDoc MP imaging system (Bio-Rad). Unsaturated signals were quantified using the Image Lab 5.1 software (Bio-Rad) lane and bands tool in order to determine the Pro-σ^K(1-127) cleavage ratio or the ratio of disulfide cross-linked complex to the total intensity of the cytTM-SpoIVFB variant monomer, dimer, and complex.

Disulfide Cross-Linking. Cells were mixed with chloramphenicol (200 μg/mL) and 2-phenanthroline (3 mM), collected by centrifugation (12,000 × *g* for 1 min), washed with 10 mM Tris-HCl pH 8.1 containing 3 mM 2-phenanthroline, and suspended in 10 mM Tris-HCl pH 8.1. Samples were treated with 1 mM Cu^{2+}(phenanthroline)$_3$ or 3 mM 2-phenanthroline (as a negative control) for 15, 30, 45 or 60 min at 37°C, followed by incubation with neocuproine (12.5 mM) for 5 min at 37°C. Cells were lysed and proteins were precipitated by addition of trichloroacetic acid (5%) and inversion every 5 min for 30 min on ice. Proteins were sedimented by centrifugation (12,000 × *g*) for 15 min at 4°C, the supernatant was removed, and the pellet was washed with cold acetone. The pellets were sedimented by centrifugation (12,000 × *g*) for 5 min at 4°C and the supernatants were discarded. The pellets were dried for 5 min at 25°C and resuspended in buffer (100 mM Tris-HCl pH 7.5, 1.5% SDS, 5 mM EDTA, 25 mM *N*-ethylmaleimide) for 30 min at 25°C. Portions were mixed with an equal volume of sample buffer (25 mM Tris-HCl pH 6.8, 2% SDS, 10% glycerol, 0.015% bromophenol blue) with or without 100 mM DTT, and were typically incubated at 37°C for 10 min, prior to immunoblot analysis. In experiments with single-Cys V70C cytTM-SpoIVFB E44Q, single-Cys Pro-σ^K(1-

127) variants, and Cys-less variants of BofA and SpoIVFA, samples were boiled 3 min prior to immunoblot analysis, which helped to resolve species (Figure S2.17E and S2.17G).

Modeling of Protein Complexes. The membrane domain of a SpoIVFB monomer was modeled initially based on the structure for the site-2 protease from *Methanocaldococcus jannaschii* (PDB code: 3B4R) [6]. The structure was combined with a CBS domain modeled based on the CBS-domain protein TM0935 from *Thermotoga martima* (PDB code: 1O50) [77]. The CBS domain provides a dimerization interface for the C-terminal part of SpoIVFB. The full-length dimer including the membrane domain was completed by considering predicted contacts from co-evolutionary coupling analysis. A tetramer was then built guided by the arrangement of transmembrane helices and orientation of CBS domains in the recently published full-length structure of the chloride proton exchanger CLC-7 (PDB code: 7JM6) [78] and again by considering contacts from co-evolutionary couplings. We note that the resulting dimer and tetramer models are different from our previous model for the SpoIVFB as we could take advantage of the new structural template and additional information from the co-evolutionary couplings. The initial model for the well-folded C-terminal part of Pro-σ^K (residues 40-114) was built based on the structure of RNA polymerase sigma subunit domain 2 (PDB code: 3UGO) [79]. Suitable templates are not available for BofA and the part of SpoIVFA modeled here. For these components, initial models were obtained based on the predicted intra-chain contacts from the co-evolutionary couplings.

The modeling under restraints was initially carried out using Cα-based coarse-grained models that were allowed to relax under restraints *via* cycles of energy minimization and short molecular dynamics simulations at elevated temperature as described in more detail previously

[46]. Restraints from cross-linking were applied as described previously [46]. Different from our previous work, we also applied extensive intra- and inter-chain restraints based on predicted contacts from co-evolutionary coupling analysis. In addition, we applied positional restraints to keep the structures of the SpoIVFB membrane and CBS domains and the folded C-terminus of Pro-σ^K close to their initial models while allowing subunits to move relative to each other as guided by the restraints. For BofA and SpoIVFA, individual helices were restrained internally but allowed to move relative to each other to find the optimal arrangement in complex with SpoIVFB, again guided by the predicted contact restraints. Contact restraints with respect to SpoIVFB were implemented as minimum distance restraints to the closest residue in any of the four subunits since contact predictions cannot distinguish between chemically equivalent oligomer units. All available experimental cross-links were applied but the list of predicted contacts was edited to exclude certain contacts incompatible with cross-linking data and previous biochemical data on the overall topology of the SpoIVFB-BofA-SpoIVFA complex when embedded into the membrane. Excluded contacts may reflect uncertainties in the prediction method as inter-chain contacts are more difficult to predict reliably. They may also indicate alternate biologically relevant interactions between SpoIVFB, BofA, and SpoIVFA that were not probed in the experiments *via* cross-linking.

Inter-residue contacts were predicted by trRosetta [80]. A multiple sequence alignment (MSA), the input of trRosetta, for a protein was generated using HHblits [81] to search against the UniClust30 database [82]. It was further curated to only include sequences that are related to spore formation and are from organisms which have both SpoIVFB and SpoIVFA sequences. To predict inter-protein contacts using trRosetta, a hybrid MSA was generated by pasting two interacting proteins' sequences that are from the same strain. Twenty glycines were inserted

between the target sequences to prevent irrelevant predictions near the pasted regions due to the proximity in the hybrid sequence. Similarly, gaps were inserted for the homologous sequences to preserve alignment with the *B. subtilis* proteins. The contact predictions for the inserted residues were ignored for further modeling.

Finally, the Cα models for the complexes were converted to an all-atom model using PyRosetta [83] with the curated predicted intra- and inter-protein contacts and the cross-linking constraints. First, the model was locally minimized in the Rosetta centroid representation. The cross-linking constraints and inter-protein contacts were used for the Cα model building. Predicted intra-protein contacts were also used only if their contact probabilities were higher than 0.15 and if they were not violated severely in the Cα model; a predicted contact was considered as a severe violation if its score was greater than 10 Rosetta energy units (REUs). The relative weights for each scoring term were 25, 0.25, and 0.1 for the cross-linking constraints, inter-protein contacts, and intra-protein contacts, respectively. To prevent large deviation from the Cα model, harmonic restraints were applied on every Cα atom with a force constant of 0.1 REU/$Å^2$. In addition, Rosetta centroid energy terms were also used: Ramachandran energy (1.0), omega angle potential (0.5), backbone hydrogen bond energy (5.0), and van der Waals energy (1.0) with weights in the parentheses. The minimization was performed for 100 steps. Then, the minimized structure was converted to an all-atom model, and the FastRelax protocol was applied to the model with the Rosetta scoring function (ref2015) [84] and the same cross-linking constraints, the contact predictions, and the harmonic restraints on Cα atoms that were used for the minimization. Eight all-atom models were generated from the Cα model, and a model with the least cross-linking constraint violations was selected. To generate final models, Zn^{2+} ions were added at the active sites of each subunit of SpoIVFB to be

coordinated with D137, H43, and H47 followed by another brief minimization using CHARMM under harmonic restraints on heavy atoms to accommodate the Zn^{2+} ions without clashes.

Table S2.1 Plasmids used in this study

Name	Description	Construction	Reference
pDR95	Ap^R Sp^R; P_{spoIID}-GFPΔ27BofA		[30]
pETproσ^K	Km^R; T7-Pro-σ^K-His_6		[85]
pPL29	Ap^R; single-Cys P135C cytTM-SpoIVFB E44Q-$FLAG_2$-His_6, which also has C35S C165L C167L C172S C246S substitutions in SpoIVFB		[45]
pSO6	Ap^R; T7-GFPΔ36BofA/SpoIVFA	pYZ46 was subjected to SDM[a] using primers SO-P13 and SO-P14, deleting residues 28-36 from GFPΔ27BofA.	This study
pSO10	Ap^R; T7-GFPΔ27+Δ85-87BofA/SpoIVFA	pYZ46 was subjected to SDM using primers SO-P11 and SO-P12, deleting residues 85-87 from GFPΔ27BofA.	This study
pSO25	Ap^R; T7-GFPΔ27BofA G40A/SpoIVFA	pYZ46 was subjected to SDM using primers SO-P48 and SO-P49, substituting G40A in GFPΔ27BofA.	This study
pSO26	Ap^R; T7-GFPΔ27BofA L44A/SpoIVFA	pYZ46 was subjected to SDM using primers SO-P50 and SO-P51, substituting L44A in GFPΔ27BofA.	This study
pSO27	Ap^R; T7-GFPΔ27BofA N48A/SpoIVFA	pYZ46 was subjected to SDM using primers SO-P52 and SO-P53, substituting N48A in GFPΔ27BofA.	This study
pSO28	Ap^R; T7-GFPΔ27BofA G51A/SpoIVFA	pYZ46 was subjected to SDM using primers SO-P54 and SO-P55, substituting G51A in GFPΔ27BofA.	This study
pSO29	Ap^R; T7-GFPΔ27BofA I60A/SpoIVFA	pYZ46 was subjected to SDM using primers SO-P56 and SO-P57, substituting I60A in GFPΔ27BofA.	This study
pSO30	Ap^R; T7-GFPΔ27BofA N61A/SpoIVFA	pYZ46 was subjected to SDM using primers SO-P58 and SO-P59, substituting N61A in GFPΔ27BofA.	This study
pSO31	Ap^R; T7-GFPΔ27BofA T64A/SpoIVFA	pYZ46 was subjected to SDM using primers SO-P60 and SO-P61, substituting T64A in GFPΔ27BofA.	This study
pSO32	Ap^R; T7-GFPΔ27BofA G69A/SpoIVFA	pYZ46 was subjected to SDM using primers SO-P62 and SO-P63, substituting G69A in GFPΔ27BofA.	This study
pSO33	Ap^R; T7-GFPΔ27BofA L71A/SpoIVFA	pYZ46 was subjected to SDM using primers SO-P64 and SO-P65, substituting L71A in GFPΔ27BofA.	This study
pSO34	Ap^R; T7-GFPΔ27BofA G72A/SpoIVFA	pYZ46 was subjected to SDM using primers SO-P66 and SO-P67, substituting G72A in GFPΔ27BofA.	This study

Table S2.1 (cont'd)

pSO35	Ap^R; T7-GFPΔ27BofA P74A/SpoIVFA	pYZ46 was subjected to SDM using primers SO-P68 and SO-P69, substituting P74A in GFPΔ27BofA.	This study
pSO36	Ap^R; T7-GFPΔ27BofA G75A/SpoIVFA	pYZ46 was subjected to SDM using primers SO-P70 and SO-P71, substituting G75A in GFPΔ27BofA.	This study
pSO37	Ap^R; T7-GFPΔ27BofA L79A/SpoIVFA	pYZ46 was subjected to SDM using primers SO-P72 and SO-P73, substituting L79A in GFPΔ27BofA.	This study
pSO38	Ap^R; T7-GFPΔ27BofA I86A/SpoIVFA	pYZ46 was subjected to SDM using primers SO-P74 and SO-P75, substituting I86A in GFPΔ27BofA.	This study
pSO39	Ap^R; T7-GFPΔ27BofA I87A/SpoIVFA	pYZ46 was subjected to SDM using primers SO-P76 and SO-P77, substituting I87A in GFPΔ27BofA.	This study
pSO40	Km^R; T7-Pro-σ^K(1-127)-His_6/T7-cytTM-SpoIVFB-$FLAG_2$-His_6/T7-GFPΔ27BofA/SpoIVFA	Fragment *T7-gfpΔ27bofA/spoIVFA* was amplified from pYZ46 using primers SO-P82 and SO-P90. Vector pYZ2 was amplified using primers SO-P80 and SO-P89. Fragment was joined to pYZ2 using GA[b].	This study
pSO42	Km^R; T7-Pro-σ^K(1-127)-His_6/T7-cytTM-SpoIVFB-$FLAG_2$-His_6/T7-GFPΔ36BofA/SpoIVFA	Fragment *gfpΔ36bofA/spoIVFA* was amplified from pSO6 using primers SO-P82 and SO-P83. Fragment was joined to pSO40 digested with NotI and NheI using GA.	This study
pSO43	Km^R; T7-Pro-σ^K(1-127)-His_6/T7-cytTM-SpoIVFB-$FLAG_2$-His_6/T7-GFPΔ27+Δ85-87BofA/SpoIVFA	Fragment *gfpΔ27+Δ85-87bofA/spoIVFA* was amplified from pSO10 using primers SO-P82 and SO-P83. Fragment was joined to pSO40 digested with NotI and NheI using GA.	This study
pSO44	Km^R; T7-Pro-σ^K(1-127)-His_6/T7-cytTM-SpoIVFB-$FLAG_2$-His_6/T7-GFPΔ27BofA G40A/SpoIVFA	Fragment *gfpΔ27bofA G40A/spoIVFA* was amplified from pSO25 using primers SO-P82 and SO-P83. Fragment was joined to pSO40 digested with NotI and NheI using GA.	This study
pSO45	Km^R; T7-Pro-σ^K(1-127)-His_6/T7-cytTM-SpoIVFB-$FLAG_2$-His_6/T7-GFPΔ27BofA L44A/SpoIVFA	Fragment *gfpΔ27bofA L44A/spoIVFA* was amplified from pSO26 using primers SO-P82 and SO-P83. Fragment was joined to pSO40 digested with NotI and NheI using GA.	This study
pSO46	Km^R; T7-Pro-σ^K(1-127)-His_6/T7-cytTM-SpoIVFB-$FLAG_2$-His_6/T7-GFPΔ27BofA N48A/SpoIVFA	Fragment *gfpΔ27bofA N48A/spoIVFA* was amplified from pSO27 using primers SO-P82 and SO-P83. Fragment was joined to pSO40 digested with NotI and NheI using GA.	This study

Table S2.1 (cont'd)

pSO47	Km^R; T7-Pro-σ^K(1-127)-His_6/T7-cytTM-SpoIVFB-$FLAG_2$-His_6/T7-GFPΔ27BofA G51A/SpoIVFA	Fragment *gfpΔ27bofA G51A/spoIVFA* was amplified from pSO28 using primers SO-P82 and SO-P83. Fragment was joined to pSO40 digested with NotI and NheI using GA.	This study
pSO48	Km^R; T7-Pro-σ^K(1-127)-His_6/T7-cytTM-SpoIVFB-$FLAG_2$-His_6/T7-GFPΔ27BofA I60A/SpoIVFA	Fragment *gfpΔ27bofA I60A/spoIVFA* was amplified from pSO29 using primers SO-P82 and SO-P83. Fragment was joined to pSO40 digested with NotI and NheI using GA.	This study
pSO49	Km^R; T7-Pro-σ^K(1-127)-His_6/T7-cytTM-SpoIVFB-$FLAG_2$-His_6/T7-GFPΔ27BofA N61A/SpoIVFA	Fragment *gfpΔ27bofA N61A/spoIVFA* was amplified from pSO30 using primers SO-P82 and SO-P83. Fragment was joined to pSO40 digested with NotI and NheI using GA.	This study
pSO50	Km^R; T7-Pro-σ^K(1-127)-His_6/T7-cytTM-SpoIVFB-$FLAG_2$-His_6/T7-GFPΔ27BofA T64A/SpoIVFA	Fragment *gfpΔ27bofA T64A/spoIVFA* was amplified from pSO31using primers SO-P82 and SO-P83. Fragment was joined to pSO40 digested with NotI and NheI using GA.	This study
pSO51	Km^R; T7-Pro-σ^K(1-127)-His_6/T7-cytTM-SpoIVFB-$FLAG_2$-His_6/T7-GFPΔ27BofA G69A/SpoIVFA	Fragment *gfpΔ27bofA G69A/spoIVFA* was amplified from pSO32 using primers SO-P82 and SO-P83. Fragment was joined to pSO40 digested with NotI and NheI using GA.	This study
pSO52	Km^R; T7-Pro-σ^K(1-127)-His_6/T7-cytTM-SpoIVFB-$FLAG_2$-His_6/T7-GFPΔ27BofA L71A/SpoIVFA	Fragment *gfpΔ27bofA L71A/spoIVFA* was amplified from pSO33 using primers SO-P82 and SO-P83. Fragment was joined to pSO40 digested with NotI and NheI using GA.	This study
pSO53	Km^R; T7-Pro-σ^K(1-127)-His_6/T7-cytTM-SpoIVFB-$FLAG_2$-His_6/T7-GFPΔ27BofA G72A/SpoIVFA	Fragment *gfpΔ27bofA G72A/spoIVFA* was amplified from pSO34 using primers SO-P82 and SO-P83. Fragment was joined to pSO40 digested with NotI and NheI using GA.	This study
pSO54	Km^R; T7-Pro-σ^K(1-127)-His_6/T7-cytTM-SpoIVFB-$FLAG_2$-His_6/T7-GFPΔ27BofA P74A/SpoIVFA	Fragment *gfpΔ27bofA P74A/spoIVFA* was amplified from pSO35 using primers SO-P82 and SO-P83. Fragment was joined to pSO40 digested with NotI and NheI using GA.	This study

Table S2.1 (cont'd)

pSO55	Km^R; T7-Pro-σ^K(1-127)-His_6/T7-cytTM-SpoIVFB-$FLAG_2$-His_6/T7-GFPΔ27BofA G75A/SpoIVFA	Fragment *gfpΔ27bofA G75A/spoIVFA* was amplified from pSO36 using primers SO-P82 and SO-P83. Fragment was joined to pSO40 digested with NotI and NheI using GA.	This study
pSO56	Km^R; T7-Pro-σ^K(1-127)-His_6/T7-cytTM-SpoIVFB-$FLAG_2$-His_6/T7-GFPΔ27BofA L79A/SpoIVFA	Fragment *gfpΔ27bofA L79A/spoIVFA* was amplified from pSO37 using primers SO-P82 and SO-P83. Fragment was joined to pSO40 digested with NotI and NheI using GA.	This study
pSO57	Km^R; T7-Pro-σ^K(1-127)-His_6/T7-cytTM-SpoIVFB-$FLAG_2$-His_6/T7-GFPΔ27BofA I86A/SpoIVFA	Fragment *gfpΔ27bofA I86A/spoIVFA* was amplified from pSO38 using primers SO-P82 and SO-P83. Fragment was joined to pSO40 digested with NotI and NheI using GA.	This study
pSO58	Km^R; T7-Pro-σ^K(1-127)-His_6/T7-cytTM-SpoIVFB-$FLAG_2$-His_6/T7-GFPΔ27BofA I87A/SpoIVFA	Fragment *gfpΔ27bofA I87A/spoIVFA* was amplified from pSO39 using primers SO-P82 and SO-P83. Fragment was joined to pSO40 digested with NotI and NheI using GA.	This study
pSO60	Km^R; T7-Pro-σ^K(1-127)-His_6/T7-cytTM-SpoIVFB-$FLAG_2$-His_6/T7-GFPΔ27BofA H57A/SpoIVFA	pSO40 was subjected to SDM using primers SO-P91 and SO-P92, substituting H57A in GFPΔ27BofA.	This study
pSO61	Km^R; T7-Pro-σ^K(1-127)-His_6/T7-cytTM-SpoIVFB-$FLAG_2$-His_6/T7-GFPΔ27BofA P59A/SpoIVFA	pSO40 was subjected to SDM using primers SO-P93 and SO-P94, substituting P59A in GFPΔ27BofA.	This study
pSO62	Km^R; T7-Pro-σ^K(1-127)-His_6/T7-cytTM-SpoIVFB-$FLAG_2$-His_6/T7-GFPΔ27BofA I82A/SpoIVFA	pSO40 was subjected to SDM using primers SO-P95 and SO-P96, substituting I82A in GFPΔ27BofA.	This study
pSO63	Km^R; T7-Pro-σ^K(1-127)-His_6/T7-cytTM-SpoIVFB-$FLAG_2$-His_6/T7-GFPΔ27BofA F85A/SpoIVFA	pSO40 was subjected to SDM using primers SO-P97 and SO-P98, substituting F85A in GFPΔ27BofA.	This study
pSO64	Km^R; T7-Pro-σ^K(1-127)-His_6/T7-cytTM-SpoIVFB-$FLAG_2$-His_6/T7-GFPΔ27BofA	Fragment *gfpΔ27bofA* was amplified from pYZ46 using primers SO-P99 and SO-P100. Fragment was joined to pSO40 digested with NotI and NheI using GA.	This study
pSO65	Km^R; T7-Pro-σ^K(1-127)-His_6/T7-cytTM-SpoIVFB-$FLAG_2$-His_6/T7-SpoIVFA	Fragment *spoIVFA* was amplified from pYZ46 using primers SO-P82 and SO-P101. Fragment was joined to pSO40 digested with NotI and NheI using GA.	This study

Table S2.1 (cont'd)

pSO67	Km^R; T7-Pro-σ^K(1-127)-His_6/T7-cytTM-SpoIVFB-$FLAG_2$-His_6/T7-GFPΔ27BofA FII85-87AAA/SpoIVFA	pSO63 was subjected to SDM using primers SO-P106 and SO-P107, substituting FII85-87AAA in GFPΔ27BofA.	This study
pSO68	Km^R; T7-Pro-σ^K(1-127)-His_6/T7-cytTM-SpoIVFB-$FLAG_2$-His_6/T7-GFPΔ27BofA/Cys-less SpoIVFA	pSO40 was subjected to SDM using primers SO-P116 and SO-P117, substituting C77L and C82L in SpoIVFA.	This study
pSO69	Km^R; T7-Pro-σ^K(1-127)-His_6/T7-cytTM-SpoIVFB-$FLAG_2$-His_6/T7-GFP-G/S linker-Δ36BofA/SpoIVFA	pSO42 was subjected to SDM using primers SO-P108 and SO-P109, adding a nine-residue G/S linker (GGSGGSGGS) to GFPΔ36BofA.	This study
pSO70	Km^R; T7-Pro-σ^K(1-127)-His_6/T7-cytTM-SpoIVFB-$FLAG_2$/T7-GFPΔ27BofA/SpoIVFA	Fragment *T7-gfpΔ27bofA/spoIVFA* was amplified from pYZ46 using primers SO-P82 and SO-P120. Vector pYZ2 was amplified using primers SO-P118 and SO-P119 (removing His_6 from cytTM-SpoIVFB). Fragment was joined to pYZ2 using GA.	This study
pSO71	Km^R; T7-Pro-σ^K(1-127)-His_6/T7-cytTM-SpoIVFB-$FLAG_2$-His_6/T7-GFP C48S-Δ27BofA/Cys-less SpoIVFA	pSO68 (Cys-less SpoIVFA) was subjected to SDM using primers SO-P112 and SO-P113, substituting C48S in GFP.	This study
pSO72	Km^R; T7-Pro-σ^K(1-127)-His_6/T7-cytTM-SpoIVFB-$FLAG_2$-His_6/T7-GFP C48S C70S-Δ27BofA/Cys-less SpoIVFA	pSO71 was subjected to SDM using primers SO-P114 and SO-P115, substituting C70S in GFP.	This study
pSO73	Km^R; T7-Pro-σ^K(1-127)-His_6/T7-cytTM-SpoIVFB E44C-$FLAG_2$/T7-GFPΔ27BofA/SpoIVFA	pSO70 was subjected to SDM using primers YZ1 and YZ2, substituting E44C in cytTM-SpoIVFB.	This study
pSO75	Ap^R Sp^R; P_{spoIID}-GFPΔ27BofA	pDR95 was subjected to SDM using primers SO-P134 and SO-P135, replacing a HindIII site with a SphI site.	This study
pSO76	Km^R; T7-Cys-less Pro-σ^K(1-127)-His_6/T7-cytTM-SpoIVFB-$FLAG_2$-His_6	pYZ2 was subjected to SDM using primers SO-P136 and SO-P137, substituting C109S in Pro-σ^K(1-127).	This study

Table S2.1 (cont'd)

pSO78	Ap^R Sp^R; P_{bofA}-GFPΔ27BofA	Fragment P_{bofA} was amplified from *B. subtilis* strain PY79 DNA using primers SO-P132 and SO-P133. Fragment was digested with EcoRI and SphI, and ligated with EcoRI-SphI-digested pSO75.	This study
pSO79	Km^R; T7-Cys-less Pro-σ^K(1-127)-His_6/T7-single-Cys E44C cytTM-SpoIVFB-$FLAG_2$-His_6	Fragment *spoIVFB* (single-Cys E44C) was amplified from pYZ40 using primers SO-P138 and SO-P139. Vector pSO76 was amplified using primers SO-P140 and SO-P141. Fragment was joined to pSO76 using GA.	This study
pSO80	Km^R; T7-Cys-less Pro-σ^K(1-127)-His_6/T7-single-Cys E44C cytTM- SpoIVFB-$FLAG_2$-His_6/T7-single-Cys GFPΔ27BofA/Cys-less SpoIVFA	Fragment *T7-gfpΔ27bofA/spoIVFA* (single-Cys GFPΔ27BofA/Cys-less SpoIVFA) was amplified from pSO72 using primers SO-P82 and SO-P90. Vector pSO79 was amplified using primers SO-P89 and SO-P80. Fragment was joined to pSO79 using GA.	This study
pSO82	Km^R; T7-Pro-σ^K(1-127)/T7-cytTM-SpoIVFB E44C-$FLAG_2$/T7-GFPΔ27BofA/SpoIVFA	pSO73 was subjected to SDM using primers SO-P148 and SO-P149, deleting His_6 from Pro-σ^K(1-127).	This study
pSO83	Km^R; T7-Cys-less Pro-σ^K(1-127)-His_6/T7-single-Cys V70C cytTM-SpoIVFB E44Q-$FLAG_2$-His_6/T7-single-Cys GFPΔ27BofA/Cys-less SpoIVFA	Fragment *spoIVFB* (single-Cys V70C) was amplified from pYZ77 using primers SO-P138 and SO-P139. Vector pSO80 was amplified using primers SO-P140 and SO-P141. Fragment was joined to pSO80 using GA.	This study
pSO84	Km^R; T7-Cys-less Pro-σ^K(1-127)-His_6/T7-single-Cys P135C cytTM-SpoIVFB E44Q-$FLAG_2$-His_6/T7-single-Cys GFPΔ27BofA/Cys-less SpoIVFA	Fragment *spoIVFB* (single-Cys P135C) was amplified from pYZ28 using primers SO-P138 and SO-P139. Vector pSO80 was amplified using primers SO-P140 and SO-P141. Fragment was joined to pSO80 using GA.	This study
pSO86	Ap^R Sp^R; P_{bofA}-GFPΔ27BofA N48A	Fragment *gfpΔ27bofA N48A* was amplified from pSO27 using primers SO-P142 and SO-P143. Fragment was joined to pSO78 digested with SphI and BamHI using GA.	This study

Table S2.1 (cont'd)

pSO87	Ap^R Sp^R; P_{bofA}-GFPΔ27BofA N61A	Fragment *gfpΔ27bofA N61A* was amplified from pSO30 using primers SO-P142 and SO-P143. Fragment was joined to pSO78 digested with SphI and BamHI using GA.	This study
pSO88	Ap^R Sp^R; P_{bofA}-GFPΔ27BofA T64A	pSO78 was subjected to SDM using primers SO-P60 and SO-P61, substituting T64A in GFPΔ27BofA	This study
pSO90	Km^R; T7-Pro-σ^K(1-127)-His_6/T7-cytTM-SpoIVFB-$FLAG_2$-His_6/T7-MBPΔ27BofA/Cys-less SpoIVFA	Fragment of *mbp* was amplified from pYZ112 using primers SO-P156 and SO-P157. Vector pSO72 was amplified using primers SO-P158 and SO-P159. Fragment was joined to pSO72 using GA.	This study
pSO91	Km^R; T7-Cys-less Pro-σ^K(1-127)-His_6/T7- single-Cys E44C cytTM-SpoIVFB-$FLAG_2$-His_6/T7-MBPΔ27BofA/Cys-less SpoIVFA	Fragment *T7-mbpΔ27bofA/spoIVFA* (single-Cys MBPΔ27BofA/Cys-less SpoIVFA) was amplified from pSO90 using primers SO-P82 and SO-P90. Vector pSO80 was amplified using primers SO-P89 and SO-P80. Fragment was joined to pSO80 using GA.	This study
pSO92	Km^R; T7-Cys-less Pro-σ^K(1-127)-His_6/T7-single-Cys V70C cytTM-SpoIVFB E44Q-$FLAG_2$-His_6/T7-MBPΔ27BofA/Cys-less SpoIVFA	Fragment *T7-mbpΔ27bofA/spoIVFA* (single-Cys MBPΔ27BofA/Cys-less SpoIVFA) was amplified from pSO90 using primers SO-P82 and SO-P90. Vector pSO83 was amplified using primers SO-P89 and SO-P80. Fragment was joined to pSO83 using GA.	This study
pSO93	Km^R; T7-Cys-less Pro-σ^K(1-127)-His_6/T7-single-Cys P135C cytTM-SpoIVFB E44Q-$FLAG_2$-His_6/T7-MBPΔ27BofA/Cys-less SpoIVFA	Fragment *T7-mbpΔ27bofA/spoIVFA* (single-Cys MBPΔ27BofA/Cys-less SpoIVFA) was amplified from pSO90 using primers SO-P82 and SO-P90. Vector pSO84 was amplified using primers SO-P89 and SO-P80. Fragment was joined to pSO84 using GA.	This study
pSO94	Km^R; T7-Cys-less Pro-σ^K(1-127)-His_6/T7-Cys-less cytTM-SpoIVFB E44Q-$FLAG_2$-His_6/T7-MBPΔ27BofA/ Cys-less SpoIVFA	pSO91 was subjected to SDM using primers LK2691 and YZ11, substituting E44Q in cytTM-SpoIVFB.	This study

Table S2.1 (cont'd)

pSO96	Km^R; T7-Cys-less Pro-σ^K(1-127)-His_6/T7-Cys-less cytTM-SpoIVFB E44Q-$FLAG_2$-His_6	pSO79 was subjected to SDM using primers LK2691 and YZ11, substituting E44Q in cytTM-SpoIVFB.	This study
pSO97	Km^R; T7-Pro-σ^K(1-127)-His_6/T7-cytTM-SpoIVFB-$FLAG_2$-His_6/T7-Cys-less MBPΔ27BofA/Cys-less SpoIVFA	pSO90 was subjected to SDM using primers SO-P152 and SO-P153, substituting C46S in MBPΔ27BofA.	This study
pSO110	Km^R; T7-Cys-less Pro-σ^K(1-127)-His_6/T7-single-Cys E44C cytTM-SpoIVFB-$FLAG_2$-His_6/T7-Cys-less MBPΔ27BofA/Cys-less SpoIVFA	Fragment *T7-mbpΔ27bofA/spoIVFA* (Cys-less MBPΔ27BofA/Cys-less SpoIVFA) was amplified from pSO97 using primers SO-P82 and SO-P90. Vector pSO80 was amplified using primers SO-P89 and SO-P80. Fragment was joined to pSO80 using GA.	This study
pSO111	Km^R; T7-Cys-less Pro-σ^K(1-127)-His_6/T7-single-Cys V70C cytTM-SpoIVFB E44Q-$FLAG_2$-His_6/T7-Cys-less MBPΔ27BofA/Cys-less SpoIVFA	Fragment *T7-mbpΔ27bofA/spoIVFA* (Cys-less MBPΔ27BofA/Cys-less SpoIVFA) was amplified from pSO97 using primers SO-P82 and SO-P90. Vector pSO83 was amplified using primers SO-P89 and SO-P80. Fragment was joined to pSO83 using GA.	This study
pSO112	Km^R; T7-Cys-less Pro-σ^K(1-127)-His_6/T7-single-Cys P135C cytTM-SpoIVFB E44Q-$FLAG_2$-His_6/T7-Cys-less MBPΔ27BofA/Cys-less SpoIVFA	Fragment *T7-mbpΔ27bofA/spoIVFA* (Cys-less MBPΔ27BofA and Cys-less SpoIVFA) was amplified from pSO97 using primers SO-P82 and SO-P90. Vector pSO84 was amplified using primers SO-P89 and SO-P80. Fragment was joined to pSO84 using GA.	This study
pSO113	Km^R; T7-single-Cys E42C Pro-σ^K(1-127)-His_6/T7-Cys-less cytTM-SpoIVFB E44Q-$FLAG_2$-His_6	pSO96 was subjected to SDM using primers SO-P162 and SO-P163, substituting E42C in Pro-σ^K(1-127).	This study
pSO114	Km^R; T7-Cys-less Pro-σ^K(1-127)-His_6/T7-single-Cys Y214C cytTM-SpoIVFB E44Q-$FLAG_2$-His_6	pSO96 was subjected to SDM using primers SO-P170 and SO-P171, substituting Y214C in cytTM-SpoIVFB.	This study
pSO115	Km^R; T7-single-Cys A97C Pro-σ^K(1-127)-His_6/T7-Cys-less cytTM-SpoIVFB E44Q-$FLAG_2$-His_6	pSO96 was subjected to SDM using primers SO-P176 and SO-P177, substituting A97C in Pro-σ^K(1-127).	This study

Table S2.1 (cont'd)

pSO116	Km^R; T7-Cys-less Pro-σ^K(1-127)-His_6/T7-single-Cys V229C cytTM-SpoIVFB E44Q-$FLAG_2$-His_6	pSO96 was subjected to SDM using primers SO-P180 and SO-P181, substituting V229C in cytTM-SpoIVFB.	This study
pSO117	Km^R; T7-single-Cys E42C Pro-σ^K(1-127)-His_6/T7-single-Cys R213C cytTM-SpoIVFB E44Q-$FLAG_2$-His_6	pSO113 was subjected to SDM using primers SO-P168 and SO-P169, substituting R213C in cytTM-SpoIVFB.	This study
pSO118	Km^R; T7-single-Cys E42C Pro-σ^K(1-127)-His_6/T7-single-Cys Y214C cytTM-SpoIVFB E44Q-$FLAG_2$-His_6	pSO113 was subjected to SDM using primers SO-P170 and SO-P171, substituting Y214C in cytTM-SpoIVFB.	This study
pSO119	Km^R; T7-single-Cys E42C Pro-σ^K(1-127)-His_6/T7-single-Cys Y215C cytTM-SpoIVFB E44Q-$FLAG_2$-His_6	pSO113 was subjected to SDM using primers SO-P172 and SO-P173, substituting Y215C in cytTM-SpoIVFB.	This study
pSO120	Km^R; T7-single-Cys L41C Pro-σ^K(1-127)-His_6/T7-single-Cys Y214C cytTM-SpoIVFB E44Q-$FLAG_2$-His_6	pSO114 was subjected to SDM using primers SO-P186 and SO-P187, substituting L41C in Pro-σ^K(1-127).	This study
pSO121	Km^R; T7-single-Cys L43C Pro-σ^K(1-127)-His_6/T7-single-Cys Y214C cytTM-SpoIVFB E44Q-$FLAG_2$-His_6	pSO114 was subjected to SDM using primers SO-P164 and SO-P165, substituting L43C in Pro-σ^K(1-127).	This study
pSO122	Km^R; T7-single-Cys A97C Pro-σ^K(1-127)-His_6/T7-single-Cys S228C cytTM-SpoIVFB E44Q-$FLAG_2$-His_6	pSO115 was subjected to SDM using primers SO-P188 and SO-P189, substituting S228C in cytTM-SpoIVFB.	This study
pSO123	Km^R; T7-single-Cys A97C Pro-σ^K(1-127)-His_6/T7-single-Cys V229C cytTM-SpoIVFB E44Q-$FLAG_2$-His_6	pSO115 was subjected to SDM using primers SO-P180 and SO-P181, substituting V229C in cytTM-SpoIVFB.	This study
pSO124	Km^R; T7-single-Cys A97C Pro-σ^K(1-127)-His_6/T7-single-Cys K230C cytTM-SpoIVFB E44Q-$FLAG_2$-His_6	pSO115 was subjected to SDM using primers SO-P182 and SO-P183, substituting K230C in cytTM-SpoIVFB.	This study
pSO125	Km^R; T7-single-Cys S96C Pro-σ^K(1-127)-His_6/T7-single-Cys V229C cytTM-SpoIVFB E44Q-$FLAG_2$-His_6	pSO116 was subjected to SDM using primers SO-P174 and SO-P175, substituting S96C in Pro-σ^K(1-127).	This study
pSO126	Km^R; T7-single-Cys G98C Pro-σ^K(1-127)-His_6/T7-single-Cys V229C cytTM-SpoIVFB E44Q-$FLAG_2$-His_6	pSO116 was subjected to SDM using primers SO-P196 and SO-P197, substituting G98C in Pro-σ^K(1-127).	This study

Table S2.1 (cont'd)

pSO127	Km^R; T7-single-Cys L41C Pro-σ^K(1-127)-His_6/T7-single-Cys Y214C cytTM-SpoIVFB E44Q-$FLAG_2$-His_6/T7-Cys-less MBPΔ27BofA/Cys-less SpoIVFA	Fragment *T7-mbpΔ27bofA/spoIVFA* (Cys-less MBPΔ27BofA/Cys-less SpoIVFA) was amplified from pSO112 using primers SO-P82 and SO-P90. Vector pSO120 was amplified using primers SO-P89 and SO-P80. Fragment was joined to pSO120 using GA.	This study
pSO128	Km^R; T7-single-Cys K24C Pro-σ^K(1-127)-His_6/T7-single-Cys E44C cytTM-SpoIVFB-$FLAG_2$-His_6	pSO79 was subjected to SDM using primers LK2473 and LK2474, substituting K24C in Pro-σ^K(1-127).	This study
pSO130	Km^R; T7-single-Cys A97C Pro-σ^K(1-127)-His_6/T7-single-Cys A231C cytTM-SpoIVFB E44Q-$FLAG_2$-His_6	pSO115 was subjected to SDM using primers SO-P184 and SO-P185, substituting A231C in cytTM-SpoIVFB.	This study
pSO131	Km^R; T7-single-Cys K24C Pro-σ^K(1-127)-His_6/T7-single-Cys E44C cytTM-SpoIVFB-$FLAG_2$-His_6/T7-Cys-less MBPΔ27BofA/Cys-less SpoIVFA	pSO110 was subjected to SDM using primers LK2473 and LK2474, substituting K24C in Pro-σ^K(1-127).	This study
pSO132	Km^R; T7-single-Cys K24C Pro-σ^K(1-127)-His_6/T7-single-Cys V70C cytTM-SpoIVFB E44Q-$FLAG_2$-His_6/T7-Cys-less MBPΔ27BofA/Cys-less SpoIVFA	pSO111 was subjected to SDM using primers LK2473 and LK2474, substituting K24C in Pro-σ^K(1-127).	This study
pSO133	Km^R; T7-single-Cys A97C Pro-σ^K(1-127)-His_6/T7-single-Cys A231C cytTM-SpoIVFB E44Q-$FLAG_2$-His_6/T7-Cys-less MBPΔ27BofA/Cys-less SpoIVFA	Fragment *T7-mbpΔ27bofA/spoIVFA* (Cys-less MBPΔ27BofA/Cys-less SpoIVFA) was amplified from pSO112 using primers SO-P82 and SO-P90. Vector pSO130 was amplified using primers SO-P89 and SO-P80. Fragment was joined to pSO130 using GA.	This study
pSO134	Km^R; T7-single-Cys K24C Pro-σ^K(1-127)-His_6/T7-single-Cys V70C cytTM-SpoIVFB E44Q-$FLAG_2$-His_6	Fragment *spoIVFB* (single-Cys V70C) was amplified from pSO111 using primers SO-P138 and SO-P139. Vector pSO128 was amplified from primers SO-P140 and SO-P141. Fragment was joined to pSO128 using GA.	This study

Table S2.1 (cont'd)

pSO136	Km^R; T7-Cys-less Pro-σ^K(1-127)-His_6/T7-single-Cys V70C cytTM-SpoIVFB E44Q-$FLAG_2$-His_6	Fragment of *spoIVFB* (single-Cys V70C) was amplified from pSO111 using primers SO-P138 and SO-P139. Vector pSO79 was amplified fromprimers SO-P140 and SO-P141. Fragment was joined to pSO79 using GA.	This study
pSO139	Km^R; T7-Cys-less Pro-σ^K(1-127)-His_6/T7-Cys-less cytTM-SpoIVFB E44Q-$FLAG_2$-His_6/T7-Cys-less MBPΔ27BofA/Cys-less SpoIVFA	pSO94 was subjected to SDM using primers SO-P152 and SO-P153, substituting C46S in MBPΔ27BofA.	This study
pSO141	Km^R; T7-Pro-σ^K(1-127)-His_6/T7-cytTM-SpoIVFB M30C-$FLAG_2$-His_6	pYZ2 was subjected to SDM using primers SO-P202 and SO-P203, substituting M30C in cytTM-SpoIVFB.	This study
pSO142	Km^R; T7-Pro-σ^K(1-127)-His_6/T7-cytTM-SpoIVFB-$FLAG_2$-His_6/T7-GFPΔ27BofA L62C/SpoIVFA	pSO40 was subjected to SDM using primers SO-P204 and SO-P205, substituting L62C in GFPΔ27BofA.	This study
pSO143	Km^R; T7-Pro-σ^K(1-127)-His_6/T7-cytTM-SpoIVFB-$FLAG_2$-His_6/T7-GFPΔ27BofA V63C/SpoIVFA	pSO40 was subjected to SDM using primers SO-P206 and SO-P207, substituting V63C in GFPΔ27BofA.	This study
pSO144	Km^R; T7-Cys-less Pro-σ^K(1-127)-His_6/T7-single-Cys M30C cytTM-SpoIVFB E44Q-$FLAG_2$-His_6/T7-Cys-less MBPΔ27BofA/Cys-less SpoIVFA	pSO139 was subjected to SDM using primers SO-P209 and SO-P210, substituting M30C in cytTM-SpoIVFB.	This study
pS0147	Km^R; T7-Cys-less Pro-σ^K(1-127)-His_6/T7-single-Cys M30C cytTM-SpoIVFB E44Q-$FLAG_2$-His_6/T7-single-Cys L62C MBPΔ27BofA/Cys-less SpoIVFA	pSO144 was subjected to SDM using primers SO-P204 and SO-P205, substituting L62C in MBPΔ27BofA.	This study
pSO148	Km^R; T7-Cys-less Pro-σ^K(1-127)-His_6/T7-single-Cys M30C cytTM-SpoIVFB E44Q-$FLAG_2$-His_6/T7-single-Cys V63C MBPΔ27BofA/Cys-less SpoIVFA	pSO144 was subjected to SDM using primers SO-P206 and SO-P207, substituting V63C in MBPΔ27BofA.	This study
pSO149	Km^R; T7-Pro-σ^K(1-127)-His_6/T7-cytTM-SpoIVFB E44C/T7-GFPΔ27BofA/SpoIVFA	pSO73 was subjected to SDM using primers SO-P211 and SO-P212, deleting $FLAG_2$ from cytTM-SpoIVFB.	This study

Table S2.1 (cont'd)

pSO157	Km^R; T7-Pro-σ^K(1-127) L41C-His_6/T7-cytTM-SpoIVFB-$FLAG_2$-His_6	pYZ2 was subjected to SDM using primers SO-P186 and SO-P187, substituting L41C in Pro-σ^K(1-127).	This study
pSO158	Km^R; T7-Pro-σ^K(1-127) A97C-His_6/T7-cytTM-SpoIVFB-$FLAG_2$-His_6	pYZ2 was subjected to SDM using primers SO-P176 and SO-P177, substituting A97C in Pro-σ^K(1-127).	This study
pSO159	Km^R; T7-Pro-σ^K(1-127)-His_6/T7-cytTM-SpoIVFB Y214C-$FLAG_2$-His_6	pYZ2 was subjected to SDM using primers SO-P170 and SO-P171, substituting Y214C in cytTM-SpoIVFB.	This study
pSO160	Km^R; T7-Pro-σ^K(1-127)-His_6/T7-cytTM-SpoIVFB A231C-$FLAG_2$-His_6	pYZ2 was subjected to SDM using primers SO-P184 and SO-P185, substituting Y231C in cytTM-SpoIVFB.	This study
pSO163	Km^R; T7-single-Cys F18C Pro-σ^K(1-127)-His_6/T7-single-Cys E44C cytTM-SpoIVFB-$FLAG_2$-His_6/T7-Cys-less MBPΔ27BofA/Cys-less SpoIVFA	pSO110 was subjected to SDM using primers LK2465 and LK2466, substituting F18C in Pro-σ^K(1-127).	This study
pSO164	Km^R; T7-single-Cys F18C Pro-σ^K(1-127)-His_6/T7-single-Cys V70C cytTM-SpoIVFB E44Q-$FLAG_2$-His_6/T7-Cys-less MBPΔ27BofA/Cys-less SpoIVFA	pSO111 was subjected to SDM using primers LK2465 and LK2466, substituting F18C in Pro-σ^K(1-127).	This study
pSO165	Km^R; T7-single-Cys V20C Pro-σ^K(1-127)-His_6/T7-single-Cys E44C cytTM-SpoIVFB-$FLAG_2$-His_6/T7-Cys-less MBPΔ27BofA/Cys-less SpoIVFA	pSO110 was subjected to SDM using primers LK2467 and LK2468, substituting V20C in Pro-σ^K(1-127).	This study
pSO166	Km^R; T7-single-Cys S21C Pro-σ^K(1-127)-His_6/T7-single-Cys E44C cytTM-SpoIVFB-$FLAG_2$-His_6/T7-Cys-less MBPΔ27BofA/Cys-less SpoIVFA	pSO110 was subjected to SDM using primers SO-P218 and SO-P219, substituting S21C in Pro-σ^K(1-127).	This study
pSO167	Km^R; T7-single-Cys F18C Pro-σ^K(1-127)-His_6/T7-single-Cys E44C cytTM-SpoIVFB-$FLAG_2$-His_6	pSO79 was subjected to SDM using primers LK2465 and LK2466, substituting F18C in Pro-σ^K(1-127).	This study
pSO168	Km^R; T7-single-Cys F18C Pro-σ^K(1-127)-His_6/T7-single-Cys V70C cytTM-SpoIVFB E44Q-$FLAG_2$-His_6	pSO136 was subjected to SDM using primers LK2465 and LK2466, substituting F18C in Pro-σ^K(1-127).	This study

Table S2.1 (cont'd)

pSO169	Km^R; T7-single Cys V20C Pro-σ^K(1-127)-His_6/T7-single-Cys E44C cytTM- SpoIVFB-$FLAG_2$-His_6	pSO79 was subjected to SDM using primers LK2467 and LK2468, substituting V20C in Pro-σ^K(1-127).	This study
pSO170	Km^R; T7-single Cys S21C Pro-σ^K(1-127)-His_6/T7-single-Cys E44C cytTM- SpoIVFB-$FLAG_2$-His_6	pSO79 was subjected to SDM using primers SO-P218 and SO-P219, substituting S21C in Pro-σ^K(1-127).	This study
pSO181	Km^R; T7-Cys-less Pro-σ^K(1-127)-His_6/T7-Cys-less cytTM-SpoIVFB E44Q-$FLAG_2$-His_6/T7-single-Cys I56C MBPΔ27BofA/Cys-less SpoIVFA	pSO139 was subjected to SDM using primers SO-P222 and SO-P223, substituting I56C in MBPΔ27BofA.	This study
pSO182	Km^R; T7-Cys-less Pro-σ^K(1-127)-His_6/T7-Cys-less cytTM-SpoIVFB E44Q-$FLAG_2$-His_6/T7-single-Cys H57C MBPΔ27BofA/Cys-less SpoIVFA	pSO139 was subjected to SDM using primers SO-P224 and SO-P225, substituting H57C in MBPΔ27BofA.	This study
pSO183	Km^R; T7-Cys-less Pro-σ^K(1-127)-His_6/T7-Cys-less cytTM-SpoIVFB E44Q-$FLAG_2$-His_6/T7-single-Cys G40C MBPΔ27BofA/Cys-less SpoIVFA	pSO139 was subjected to SDM using primers SO-P226 and SO-P227, substituting G40C in MBPΔ27BofA.	This study
pSO184	Km^R; T7-Cys-less Pro-σ^K(1-127)-His_6/T7-Cys-less cytTM-SpoIVFB E44Q-$FLAG_2$-His_6/T7-single-Cys A41C MBPΔ27BofA/Cys-less SpoIVFA	pSO139 was subjected to SDM using primers SO-P228 and SO-P229, substituting A41C in MBPΔ27BofA.	This study
pSO186	Km^R; T7-Cys-less Pro-σ^K(1-127)-His_6/T7-single-Cys A32C cytTM-SpoIVFB E44Q-$FLAG_2$-His_6/T7-single-Cys I56C MBPΔ27BofA/Cys-less SpoIVFA	pSO181 was subjected to SDM using primers SO-P232 and SO-P233, substituting A32C in cytTM-SpoIVFB.	This study
pSO187	Km^R; T7-Cys-less Pro-σ^K(1-127)-His_6/T7-single-Cys L33C cytTM-SpoIVFB E44Q-$FLAG_2$-His_6/T7-single-Cys I56C MBPΔ27BofA/Cys-less SpoIVFA	pSO181 was subjected to SDM using primers SO-P234 and SO-P235, substituting L33C in cytTM-SpoIVFB.	This study

Table S2.1 (cont'd)

pSO188	Km^R; T7-Cys-less Pro-σ^K(1-127)-His_6/T7-single-Cys Q181C cytTM-SpoIVFB E44Q-$FLAG_2$-His_6/T7-single-Cys H57C MBPΔ27BofA/Cys-less SpoIVFA	pSO182 was subjected to SDM using primers SO-P236 and SO-P237, substituting Q181C in cytTM-SpoIVFB.	This study
pSO189	Km^R; T7-Cys-less Pro-σ^K(1-127)-His_6/T7-single-Cys V86C cytTM-SpoIVFB E44Q-$FLAG_2$-His_6/T7-single-Cys G40C MBPΔ27BofA/Cys-less SpoIVFA	pSO183 was subjected to SDM using primers SO-P238 and SO-P239, substituting V86C in cytTM-SpoIVFB.	This study
pSO190	Km^R; T7-Cys-less Pro-σ^K(1-127)-His_6/T7-single-Cys V86C cytTM-SpoIVFB E44Q-$FLAG_2$-His_6/T7-single-Cys A41C MBPΔ27BofA/Cys-less SpoIVFA	pSO184 was subjected to SDM using primers SO-P238 and SO-P239, substituting V86C in cytTM-SpoIVFB.	This study
pSO192	Ap^R; T7-SpoIVB S378A-His_6	pZR53 was subjected to SDM using primers SO-P244 and SO-P245, substituting S378A in SpoIVB.	This study
pSO193	Km^R; T7-Pro-σ^K(1-127)-His_6/T7-cytTM- SpoIVFB F66A-$FLAG_2$-His_6/T7-GFPΔ27BofA/SpoIVFA	pSO40 was subjected to SDM using primers SO-P242 and SO-P243, substituting F66A in cytTM-SpoIVFB	This study
pSO203	Km^R; T7-Pro-σ^K(1-127)-His_6/T7-cytTM-SpoIVFB-$FLAG_2$-His_6/T7-GFPΔ27BofA N48D/SpoIVFA	pSO40 was subjected to SDM using primers SO-P251 and SO-P252, substituting N48D in GFPΔ27BofA.	This study
pSO211	Km^R; T7-Pro-σ^K-His_6/T7-cytTM- SpoIVFB E44C-$FLAG_2$/T7-GFPΔ27BofA/SpoIVFA	Fragment of 5' end of *pro*-σ^K-*His_6* was amplified from pETproσ^K using primers SO-P260 and SO-P270. Vector pSO73 was amplified using primers SO-P257 and SO-P269. Fragment was joined to pSO73 using GA.	This study
pSO212	Ap^R; T7-BofA/SpoIVFA	Fragment of native *bofA* was amplified from *B. subtilis* strain PY79 DNA using primers SO-P271 and SO-P272. Fragment was used as template with primers SO-P277 and SO-P276 to add regions of homology to pYZ46. Vector pYZ46 was amplified with primers SO-P273 and SO-P280. Fragment with homology was joined to pYZ46 using GA.	This study

Table S2.1 (cont'd)

pSO213	Km^R; T7-Pro-σ^K(1-127)-His_6/T7-cytTM-SpoIVFB-$FLAG_2$-His_6/T7-BofA/SpoIVFA	Fragment *T7-bofA/spoIVFA* was amplified from pSO212 using primers SO-P82 and SO-P90. Vector pYZ2 was amplified using primers SO-P89 and SO-P80. Fragment was joined to pYZ2 using GA.	This study
pSO215	Km^R; T7-Pro-σ^K(1-127)-His_6/T7-cytTM-SpoIVFB E44C-$FLAG_2$/T7-BofA/SpoIVFA	Fragment *spoIVFB/T7-bofA/spoIVFA* was made by OEPCR[c]. Fragment #1 (*T7-bofA/spoIVFA*) was amplified from pSO212 using primers SO-P120 and SO-P286. Fragment #2 (*spoIVFB*) was amplified from pSO70 using primers SO-P288 and SO-P293. Fragments #1 and #2 were used as template for OEPCR using primers SO-P294 and SO-P286 (removing His_6 from cytTM-SpoIVFB). Vector pSO73 was amplified using primers SO-P287 and SO-P295. Product from OEPCR was joined to pSO73 using GA.	This study
pSO216	Km^R; T7-Pro-σ^K(1-127)/T7-cytTM-SpoIVFB E44C-$FLAG_2$/T7-BofA/SpoIVFA	pSO215 was subjected to SDM using primers SO-P148 and SO-P149, deleting His_6 from Pro-σ^K(1-127).	This study
pSO217	Km^R; T7-Pro-σ^K(1-127)-His_6/T7-cytTM-SpoIVFB E44C/T7-BofA/SpoIVFA	pSO215 was subjected to SDM using primers SO-P211 and SO-P212, deleting $FLAG_2$ from cytTM-SpoIVFB.	This study
pSO220	Km^R; T7-Pro-σ^K/T7-cytTM-SpoIVFB E44C-$FLAG_2$/T7-GFPΔ27BofA/SpoIVFA	pSO211 was subjected to SDM using primers SO-P148 and SO-P149, deleting His_6 from Pro-σ^K	This study
pSO221	Km^R; T7-Pro-σ^K-His_6/T7-cytTM- SpoIVFB E44C/T7-GFPΔ27BofA/SpoIVFA	pSO211 was subjected to SDM using primers: SO-P211 and SO-P212, deleting $FLAG_2$ from cytTM-SpoIVFB	This study
pSO224	Km^R; T7-Cys-less Pro-σ^K(1-127)-His_6/T7-cytTM-SpoIVFB-$FLAG_2$-His_6/T7-BofA/SpoIVFA	pSO213 was subjected to SDM using primers SO-P136 and SO-P137, substituting C109S in Pro-σ^K(1-127).	This study
pSO225	Km^R; T7-Cys-less Pro-σ^K(1-127)-His_6/T7-cytTM-SpoIVFB-$FLAG_2$-His_6/T7-BofA/Cys-less SpoIVFA	pSO224 was subjected to SDM using primers SO-P116 and SO-P117, substituting C77L and C82L in SpoIVFA.	This study

Table S2.1 (cont'd)

pSO226	Km^R; T7-Cys-less Pro-σ^K(1-127)-His_6/T7-single-Cys E44C cytTM-SpoIVFB-$FLAG_2$-His_6/T7-BofA/Cys-less SpoIVFA	Fragment of *spoIVFB* (single-Cys E44C) was amplified from pSO91 using primers SO-P138 and SO-P139. Vector pSO225 was amplified using primers SO-P140 and SO-P141. Fragment was joined to pSO225 using GA.	This study
pSO227	Km^R; T7-Cys-less Pro-σ^K(1-127)-His_6/T7-single-Cys V70C cytTM-SpoIVFB E44Q-$FLAG_2$-His_6/T7-BofA/Cys-less SpoIVFA	Fragment of *spoIVFB* (single-Cys V70C) was amplified from pSO92 using primers SO-P138 and SO-P139. Vector pSO225 was amplified using primers SO-P140 and SO-P141. Fragment was joined to pSO225 using GA.	This study
pSO228	Km^R; T7-Cys-less Pro-σ^K(1-127)-His_6/T7-single-Cys P135C cytTM-SpoIVFB E44Q-$FLAG_2$-His_6/T7-BofA/Cys-less SpoIVFA	Fragment of *spoIVFB* (single-Cys P135C) was amplified from pSO93 using primers SO-P138 and SO-P139. Vector pSO225 was amplified using primers SO-P140 and SO-P141. Fragment was joined to pSO225 using GA.	This study
pSO229	Km^R; T7-Cys-less Pro-σ^K(1-127)-His_6/T7-single-Cys E44C cytTM-SpoIVFB-$FLAG_2$-His_6/T7-Cys-less BofA/Cys-less SpoIVFA	pSO226 was subjected to SDM using primers SO-P152 and SO-P153, substituting C46S in BofA.	This study
pSO230	Km^R; T7-Cys-less Pro-σ^K(1-127)-His_6/T7-single-Cys V70C cytTM-SpoIVFB E44Q-$FLAG_2$-His_6/T7-Cys-less BofA/Cys-less SpoIVFA	pSO227 was subjected to SDM using primers SO-P152 and SO-P153, substituting C46S in BofA.	This study
pSO231	Km^R; T7-Cys-less Pro-σ^K(1-127)-His_6/T7-single-Cys P135C cytTM-SpoIVFB E44Q-$FLAG_2$-His_6/T7-Cys-less BofA/Cys-less SpoIVFA	pSO228 was subjected to SDM using primers SO-P152 and SO-P153, substituting C46S in BofA.	This study

Table S2.1 (cont'd)

pSO232	Ap^R; T7-GFPΔ27BofA/SpoIVFA/SpoIVB S378A	Fragment *spoIVFA/spoIVB S378A* was made by OEPCR. Fragment #1 (*spoIVB S378A*) was amplified from pSO192 using primers SO-P302 and SO-P282. Fragment #2 (*spoIVFA*) was amplified from pYZ46 using primers SO-P289 and SO-P303. Fragments #1 and #2 were used as template for OEPCR using primers SO-P304 and SO-305. Vector pYZ46 was amplfied using primers SO-P306 and SO-P307. Product from OEPCR was joined to pYZ46 using GA.	This study
pSO233	Ap^R; T7-GFPΔ27BofA/SpoIVFA/SpoIVB	Fragment *spoIVFA/spoIVB* was made by OEPCR. Fragment #1 (*spoIVB*) was amplified from pZR53 using primers SO-P302 and SO-P282. Fragment #2 (*spoIVFA*) was amplified from pYZ46 using primers SO-P289 and SO-P303. Fragments #1 and #2 were used as template for OEPCR using primers SO-P304 and SO-305. Vector pYZ46 was amplified using primers SO-P306 and SO-P307. Product from OEPCR was joined to pYZ46 using GA.	This study
pSO234	Km^R; T7-single-Cys V20C Pro-σ^K(1-127)-His_6/T7-single-Cys E44C cytTM-SpoIVFB-$FLAG_2$-His_6/T7-Cys-less BofA/Cys-less SpoIVFA	pSO229 was subjected to SDM using primers LK2467 and LK2468, substituting V20C in Pro-σ^K(1-127).	This study
pSO235	Km^R; T7-single-Cys S21C Pro-σ^K(1-127)-His_6/T7-single-Cys E44C cytTM-SpoIVFB-$FLAG_2$-His_6/T7-Cys-less BofA/Cys-less SpoIVFA	pSO229 was subjected to SDM using primers SO-P218 and SO-P219, substituting S21C in Pro-σ^K(1-127).	This study
pSO236	Km^R; T7-single-Cys F18C Pro-σ^K(1-127)-His_6/T7-single-Cys V70C cytTM-SpoIVFB E44Q-$FLAG_2$-His_6/T7-Cys-less BofA/Cys-less SpoIVFA	pSO230 was subjected to SDM using primers LK2465 and LK2466, substituting F18C in Pro-σ^K(1-127).	This study
pSO237	Km^R; T7-single-Cys K24C Pro-σ^K(1-127)-His_6/T7-single-Cys V70C cytTM-SpoIVFB E44Q-$FLAG_2$-His_6/T7-Cys-less BofA/Cys-less SpoIVFA	pSO230 was subjected to SDM using primers LK2473 and LK2474, substituting K24C in Pro-σ^K(1-127).	This study

Table S2.1 (cont'd)

pSO238	Km^R; T7-single-Cys F18C Pro-σ^K(1-127)-His_6/T7-single-Cys E44C cytTM-SpoIVFB-$FLAG_2$-His_6/T7-Cys-less BofA/Cys-less SpoIVFA	pSO229 was subjected to SDM using primers LK2465 and LK2466, substituting F18C in Pro-σ^K(1-127).	This study
pSO239	Km^R; T7-single-Cys K24C Pro-σ^K(1-127)-His_6/T7-single-Cys E44C cytTM-SpoIVFB-$FLAG_2$-His_6/T7-Cys-less BofA/Cys-less SpoIVFA	pSO229 was subjected to SDM using primers LK2473 and LK2474, substituting K24C in Pro-σ^K(1-127).	This study
pSO240	Km^R; T7-Pro-σ^K(1-127)-His_6/T7-cytTM-SpoIVFB-$FLAG_2$-His_6/T7-GFPΔ27BofA/SpoIVFA/SpoIVB S378A	Fragment *gfpΔ27bofA/spoIVFA/spoIVB S378A* was amplified from pSO232 using primers SO-P284 and SO-P285. Vector pSO40 was amplified using primers SO-P80 and SO-P283. Fragment was joined to pSO40 using GA.	This study
pSO241	Km^R; T7-Pro-σ^K(1-127)-His_6/T7-cytTM-SpoIVFB-$FLAG_2$-His_6/T7-GFPΔ27BofA/SpoIVFA/SpoIVB	Fragment *gfpΔ27bofA/spoIVFA/spoIVB* was amplified from pSO233 using primers SO-P284 and SO-P285. Vector pSO40 was amplified using primers SO-P80 and SO-P283. Fragment was joined to pSO40 using GA.	This study
pSO242	Km^R; T7-Cys-less Pro-σ^K(1-127)-His_6/T7-Cys-less cytTM-SpoIVFB E44Q-$FLAG_2$-His_6/T7-Cys-less BofA/Cys-less SpoIVFA	pSO229 was subjected to SDM using primers LK2691 and YZ11, substituting E44Q in cytTM-SpoIVFB.	This study
pSO243	Km^R; T7-Cys-less Pro-σ^K(1-127)-His_6/T7-single-Cys Y214C cytTM-SpoIVFB E44Q-$FLAG_2$-His_6/T7-Cys-less BofA/Cys-less SpoIVFA	pSO242 was subjected to SDM using primers SO-P170 and SO-P171, substituting Y214C in cytTM-SpoIVFB.	This study
pSO244	Km^R; T7-Cys-less Pro-σ^K(1-127)-His_6/T7-single-Cys A231C cytTM-SpoIVFB E44Q-$FLAG_2$-His_6/T7-Cys-less BofA/Cys-less SpoIVFA	pSO242 was subjected to SDM using primers SO-P184 and SO-P185, substituting A231C in cytTM-SpoIVFB.	This study
pSO245	Km^R; T7-single-Cys L41C Pro-σ^K(1-127)-His_6/T7-single-Cys Y214C cytTM-SpoIVFB E44Q-$FLAG_2$-His_6/T7-Cys-less BofA/Cys-less SpoIVFA	pSO243 was subjected to SDM using primers SO-P186 and SO-P187, substituting L41C in Pro-σ^K(1-127).	This study

Table S2.1 (cont'd)

pSO246	Km^R; T7-single-Cys A97C Pro-σ^K(1-127)-His_6/T7-single-Cys A231C cytTM-SpoIVFB E44Q-$FLAG_2$-His_6/T7-Cys-less BofA/Cys-less SpoIVFA	pSO244 was subjected to SDM using primers SO-P176 and SO-P177, substituting A97C in Pro-σ^K(1-127).	This study
pSO247	Ap^R; T7-GFPΔ27BofA/SpoIVFA/T7-SpoIVB S378A	Fragment *spoIVFA/T7-spoIVB S378A* was made by OEPCR. Fragment #1 (*T7-spoIVB S378A*) was amplified from pSO192 using primers SO-P248 and SO-P282. Fragment #2 (*spoIVFA*) was amplified from pYZ46 using primers SO-P289 and SO-P290. Fragments #1 and #2 were used as template for OEPCR using primers SO-P304 and SO-305. Vector pYZ46 was amplified using primers SO-P306 and SO-P307. Product from OEPCR was joined to pYZ46 using GA.	This study
pSO248	Ap^R; T7-BofA/SpoIVFA/SpoIVB	Fragment *spoIVFA/spoIVB* was made by OEPCR. Fragment #1 (*spoIVB*) was amplified from pZR53 using primers SO-P302 and SO-P282. Fragment #2 (*spoIVFA*) was amplified from pYZ46 using primers SO-P289 and SO-P303. Fragments #1 and #2 were used as template for OEPCR using primers SO-P304 and SO-305. Vector pSO212 was amplified using SO-P306 and SO-P307. Product from OEPCR was joined to pSO212 using GA.	This study
pSO249	Ap^R; T7-BofA/SpoIVFA/SpoIVB S378A	Fragment *spoIVFA/spoIVB S378A* was made by OEPCR. Fragment #1 (*spoIVB S378A*) was amplified from pSO192 using primers SO-P302 and SO-P282. Fragment #2 (*spoIVFA*) was amplified from pYZ46 using primers SO-P289 and SO-P303. Fragments #1 and #2 were used as template for OEPCR using primers SO-P304 and SO-305. Vector pSO212 was amplified using SO-P306 and SO-P307. Product from OEPCR was joined to pSO212 using GA.	This study

Table S2.1 (cont'd)

pSO250	Ap^R; T7-BofA/SpoIVFA/T7-SpoIVB S378A	Fragment *spoIVFA/T7-spoIVB S378A* was made by OEPCR. Fragment #1 (*T7-spoIVB S378A*) was amplified from pSO192 using primers SO-P248 and SO-P282. Fragment #2 (*spoIVFA*) was amplified from pYZ46 using primers SO-P289 and SO-P290. Fragments #1 and #2 were used as template for OEPCR using primers SO-P304 and SO-305. Vector pSO212 was amplified using primers SO-P306 and SO-P307. Product from OEPCR was joined to pYZ46 using GA.	This study
pSO251	Km^R; T7-Pro-σ^K(1-127)-His_6/T7-cytTM-SpoIVFB-$FLAG_2$-His_6/T7-GFPΔ27BofA/SpoIVFA/T7-SpoIVB S378A	Fragment *gfpΔ27bofA/spoIVFA/T7-spoIVB S378A* was amplified from pSO247 using primers SO-P284 and SO-P285. Vector pSO40 was amplified using primers SO-P80 and SO-P283. Fragment was joined to pSO40 using GA.	This study
pSO252	Km^R; T7-Pro-σ^K(1-127)-His_6/T7-cytTM-SpoIVFB-$FLAG_2$-His_6/T7-BofA/SpoIVFA/SpoIVB	Fragment *bofA/spoIVFA/spoIVB* was amplified from pSO248 usng primers SO-P310 and SO-P285. Vector pSO213 was amplified using primers SO-P80 and SO-P311. Fragment was joined to pSO213 using GA.	This study
pSO253	Km^R; T7-Pro-σ^K(1-127)-His_6/T7-cytTM-SpoIVFB-$FLAG_2$-His_6/T7-BofA/SpoIVFA/SpoIVB S378A	Fragment *bofA/spoIVFA/spoIVB S378A* was amplified from pSO249 usng primers SO-P310 and SO-P285. Vector pSO213 was amplified using primers SO-P80 and SO-P311. Fragment was joined to pSO213 using GA.	This study
pSO254	Km^R; T7-Pro-σ^K(1-127)-His_6/T7-cytTM-SpoIVFB-$FLAG_2$-His_6/T7-BofA/SpoIVFA/T7-SpoIVB S378A	Fragment *bofA/spoIVFA/T7-spoIVB S378A* was amplified from pSO250 using primers SO-P310 and SO-P285. Vector pSO213 was amplified using primers SO-P80 and SO-P311. Fragment was joined to pSO213 using GA.	This study
pSO255	Km^R; T7-Cys-less Pro-σ^K(1-127)-His_6/T7-single-Cys A231C cytTM-SpoIVFB E44Q-$FLAG_2$-His_6	pSO96 was subjected to SDM using primers SO-P184 and SO-P185, substituting A231C in cytTM-SpoIVFB.	This study

Table S2.1 (cont'd)

pSO256	Km^R; T7-Pro-σ^K(1-127)-His_6/T7-cytTM-SpoIVFB A32C C35S-$FLAG_2$-His_6	pYZ2 was subjected to SDM using primers SO-P232 and SO-P233, substituting A32C and C35S in cytTM-SpoIVFB.	This study
pSO257	Km^R; T7-Pro-σ^K(1-127)-His_6/T7-cytTM-SpoIVFB L33C C35S-$FLAG_2$-His_6	pYZ2 was subjected to SDM using primers SO-P234 and SO-P235, substituting L33C and C35S in cytTM-SpoIVFB.	This study
pSO258	Km^R; T7-Pro-σ^K(1-127)-His_6/T7-cytTM-SpoIVFB V86C-$FLAG_2$-His_6	pYZ2 was subjected to SDM using primers SO-P238 and SO-P239, substituting V86C in cytTM-SpoIVFB.	This study
pSO259	Km^R; T7-Pro-σ^K(1-127)-His_6/T7-cytTM-SpoIVFB Q181C-$FLAG_2$-His_6	pYZ2 was subjected to SDM using primers SO-P236 and SO-P237, substituting Q181C in cytTM-SpoIVFB.	This study
pSO260	Km^R; T7-Pro-σ^K(1-127)-His_6/T7-cytTM-SpoIVFB-$FLAG_2$-His_6/T7-GFPΔ27BofA G40C/SpoIVFA	pSO40 was subjected to SDM using primers SO-P226 and SO-P227, substituting G40C in GFPΔ27BofA.	This study
pSO261	Km^R; T7-Pro-σ^K(1-127)-His_6/T7-cytTM-SpoIVFB-$FLAG_2$-His_6/T7-GFPΔ27BofA A41C/SpoIVFA	pSO40 was subjected to SDM using primers SO-P228 and SO-P229, substituting A41C in GFPΔ27BofA.	This study
pSO262	Km^R; T7-Pro-σ^K(1-127)-His_6/T7-cytTM-SpoIVFB-$FLAG_2$-His_6/T7-GFPΔ27BofA I56C/SpoIVFA	pSO40 was subjected to SDM using primers SO-P222 and SO-P223, substituting I56C in GFPΔ27BofA.	This study
pSO263	Km^R; T7-Pro-σ^K(1-127)-His_6/T7-cytTM-SpoIVFB-$FLAG_2$-His_6/T7-GFPΔ27BofA H57C/SpoIVFA	pSO40 was subjected to SDM using primers SO-P224 and SO-P225, substituting H57C in GFPΔ27BofA.	This study
pSO289	Km^R; T7-Pro-σ^K-His_6/T7-cytTM- SpoIVFB-$FLAG_2$/T7-GFPΔ27BofA/SpoIVFA	Fragment *spoIVFB* was amplified from pSO40 using primers SO-P138 and SO-P139. Vector pSO211 was amplified using primers SO-P140 and SO-P141. Fragment was joined to pSO211 using GA.	This study
pSO290	Km^R; T7-Pro-σ^K-His_6/T7-cytTM- SpoIVFB-$FLAG_2$	Vector pSO289 was amplified using primers SO-P319 and SO-P320, deleting *T7-gfpΔ27bofA/spoIVFA*. Vector was joined using GA.	This study
pYZ2	Km^R; T7-Pro-σ^K(1-127)-His_6/T7-cytTM-SpoIVFB-$FLAG_2$-His_6	pZR209 was digested with BglII and XhoI, and fragment *T7-cytTM-SpoIVFB-$FLAG_2$-His_6* was ligated with BglII-XhoI-digested pZR27.	Zhang, Y. unpublished

Table S2.1 (cont'd)

pYZ28	Km^R; T7-single-Cys P135C cytTM-SpoIVFB E44Q-$FLAG_2$-His_6	pPL29 was digested with XbaI and XhoI, and fragment *T7-single-Cys P135C cytTM-SpoIVFB E44Q-$FLAG_2$-His_6* was ligated with XbaI-XhoI-digested pZR8.	Zhang, Y. unpublished
pYZ40	Ap^R; T7-single-Cys E44C cytTM-SpoIVFB-$FLAG_2$-His_6, which also has C35S C165L C167L C172S C246S		[45]
pYZ46	Ap^R; T7-GFPΔ27BofA/SpoIVFA	pZR33 was digested with BamHI and NotI, and fragment *spoIVFA* was ligated with BamHI-NotI-digested pZR62	Zhang, Y. unpublished
pYZ77	Ap^R; T7-single-Cys V70C cytTM-SpoIVFB E44Q-$FLAG_2$-His_6, which also has C35S C165L C167L C172S C246S		[45]
pYZ112	Ap^R; T7-His_6-MBP-FtsL(23-117)		[86]
pZR8	Km^R; T7-Pro-σ^K(1-109)-His_6		[31]
pZR27	Km^R; T7-Pro-σ^K(1-127)-His_6		[31]
pZR33	Ap^R; T7-His_{10}-SpoIVFB-GFP/SpoIVFA		[31]
pZR53	Ap^R; T7-SpoIVB-His_6		[39]
pZR62	Ap^R; T7-GFPΔ27BofA		[31]
pZR209	Ap^R; T7-cytTM-SpoIVFB-$FLAG_2$-His_6		[42]

[a]Site-directed mutagenesis using the QuikChange kit (Stratagene).
[b]Gibson assembly [87].
[c]Overlap extension polymerase chain reaction.

Table S2.2 Primers used in this study

Primer	Sequence
SO-P11	GTTAGTCGTCATTAAGCAATAAGATCCGAAGGAGATATAC
SO-P12	GTATATCTCCTTCGGATCTTATTGCTTAATGACGACTAAC
SO-P13	GAACTATACAAACTCGAGTTTGTGGCAGGTGCTTTG
SO-P14	CAAAGCACCTGCCACAAACTCGAGTTTGTATAGTTC
SO-P48	CTGTTAAATTTGTGGCAGCTGCTTTGCTGCTGGTTTG
SO-P49	CAAACCAGCAGCAAAGCAGCTGCCACAAATTTAACAG
SO-P50	GTGGCAGGTGCTTTGCTGGCGGTTTGTGTAAATATGTT
SO-P51	AACATATTTACACAAACCGCCAGCAAAGCACCTGCCAC
SO-P52	TTGCTGCTGGTTTGTGTAGCTATGTTTGGCGGCAGTCT
SO-P53	AGACTGCCGCCAAACATAGCTACACAAACCAGCAGCAA
SO-P54	GTTTGTGTAAATATGTTTGCCGGCAGTCTTGGCATTCA
SO-P55	TGAATGCCAAGACTGCCGGCAAACATATTTACACAAAC
SO-P56	CTTGGCATTCATGTGCCGGCTAATCTGGTTACAACAGC
SO-P57	GCTGTTGTAACCAGATTAGCCGGCACATGAATGCCAAG
SO-P58	GGCATTCATGTGCCGATTGCTCTGGTTACAACAGCTATC
SO-P59	GATAGCTGTTGTAACCAGAGCAATCGGCACATGAATGCC
SO-P60	GTGCCGATTAATCTGGTTGCAACAGCTATCAGCGGAA
SO-P61	TTCCGCTGATAGCTGTTGCAACCAGATTAATCGGCAC
SO-P62	GTTACAACAGCTATCAGCGCAATTTTAGGAATACCCGG
SO-P63	CCGGGTATTCCTAAAATTGCGCTGATAGCTGTTGTAAC
SO-P64	ACAGCTATCAGCGGAATTGCAGGAATACCCGGAATAGC
SO-P65	GCTATTCCGGGTATTCCTGCAATTCCGCTGATAGCTGT
SO-P66	CTATCAGCGGAATTTTAGCAATACCCGGAATAGCTGC
SO-P67	CTATCAGCGGAATTTTAGCAATACCCGGAATAGCTGC
SO-P68	CAGCGGAATTTTAGGAATAGCCGGAATAGCTGCGTTAG
SO-P69	CTAACGCAGCTATTCCGGCTATTCCTAAAATTCCGCTG
SO-P70	GAATTTTAGGAATACCCGCAATAGCTGCGTTAGTCGTC
SO-P71	GACGACTAACGCAGCTATTGCGGGTATTCCTAAAATTC
SO-P72	ATACCCGGAATAGCTGCGGCAGTCGTCATTAAGCAATT
SO-P73	AATTGCTTAATGACGACTGCCGCAGCTATTCCGGGTAT
SO-P74	GTCGTCATTAAGCAATTTGCCATTTAAGGATCCGAAGG
SO-P75	CCTTCGGATCCTTAAATGGCAAATTGCTTAATGACGAC
SO-P76	GTCATTAAGCAATTTATCGCTTAAGGATCCGAAGGAGA
SO-P77	TCTCCTTCGGATCCTTAAGCGATAAATTGCTTAATGAC
SO-P80	TGAGATCCGGCTGCTAACAAAGCCC
SO-P82	GGCTTTGTTAGCAGCCGGATCTCAGCGGCCGCTTATTCAAATGAAATC
SO-P83	CTTTAAGAAGGAGATATACATATGGCTAGCATGA
SO-P89	CTTTAAGAAGGAGATATACATATGGCTAGCATGA
SO-P90	ATGACAAGCTCGAGCACCACCACCACCACCACTGAGATCTCGATCCCGCGAAATTAAT A
SO-P91	GGCGGCAGTCTTGGCATTGCTGTGCCGATTAATCTGGT
SO-P92	ACCAGATTAATCGGCACAGCAATGCCAAGACTGCCGCC
SO-P93	CAGTCTTGGCATTCATGTGGCGATTAATCTGGTTACAAC
SO-P94	GTTGTAACCAGATTAATCGCCACATGAATGCCAAGACTG
SO-P95	ATAGCTGCGTTAGTCGTCGCTAAGCAATTTATCATTTA
SO-P96	TAAATGATAAATTGCTTAGCGACGACTAACGCAGCTAT

Table S2.2 (cont'd)

SO-P97	GTTAGTCGTCATTAAGCAAGCTATCATTTAAGGATCCGAAG
SO-P98	CTTCGGATCCTTAAATGATAGCTTGCTTAATGACGACTAAC
SO-P99	TAAGAAGGAGATATACATATGGCTAGC
SO-P100	GGCTTTGTTAGCAGCCGGATCTCAGCGGCCGCGGATCCTTAAATGATAAATTGCTTAA TG
SO-P101	CTTTAAGAAGGAGATATACATATGGCTAGCATGAGTCACAGAGCAGATGAAATCAG
SO-P106	GTCGTCATTAAGCAAGCTGCCGCTTAAGGATCCGAAGGAGA
SO-P107	TCTCCTTCGGATCCTTAAGCGGCAGCTTGCTTAATGACGAC
SO-P108	GAACTATACAAACTCGAGGGCGGCAGCGGCGGCAGCGGCGGCAGCTTTGTGGCAGGT GCTTTG
SO-P109	CAAAGCACCTGCCACAAAGCTGCCGCCGCTGCCGCCGCTGCCGCCCTCGAGTTTGTAT AGTTC
SO-P112	CTTACCCTTAAATTTATTAGCACTACTGGAAAACTAC
SO-P113	GTAGTTTTCCAGTAGTGCTAATAAATTTAAGGGTAAG
SO-P114	TTCGCGTATGGTCTTCAAAGCTTTGCGAGATACCCAG
SO-P115	CTGGGTATCTCGCAAAGCTTTGAAGACCATACGCGAA
SO-P116	GATTCAATTATCCTGAAATTACTTCTGTCGGCCTTACTTGTTCTCGTTTCAGCT
SO-P117	AGCTGAAACGAGAACAAGTAAGGCCGACAGAAGTAATTTCAGGATAATTGAATC
SO-P118	TGAGATCCGGCTGCTAACA
SO-P119	CTTGTCATCGTCATCCTTGTAATCC
SO-P120	GGATTACAAGGATGACGATGACAAGTAATGAGATCTCGATCCCGCGAAATTAATA
SO-P132	GCATGAATTCTTTTCTTCGCAAGAAAACATTAAGAAG
SO-P133	GCATGCATGCGCTTGTTCTAGTACAAGCTTATGAG
SO-P134	GACTAGAGTCGAATCCCGGCATGCACATAAGGAGGAACTACT
SO-P135	AGTAGTTCCTCCTTATGTGCATGCCGGGATTCGACTCTAGTC
SO-P136	GCGACGTATGCAGCGAGGAGTATTGAAAATGAAATCC
SO-P137	GGATTTCATTTTCAATACTCCTCGCTGCATACGTCGC
SO-P138	ATGAATAAATGGCTCGACCTTATCTTAAAG
SO-P139	GTAGGGCAGAAGCAGTTCC
SO-P140	CTTCCATGGAGGAACTGCTTC
SO-P141	GATAAGGTCGAGCCATTTATTCATGG
SO-P142	GCATGCACATAAGGAGGAACTACTATGAGTAAAGGAGAAGAACTTTTC
SO-P143	CGACCGGCGCTCAGGATCCTTAAATGATAAATTGCTT
SO-P148	CGCATTGAAAAAAACAAAAAAATAAGATCCATGAGTAAAGGAGAAGATCT
SO-P149	AGATCTTCTCCTTTACTCATGGATCTTATTTTTTTGTTTTTTTCAATGCG
SO-P152	GGTGCTTTGCTGCTGGTTAGTGTAAATATGTTTGGCG
SO-P153	CGCCAAACATATTTACACTAACCAGCAGCAAAGCACC
SO-P156	GAGATATACATATGGCTAGCATGGAAACTGAAGAAGGTAAACTGGTAATCTGGATTA ACG
SO-P157	CTGATGCCAATCCACTTCTCGAGGGCCGCCGCGTCTTT
SO-P158	CTCGAGAAGTGGATTGGC
SO-P159	CATGCTAGCCATATGTATATCTCC
SO-P162	GAAGAAAAAAAATACTTATGCCTCATGGCTAAAGGGGATG
SO-P163	CATCCCCTTTAGCCATGAGGCATAAGTATTTTTTTTCTTC
SO-P164	AGAAAAAAAATACTTAGAGTGCATGGCTAAAGGGGATGA
SO-P165	TCATCCCCTTTAGCCATGCACTCTAAGTATTTTTTTTCT
SO-P168	GTGAGATTTCTCCTCGAATGCTATTACGGAAAAAACAGG
SO-P169	CCTGTTTTTTCCGTAATAGCATTCGAGGAGAAATCTCAC
SO-P170	GATTTCTCCTCGAAAGGTGCTACGGAAAAAACAGGGAG

Table S2.2 (cont'd)

SO-P171	CTCCCTGTTTTTTCCGTAGCACCTTTCGAGGAGAAATC
SO-P172	TTCTCCTCGAAAGGTATTGCGGAAAAAACAGGGAGC
SO-P173	GCTCCCTGTTTTTTCCGCAATACCTTTCGAGGAGAA
SO-P174	AAGGAATTGAAAGCTATTGCGCTGGAAAAGGGACAAAG
SO-P175	CTTTGTCCCTTTTCCAGCGCAATAGCTTTCAATTCCTT
SO-P176	GGAATTGAAAGCTATTCCTGTGGAAAAGGGACAAAGCTG
SO-P177	CAGCTTTGTCCCTTTTCCACAGGAATAGCTTTCAATTCC
SO-P180	GAAACTTCTGCCGCTGACATGCAAGGCGGAGGATAAAGTC
SO-P181	GACTTTATCCTCCGCCTTGCATGTCAGCGGCAGAAGTTTC
SO-P182	CTTCTGCCGCTGACAGTATGCGCGGAGGATAAAGTCTATC
SO-P183	GATAGACTTTATCCTCCGCGCATACTGTCAGCGGCAGAAG
SO-P184	CTGCCGCTGACAGTAAAGTGCGAGGATAAAGTCTATCATG
SO-P185	CATGATAGACTTTATCCTCGCACTTTACTGTCAGCGGCAG
SO-P186	GCGAAGAAAAAAAAATACTGCGAGCTCATGGCTAAAGGG
SO-P187	CCCTTTAGCCATGAGCTCGCAGTATTTTTTTTCTTCGC
SO-P188	GAGAAACTTCTGCCGCTGTGCGTAAAGGCGGAGGATAAAG
SO-P189	CTTTATCCTCCGCCTTTACGCACAGCGGCAGAAGTTTCTC
SO-P196	GGAATTGAAAGCTATTCCGCTTGCAAAGGGACAAAGCTGG
SO-P197	CCAGCTTTGTCCCTTTGCAAGCGGAATAGCTTTCAATTCC
SO-P202	GGCTTGCTCACAGGCCATTGCAAAGCATTATTATGTCTG
SO-P203	CAGACATAATAATGCTTTGCAATGGCCTGTGAGCAAGCC
SO-P204	CATTCATGTGCCGATTAATTGCGTTACAACAGCTATCAGC
SO-P205	GCTGATAGCTGTTGTAACGCAATTAATCGGCACATGAATG
SO-P206	CATGTGCCGATTAATCTGTGTACAACAGCTATCAGCGGA
SO-P207	TCCGCTGATAGCTGTTGTACACAGATTAATCGGCACATG
SO-P209	GGCTTGCTCACAGGCCATTGCAAAGCATTATTATCTCTG
SO-P210	CAGAGATAATAATGCTTTGCAATGGCCTGTGAGCAAGCC
SO-P211	GCTTCTGCCCTACAAGCTTTAATGAGATCTCGATCCC
SO-P212	GGGATCGAGATCTCATTAAAGCTTGTAGGGCAGAAGC
SO-P218	GAGCTTGTCTTTTTAGTATGTTACGTGAAAAACAATGC
SO-P219	GCATTGTTTTTCACGTAACATACTAAAAAGACAAGCTC
SO-P222	GTTTGGCGGCAGTCTTGGCTGTCATGTGCCGATTAATCTG
SO-P223	CAGATTAATCGGCACATGACAGCCAAGACTGCCGCCAAAC
SO-P224	GGCGGCAGTCTTGGCATTTGTGTGCCGATTAATCTGGT
SO-P225	ACCAGATTAATCGGCACACAAATGCCAAGACTGCCGCC
SO-P226	GCTGTTAAATTTGTGGCATGTGCTTTGCTGCTGGTTAG
SO-P227	CTAACCAGCAGCAAAGCACATGCCACAAATTTAACAGC
SO-P228	GTTAAATTTGTGGCAGGTTGTTTGCTGCTGGTTAGTGT
SO-P229	ACACTAACCAGCAGCAAACAACCTGCCACAAATTTAAC
SO-P232	CTCACAGGCCATATGAAATGTTTATTATCTCTGCTCCTG
SO-P233	CAGGAGCAGAGATAATAAACATTTCATATGGCCTGTGAG
SO-P234	CAGGCCATATGAAAGCATGTTTATCTCTGCTCCTGATTG
SO-P235	CAATCAGGAGCAGAGATAAACATGCTTTCATATGGCCTG
SO-P236	TTATTCGTGATTCCTCTGTGTATCAGCGCATGGGTTTTG
SO-P237	CAAAACCCATGCGCTGATACACAGAGGAATCACGAATAA
SO-P238	GTTAAAGGAAGAGTTTGCGTGCATTATTGCCGGACCTCT
SO-P239	AGAGGTCCGGCAATAATGCACGCAAACTCTTCCTTTAAC
SO-P242	CGTGTTTTTTTGCTGCCGGCTGGCGGAACGGTCGAAGTG

Table S2.2 (cont'd)

SO-P243	CACTTCGACCGTTCCGCCAGCCGGCAGCAAAAAAACACG
SO-P244	GGCATCGTACAGGGGATGGCCGGAAGCCCGATCATTCAA
SO-P245	TTGAATGATCGGGCTTCCGGCCATCCCCTGTACGATGCC
SO-P248	GATTTCATTTGAATAAGCGGCCGCGTCCGGCGTAGAGGATCG
SO-P251	TTGCTGCTGGTTTGTGTAGATATGTTTGGCGGCAGTC
SO-P252	GACTGCCGCCAAACATATCTACACAAACCAGCAGCAA
SO-P257	AAAGGATCCCACCACCAC
SO-P260	GATCTTAGTGGTGGTGGTGGTGGGATCCTTTCCCCTTCGCCTTCTTC
SO-P269	CAATGCGCGCAAATGCATG
SO-P270	TGAAATCCTCATGCATTTGCGC
SO-P271	CTTAAGGGAAGCGAAGCAGC
SO-P272	CCGCTACTGTCAACAACTTTTTAGC
SO-P273	TAAGGATCCGAAGGAGATATACATATGAG
SO-P276	GACTCATATGTATATCTCCTTCGGATCCTTAAATGATAAATTGCTTAATGACGACTAACG
SO-P277	TTAAGAAGGAGATATACATATGGCTAGCATGGAGCCTATTTTTATTATTGGGATTATTTT
SO-P280	CATGCTAGCCATATGTATATCTCCTTCTTAAAG
SO-P282	CTCAGTGGTGGTGGTGGTGGTGCTCGAGGCTTGCTTTTTCTTTTCCATAAATATCGATTC
SO-P283	CTGCTAGTTGAACGCTTCCATCTTCAATGTTG
SO-P284	CAACATTGAAGATGGAAGCGTTCAACTAGCAG
SO-P285	GGCTTTGTTAGCAGCCGGATCTCAGTG
SO-P286	CTAATCGTTTTCTGATTTCATCTGCTCTGTG
SO-P287	ATGAGTCACAGAGCAGATGAAATCAGAAAACGATTAG
SO-P288	ATCTCATTACTTGTCATCGTCATCCTTGTAATCCTTGTCATCGTCATCCTTGTAATC
SO-P289	CTTGCTTTCCTGGCTCCTGAA
SO-P290	CGATCCTCTACGCCGGACGCGGCCGCTTATTCAAATGAAATC
SO-P293	GCAAATCAGCGCATGGGTTTTGTTTGTCTTTCTGG
SO-P294	GCAAATCAGCGCATGGGTTTTG
SO-P295	CAAACAAAACCCATGCGCTGATTTGC
SO-P302	GATTTCATTTGAATAAGCGGCCGCTGAAGGAGATATACATATGCCCGATAAC
SO-P303	ATGTTATCGGGCATATGTATATCTCCTTCAGCGGCCGCTTATTCAAATG
SO-P304	CTTGCTTTCCTGGCTCCTGAACACAAAAATAAGGAACAGC
SO-P305	CTCAGTGGTGGTGGTGGTGGTGCTC
SO-P306	GAGCACCACCACCACCACCACTG
SO-P307	CTGTTCCTTATTTTTGTGTTCAGGAGCCAGGAAAGCAAG
SO-P310	GCTGTTAAATTTGTGGCAGGTGCTTTGCTG
SO-P311	CAGCAAAGCACCTGCCACAAATTTAACAGC
SO-P319	CGATGACAAGTAATGAGATCCGGCTGCTAACAAAGCCC
SO-P320	GATCTCATTACTTGTCATCGTCATCCTTGTAATCCTTGTCATCGTCATCCTTGTAATCAA
LK2465	AAAGAGCTTGTCTGTTTAGTATCTTAC
LK2466	GTAAGATACTAAACAGACAAGCTCTTT
LK2467	CTTGTCTTTTTATGTTCTTACGTGAAA
LK2468	TTTCACGTAAGAACATAAAAAGACAAC
LK2473	GTATCTTACGTGTGTAACAATGCCTTT
LK2474	AAAGGCATTGTTACACACGTAAGATAC
LK2691	GCAGCATGCCCCAGCTGATGAATCAATACAATC

Table S2.2 (cont'd)

YZ1	GATTGTATTGATTCATTGCCTGGGGCATGCTGCTC
YZ2	GAGCAGCATGCCCCAGGCAATGAATCAATACAATC
YZ11	GATTGTATTGATTCATCAGCTGGGGCATGCTGC

Table S2.3 Sequencing primers used in this study

Primer	Sequence	Notes
SO-P23	CATTACCTGTCCACACAATCTGC	Forward primer. Binds in GFP.
SO-P84	CATACCCACGCCGAAACAAG	Forward primer. Binds upstream of the T7 promoter in pET29b.
SO-P86	GAGTAAAGGAGAAGATCTCGATCC	Forward primer. Binds in Pro-σ^K.
SO-P87	CTCCAGTGAAAAGTTCTTCTCC	Reverse primer. Binds in GFP.
SO-P104	CATGGAGGAACTGCTTCTGC	Forward primer. Binds in SpoIVFB.
SO-P121	GCAGATTGTGTGGACAGGTAATG	Reverse primer. Binds in GFP.
SO-P122	CTGTCAGTGGAGAGGGTGA	Forward primer. Binds in GFP.
SO-P123	TCACCCTCTCCACTGACAG	Reverse primer. Binds in GFP.
SO-P157	CTGATGCCAATCCACTTCTCGAGGGCCGCCGCGTCTTT	Reverse primer. Binds in MBP.
SO-P160	CTTCAGCGAGACCGTTATAGC	Reverse primer. Binds in MBP.
SO-P161	ACTGACGGGTCCAATGTTTG	Reverse primer. Binds in SpoIVFA.
SO-P276	GACTCATATGTATATCTCCTTCGGATCCTTAAATGATAAATT GCTTAATGACGACTAACG	Reverse primer. Binds in BofA
SO-P279	GACTGACGGTTAAGGTGCAG	Forward primer. Binds in SpoIVFA
DP18	GCTAGTTATTGCTCAGCGG	Reverse primer. Binds T7 terminator
DP89	TAATACGACTCACTATAGGG	Forward primer. Binds T7 promoter.

Table S2.4 *B. subtilis* strains used in this study

Strain	Genotype	Construction	Citation
PY79	Prototrophic wild-type strain		[88]
BK754	*spoIVB165*		[33]
ZR264	*spoIVB165 bofA*::*erm*		[31]
SO3	*spoIVB165 bofA*::*erm amyE*::P_{bofA}-*gfpΔ27bofA*	ZR264 was transformed with pSO78	This study
SO6	*spoIVB165 bofA*::*erm amyE*::P_{bofA}-*gfpΔ27bofA N48A*	ZR264 was transformed with pSO86	This study
SO8	*spoIVB165 bofA*::*erm amyE*::P_{bofA}-*gfpΔ27bofA N61A*	ZR264 was transformed with pSO87	This study
SO10	*spoIVB165 bofA*::*erm amyE*::P_{bofA}-*gfpΔ27bofA T64A*	ZR264 was transformed with pSO88	This study

REFERENCES

REFERENCES

1. Brown, M.S., et al., *Regulated intramembrane proteolysis: a control mechanism conserved from bacteria to humans.* Cell, 2000. **100**(4): p. 391-398.

2. Urban, S., *Mechanisms and cellular functions of intramembrane proteases.* Biochim. Biophys. Acta - Biomembr., 2013. **1828**: p. 2797-2800.

3. Manolaridis, I., et al., *Mechanism of farnesylated CAAX protein processing by the intramembrane protease Rce1.* Nature, 2013. **504**(7479): p. 301-305.

4. Hu, J., et al., *The crystal structure of GXGD membrane protease FlaK.* Nature, 2011. **475**(7357): p. 528-531.

5. Li, X., et al., *Structure of a presenilin family intramembrane aspartate protease.* Nature, 2013. **493**(7430): p. 56-61.

6. Feng, L., et al., *Structure of a site-2 protease family intramembrane metalloprotease.* Science, 2007. **318**(5856): p. 1608-1612.

7. Wang, Y., Y. Zhang, and Y. Ha, *Crystal structure of a rhomboid family intramembrane protease.* Nature, 2006. **444**(7116): p. 179-183.

8. Wu, Z., et al., *Structural analysis of a rhomboid family intramembrane protease reveals a gating mechanism for substrate entry.* Nat. Struct. Mol. Biol., 2006. **13**(12): p. 1084-1091.

9. Cho, S., S.W. Dickey, and S. Urban, *Crystal structures and inhibition kinetics reveal a two-stage catalytic mechanism with drug design implications for rhomboid proteolysis.* Mol. Cell, 2016. **61**(3): p. 329-340.

10. Zoll, S., et al., *Substrate binding and specificity of rhomboid intramembrane protease revealed by substrate-peptide complex structures.* EMBO J., 2014. **33**(20): p. 2408-2421.

11. Yang, G., et al., *Structural basis of Notch recognition by human γ-secretase.* Nature, 2019. **565**(7738): p. 192-197.

12. Zhou, R., et al., *Recognition of the amyloid precursor protein by human γ-secretase.* Science, 2019. **363**(6428): p. eaaw0930.

13. Rawson, R.B., *The site-2 protease.* Biochim. Biophys. Acta - Biomembr., 2013. **1828**(12): p. 2801-2807.

14. Ye, J., *Roles of regulated intramembrane proteolysis in virus infection and antiviral immunity.* Biochim. Biophys. Acta - Biomembr., 2013. **1828**(12): p. 2926-2932.

15. Adam, Z., *Emerging roles for diverse intramembrane proteases in plant biology.* Biochim. Biophys. Acta - Biomembr., 2013. **1828**(12): p. 2933-2936.

16. Chang, Y.C., et al., *Sre1p, a regulator of oxygen sensing and sterol homeostasis, is required for virulence in Cryptococcus neoformans.* Mol. Microbiol., 2007. **64**(3): p. 614-629.

17. Urban, S., *Making the cut: central roles of intramembrane proteolysis in pathogenic microorganisms.* Nat. Rev. Microbiol., 2009. **7**: p. 411-423.

18. Kroos, L. and Y. Akiyama, *Biochemical and structural insights into intramembrane metalloprotease mechanisms.* Biochim. Biophys. Acta - Biomembr., 2013. **1828**(12): p. 2873-2885.

19. Schneider, J.S. and M.S. Glickman, *Function of site-2 proteases in bacteria and bacterial pathogens.* Biochim. Biophys. Acta - Biomembr., 2013. **1828**(12): p. 2808-2814.

20. Galperin, M.Y., et al., *Genomic determinants of sporulation in Bacilli and Clostridia: towards the minimal set of sporulation-specific genes.* Environ. Microbiol., 2012. **14**(11): p. 2870-2890.

21. McKenney, P.T., A. Driks, and P. Eichenberger, *The Bacillus subtilis endospore: assembly and functions of the multilayered coat.* Nat. Rev. Microbiol., 2013. **11**(1): p. 33-44.

22. Al-Hinai, M.A., S.W. Jones, and E.T. Papoutsakis, *The Clostridium sporulation programs: diversity and preservation of endospore differentiation.* Microbiol. Mol. Biol. Rev., 2015. **79**(1): p. 19-37.

23. Checinska, A., A. Paszczynski, and M. Burbank, *Bacillus and other spore-forming genera: variations in responses and mechanisms for survival.* Annu. Rev. Food Sci. Technol., 2015. **6**: p. 351-369.

24. Cutting, S., et al., *A forespore checkpoint for mother-cell gene expression during development in Bacillus subtilis.* Cell, 1990. **62**: p. 239-250.

25. Cutting, S., S. Roels, and R. Losick, *Sporulation operon spoIVF and the characterization of mutations that uncouple mother-cell from forespore gene expression in Bacillus subtilis.* J. Mol. Biol., 1991. **221**: p. 1237-1256.

26. Ricca, E., S. Cutting, and R. Losick, *Characterization of bofA, a gene involved in intercompartmental regulation of pro-σ^K processing during sporulation in Bacillus subtilis.* J. Bacteriol., 1992. **174**: p. 3177-3184.

27. Tan, I.S. and K.S. Ramamurthi, *Spore formation in Bacillus subtilis.* Environ. Microbiol. Rep., 2014. **6**(3): p. 212-225.

28. Resnekov, O., S. Alper, and R. Losick, *Subcellular localization of proteins governing the proteolytic activation of a developmental transcription factor in Bacillus subtilis.* Genes Cells, 1996. **1**(6): p. 529-542.

29. Rudner, D.Z., Q. Pan, and R.M. Losick, *Evidence that subcellular localization of a bacterial membrane protein is achieved by diffusion and capture.* Proc Natl Acad Sci U S A, 2002. **99**(13): p. 8701-6.

30. Rudner, D.Z. and R. Losick, *A sporulation membrane protein tethers the pro-σ^K processing enzyme to its inhibitor and dictates its subcellular localization.* Genes Dev., 2002. **16**(8): p. 1007-1018.

31. Zhou, R. and L. Kroos, *BofA protein inhibits intramembrane proteolysis of pro-σ^K in an intercompartmental signaling pathway during Bacillus subtilis sporulation.* Proc. Natl. Acad. Sci. USA, 2004. **101**(17): p. 6385-6390.

32. Kroos, L., et al., *Forespore signaling is necessary for pro-σ^K processing during Bacillus subtilis sporulation despite the loss of SpoIVFA upon translational arrest.* J. Bacteriol., 2002. **184**(19): p. 5393-5401.

33. Cutting, S., et al., *Forespore-specific transcription of a gene in the signal transduction pathway that governs pro-σ^K processing in Bacillus subtilis.* Genes Dev., 1991. **5**: p. 456-466.

34. Pan, Q., R. Losick, and D.Z. Rudner, *A second PDZ-containing serine protease contributes to activation of the sporulation transcription factor σ^K in Bacillus subtilis.* J. Bacteriol., 2003. **185**(20): p. 6051-6056.

35. Dong, T.C. and S.M. Cutting, *SpoIVB-mediated cleavage of SpoIVFA could provide the intercellular signal to activate processing of Pro-σ^K in Bacillus subtilis.* Mol. Microbiol., 2003. **49**(5): p. 1425-1434.

36. Campo, N. and D.Z. Rudner, *A branched pathway governing the activation of a developmental transcription factor by regulated intramembrane proteolysis.* Mol. Cell, 2006. **23**(1): p. 25-35.

37. Campo, N. and D.Z. Rudner, *SpoIVB and CtpB are both forespore signals in the activation of the sporulation transcription factor σ^K in Bacillus subtilis.* J. Bacteriol., 2007. **189**(16): p. 6021-6027.

38. Mastny, M., et al., *CtpB assembles a gated protease tunnel regulating cell-cell signaling during spore formation in Bacillus subtilis.* Cell, 2013. **155**(3): p. 647-658.

39. Zhou, R. and L. Kroos, *Serine proteases from two cell types target different components of a complex that governs regulated intramembrane proteolysis of pro-σ^K during Bacillus subtilis development.* Mol. Microbiol., 2005. **58**(3): p. 835-846.

40. Rudner, D., P. Fawcett, and R. Losick, *A family of membrane-embedded metalloproteases involved in regulated proteolysis of membrane-associated transcription factors.* Proc. Natl. Acad. Sci. USA, 1999. **96**: p. 14765-14770.

41. Yu, Y.-T.N. and L. Kroos, *Evidence that SpoIVFB is a novel type of membrane metalloprotease governing intercompartmental communication during Bacillus subtilis sporulation.* J. Bacteriol., 2000. **182**: p. 3305-3309.

42. Zhou, R., et al., *Intramembrane proteolytic cleavage of a membrane-tethered transcription factor by a metalloprotease depends on ATP.* Proc. Natl. Acad. Sci. USA, 2009. **106**: p. 16174-16179.

43. Kroos, L., B. Kunkel, and R. Losick, *Switch protein alters specificity of RNA polymerase containing a compartment-specific sigma factor.* Science, 1989. **243**: p. 526-529.

44. Eichenberger, P., et al., *The program of gene transcription for a single differentiating cell type during sporulation in Bacillus subtilis.* PLoS Biol., 2004. **2**(10): p. e328.

45. Zhang, Y., et al., *Residues in conserved loops of intramembrane metalloprotease SpoIVFB interact with residues near the cleavage site in Pro-σ^K.* J. Bacteriol., 2013. **195**(21): p. 4936-4946.

46. Halder, S., et al., *Interaction of intramembrane metalloprotease SpoIVFB with substrate Pro-σ^K.* Proc. Natl. Acad. Sci. USA, 2017. **114**: p. E10677-E10686.

47. Saribas, A.S., L. Gruenke, and L. Waskell, *Overexpression and purification of the membrane-bound cytochrome P450 2B4.* Protein Expr. Purif., 2001. **21**(2): p. 303-309.

48. Prince, H., R. Zhou, and L. Kroos, *Substrate requirements for regulated intramembrane proteolysis of Bacillus subtilis pro-σ^K.* J. Bacteriol., 2005. **187**: p. 961-971.

49. Ramirez-Guadiana, F.H., et al., *Evidence that regulation of intramembrane proteolysis is mediated by substrate gating during sporulation in Bacillus subtilis.* PLoS Genet., 2018. **14**(11): p. e1007753.

50. de Hoon, M.J., P. Eichenberger, and D. Vitkup, *Hierarchical evolution of the bacterial sporulation network.* Curr. Biol., 2010. **20**(17): p. R735-R745.

51. Varcamonti, M., et al., *Membrane topology analysis of the Bacillus subtilis BofA protein involved in pro-σ^K processing.* Microbiol., 1997. **143**(Pt 4): p. 1053-1058.

52. Zhang, Y., et al., *Complex formed between intramembrane metalloprotease SpoIVFB and its substrate, Pro-σ^K.* J. Biol. Chem., 2016. **291**: p. 10347-10362.

53. Arolas, J.L., et al., *Multiple architectures and mechanisms of latency in metallopeptidase zymogens.* Chem. Rev., 2018. **118**(11): p. 5581-5597.

54. Akiyama, K., et al., *Roles of the membrane-reentrant β-hairpin-like loop of RseP protease in selective substrate cleavage.* eLife, 2015. **4**: p. e08928

55. Moss, M.L., et al., *The ADAM10 prodomain is a specific inhibitor of ADAM10 proteolytic activity and inhibits cellular shedding events.* J. Biol. Chem., 2007. **282**(49): p. 35712-35721.

56. Wong, E., et al., *Harnessing the natural inhibitory domain to control TNFα Converting Enzyme (TACE) activity in vivo.* Sci. Rep., 2016. **6**: p. 35598.

57. Gomis-Ruth, F.X., *Third time lucky? Getting a grip on matrix metalloproteinases.* J. Biol. Chem., 2017. **292**(43): p. 17975-17976.

58. Driks, A. and P. Eichenberger, eds. *The bacterial spore: from molecules to systems*. 2016, ASM Press: Washington, DC. 397.

59. Zorzi, A., K. Deyle, and C. Heinis, *Cyclic peptide therapeutics: past, present and future.* Curr. Opin. Chem. Biol., 2017. **38**: p. 24-29.

60. Sohrabi, C., A. Foster, and A. Tavassoli, *Methods for generating and screening libraries of genetically encoded cyclic peptides in drug discovery.* Nat. Rev. Chem., 2020. **4**(2): p. 90-101.

61. Grigorova, I.L., et al., *Fine-tuning of the Escherichia coli σ^E envelope stress response relies on multiple mechanisms to inhibit signal-independent proteolysis of the transmembrane anti-sigma factor, RseA.* Genes Dev., 2004. **18**(21): p. 2686-2697.

62. Inaba, K., et al., *A pair of circularly permutated PDZ domains control RseP, the S2P family intramembrane protease of Escherichia coli.* J. Biol. Chem., 2008. **283**(50): p. 35042-35052.

63. Kanehara, K., K. Ito, and Y. Akiyama, *YaeL proteolysis of RseA is controlled by the PDZ domain of YaeL and a Gln-rich region of RseA.* EMBO J., 2003. **22**(23): p. 6389-6398.

64. Ades, S.E., et al., *The Escherichia coli s^E-dependent extracytoplasmic stress response is controlled by the regulated proteolysis of an anti-sigma factor.* Genes Dev., 1999. **13**(18): p. 2449-2461.

65. Alba, B.M., et al., *DegS and YaeL participate sequentially in the cleavage of RseA to activate the σ^E-dependent extracytoplasmic stress response.* Genes Dev., 2002. **16**(16): p. 2156-2168.

66. Kanehara, K., K. Ito, and Y. Akiyama, *YaeL (EcfE) activates the σ^E pathway of stress response through a site-2 cleavage of anti-σ^E, RseA.* Genes Dev., 2002. **16**(16): p. 2147-2155.

67. Hizukuri, Y., et al., *A structure-based model of substrate discrimination by a noncanonical PDZ tandem in the intramembrane-cleaving protease RseP.* Structure, 2014. **22**(2): p. 326-336.

68. Konovalova, A., et al., *Inhibitor of intramembrane protease RseP blocks the σ^E response causing lethal accumulation of unfolded outer membrane proteins.* Proc. Natl. Acad. Sci. USA, 2018. **115**(28): p. E6614-E6621.

69. Jacobsen, J.A., et al., *To bind zinc or not to bind zinc: an examination of innovative approaches to improved metalloproteinase inhibition.* Biochim. Biophys. Acta, 2010. **1803**(1): p. 72-94.

70. Fields, G.B., *New strategies for targeting matrix metalloproteinases.* Matrix Biol., 2015. **44-46**: p. 239-246.

71. Hanahan, D., *Studies on transformation of Escherichia coli with plasmids.* J. Mol. Biol., 1983. **166**: p. 557-580.

72. Notredame, C., D.G. Higgins, and J. Heringa, *T-Coffee: A novel method for fast and accurate multiple sequence alignment.* J. Mol. Biol., 2000. **302**(1): p. 205-217.

73. Harwood, C.R. and S.M. Cutting, *Molecular Biological Methods for Bacillus*. 1990, Chichester, England: John Wiley & Sons. 581.

74. Parrell, D. and L. Kroos, *Channels modestly impact compartment-specific ATP levels during Bacillus subtilis sporulation and a rise in the mother cell ATP level is not necessary for Pro-σ^K cleavage.* Mol. Microbiol., 2020. **114**: p. 563-581.

75. Koide, K., K. Ito, and Y. Akiyama, *Substrate recognition and binding by RseP, an Escherichia coli intramembrane protease.* J. Biol. Chem., 2008. **283**(15): p. 9562-9570.

76. Lu, S., R. Halberg, and L. Kroos, *Processing of the mother-cell σ factor, σ^K, may depend on events occurring in the forespore during Bacillus subtilis development.* Proc. Natl. Acad. Sci. USA, 1990. **87**: p. 9722-9726.

77. Miller, M.D., et al., *Crystal structure of a tandem cystathionine-beta-synthase (CBS) domain protein (TM0935) from Thermotoga maritima at 1.87 Angstrom resolution.* Proteins, 2004. **57**(1): p. 213-217.

78. Schrecker, M., J. Korobenko, and R.K. Hite, *Cryo-EM structure of the lysosomal chloride-proton exchanger CLC-7 in complex with OSTM1.* eLife, 2020. **9**: p. e59555.

79. Feklistov, A. and S.A. Darst, *Structural basis for promoter-10 element recognition by the bacterial RNA polymerase sigma subunit.* Cell, 2011. **147**(6): p. 1257-1269.

80. Yang, J., et al., *Improved protein structure prediction using predicted interresidue orientations.* Proc. Natl. Acad. Sci. USA, 2020. **117**(3): p. 1496-1503.

81. Remmert, M., et al., *HHblits: lightning-fast iterative protein sequence searching by HMM-HMM alignment.* Nat. Methods, 2011. **9**(2): p. 173-175.

82. Mirdita, M., et al., *Uniclust databases of clustered and deeply annotated protein sequences and alignments.* Nucleic Acids Res., 2017. **45**(D1): p. D170-D176.

83. Chaudhury, S., S. Lyskov, and J.J. Gray, *PyRosetta: a script-based interface for implementing molecular modeling algorithms using Rosetta.* Bioinformatics, 2010. **26**(5): p. 689-691.

84. Park, H., et al., *Simultaneous optimization of biomolecular energy functions on features from small molecules and macromolecules.* J. Chem. Theory Comput., 2016. **12**(12): p. 6201-6212.

85. Green, D. and S. Cutting, *Membrane topology of the Bacillus subtilis Pro-σ^K processing complex.* J. Bacteriol., 2000. **182**: p. 278-285.

86. Parrell, D., et al., *Bacillus subtilis intramembrane protease RasP activity in Escherichia coli and in vitro.* J. Bacteriol., 2017. **199**: p. e00381-17.

87. Gibson, D.G., et al., *Enzymatic assembly of DNA molecules up to several hundred kilobases.* Nat. Methods, 2009. **6**(5): p. 343-345.

88. Youngman, P., J.B. Perkins, and R. Losick, *Construction of a cloning site near one end of Tn917 into which foreign DNA may be inserted without affecting transposition in*

Bacillus subtilis or expression of the transposon-borne erm gene. Plasmid, 1984. **12**: p. 1-9.

CHAPTER 3: Conserved Proline Residues of *Bacillus subtilis* Intramembrane Metalloprotease SpoIVFB Are Important for Substrate Interaction and Cleavage

We plan to submit this chapter for publication with the following citation:

Olenic S, Buchanan F*, VanPorfliet J*, Parrell D, and Kroos L. Conserved Proline Residues of *Bacillus subtilis* Intramembrane Metalloprotease SpoIVFB Are Important for Substrate Interaction and Cleavage

I contributed significantly to the writing, editing and work in this manuscript in addition to using plasmids generated by Fiona Buchanan, Jordyn VanPorfliet, and Daniel Parrell to prepare final figures and build from their preliminary work.

*Equal contributions

Abstract

Intramembrane metalloproteases regulate diverse biological processes by cleaving membrane-associated substrates within the membrane or near its surface. SpoIVFB is an intramembrane metalloprotease of *Bacillus subtilis* that cleaves Pro-σ^K during endosporulation. Intramembrane metalloproteases have a broadly conserved NPDG motif, which in the structure of an archaeal enzyme is located in a short loop that interrupts a transmembrane segment facing the active site. The aspartate residue of the NPDG motif acts as a ligand of the zinc ion involved in catalysis. The functions of other residues in the short loop are less well understood. We found that the predicted short loop of SpoIVFB contains two highly conserved proline residues, P132 of the NPDG motif and P135. Mutational analysis revealed that both proline residues are important for Pro-σ^K cleavage in *Escherichia coli* engineered to synthesize the proteins. Substitutions for either residue also impaired Pro-σ^K interaction with SpoIVFB in co-purification assays. Disulfide cross-linking experiments showed that the predicted short loop of SpoIVFB is in proximity to the Proregion of Pro-σ^K. Alanine substitutions for N129 and P132 of the SpoIVFB NPDG motif reduced cross-linking between its predicted short loop and the Proregion more than a P135A substitution. Conversely, the SpoIVFB P135A substitution reduced Pro-σ^K cleavage more than the N129A and P132A substitutions during sporulation of *B. subtilis*. We conclude that all three conserved residues of SpoIVFB are important for substrate interaction and cleavage, and we propose that P135 is necessary to position D137 to act as a zinc ligand.

Introduction

Regulated intramembrane proteolysis (RIP) controls many biological processes in all three domains of life [1, 2]. RIP utilizes intramembrane proteases (IPs), which cleave membrane-associated substrates within a transmembrane segment (TMS) or near the membrane surface. There are four known IP families: aspartyl proteases like presenilin (a component of γ-secretase), serine proteases (also referred to as rhomboids), the glutamyl protease Rce1, and intramembrane metalloproteases (IMMPs) [2, 3]. Crystal structures have been solved for representatives of each IP family [3-8]. Additionally, structures have been solved for rhomboid·peptide inhibitor complexes [9, 10] and for γ-secretase·substrate complexes [11, 12]; however, more work is needed in order to determine how IPs recognize and bind their substrates.

IMMPs activate transcription factors in numerous signaling pathways [1, 2]. S2P, an IMMP in humans, is involved in regulation of cholesterol homeostasis and responses to endoplasmic reticulum stress and viral infection [13, 14]. Bacterial IMMPs control endosporulation, enhance pathogenicity, regulate stress responses and polar morphogenesis, produce mating signals, and clear signal peptides from the membrane [15-19]. During endosporulation of *Bacillus* and *Clostridium* species, the IMMP SpoIVFB cleaves Pro-σ^K to make active σ^K, which directs RNA polymerase to transcribe genes necessary for mature spore formation [16, 20]. Endospores are dormant and can survive harsh environmental conditions [21], enhancing the persistence of pathogenic species [22, 23]. Thus, knowledge about SpoIVFB substrate recognition and binding could lead to new strategies to manipulate endosporulation and other processes involving IMMPs in bacteria and eukaryotes.

During endosporulation, *B. subtilis* forms two separate compartments, the mother cell (MC) and the forespore (FS) [24] (Figure 3.1A). SpoIVFB is held inactive in the outer FS

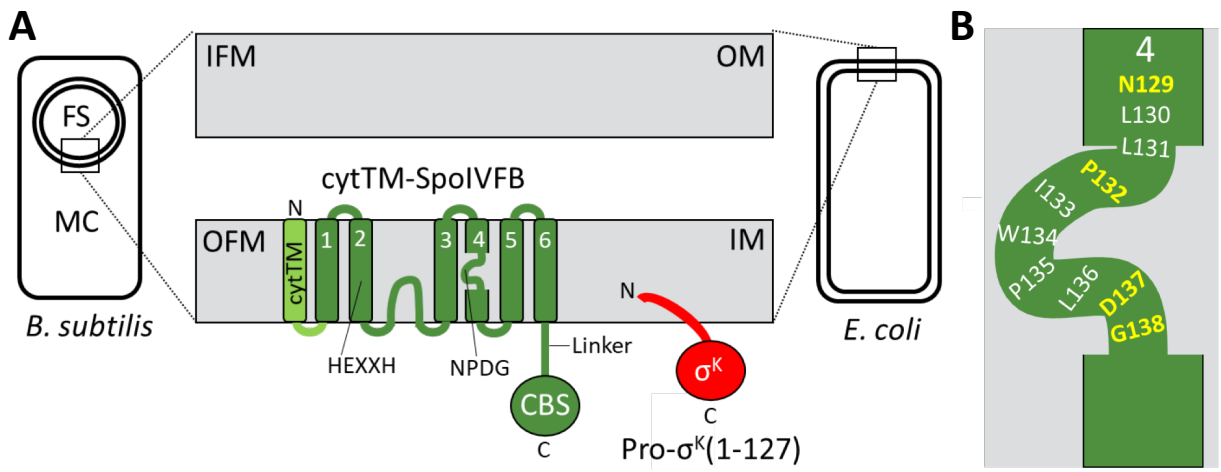

Figure 3.1 Cartoon depictions of SpoIVFB and Pro-σ^K. (*A*) Membrane topology of SpoIVFB during endosporulation of *B. subtilis* and when synthesized in *E. coli*. During endosporulation, the forespore (FS) is engulfed by the mother cell (MC), resulting in two membranes surrounding the FS (left). SpoIVFB (green) and Pro-σ^K (red) are synthesized in the MC and inserted into the outer FS membrane (OFM). When these proteins are produced in the *E. coli* cytosol (right), they insert into the inner membrane (IM). The expanded view of the membranes (middle) shows SpoIVFB with an extra transmembrane segment (cytTM) at its N terminus, the six predicted transmembrane segments (TMSs) and the interdomain linker that connects the C-terminal cystathionine-β-synthase (CBS) domain with TMS6. The locations of the HEXXH and NPDG motifs of SpoIVFB are indicated. When produced in *E. coli*, cytTM-SpoIVFB recognizes C-terminally truncated Pro-σ^K(1-127) as substrate and cleaves the N-terminal 21-residue Proregion, which appears to associate peripherally with the OFM in *B. subtilis* and the IM in *E. coli*. See the text for references. (*B*) Expanded view of the short loop predicted to interrupt TMS4 of SpoIVFB. Residues comprising the conserved NPDG motif are indicated by yellow.

membrane by the inhibitory proteins BofA and SpoIVFA [25-29]. A proteolytic cascade, initiated by FS secreted serine proteases SpoIVB and CtpB, relieves inhibition of SpoIVFB [30-32]. SpoIVB cleaves the C-terminal end of SpoIVFA [33, 34] and CtpB can cleave the C-terminal ends of both SpoIVFA and BofA [34-36]. Once inhibition is removed, SpoIVFB cleaves the N-terminal 21-residue Proregion from Pro-σ^K, releasing σ^K into the MC [37-39]. σ^K directs RNA polymerase to transcribe genes whose products form the spore coat and lyse the MC, releasing a mature spore [40, 41].

A structural model of SpoIVFB has been built based on the crystal structure of an archaeal homolog [6] and constraints from cross-linking and co-evolutionary analyses [42-44]. In the model, SpoIVFB has an N-terminal domain with six TMSs [45, 46] including an HEXXH metalloprotease motif in TMS2 and an NPDG motif in TMS4 [37, 38], and a C-terminal cystathionine-β-synthase (CBS) domain [39, 47] (Figure 1A). Both H43 and H47 residues in the HEXXH motif and D137 in the NPDG motif are predicted zinc ligands that form a catalytic core [37, 38, 47-49]. Most of the NPDG motif is predicted to reside in a short loop that interrupts TMS4 [42-44] (Figure 1B)[6]. Substitutions for N129, P132, and D137 in the NPDG motif of SpoIVFB impaired RIP of Pro-σ^K during sporulation [37, 38], demonstrating that residues of the NPDG motif are important for substrate cleavage. Disulfide cross-linking experiments showed proximity between SpoIVFB P135 in the predicted short loop and residues near the cleavage site in Pro-σ^K [42].

Cleavage of Pro-σ^K by SpoIVFB can be reproduced by expressing these proteins in *E. coli* [29] (Figure 1A). Using this assay and bioinformatics, we found that both P132 and P135 in the predicted SpoIVFB short loop are important for Pro-σ^K cleavage and are highly conserved in SpoIVFB orthologs. Changes to these proline residues impaired the interaction between

catalytically-inactive SpoIVFB and Pro-σ^K produced in *E. coli*, as determined by co-purification (pull-down) assays. However, the effects of alanine substitutions for P132 and P135 differed, both in disulfide cross-linking experiments between the predicted SpoIVFB short loop and a residue near the cleavage site in Pro-σ^K, and in experiments that measured Pro-σ^K cleavage during *B. subtilis* sporulation. Our results provide new insights into functions of residues in the predicted SpoIVFB short loop and the NPDG motif that is broadly conserved in IMMPs.

Results

Two Conserved Proline Residues in the Predicted Short Loop of SpoIVFB Are Important for Cleavage of Pro-σ^K in *E. coli*. The predicted SpoIVFB short loop located in TMS4 contains most of the broadly conserved NPDG (N129, P132, D137, G138) motif (also referred to as the LDG motif) in IMMPs (Figure 3.1A and 3.1B) [37, 47, 50]. To identify additional residues that may play a role in substrate interaction and cleavage, an alignment of 136 SpoIVFB orthologs was made (Figure 3.2A; see Figure S3.1 in the supplemental material). The predicted short loop region is highly conserved, with little variability in residues and no variability in length. Interestingly, a second Pro residue, P135 in *B. subtilis* SpoIVFB, is conserved in all orthologs. Previous alignments of diverse IMMPs showed that some contain two or three Pro residues at variable positions within the predicted short loop region, while others contain only one Pro residue [37, 47]. Therefore, we tested whether *B. subtilis* SpoIVFB P135 is important for Pro-σ^K cleavage. We also tested the functional importance of I133 and W134, which are not highly conserved in orthologs (Figure 3.2A and S3.1). We compared them with two residues of the broadly conserved NPDG motif, N129 and P132, which have previously been shown to be important for RIP of Pro-σ^K during *B. subtilis* sporulation [37].

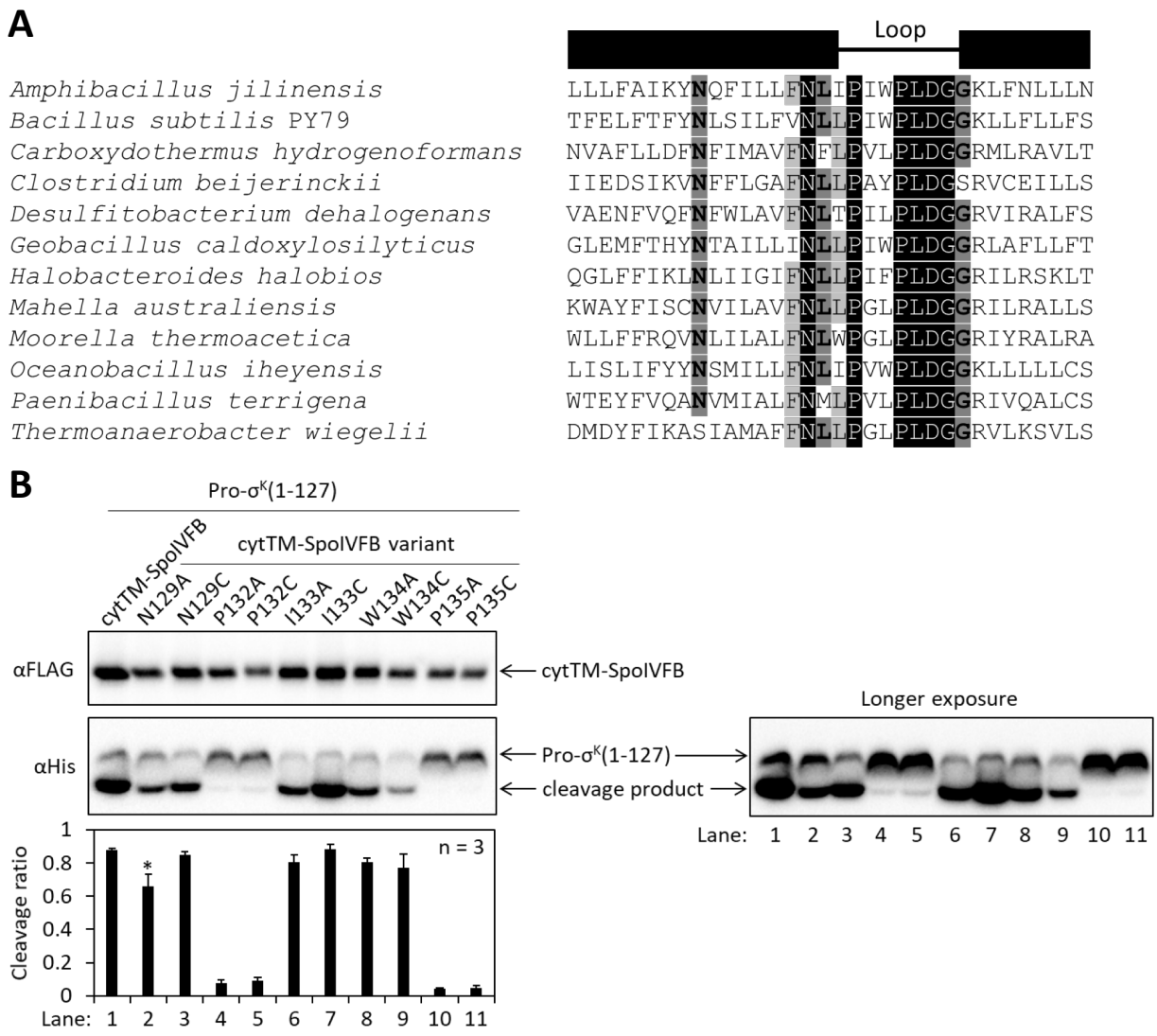

Figure 3.2 Conserved residues in the predicted short loop region of SpoIVFB and effects of substitutions on cleavage of Pro-σ^K(1-127) in *E. coli*. (*A*) Alignment of the predicted short loop region of *B. subtilis* SpoIVFB with representative orthologs. Here and in the full alignment (Figure S3.1), highlighted residues are 100% conserved (black), at least 90% conserved (dark gray), or at least 70% conserved (light gray). (*B*) Effects of Ala and Cys substitutions in SpoIVFB on cleavage of Pro-σ^K(1-127). Plasmids were used to express Pro-σ^K(1-127) and cytTM-SpoIVFB (lane 1, pFB9) or the indicated cytTM-SpoIVFB variant (lanes 2 to 11, pEN14, pEN18, pFB10, pFB12 to pFB16, pJV22, or pSO288) in *E. coli*. Samples collected after 2 h of IPTG induction were subjected to immunoblot analysis with FLAG (*Top*) and penta-His antibodies (*Bottom*, 7 and 30 s exposures). The graph shows quantification of the cleavage ratio (cleavage product/[Pro-σ^K(1-127) + cleavage product]) for three biological replicates. Error bars, 1 standard deviation. *, $p = 0.006$ in a Student's two-tailed *t* test comparing the cleavage ratio of the N129A variant (lane 2) with cytTM-SpoIVFB (lane 1).

To test cleavage of Pro-σ^K by SpoIVFB easily and in the absence of other *B. subtilis* proteins, *E. coli* was used to express variants of SpoIVFB and Pro-σ^K in various combinations. The SpoIVFB variant cytTM-SpoIVFB-$FLAG_2$ (cytTM-SpoIVFB) (Figure 3.1A) contains cytTM [51], which improves accumulation [39]. The substrate variant Pro-σ^K(1-127)-His_6 [Pro-σ^K(1-127)] lacks the C-terminal half of Pro-σ^K, but can be cleaved by SpoIVFB and the cleavage product can easily be separated from Pro-σ^K(1-127) by SDS-PAGE [52] [Note: Pro-σ^K(1-126) was renamed Pro-σ^K(1-127) as explained in [43]]. When Pro-σ^K(1-127) was produced with cytTM-SpoIVFB, cleavage was abundant (Figure 3.2B, lane 1). To quantify cleavage, we measured the amount of cleavage product and divided that by the amount of Pro-σ^K(1-127) plus cleavage product, which resulted in a cleavage ratio of 0.88 ± 0.01.

When Ala and Cys substitutions were made for P132 and P135, very little cleavage product was observed (Figure 3.2B, lanes 4, 5, 10, and 11), demonstrating that both conserved Pro residues are important for substrate cleavage in *E. coli*. A longer exposure of the immunoblot revealed small amounts of cleavage product. Interestingly, the N129A variant showed a small but reproducible decrease in cleavage product (lane 2) as compared with cytTM-SpoIVFB (lane 1) or the N129C variant (lane 3). The N129A variant produces a breakdown species, which appears to reduce accumulation of the full-length variant slightly (see Figure S3.2 in the supplemental material). Accumulation of the P132 and P135 variants, as well as the W134C variant, was also reduced, yet the cleavage ratio of the W134C variant (Figure 3.2B, lane 9) was similar to cytTM-SpoIVFB (lane 1) or the W134A variant (lane 8). Ala and Cys substitutions for I133 also had no measurable effect on the cleavage ratio (lanes 6 and 7). Since substitutions for P132 and P135 strongly impaired Pro-σ^K(1-127) cleavage in *E. coli*, we focused on these substitutions to test substrate binding as described below.

Substitutions for P132 and P135 of SpoIVFB Reduce Interaction with Pro-σ^K(1-127). To test substrate binding, *E. coli* was used to express Pro-σ^K(1-127) in combination with catalytically-inactive cytTM-SpoIVFB E44Q variants (which have a $FLAG_2$ tag), and pull-down assays were performed by mixing cell extracts with cobalt resin, which binds to the His_6 tag on Pro-σ^K(1-127). As expected, the cytTM-SpoIVFB variant co-purified with Pro-σ^K(1-127) (Figure 3.3A). Both proteins were observed in the diluted (to match the input concentration) bound sample (lane 6), indicative of a strong interaction, as well as in the concentrated bound sample (lane 7). The cytTM-SpoIVFB variant was undetectable in the bound samples of a negative control with Pro-σ^K(1-127) lacking the His_6 tag (lanes 13 and 14), indicating that the cytTM-SpoIVFB variant does not bind nonspecifically to the resin. As expected, none of the negative control samples showed a detectable signal with penta-His antibodies (Figure 3.3, lanes 8 to 14, top panel), and with Pro-σ^K antibodies only the input and unbound negative control samples showed Pro-σ^K(1-127) (see Figure S3.3 in the supplemental material, lanes 8 to 14, middle panel).

Ala and Cys substitutions for P132 and P135 of the cytTM-SpoIVFB variant appeared to reduce interaction with Pro-σ^K(1-127), since less of each variant appeared to be present in the bound samples (Figure 3.3A, lanes 20, 21, 27, 28, 34, 35, 41, and 42) as compared with the control (lanes 6 and 7). To quantify binding, we measured the amount of the cytTM-SpoIVFB variant in the diluted bound sample and divided that by the amount in the unbound, wash, plus diluted bound samples (Figure 3.3B). On average, the Ala- or Cys-substituted P132 variants exhibited about twofold less binding to Pro-σ^K(1-127), as compared with the cytTM-SpoIVFB E44Q control (p = 0.044 and 0.061 for the P132A and P132C variants, respectively), and the P135 variants exhibited about fourfold less binding (p = 0.0096 and 0.020 for the P135A and

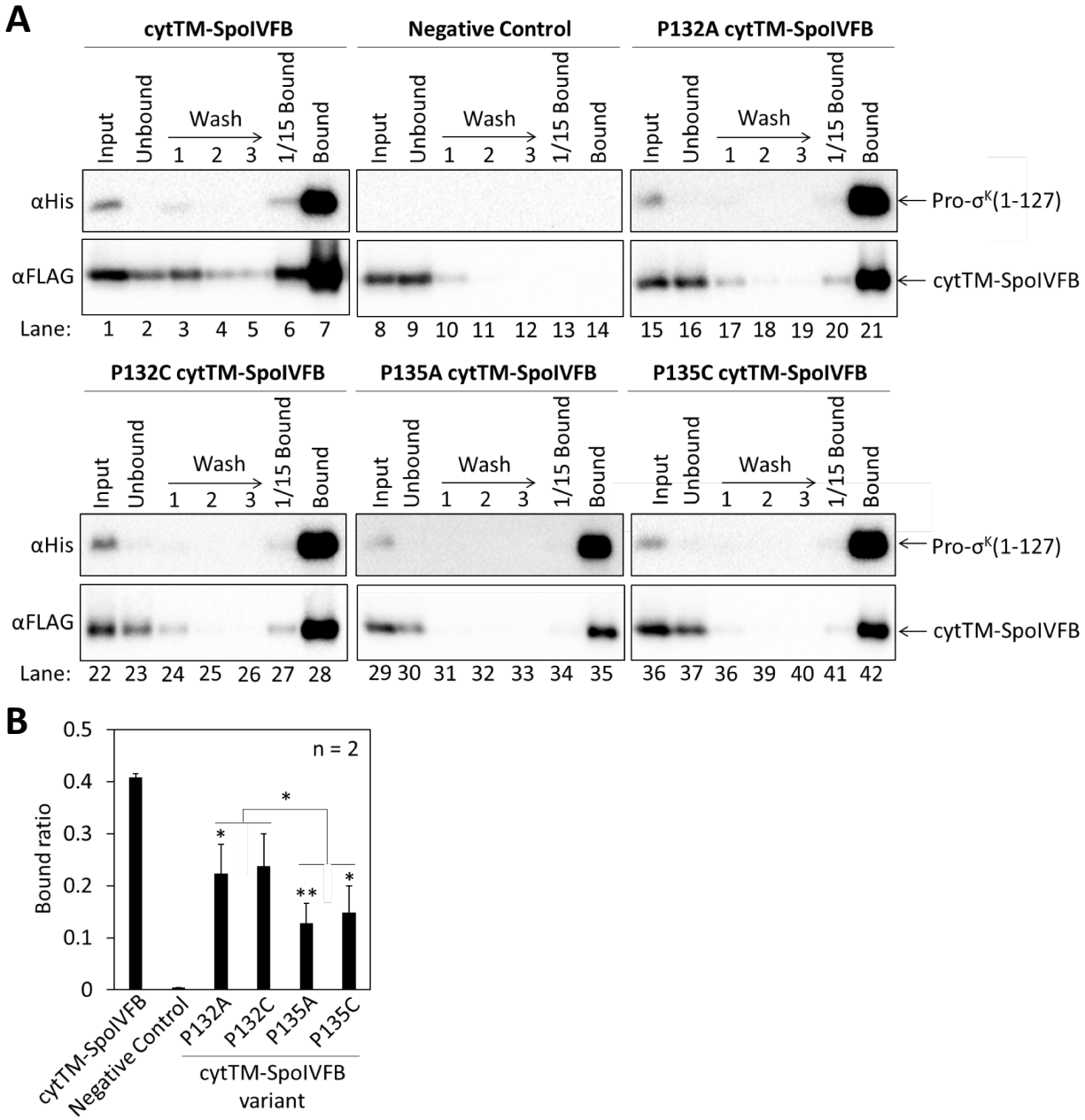

Figure 3.3 Effects of substitutions for SpoIVFB P132 or P135 on co-purification with Pro-σ^K(1-127). Plasmids were used to express Pro-σ^K(1-127) or a variant lacking the His_6 tag (as a negative control) in combination with catalytically-inactive cytTM-SpoIVFB E44Q variants in *E. coli*. Samples collected after 2 h of IPTG induction were subjected to co-purification with cobalt resin. Input, unbound, wash, 1/15 bound (diluted to match input), and (undiluted) bound samples were subjected to immunoblot analysis with penta-His and FLAG antibodies as indicated. (*A*) Representative results from two biological replicates. cytTM-SpoIVFB E44Q was produced in combination with Pro-σ^K(1-127) (lanes 1 to 7, pJV26) or a variant lacking the

Figure 3.3 (cont'd)
His_6 tag (Negative Control) (lanes 8 to 14, pSO292), or Pro-σ^K(1-127) was produced in combination with the indicated cytTM-SpoIVFB E44Q variant (lanes 15 to 21, pJV25; lanes 22 to 28, pJV29; lanes 29 to 35, pSO291; lanes 36 to 42, pJV23). (*B*) Quantification of binding. The graph shows quantification of the bound ratio (diluted bound/[unbound + washes + diluted bound]) for two biological replicates of the indicated cytTM-SpoIVFB E44Q variants. Error bars, 1 standard deviation. Results of Student's two-tailed *t* tests comparing Ala- or Cys-substituted variants with the cytTM-SpoIVFB E44Q control are summarized above the error bars, and the result of comparing the combined bound ratios of the P132 variants with the P135 variants is summarized above the bracket (*, $p < 0.05$; **, $p < 0.01$).

P135C variants, respectively). Pairwise comparisons of P132A and P135A variants or P132C and P135C variants yielded $p > 0.05$, but comparison of the combined bound ratios of the P132 variants with the P135 variants yielded $p = 0.026$ (Figure 3.3B). We conclude that both P132 and P135 in the predicted short loop of SpoIVFB are important for interaction with Pro-σ^K(1-127), and P135 is more important for the substrate interaction than P132 of the NPDG motif.

The Predicted Short Loop of SpoIVFB Is in Proximity to the Proregion of Pro-σ^K(1-127) When the Proteins Interact. SpoIVFB cleaves Pro-σ^K [40] and Pro-σ^K(1-127) [29] between residues S21 and Y22. In previous disulfide cross-linking experiments, Cys substitutions for several residues near the cleavage site of otherwise Cys-less Pro-σ^K(1-127) formed a cross-linked complex with catalytically-inactive single-Cys (E44C, V70C, or P135C) cytTM-SpoIVFB variants in *E. coli* [42]. However, formation of cross-linked complex was weak between single-Cys P135C cytTM-SpoIVFB E44Q and single-Cys residues near the cleavage site in Pro-σ^K(1-127). To examine proximity between other residues in the predicted SpoIVFB short loop region and the Proregion of Pro-σ^K(1-127), we performed additional disulfide cross-linking experiments.

For comparison as positive controls, we co-produced single-Cys (F18C or V20C) Pro-σ^K(1-127) variants with catalytically-inactive single-Cys (E44C or V70C) cytTM-SpoIVFB variants in *E. coli*. Cells were treated with the oxidant Cu^{2+}(phenanthroline)$_3$ to promote disulfide bond formation. As expected, formation of a species of the expected size for a cross-linked complex between the two proteins was detected by immunoblot with anti-FLAG antibodies (Figure 3.4, lanes 1 to 12). Formation of cross-linked complex was weaker between

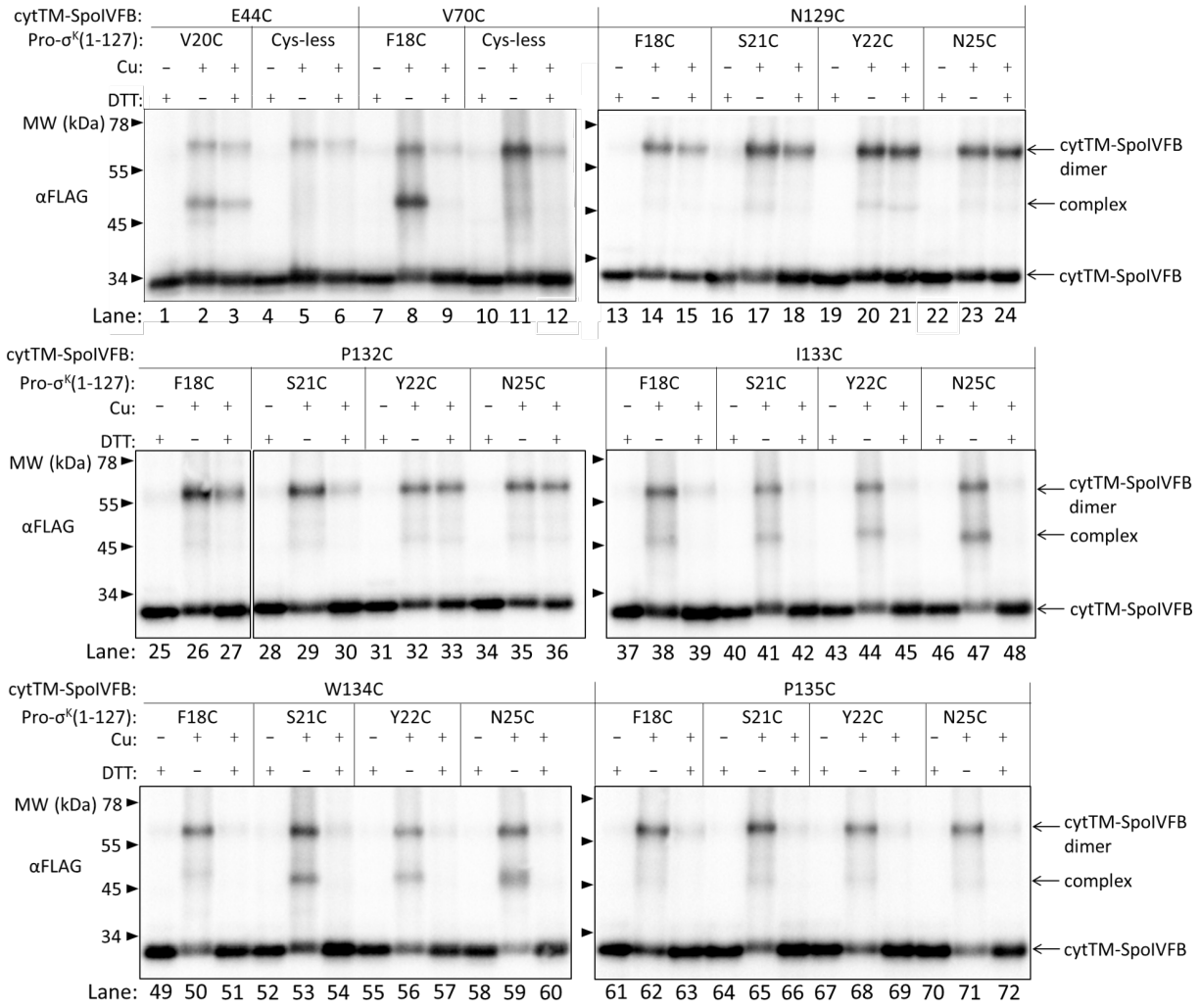

Figure 3.4 Disulfide cross-linking between the predicted short loop region of SpoIVFB and the Proregion of Pro-σ^K(1-127). Plasmids were used to express catalytically-inactive single-Cys cytTM-SpoIVFB variants in combination with Cys-less (as a negative control) or single-Cys Pro-σ^K(1-127) variants in *E. coli*. Samples collected after 2 h of IPTG induction were treated with Cu^{2+}(phenanthroline)$_3$ (Cu +) for 60 min or with 2-phenanthroline (Cu –) as a control. Samples were treated with TCA to precipitate proteins and resuspended in sample buffer with DTT (+) or without (–) and subjected to immunoblot analysis with FLAG antibodies to visualize cytTM-SpoIVFB monomer, dimer, and complex with Pro-σ^K(1-127). Representative results from two biological replicates are shown. As controls for cross-linked complex formation, single-Cys E44C cytTM-SpoIVFB was produced in combination with single-Cys V20C (lanes 1 to 3, pSO169) or Cys-less (lanes 4 to 6, pSO79) Pro-σ^K(1-127), and single-Cys V70C cytTM-SpoIVFB E44Q was produced in combination with single-Cys F18C (lanes 7 to 9, pSO168) or Cys-less (lanes 10 to 12, pSO136) Pro-σ^K(1-127). Single-Cys N129C cytTM-SpoIVFB E44Q was produced in combination with single-Cys F18C (lanes 13 to 15, pSO283), S21C (lanes 16 to 18, pJV12), Y22C (lanes 19 to 21, pJV1), or N25C (lanes 22 to 24, pSO277) Pro-σ^K(1-127). Likewise, single-Cys P132C cytTM-SpoIVFB E44Q was produced in combination with the

Figure 3.4 (cont'd)
indicated single-Cys Pro-σ^K(1-127) variants (lanes 25 to 36; pSO284, pSO269, pSO272, and pSO278), single-Cys I133C cytTM-SpoIVFB E44Q was produced in combination with the indicated single-Cys Pro-σ^K(1-127) variants (lanes 37 to 48; pSO285, pSO270, pSO273, and pSO279), single-Cys W134C cytTM-SpoIVFB E44Q was produced in combination with the indicated single-Cys Pro-σ^K(1-127) variants (lanes 49 to 60; pSO286, pSO271, pSO274, and pSO280), and single-Cys P135C cytTM-SpoIVFB E44Q was produced in combination with the indicated single-Cys Pro-σ^K(1-127) variants (lanes 61 to 72; pSO287, pJV28, pJV5, and pSO281).

single-Cys E44C cytTM-SpoIVFB and single-Cys V20C Pro-σ^K(1-127) (lane 2) than between single-Cys V70C cytTM-SpoIVFB E44Q and single-Cys F18C Pro-σ^K(1-127) (lane 8), in agreement with previous results [42]. Also in agreement, treatment with the reducing agent DTT was more effective at decreasing the abundance of cross-linked complex between the V70C cytTM-SpoIVFB and F18C Pro-σ^K(1-127) variants (lane 9) than the complex containing the E44C cytTM-SpoIVFB and V20C Pro-σ^K(1-127) variants (lane 3), indicating that the latter cross-link is not as readily reversible. As expected for negative controls, a cross-linked complex was not observed with Cys-less Pro-σ^K(1-127) (lanes 5 and 11). A species of the expected size for a cross-linked dimer of single-Cys cytTM-SpoIVFB was also observed in samples treated with the oxidant. Formation of the apparent dimer varies, as reported previously [42].

Single-Cys (F18C, S21C, Y22C, or N25C) Pro-σ^K(1-127) variants were co-produced with catalytically-inactive single-Cys (N129C, P132C, I133C, W134C, or P135C) cytTM-SpoIVFB E44Q variants and disulfide cross-linking experiments were performed as described above. The I133C and W134C cytTM-SpoIVFB variants formed cross-linked complex with all four Pro-σ^K(1-127) variants (Figure 3.4, lanes 37 to 48 and 49 to 60). The I133C cytTM-SpoIVFB variant formed the most complex with the N25C Pro-σ^K(1-127) variant (lane 47), while the W134C cytTM-SpoIVFB variant showed abundant complex formation with both the S21C and N25C Pro-σ^K(1-127) variants (lanes 53 and 59). The N129C, P132C, and P135C cytTM-SpoIVFB variants formed small amounts of cross-linked complex with the Pro-σ^K(1-127) variants (lanes 13 to 24, 25 to 36, and 61 to 72). The results for the P135C cytTM-SpoIVFB variant were consistent with those reported previously [42]. We conclude that all five residues in the predicted short loop of SpoIVFB are in proximity to several residues near the cleavage site in Pro-σ^K(1-127) when the two proteins interact.

Alanine Substitutions for N129 and P132 of SpoIVFB Reduce Cross-linking Between its Predicted Short Loop and the Proregion of Pro-σ^K(1-127) More Than a P135A Substitution. To better understand the effects of Ala substitutions for N129, P132, and P135 of SpoIVFB on substrate cleavage (Figure 3.2B) and interaction (Figure 3.3), we examined whether the substitutions affect disulfide cross-linking between catalytically-inactive single-Cys (I133C or W134C) cytTM-SpoIVFB E44Q variants and the single-Cys N25C Pro-σ^K(1-127) variant in experiments similar to those shown in Figure 3.4. We reasoned that changes in cross-linking may reflect changes in proximity between the predicted SpoIVFB short loop and the Proregion, due to the N129A, P132A, and P135A substitutions.

The N129A and P132A substitutions appeared to reduce cross-linking between the I133C cytTM-SpoIVFB and N25C Pro-σ^K(1-127) variants more than the P135A substitution (Figure 3.5A, lanes 8, 11, and 14). Control experiments with no Ala substitution in the I133C cytTM-SpoIVFB variant, in combination with the N25C Pro-σ^K(1-127) variant (lane 5) or with Cys-less Pro-σ^K(1-127) (lane 2) were performed for comparison. The N129A and P132A substitutions also appeared to reduce cross-linking between the W134C cytTM-SpoIVFB and N25C Pro-σ^K(1-127) variants more than the P135A substitution (see Figure S3.4 in the supplemental material, lanes 8, 11, and 14). To quantify cross-linking in the samples treated only with Cu^{2+}(phenanthroline)$_3$, we measured the amount of the cytTM-SpoIVFB variant in the cross-linked complex and divided that by the amount in the monomer, dimer, plus complex (Figure 3.5B). The N129A and P132A substitutions reduced the cross-linked ratio to values similar to the Cys-less Pro-σ^K(1-127) negative controls, whereas the P135A substitution reduced the cross-linked ratio by about one-third on average compared with the corresponding I133C or W134C

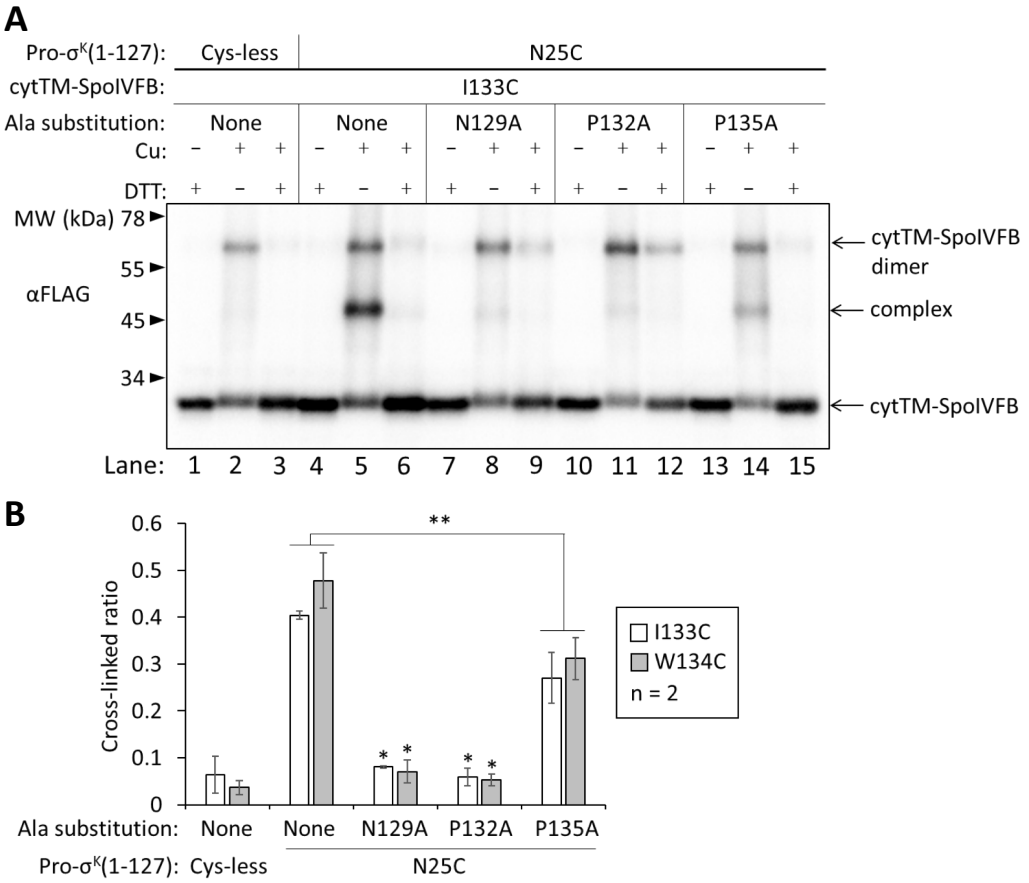

Figure 3.5 Effects of alanine substitutions for SpoIVFB N129, P132, and P135 on disulfide cross-linking between the predicted short loop and the Proregion of Pro-σ^K(1-127). Plasmids were used to express Cys-less or single-Cys N25C Pro-σ^K(1-127) variants in combination with catalytically-inactive single-Cys I133C cytTM-SpoIVFB E44Q variants in *E. coli*. Samples collected after 2 h of IPTG induction were treated with Cu^{2+}(phenanthroline)$_3$ (Cu +) for 60 min or with 2-phenanthroline (Cu –) as a control. Samples were treated with TCA to precipitate proteins and resuspended in sample buffer with DTT (+) or without (–) and subjected to immunoblot analysis with FLAG antibodies to visualize cytTM-SpoIVFB monomer, dimer, and complex with Pro-σ^K(1-127). (*A*) Representative result from two biological replicates. As controls, single-Cys I133C cytTM-SpoIVFB E44Q was produced in combination with Cys-less (lanes 1 to 3, pSO295) or single-Cys N25C (lanes 4 to 6, pSO279) Pro-σ^K(1-127). Single-Cys I133C cytTM-SpoIVFB E44Q with an Ala substitution at N129 (lanes 7 to 9, pSO296), P132 (lanes 10 to 12, pSO297), or P135A (lanes 13 to 15, pSO298) was produced in combination with single-Cys N25C Pro-σ^K(1-127). (*B*) Quantification of cross-linking. The graph shows quantification of the cross-linked ratio (complex/[monomer + dimer + complex]) for two biological replicates of the indicated cytTM-SpoIVFB E44Q variants. Error bars, 1 standard deviation. Results of Student's two-tailed *t* tests comparing the N129A- or P132A-substituted I133C or W134C cytTM-SpoIVFB E44Q variants pairwise with the corresponding P135A-substituted variant are summarized above the error bars, and the result of comparing the combined cross-linked ratios of the I133C and W134C cytTM-SpoIVFB positive controls lacking an Ala substitution with the combined ratios of the P135A-substituted variants is summarized above the bracket (*, $p < 0.05$; **, $p < 0.01$).

cytTM-SpoIVFB positive control lacking an Ala substitution ($p = 0.075$ and 0.087 for I133C and W134C, respectively). Comparison of the combined cross-linked ratios of the positive controls with the P135A-substituted variants yielded $p = 0.0061$ (Figure 3.5B). Pairwise comparisons of the P135A-substituted I133C or W134C cytTM-SpoIVFB variants with the corresponding N129A- or P132A-substituted variants supported that the latter substitutions reduce cross-linking more than the P135A substitution ($p < 0.05$).

We infer that the N129A and P132A substitutions reduce proximity between the predicted SpoIVFB short loop and the Proregion of Pro-σ^K(1-127), perhaps decreasing substrate cleavage (Figure 3.2B) and interaction (at least in the case of the P132A substitution; Figure 3.3). In contrast, the P135A substitution appears to have less effect on proximity between the predicted SpoIVFB short loop and the Proregion, yet substrate cleavage (Figure 3.2B) and interaction (Figure 3.3) are strongly impaired, suggesting that P135 plays a different role (see Discussion).

SpoIVFB P135 Is Crucial for Pro-σ^K Cleavage During *B. subtilis* Sporulation. A *B. subtilis spoIVFΔAB*::*cat* deletion mutant provides a genetic background to test the effects of Ala substitutions in SpoIVFB during sporulation [53]. The effects of SpoIVFB variants (N129A, P132A, I133A, W134A, P135A) were tested by ectopically integrating mutant versions of the *spoIVFAB* operon into the chromosome of the *spoIVFΔAB*::*cat* mutant lacking the endogenous *spoIVFAB* operon. The strains were starved to induce sporulation and samples were collected at appropriate times to observe Pro-σ^K cleavage as well as the SpoIVFA and SpoIVFB levels by immunoblot. To quantify cleavage of Pro-σ^K, we measured the amount of σ^K and divided that by the amount of Pro-σ^K plus σ^K. As a control, in wild-type *B. subtilis* strain PY79, Pro-σ^K cleavage

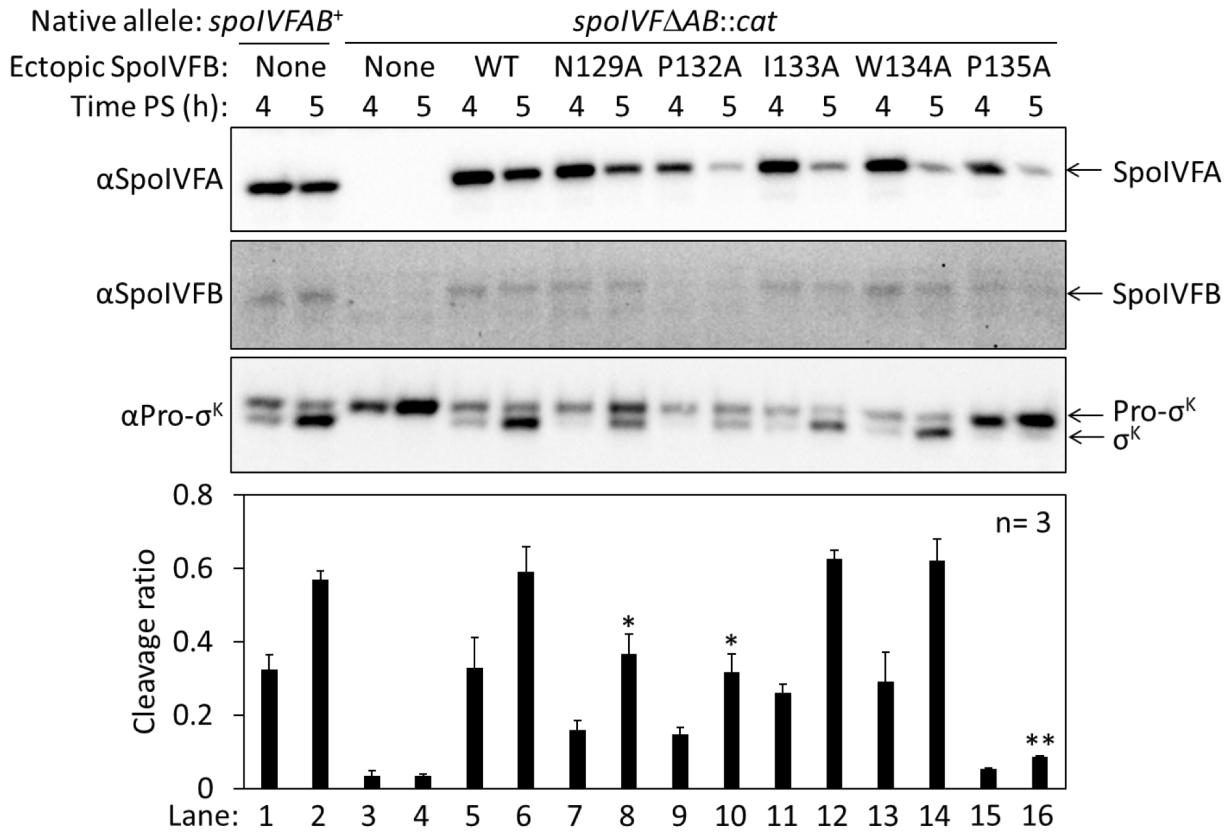

Figure 3.6 Effects of alanine substitutions in SpoIVFB on Pro-σ^K cleavage during *B. subtilis* sporulation. Wild-type strain PY79 (lanes 1 and 2), a *spoIVF*Δ*AB*::*cat* deletion mutant (lanes 3 and 4), and the deletion mutant with either the wild-type (WT) *spoIVF* operon (lanes 5 and 6) or the indicated mutant version (lanes 7 to 16) integrated ectopically at *amyE*, were starved to induce sporulation. Samples collected at 4 and 5 h poststarvation (PS) were subjected to immunoblot analysis with antibodies against SpoIVFA, SpoIVFB, and Pro-σ^K. The graph shows quantification of the cleavage ratio [cleavage product/(Pro-σ^K + cleavage product)] for three biological replicates. Error bars, 1 standard deviation. Student's two-tailed *t* tests were performed to compare certain cleavage ratios; *, $p \leq 0.01$ and **, $p = 0.0002$ in comparison with the data for the deletion mutant with the WT *spoIVF* operon at *amyE* (lane 6).

was observed at 4 and 5 h poststarvation (PS), resulting in cleavage ratios of 0.32 $\pm$ 0.04 and 0.57 $\pm$ 0.02, respectively, (Figure 3.6, lanes 1 and 2). For the *spoIVF*Δ*AB*::*cat* deletion mutant, no Pro-σ^K cleavage was observed, as expected, since SpoIVFA and SpoIVFB were absent (lanes 3 and 4). When SpoIVFA and wild-type SpoIVFB were produced ectopically in the deletion mutant, Pro-σ^K cleavage as well as the SpoIVFA and SpoIVFB levels were restored (lanes 5 and 6) to normal (lanes 1 and 2).

Ectopic production of the I133A and W134A SpoIVFB variants in the deletion mutant restored cleavage of Pro-σ^K (Figure 3.6, lanes 11 to 14). Cleavage was comparable to wild-type strain PY79 (lanes 1 and 2) and to the deletion mutant with ectopic production of SpoIVFA and wild-type SpoIVFB (lanes 5 and 6). The I133A and W134A SpoIVFB variants accumulated normally (Figure 3.6; see Figure S3.5 in the supplemental material for a longer exposure of the immunoblot), but less SpoIVFA accumulated at 5 h PS (Figure 3.6, lanes 12 and 14).

Production of the N129A and P132A SpoIVFB variants only partially restored Pro-σ^K cleavage in the deletion mutant (Figure 3.6, lanes 7 to 10). SpoIVFB N129A accumulated normally but very little SpoIVFB P132A accumulated (Figure 3.6 and S3.5), and less SpoIVFA accumulated at 5 h PS in the latter strain (Figure 3.6, lane 10). Despite very little accumulation of SpoIVFB P132A, cleavage of Pro-σ^K was comparable to that observed for SpoIVFB N129A (lanes 7 to 10). We note that the N129A and P132A cytTM-SpoIVFB variants accumulated comparably when expressed in *E. coli* (albeit accumulation of both was reduced in comparison with cytTM-SpoIVFB) (Figure 3.2B and S3.2), but the P129A variant cleaved Pro-σ^K(1-127) much more efficiently than the P132A variant, indicating differences in protein accumulation and activity in *E. coli* versus sporulating *B. subtilis* (see Discussion).

The P135A substitution in SpoIVFB had the largest impact on Pro-σ^K cleavage in sporulating *B. subtilis* (Figure 3.6, lanes 15 and 16). Very little σ^K was observed at 4 or 5 h PS. SpoIVFB P135A accumulated normally (Figure 3.6 and S3.5), but less SpoIVFA accumulated at 5 h PS (Figure 3.6, lane 16), as observed for several other strains (lanes 10, 12, and 14). Thus, P135 is crucial for Pro-σ^K cleavage during *B. subtilis* sporulation, as reported previously for nearby D137 of the NPDG motif [37, 38].

Discussion

Our results provide evidence that residues in the predicted short loop of SpoIVFB are important for substrate interaction and cleavage. Although bioinformatics identified a broadly conserved NPDG motif in IMMPs [37, 47, 49] that is predicted to be located in a short loop near the active site based on the structure of an archaeal enzyme [6], functional analysis of predicted short loop residues has been reported only for *E. coli* RseP [50]. Our results reveal notable differences in function between residues in the predicted short loop regions of SpoIVFB and RseP, yet both studies support the conclusion that residues in the predicted short loop region are important for substrate interaction and cleavage, suggesting this is a broadly conserved feature of IMMPs.

IMMPs Have a Variable Number of Proline Residues in Their Predicted Short Loop. Phylogenetic analysis of IMMPs defined four groups, including those that contain a C-terminal CBS domain like SpoIVFB (Group III), those that contain one or more PDZ domain(s) such as RseP and human S2P (Group I), one devoid of additional domains (Group II), and one with a conserved N-terminal extension that may form a soluble domain (Group IV) [47]. All

four groups contain the NPDG motif, but conservation of additional Pro residues in the predicted short loop varies. SpoIVFB and its orthologs have one additional Pro residue (P135 in *B. subtilis*) between the Pro and Asp of their NPDG motif (Figure 3.2A and S3.1), as do diverse bacterial and archaeal Group III IMMPs [47]. RseP also has one additional Pro residue (P399) between the Pro and Asp of its NPDG motif [37], as do diverse bacterial and predicted chloroplast Group I IMMPs [47], but in these IMMPs the additional Pro residue is one position closer to the Pro of the NPDG motif than in SpoIVFB. Archaeal Group I IMMPs have one additional Pro residue in the same position as in SpoIVFB, or they lack an additional Pro residue, as do eukaryotic Group I IMMPs like human S2P and Group IV IMMPs [47]. Group II IMMPs are the most variable in terms of additional Pro residues in their predicted short loop, ranging from zero to two additional Pro residues between the Pro and Asp of their NPDG motif [47]. Our analysis of *B. subtilis* YydH suggests it is a Group II IMMP which lacks an additional Pro residue. YydH has been suggested to cleave YydF, resulting in an exported peptide that causes cell envelope stress sensed by the well-characterized LiaRS two-component system [54], so it may be feasible to study the functions of residues in the predicted short loop of YydH. Interestingly, Group II IMMPs with two additional Pro residues in their predicted short loop are encoded in genomes of hyperthermophilic archaea and bacteria [47], perhaps suggesting an important role of additional Pro residues under extreme conditions.

Residues in the Predicted Short Loop of SpoIVFB Function Differently in Substrate Interaction and Cleavage Than in RseP. As noted above, both SpoIVFB and RseP contain one additional Pro residue between the Pro and Asp of their NPDG motif, albeit at a slightly different position. The NPDG motif of RseP spans from N394 to G403, interrupting TMS3, with

P397 of the NPDG motif, and P399 the additional Pro residue. Cys substitutions for N394, P397, and P399 of RseP reduced substrate cleavage [50], but not as dramatically as Cys substitutions for P132 and P135 of SpoIVFB reduced substrate cleavage in *E. coli* (Figure 3.2B). Each of the three Cys substitutions in RseP strongly impaired substrate interaction based on pull-down assays [50], whereas a Cys substitution for P135 of SpoIVFB impaired substrate interaction more strongly than a Cys substitution for P132 (Figure 3.3). Finally, Cys substitutions for P397 and P399 of RseP resulted in readily detectable disulfide cross-linking with Cys substitutions for substrate residues near the cleavage site, but a Cys substitution for N394 of RseP gave no detectable cross-linking [50]. In contrast, Cys substitutions for N129, P132, and P135 of SpoIVFB resulted in weak cross-linking with Cys substitutions near the substrate cleavage site (Figure 3.4). The differing results for predicted short loop residues of RseP and SpoIVFB suggest somewhat different roles in substrate interaction and cleavage, which is not surprising given the complexity of IMMP-substrate interactions so far uncovered for RseP [50, 55-58] and SpoIVFB [42-44, 59, 60]. Yet, both our results for SpoIVFB reported here and the work by Akiyama's group on RseP [50] demonstrate that the Asn and Pro of the NPDG motif as well as the additional Pro in the predicted short loop are important for substrate interaction and cleavage. As explained above, SpoIVFB and RseP are in distinct IMMP groups [47, 49], so the importance of predicted short loop residues in substrate interaction and cleavage may be a broadly conserved feature of IMMPs.

SpoIVFB P135 Functions Differently Than N129 and P132 in Substrate Interaction and Cleavage. The effects of an Ala substitution for P135 in the predicted short loop of SpoIVFB differed strikingly from the effects of both N129A and P132A substitutions in two

experiments. First, the P135A substitution appeared to have less effect on proximity between the predicted SpoIVFB short loop and the Proregion of Pro-σ^K(1-127) (Figure 3.5). Second, the P135A substitution impaired cleavage of Pro-σ^K more strongly during *B. subtilis* sporulation (Figure 3.6). These two observations, taken together with our finding that Ala and Cys substitutions for P135 impaired interaction with Pro-σ^K(1-127) more strongly than Ala and Cys substitutions for P132 (Figure 3.3), suggest that P135 plays a different role in substrate interaction and cleavage than P132 and N129.

We propose that SpoIVFB P135 positions nearby D137 to act as a zinc ligand. Like the P135A substitution (Figure 3.6), substitutions for D137 (to A, E, or N) allowed the SpoIVFB variant to accumulate but strongly impaired Pro-σ^K cleavage in sporulating *B. subtilis*, as did substitutions for H43 or H47, the other two predicted zinc ligands [37, 38]. Improper zinc binding by SpoIVFB P135A could also explain the observed differences in substrate interaction as compared with SpoIVFB P132A (Figure 3.3 and 3.5), if P132A primarily affects the local interaction between the predicted short loop and the Proregion, whereas P135A permits the local interaction but impairs several other interactions between SpoIVFB and Pro-σ^K. Like P132A, N129A may primarily affect the local interaction, which could explain their similar effects on substrate interaction (Figure 3.5) and Pro-σ^K cleavage during *B. subtilis* sporulation (Figure 3.6). However, N129A had much less effect than P132A on Pro-σ^K(1-127) cleavage in *E. coli* (Figure 3.2B). At present, we cannot account for this difference, but we note that differences between heterologous overexpression in growing *E. coli* compared with expression in sporulating *B. subtilis* have been observed in several studies of IMMP activity [43, 60, 61].

The Predicted Short Loop of SpoIVFB May Orient Pro-σ^K for Cleavage. Previous disulfide cross-linking suggested that side chains of certain residues near the cleavage site in Pro-σ^K adopt preferred orientations in the active site of SpoIVFB [42]. The Pro-σ^K S21 side chain was suggested to point toward P135 of the predicted SpoIVFB short loop. In agreement, our results suggest that the S21 side chain is in proximity to all five residues of the predicted short loop region that were tested (Figure 3.4). In contrast, the Pro-σ^K S21 side chain appears to point away from the catalytic E44 residue of SpoIVFB [42]. During catalysis, E44 within the HEXXH motif is thought to activate a zinc-bound water molecule for hydrolysis of the peptide bond between S21 and Y22 of Pro-σ^K [37, 38, 40]. Unlike the S21 side chain, the Pro-σ^K Y22 side chain appears to be in proximity to both E44 [42] and the predicted short loop region of SpoIVFB (Figure 3.4).

Based on the apparent preferred orientation of the Pro-σ^K S21 side chain [42] and on the preference of SpoIVFB for a residue with a small side chain at position 21 of Pro-σ^K [39, 60], it has been proposed that SpoIVFB has a binding pocket for the residue at position 21 of the substrate, which ensures efficient hydrolysis of the correct peptide bond [42, 60]. In a structural model of SpoIVFB in complex with Pro-σ^K, P132 and P135 constrain the predicted SpoIVFB short loop so that the side chains of W134, P135, and L136 form a hydrophobic face of the active site region [43, 44]. Conceivably, the hydrophobic face limits the side chain size at position 21 of the substrate, and the Ser of Pro-σ^K at that position is oriented by interactions with residues of the predicted short loop. Since an Ala substitution for W134 in the predicted short loop of SpoIVFB did not impair Pro-σ^K cleavage in *E. coli* (Figure 3.2B) or sporulating *B. subtilis* (Figure 3.6), perhaps the SpoIVFB W134A variant would cleave Pro-σ^K variants with a residue at position 21 having a larger side chain than tolerated by wild-type SpoIVFB. More work will

be needed to test this prediction and more broadly to utilize the knowledge generated in this study to manipulate IMMP activity. Taken together with the previous investigation of the *E. coli* RseP predicted short loop [50], our results suggest that a broadly conserved feature of IMMPs is the importance of short loop residues for substrate interaction and cleavage. Yet, residues in the predicted short loop regions of SpoIVFB and RseP do not appear to function identically. The differences may provide opportunities to develop selective modulators of IMMPs for therapeutic and other purposes.

Materials and Methods

Plasmids, Primers, and Strains. Plasmids used in this study are described in Table S1 in the supplemental material. Primers used in plasmid construction are listed in Table S2 in the supplemental material. Plasmids were cloned in *E. coli* strain DH5α [62]. Relevant parts of plasmids were verified by DNA sequencing with primers listed in Table S3 in the supplemental material. *B. subtilis* strains used in this study are described in Table S4 in the supplemental material.

Sequence Analysis of SpoIVFB Orthologs. Orthologs of *B. subtilis* SpoIVFB were collected from the NCBI and Uniprot databases by searching for genes annotated as *spoIVFB* in endospore-forming bacterial species [20]. The protein sequences of SpoIVFB orthologs were aligned using the T-Coffee multiple sequence alignment package [63]. Residues identical in at least 70% of the sequences were considered conserved.

Pro-σ^K(1-127) Cleavage in *E. coli*. Strain BL21(DE3) (Novagen) was used to express proteins in *E. coli*. Plasmid transformants were selected on Luria-Bertani (LB) agar supplemented with kanamycin sulfate (50 μg/mL). Transformants (4-5 colonies) were grown in LB medium with 50 μg/mL kanamycin sulfate at 37°C with shaking (200 rpm). Overnight culture (200 μL) was transferred to 10 mL of LB medium with antibiotics, cultures were grown at 37°C with shaking (250 rpm) to an optical density of 60 to 80 Klett units, and isopropyl β-D-thiogalactopyranoside (IPTG) (0.5 mM) was added to induce protein production for 2 h. Equivalent amounts of cells (based on optical density in Klett units) were collected (12,000 × *g* for 1 min) and extracts were prepared [29], then subjected to immunoblot analysis.

Immunoblot Analysis. Samples were subjected to immunoblot analysis as described [64]. Briefly, proteins were separated by SDS-PAGE using either 14% or 10% Prosieve (Lonza) polyacrylamide gels and electroblotted to Immobilon-P membranes (Millipore). Protein migration was monitored using SeeBlue Plus2 Prestained Standard (Invitrogen) and blots were blocked with 5% nonfat dry milk (Meijer) in TBST (20 mM Tris-HCl pH 7.5, 0.5 M NaCl, 0.1% Tween 20) for 1 h at 25°C with shaking. Blots were probed with antibodies against His_6 (penta-His Qiagen #34460; 1:10,000), $FLAG_2$ (Sigma #A8592; 1:10,000), Pro-σ^K [65] (1:3,000), SpoIVFA [64] (1:3,000), and/or SpoIVFB [38, 43] (1:5,000) diluted in TBST with 2% milk, overnight at 4°C with shaking. Since the Pro-σ^K, SpoIVFA, and SpoIVFB antibodies were not HRP-conjugated, they were detected with goat anti-rabbit-HRP antibody (Bio-Rad #170-6515; 1:10,000) diluted in TBST with 2% milk, 1 h at 25°C with shaking. Signals were generated using the Western Lightning Plus ECL reagent (PerkinElmer) and detected using a ChemiDoc

MP imaging system (Bio-Rad). Unsaturated signals were quantified using the Image Lab 5.1 software (Bio-Rad) lane and bands tool in order to determine the Pro-σ^K(1-127) cleavage ratio.

Colbalt Affinity Purification. *E. coli* BL21(DE3) was transformed with a plasmid, grown in LB (1 L), and induced with IPTG as described above. The culture was split, cells were harvested, and cell pellets were stored at -80°C. Each cell pellet was resuspended in 20 mL of lysis buffer containing PBS pH 7.4 and cell lysates were prepared as described [59]. Cell lysates were centrifuged (15,000 × *g* for 15 min at 4 °C) to sediment cell debris. The supernatant was treated with 1% *n*-dodecyl-β-D-maltoside (DDM) (Anatrace) for 1 h at 4 °C to solubilize membrane proteins, then centrifuged at 150,000 × *g* for 1 h at 4 °C. The supernatant was designated the input sample and 15 mL was mixed with imidazole (5 mM) and 0.5 mL of Talon superflow metal affinity resin (Clontech) that had been equilibrated with buffer (PBS pH 7.4, 0.1% DDM, 5 mM 2-mercaptoethanol, 10% glycerol). The mixture was rotated for 1 h at 4°C. The cobalt resin was sedimented by centrifugation at 708 × *g* for 2 min at 4 °C and the supernatant was saved (unbound sample). The resin was washed three times with 5 mL wash buffer (PBS pH 7.4, 150 mM NaCl, 10% glycerol, 0.1% DDM, 20 mM imidazole), each time gently mixing for 1 min on a Vortexer II (VWR) set at 4, then sedimenting the resin as above. The resin was mixed with 0.5 mL 2× sample buffer and boiled for 3 min (bound sample). A portion of the bound sample was diluted fifteenfold (1/15 bound sample) with 1× sample buffer to match the concentration of the input sample. Samples were subjected to immunoblot analysis using 14% Prosieve (Lonza) polyacrylamide gels.

Disulfide Cross-linking. As described above for Pro-σ^K(1-127) cleavage, *E. coli* BL21(DE3) was transformed with a plasmid, grown in LB (10 mL), induced with IPTG, and equivalent amounts of cells were collected. Cells were mixed with chloramphenicol (200 μg/mL) and 2-phenanthroline (3 mM), collected by centrifugation (12,000 × *g* for 1 min), washed with 10 mM Tris-HCl pH 8.1 containing 3 mM 2-phenanthroline, and suspended in 10 mM Tris-HCl pH 8.1. Samples were treated with 1 mM Cu^{2+}(phenanthroline)$_3$ or 3 mM 2-phenanthroline (as a negative control) for 60 min at 37°C, followed by incubation with neocuproine (12.5 mM) for 5 min at 37°C. Cells were lysed and proteins were precipitated by addition of trichloroacetic acid (5%) and inversion every 5 min for 30 min on ice. Proteins were sedimented by centrifugation (12,000 × *g*) for 15 min at 4°C, the supernatant was removed, and the pellet was washed with cold acetone. The pellets were sedimented by centrifugation (12,000 × *g*) for 5 min at 4°C and the supernatants were discarded. The pellets were dried for 5 min at 25°C and resuspended in buffer (100 mM Tris-HCl pH 7.5, 1.5% SDS, 5 mM EDTA, 25 mM *N*-ethylmaleimide) for 30 min at 25°C. Portions were mixed with an equal volume of sample buffer (25 mM Tris-HCl pH 6.8, 2% SDS, 10% glycerol, 0.015% bromophenol blue) with or without 100 mM DTT, and were incubated at 37°C for 10 min, prior to immunoblot analysis using 10% Prosieve (Lonza) polyacrylamide gels.

***B. subtilis* Sporulation.** Wild-type *B. subtilis* strain PY79 and its derivative BSL51 in which the *spoIVFAB* operon was replaced with a chloramphenicol resistance gene served as controls. Plasmids bearing the wild-type *spoIVF* operon or a mutant version, bordered by regions of homology to *B. subtilis amyE*, were transformed into strain BSL51. Transformants with a gene replacement at *amyE* were selected on LB agar with spectinomycin sulfate

(100 μg/mL) and identified by loss of amylase activity [66]. Sporulation was induced by growing cells in the absence of antibiotics and resuspension of cells in SM medium [66]. At indicated times PS, equivalent amounts of cells (based on optical density in Klett units) were centrifuged (12,000 × *g* for 1 min), supernatants were removed, and cell pellets were stored at -80°C. Whole-cell extracts were prepared as described for *E. coli* [29], except samples were incubated at 50°C for 3 min instead of boiling for 3 min [43], and proteins were subjected to immunoblot analysis using 14% Prosieve (Lonza) polyacrylamide gels.

Acknowledgments. We thank Erica Nowosielski for constructing the plasmids designated pEN, David Rudner for sharing pDR18a, and Jon Kaguni for helpful comments on the manuscript. This research was supported by National Institutes of Health Grant R01 GM43585 and by Michigan State University AgBioResearch.

APPENDIX

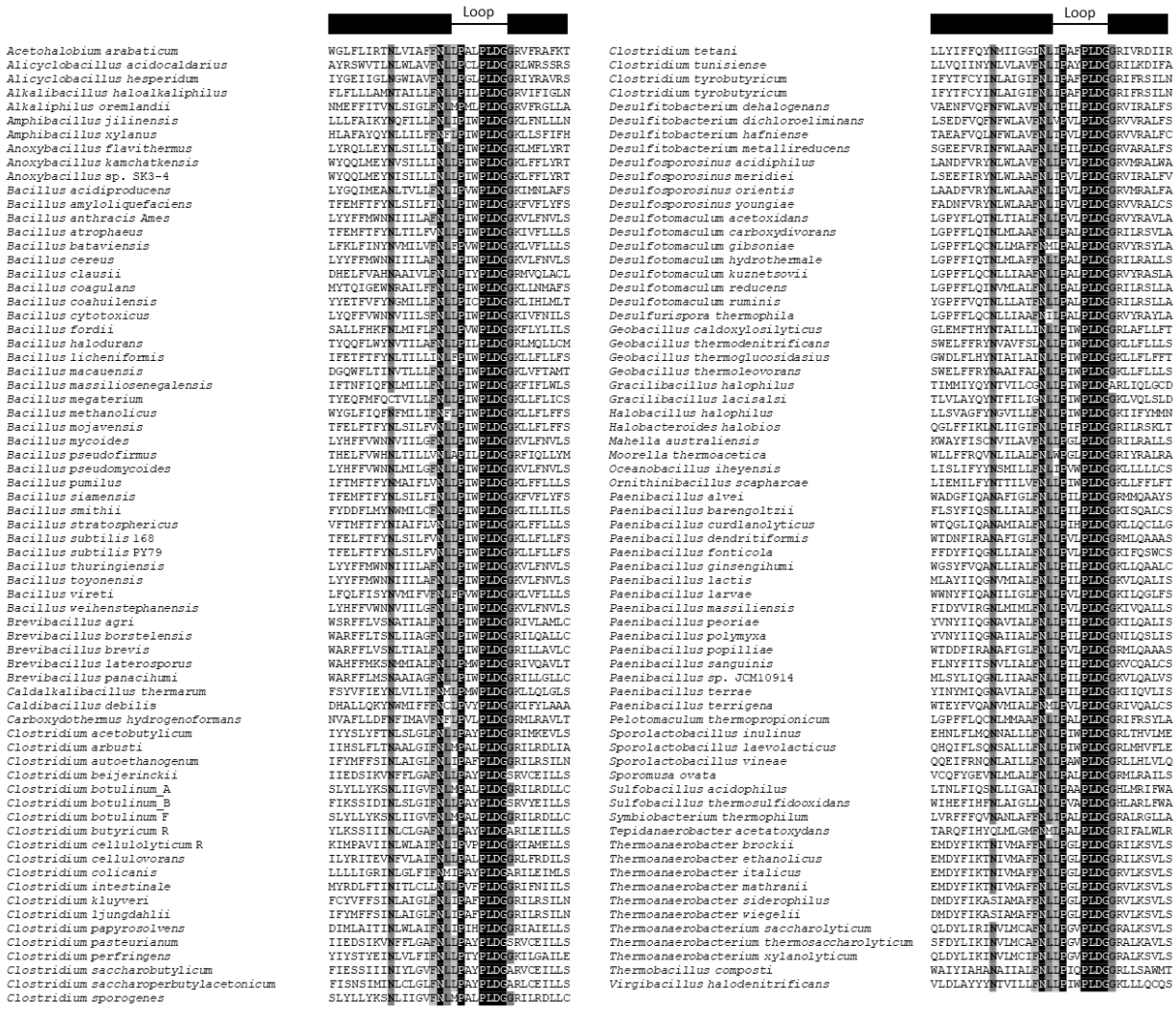

Figure S3.1 Alignment of the predicted short loop region of *B. subtilis* SpoIVFB with 135 orthologs. Highlighted residues are 100% conserved (black) (N129, P132, P135, L136, D137, and G138 in SpoIVFB of *B. subtilis*), at least 90% conserved (dark gray) (N122, L130, and G139), or at least 70% conserved (light gray) (F128, L131).

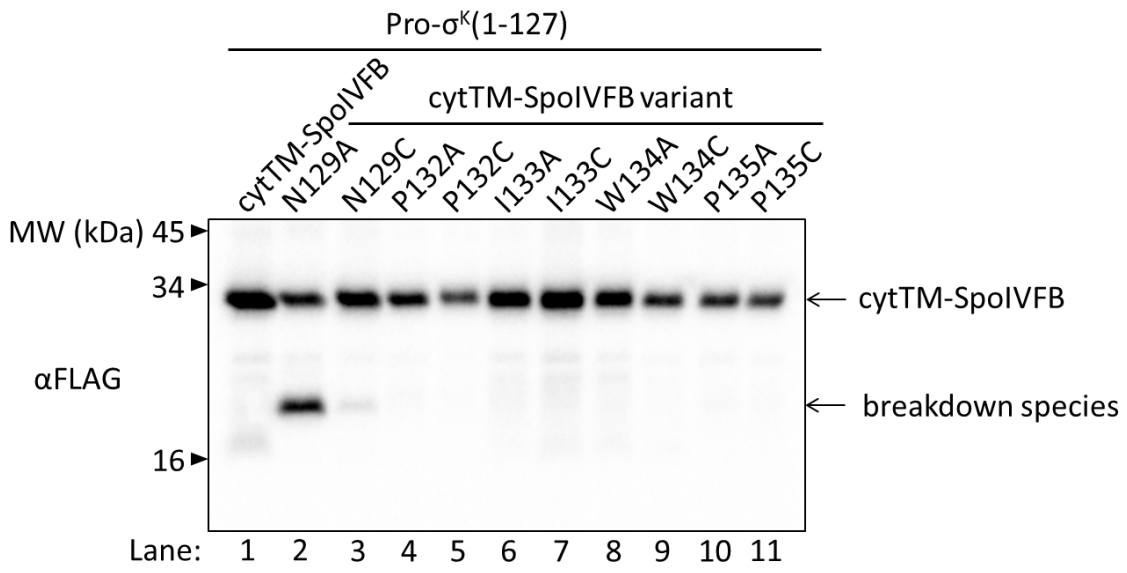

Figure S3.2 Effects of alanine and cysteine substitutions in SpoIVFB on cleavage of Pro-σ^K(1-127). Plasmids were used to produce Pro-σ^K(1-127) and cytTM-SpoIVFB (lane 1, pFB9) or the indicated cytTM-SpoIVFB variant (lanes 2 to11, pEN14, pEN18, pFB10, pFB12 to pFB16, pJV22, or pSO288). Samples collected after 2 h of IPTG induction were subjected to immunoblot analysis with FLAG antibodies. The N129A and N129C variants produce a breakdown species (lanes 2 and 3). A smaller portion of the same immunoblot is shown in Figure 3.2B (top panel).

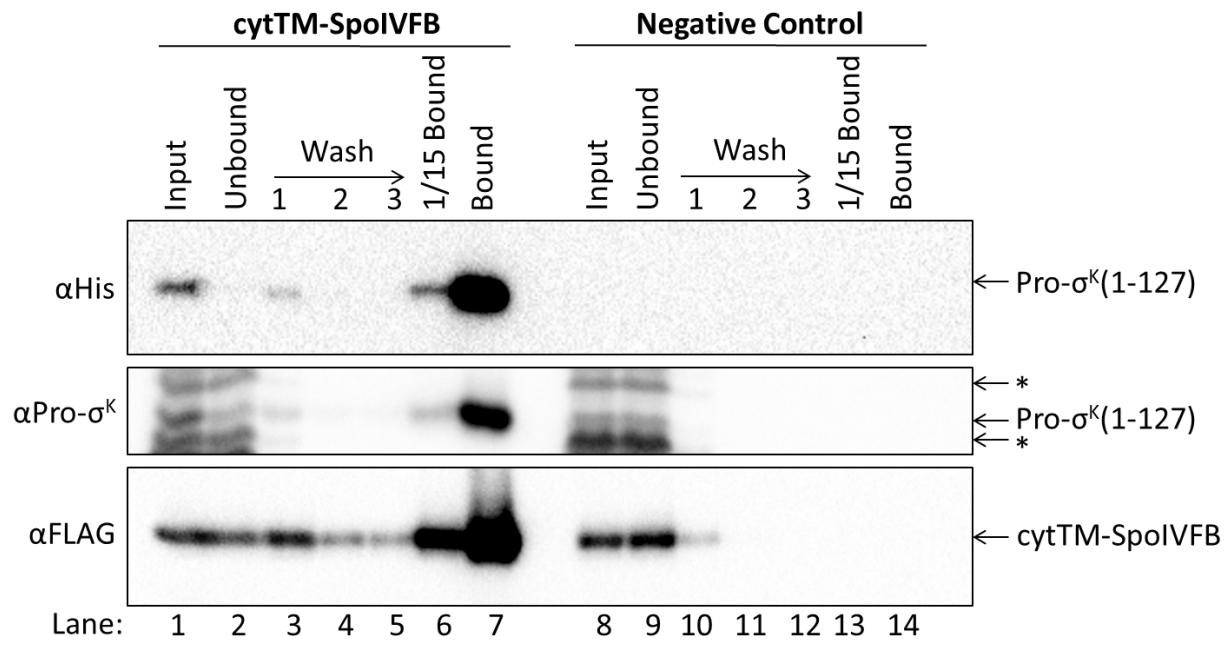

Figure S3.3 SpoIVFB co-purifies with Pro-σ^K(1-127). Plasmids were used to produce catalytically-inactive cytTM-SpoIVFB E44Q in combination with Pro-σ^K(1-127) (lanes 1 to 7, pJV26) or a variant lacking the His_6 tag (Negative Control) (lanes 8 to 14, pSO292) in *E. coli*. Samples collected after 2 h of IPTG induction were subjected to co-purification with cobalt resin. Input, unbound, wash, 1/15 bound (diluted to match input), and (undiluted) bound samples were subjected to immunoblot analysis with penta-His, Pro-σ^K, and FLAG antibodies as indicated. A representative result from two biological replicates is shown. The single stars (*) indicate cross-reacting proteins above and below Pro-σ^K(1-127) that fail to co-purify. For the Negative Control, the middle panel shows that Pro-σ^K(1-127) lacking the His_6 tag was produced and does not bind nonspecifically to the resin (lanes 8 to 14). Cropped portions of the immunoblots shown in the top and bottom panels are shown in Figure 3.3A.

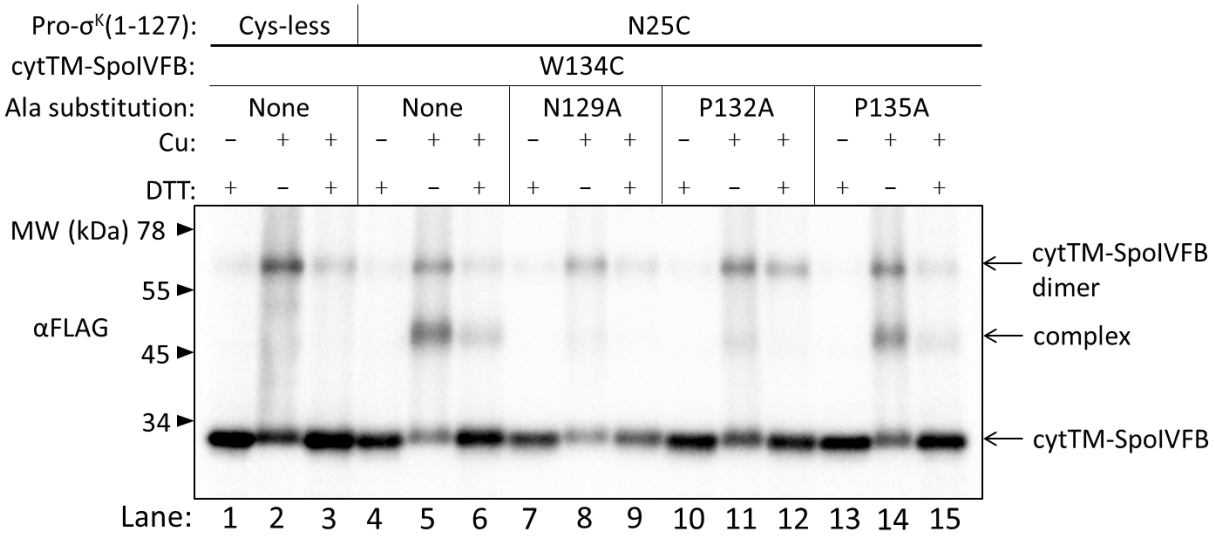

Figure S3.4 Effects of alanine substitutions for SpoIVFB N129, P132, and P135 on disulfide cross-linking between W134C in the predicted short loop and N25C in the Proregion of Pro-σ^K(1-127). Plasmids were used to produce Cys-less or single-Cys N25C Pro-σ^K(1-127) variants in combination with catalytically-inactive single-Cys W134C cytTM-SpoIVFB E44Q variants in *E. coli*. Samples collected after 2 h of IPTG induction were treated with Cu^{2+}(phenanthroline)$_3$ (Cu +) for 60 min or with 2-phenanthroline (Cu –) as a control. Samples were treated with TCA to precipitate proteins and resuspended in sample buffer with DTT (+) or without (–) and subjected to immunoblot analysis with FLAG antibodies to visualize cytTM-SpoIVFB monomer, dimer, and complex with Pro-σ^K(1-127). (A) Representative result from two biological replicates. As controls, single-Cys W134C cytTM-SpoIVFB E44Q was produced in combination with Cys-less (lanes 1 to 3, pSO276) or single-Cys N25C (lanes 4 to 6, pSO280) Pro-σ^K(1-127). Single-Cys W134C cytTM-SpoIVFB E44Q with an Ala substitution at N129A (lanes 7 to 9, (pSO299), P132A (lanes 10 to 12, (pSO300), or P135A (lanes 13 to 15, pSO301) was produced in combination with single-Cys N25C Pro-σ^K(1-127). Quantification of cross-linking is shown in Figure 3.5B.

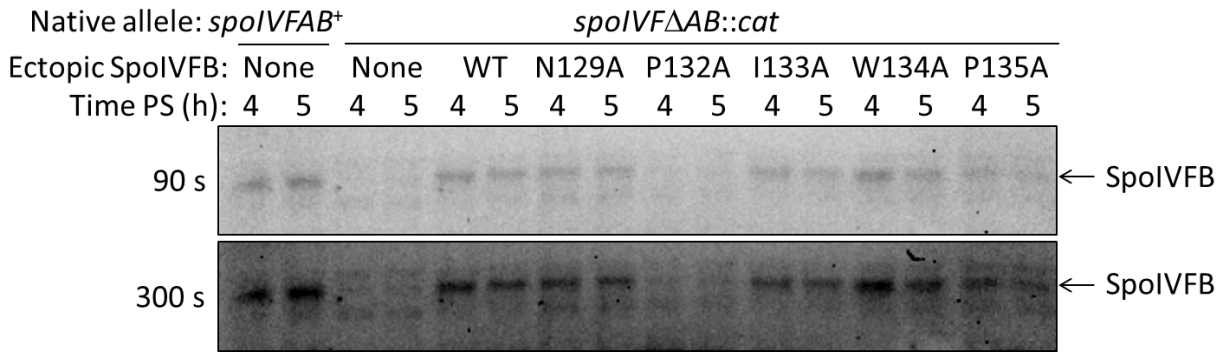

Figure S3.5 Effects of alanine substitutions in SpoIVFB on Pro-σ^K cleavage during *B. subtilis* sporulation. Wild-type strain PY79 (lanes 1 and 2), a *spoIVF*Δ*AB*::*cat* deletion mutant (lanes 3 and 4), and the deletion mutant with either the wild-type (WT) *spoIVF* operon (lanes 5 and 6) or the indicated mutant version (lanes 7 to 16) integrated ectopically at *amyE*, were starved to induce sporulation. Samples collected at 4 and 5 h poststarvation (PS) were subjected to immunoblot analysis with antibodies against SpoIVFB. The top panel shows a 90 s exposure of the immunoblot, which is also shown in Figure 3.6 (middle panel). The bottom panel shows a 300 s exposure of the same immunoblot.

Table S3.1 Plasmids used in this study

Name	Description	Construction	Reference
pDP81	Km^R; T7-Cys-less Pro-σ^K(1-127)-His_6/T7-cyTM	pFB6 was subjected to SDM PCR using primers LK1123 and LK1124, substituting C109S in Pro-σ^K(1-127).	This study
pDR18a	Ap^R Sp^R; amyE::spoIVF	The intact *spoIVF* operon was cloned into pLD30	[37]
pEN1[a]	Km^R; T7-single Cys F18C Pro-σ^K(1-127)-His_6/T7-cytTM	pDP81 was subjected to SDM[b] PCR using primers LK2465 and LK2466, substituting F18C in Pro-σ^K(1-127)	This study
pEN2	Km^R; T7-single Cys S21C Pro-σ^K(1-127)-His_6/T7-cytTM	pDP81 was subjected to SDM PCR using primers LK1481 and LK1482, substituting S21C in Pro-σ^K(1-127)	This study
pEN4	Km^R; T7-single Cys N25C P29A Pro-σ^K(1-127)-His_6/T7-cytTM	pDP81 was subjected to SDM PCR using primers LK2062 and LK2063, substituting N25C and P29A in Pro-σ^K(1-127)	This study
pEN5	Km^R; T7-single Cys Y22C Pro-σ^K(1-127)-His_6/T7-cytTM	pDP81 was subjected to SDM PCR using primers LK2469 and LK2470, substituting Y22C in Pro-σ^K(1-127)	This study
pEN6[a]	Km^R; T7-Single Cys F18C Pro-σ^K(1-127) C109S-His_6/T7-cytTM Single-Cys N129C SpoIVFB E44Q-$FLAG_2$	Fragment of *spoIVFB* N129C with no His_6 epitope tag and a BamHI cut site was made by OEPCR[c]. Fragment #1 (5' end of *spoIVFB* N129C) was amplified from pYZ107 and made with primers pFB15 and pFB16. Fragment #2 (3' end of *spoIVFB* N129C) was amplified from pYZ107 and made with primers pFB17 and pFB18. Fragments #1 and #2 were used as template for OEPCR using primers pFB15 and pFB18. Vector pEN1 was digested with BamHI. Product from OEPCR was joined to digested pEN1 using GA[d].	This study
pEN14	KmR; T7-Pro-σK(1-127)-His_6/T7-cytTM-SpoIVFB N129A-$FLAG_2$	pFB9 was subjected to SDM PCR using primers pFB9 and pFB10, substituting N129A in SpoIVFB	This study
pEN18	KmR; T7-Pro-σK(1-127)-His_6/T7-cytTM-SpoIVFB I133A-$FLAG_2$	pFB9 was subjected to SDM PCR using primers LK2517 and LK2518, substituting I133C in SpoIVFB	This study

Table S3.1 (cont'd)

pFB6	Km^R; T7-Pro-σ^K(1-127)-His_6/T7-cytTM	Fragment of *cytTM* was amplified from pYZ2 using primers pFB13 and pFB14. Vector was amplified from pYZ2 using primers pFB11 and pFB12 (containing pET29b backbone and *T7-pro-sigK* and changing GGATCC BamHI cut site between Pro-σ^K and His_6 to GGCTCC). Fragment was joined to vector using GA.	This study
pFB9	Km^R; T7-Pro-σ^K(1-127)-His_6/T7-cytTM-SpoIVFB-$FLAG_2$	Fragment of *cytTM-spoIVFB* (removing the His_6 epitope tag) was amplified from pYZ2 using primers pFB15 and pFB18. Vector pFB6 was digested with BamHI. Insert was added to vector using GA.	This study
pFB10	Km^R; T7-Pro-σ^K(1-127)-His_6/T7-cytTM-SpoIVFB N129C-$FLAG_2$	Fragment of *spoIVFB* N129C with no His_6 epitope tag and a BamHI cut site was made by OEPCR. Fragment #1 (5' end of *spoIVFB* N129C) was amplified from pYZ2 and made with primers pFB15 and pFB16. Fragment #2 (3' end of *spoIVFB* N129C) was amplified from pYZ2 and made with primers pFB17 and pFB18. Fragments #1 and #2 were used as template for OEPCR using primers pFB15 and pFB19. Vector pFB6 was digested with BamHI. Product from OEPCR was joined to digested pFB6 using GA.	This study
pFB12	Km^R; T7-Pro-σ^K(1-127)-His_6/T7-cytTM-SpoIVFB W134C-$FLAG_2$	Fragment of *spoIVFB* W134C with no His_6 epitope tag and a BamHI cut site was made by OEPCR. Fragment #1 (5' end of *spoIVFB* W134C) was amplified from pYZ2 and made with primers pFB15 and pFB26. Fragment #2 (3' end of *spoIVFB* W134C) was amplified from pYZ2 and made with primers pFB18 and pFB25. Fragments #1 and #2 were used as template for OEPCR using primers pFB15 and pFB19. Vector pFB6 was digested with BamHI. Product from OEPCR was joined to digested pFB6 using GA.	This study

Table S3.1 (cont'd)

pFB13	Km^R; T7-Pro-σ^K(1-127)-His_6/T7-cytTM-SpoIVFB P135C-$FLAG_2$	Fragment of *spoIVFB* P135C with no His_6 epitope tag and a BamHI cut site was made by OEPCR. Fragment #1 (5' end of *spoIVFB* P135C) was amplified from pYZ2 and made with primers pFB15 and pFB24. Fragment #2 (3' end of *spoIVFB* P135C) was amplified from pYZ2 and made with primers pFB18 and pFB23. Fragments #1 and #2 were used as template for OEPCR using primers pFB15 and pFB19. Vector pFB6 was digested with BamHI. Product from OEPCR was joined to digested pFB6 using GA.	This study
pFB14	Km^R; T7-Pro-σ^K(1-127)-His_6/T7-cytTM-SpoIVFB I133C-$FLAG_2$	Fragment of *spoIVFB* I133C with no His_6 epitope tag and a BamHI cut site was made by OEPCR. Fragment #1 (5' end of *spoIVFB* I133C) was amplified from pYZ2 and made with primers pFB15 and pFB30. Fragment #2 (3' end of *spoIVFB* I133C) was amplified from pYZ2 and made with primers pFB18 and pFB29. Fragments #1 and #2 were used as template for OEPCR using primers pFB15 and pFB19. Vector pFB6 was digested with BamHI. Product from OEPCR was joined to digested pFB6 using GA.	This study
pFB15	Km^R; T7-Pro-σ^K(1-127)-His_6/T7-cytTM-SpoIVFB P132C-$FLAG_2$	Fragment of *spoIVFB* P132C with no His_6 epitope tag and a BamHI cut site was made by OEPCR. Fragment #1 (5' end of *spoIVFB* P132C) was amplified from pYZ2 and made with primers pFB15 and pFB28. Fragment #2 (3' end of *spoIVFB* N129C) was amplified from pYZ2 and made with primers pFB18 and pFB27. Fragments #1 and #2 were used as template for OEPCR using primers pFB15 and pFB19. Vector pFB6 was digested with BamHI. Product from OEPCR was joined to digested pFB6 using GA.	This study

Table S3.1 (cont'd)

pFB16	Km^R; T7-Pro-σ^K(1-127)-His_6/T7-cytTM-SpoIVFB P132A-$FLAG_2$	Fragment of *spoIVFB* P132A with no His_6 epitope tag and a BamHI cut site was made by OEPCR. Fragment #1 (5' end of *spoIVFB* P132A) was amplified from pYZ2 and made with primers pFB15 and pFB35. Fragment #2 (3' end of *spoIVFB* P132A) was amplified from pYZ2 and made with primers pFB18 and pFB34. Fragments #1 and #2 were used as template for OEPCR using primers pFB15 and pFB19. Vector pFB6 was digested with BamHI. Product from OEPCR was joined to digested pFB6 using GA.	This study
pJV1	Km^R; T7-single-Cys Y22C Pro-σ^K(1-127)-His_6/T7-single-Cys N129C cytTM-SpoIVFB E44Q-$FLAG_2$	Fragment of *spoIVFB* N129C was amplified from pEN6 using primers pFB15 and pFB18. Vector pEN5 was digested with BamHI. The *spoIVFB* N129C fragment was added to pEN5 using GA.	This study
pJV5	Km^R; T7-single-Cys Y22C Pro-σ^K(1-127)-His_6/T7-single-Cys P135C cytTM-SpoIVFB E44Q-$FLAG_2$	Fragment of *spoIVFB* P135C was amplified from pSO135 using primers pFB15 and pFB18. Vector pEN5 was digested with BamHI. The *spoIVFB* P135C fragment was added to pEN5 using GA.	This study
pJV8	Km^R; T7-single-Cys N25C Pro-σ^K(1-127) P29A-His_6/T7-single-Cys P132C cytTM-SpoIVFB E44Q-$FLAG_2$	Fragment of *spoIVFB* P132C with no His_6 epitope tag and a BamHI cut site was made by OEPCR. Fragment #1 (5' end of *spoIVFB* P132C) was amplified from pYZ107 and made with primers pFB15 and pFB28. Fragment #2 (3' end of *spoIVFB* N129C) was amplified from pYZ107 and made with primers pFB27 and pFB18. Fragments #1 and #2 were used as template for OEPCR using primers pFB15 and pFB18. Vector pEN4 was digested with BamHI. Product from OEPCR was joined to digested pEN4 using GA.	This study
pJV12	Km^R; T7-single-Cys S21C Pro-σ^K(1-127)-His_6/T7-single-Cys N129C cytTM-SpoIVFB E44Q-$FLAG_2$	Fragment of *spoIVFB* N129C was amplified from pEN6 using primers pFB15 and pFB18. Vector pEN2 was digested with BamHI. The *spoIVFB* N129C fragment was added to pEN2 using GA.	This study
pJV22	Km^R; T7-Pro-σK(1-127)-His_6/T7-cytTM-SpoIVFB W134A-$FLAG_2$	pFB9 was subjected to SDM PCR using primers W134A F and W134A R, substituting W134A in SpoIVFB	This study

Table S3.1 (cont'd)

pJV23	Km^R; T7-Pro-σK(1-127)-His_6/T7-cytTM-P135C SpoIVFB E44Q-$FLAG_2$	pFB13 was subjected to SDM PCR using primers LK2691 and YZ11, substituting E44Q in SpoIVFB	This study
pJV25	Km^R; T7-Pro-σK(1-127)-His_6/T7-cytTM-P132A SpoIVFB E44Q-$FLAG_2$	pFB16 was subjected to SDM PCR using primers LK2691 and YZ11, substituting E44Q in SpoIVFB	This study
pJV26	Km^R; T7-Pro-σ^K(1-127)-His_6/T7-cytTM-SpoIVFB E44Q-$FLAG_2$	pFB9 was subjected to SDM PCR using primers LK2691 and YZ11, substituting E44Q in SpoIVFB	This study
pJV29	Km^R; T7-Pro-σK(1-127)-His_6/T7-cytTM-P132C SpoIVFB E44Q-$FLAG_2$	pFB15 was subjected to SDM PCR using primers LK2691 and YZ11, substituting E44Q in SpoIVFB	This study
pJV28	Km^R; T7-single-Cys S21C Pro-σK(1-127)-His_6/T7-single-Cys P135C cytTM-SpoIVFB E44Q-$FLAG_2$	Fragment of *spoIVFB* P135C was amplified from pSO135 using primers pFB15 and pFB18. Vector pEN2 was digested with BamHI. The *spoIVFB* P135C fragment was added to pEN2 using GA.	This study
pSO79	Km^R; T7-Cys-less Pro-σ^K(1-127)-His_6/T7-single-Cys E44C cytTM-SpoIVFB-$FLAG_2$-His_6	Fragment *spoIVFB* (single-Cys E44C) was amplified from pYZ40 using primers SO-P138 and SO-P139. Vector pSO76 was amplified using primers SO-P140 and SO-P141. Fragment was joined to pSO76 using GA.	Chapter 2
pSO112	Km^R; T7-Cys-less Pro-σ^K(1-127)-His_6/T7-single-Cys P135C cytTM-SpoIVFB E44Q-$FLAG_2$-His_6/T7-Cys-less MBPΔ27BofA/Cys-less SpoIVFA	Fragment *T7-mbpΔ27bofA/spoIVFA* (Cys-less MBPΔ27BofA and Cys-less SpoIVFA) was amplified from pSO97 using primers SO-P82 and SO-P90. Vector pSO84 was amplified using primers SO-P89 and SO-P80. Fragment was joined to pSO84 using GA.	Chapter 2
pSO128	Km^R; T7-single-Cys K24C Pro-σ^K(1-127)-His_6/T7-single-Cys E44C cytTM-SpoIVFB-$FLAG_2$-His_6	pSO79 was subjected to SDM using primers LK2473 and LK2474, substituting K24C in Pro-σ^K(1-127).	Chapter 2
pSO129	Km^R; T7-single-Cys K24C Pro-σ^K(1-127)-His_6/T7-single-Cys P135C cytTM-SpoIVFB E44Q-$FLAG_2$-His_6/T7-Cys-less MBPΔ27BofA/Cys-less SpoIVFA	pSO112 was subjected to SDM PCR using primers LK2473 and LK2474, substituting K24C in Pro-σ^K(1-127)	Olenic, unpublished
pSO135	Km^R; T7-single-Cys K24C Pro-σ^K(1-127)-His_6/T7-single-Cys P135C cytTM-SpoIVFB E44Q-$FLAG_2$-His_6	Fragment of *spoIVFB* P135C was amplified from pSO129 using primers SO-P138 and SO-P139. Vector was amplified from pSO128 using primers SO-P140 and SO-P141, removing *spoIVFB* E44C. The *spoIVFB* P135C fragment was added to pSO128 vector by GA.	Olenic, unpublished

Table S3.1 (cont'd)

pSO136	Km^R; T7-Cys-less Pro-σ^K(1-127)-His_6/T7-single-Cys V70C cytTM-SpoIVFB E44Q-$FLAG_2$-His_6	Fragment of *spoIVFB* (single-Cys V70C) was amplified from pSO111 using primers SO-P138 and SO-P139. Vector pSO79 was amplified fromprimers SO-P140 and SO-P141. Fragment was joined to pSO79 using GA.	Chapter 2
pSO168	Km^R; T7-single-Cys F18C Pro-σ^K(1-127)-His_6/T7-single-Cys V70C cytTM-SpoIVFB E44Q-$FLAG_2$-His_6	pSO136 was subjected to SDM using primers LK2465 and LK2466, substituting F18C in Pro-σ^K(1-127).	Chapter 2
pSO169	Km^R; T7-single Cys V20C Pro-σ^K(1-127)-His_6/T7-single-Cys E44C cytTM-SpoIVFB-$FLAG_2$-His_6	pSO79 was subjected to SDM using primers LK2467 and LK2468, substituting V20C in Pro-σ^K(1-127).	Chapter 2
pSO264	Km^R; T7-single Cys N25C Pro-σ^K(1-127)-His_6/T7-cytTM	pEN4 was subjected to SDM PCR using primers SO-P316 and SO-P317, fixing P29A to P29 in Pro-σ^K(1-127)	This study
pSO269	Km^R; T7-single-Cys S21C Pro-σ^K(1-127)-His_6/T7-single-Cys P132C cytTM-SpoIVFB E44Q-$FLAG_2$	Fragment of *spoIVFB* P132C was amplified from pJV8 using primers pFB15 and SO-P318. Vector pEN2 was digested with BamHI. The *spoIVFB* P132C fragment was added to pEN2 using GA.	This study
pSO270	Km^R; T7-single-Cys S21C Pro-σ^K(1-127)-His_6/T7-single-Cys I133C cytTM-SpoIVFB E44Q-$FLAG_2$	Fragment of *spoIVFB* I133C with no His6 epitope tag and a BamHI cut site was made by OEPCR. Fragment #1 (5' end of *spoIVFB* I133C) was amplified from pYZ107 and made with primers pFB15 and pFB30. Fragment #2 (3' end of *spoIVFB* I133C) was amplified from pYZ107 and made with primers pFB29 and SO-P318. Fragments #1 and #2 were used as template for OEPCR using primers pFB15 and SO-P318. Vector pEN2 was digested with BamHI. Product from OEPCR was joined to digested pEN2 using GA.	This study

Table S3.1 (cont'd)

pSO271	Km^R; T7-single-Cys S21C Pro-σ^K(1-127)-His_6/T7-single-Cys W134C cytTM-SpoIVFB E44Q-$FLAG_2$	Fragment of *spoIVFB* W134C with no His_6 epitope tag and a BamHI cut site was made by OEPCR. Fragment #1 (5' end of *spoIVFB* W134C) was amplified from pYZ107 and made with primers pFB15 and pFB26. Fragment #2 (3' end of *spoIVFB* W134C) was amplified from pYZ107 and made with primers pFB25 and SO-P318. Fragments #1 and #2 were used as template for OEPCR using primers pFB15 and SO-P318. Vector pEN2 was digested with BamHI. Product from OEPCR was joined to digested pEN2 using GA.	This study
pSO272	Km^R; T7-single-Cys Y22C Pro-σ^K(1-127)-His_6/T7-single-Cys P132C cytTM-SpoIVFB E44Q-$FLAG_2$	Fragment of *spoIVFB* P132C was amplified from pJV8 using primers pFB15 and SO-P318. Vector pEN5 was digested with BamHI. The *spoIVFB* P132C fragment was added to pEN5 using GA.	This study
pSO273	Km^R; T7-single-Cys Y22C Pro-σ^K(1-127)-His_6/T7-single-Cys I133C cytTM-SpoIVFB E44Q-$FLAG_2$	Fragment of *spoIVFB* I133C with no His_6 epitope tag and a BamHI cut site was made by OEPCR. Fragment #1 (5' end of *spoIVFB* I133C) was amplified from pYZ107 and made with primers pFB15 and pFB30. Fragment #2 (3' end of *spoIVFB* I133C) was amplified from pYZ107 and made with primers pFB29 and SO-P318. Fragments #1 and #2 were used as template for OEPCR using primers pFB15 and SO-P318. Vector pEN5 was digested with BamHI. Product from OEPCR was joined to digested pEN5 using GA.	This study
pSO274	Km^R; T7-single-Cys Y22C Pro-σ^K(1-127)-His_6/T7-single-Cys W134C cytTM-SpoIVFB E44Q-$FLAG_2$	Fragment of *spoIVFB* W134C with no His_6 epitope tag and a BamHI cut site was made by OEPCR. Fragment #1 (5' end of *spoIVFB* W134C) was amplified from pYZ107 and made with primers pFB15 and pFB26. Fragment #2 (3' end of *spoIVFB* W134C) was amplified from pYZ107 and made with primers pFB25 and SO-P318. Fragments #1 and #2 were used as template for OEPCR using primers pFB15 and SO-P318. Vector pEN5 was digested with BamHI. Product from OEPCR was joined to digested pEN5 using GA.	This study

Table S3.1 (cont'd)

pSO276	Km^R; T7-Cys-less Pro-σ^K(1-127)-His_6/T7-single-Cys W134C cytTM-SpoIVFB E44Q-$FLAG_2$	Fragment of *spoIVFB* W134C with no His_6 epitope tag and a BamHI cut site was made by OEPCR. Fragment #1 (5' end of *spoIVFB* W134C) was amplified from pYZ107 and made with primers pFB15 and pFB26. Fragment #2 (3' end of *spoIVFB* W134C) was amplified from pYZ107 and made with primers pFB25 and SO-P318. Fragments #1 and #2 were used as template for OEPCR using primers pFB15 and SO-P318. Vector pDP81 was digested with BamHI. Product from OEPCR was joined to digested pDP81 using GA.	This study
pSO277	Km^R; T7-single-Cys N25C Pro-σ^K(1-127)-His_6/T7-single-Cys N129C cytTM-SpoIVFB E44Q-$FLAG_2$	Fragment of *spoIVFB* N129C was amplified from pJV1 using primers pFB15 and SO-P318. Vector pSO264 was digested with BamHI. The *spoIVFB* N129C fragment was added to pSO264 using GA.	This study
pSO278	Km^R; T7-single-Cys N25C Pro-σ^K(1-127)-His_6/T7-single-Cys P132C cytTM-SpoIVFB E44Q-$FLAG_2$	Fragment of *spoIVFB* P132C was amplified from pJV8 using primers pFB15 and SO-P318. Vector pSO264 was digested with BamHI. The *spoIVFB* P132C fragment was added to pSO264 using GA.	This study
pSO279	Km^R; T7-single-Cys N25C Pro-σ^K(1-127)-His_6/T7-single-Cys I133C cytTM-SpoIVFB E44Q-$FLAG_2$	Fragment of *spoIVFB* I133C with no His_6 epitope tag and a BamHI cut site was made by OEPCR. Fragment #1 (5' end of *spoIVFB* I133C) was amplified from pYZ107 and made with primers pFB15 and pFB30. Fragment #2 (3' end of *spoIVFB* I133C) was amplified from pYZ107 and made with primers pFB29 and SO-P318. Fragments #1 and #2 were used as template for OEPCR using primers pFB15 and SO-P318. Vector pSO264 was digested with BamHI. Product from OEPCR was joined to digested pSO264 using GA.	This study

Table S3.1 (cont'd)

pSO280	Km^R; T7-single-Cys N25C Pro-σ^K(1-127)-His_6/T7-single-Cys W134C cytTM-SpoIVFB E44Q-$FLAG_2$	Fragment of *spoIVFB* W134C with no His_6 epitope tag and a BamHI cut site was made by OEPCR. Fragment #1 (5' end of *spoIVFB* W134C) was amplified from pYZ107 and made with primers pFB15 and pFB26. Fragment #2 (3' end of *spoIVFB* W134C) was amplified from pYZ107 and made with primers pFB25 and SO-P318. Fragments #1 and #2 were used as template for OEPCR using primers pFB15 and SO-P318. Vector pSO264 was digested with BamHI. Product from OEPCR was joined to digested pSO264 using GA.	This study
pSO281	Km^R; T7-single-Cys N25C Pro-σ^K(1-127)-His_6/T7-single-Cys P135C cytTM-SpoIVFB E44Q-$FLAG_2$	Fragment of *spoIVFB* P135C was amplified from pJV5 using primers pFB15 and SO-P318. Vector pSO264 was digested with BamHI. The *spoIVFB* P135C fragment was added to pSO264 using GA.	This study
pSO282[a]	Km^R; T7-single Cys F18C Pro-σ^K(1-127)-His_6/T7-cytTM	pDP81 was subjected to SDM PCR using primers LK2465 and LK2466, substituting F18C in Pro-σ^K(1-127)	This study
pSO283[a]	Km^R; T7-single Cys F18C Pro-σ^K(1-127)-His_6/T7-single-Cys N129C cytTM-SpoIVFB E44Q-$FLAG_2$	Fragment of *spoIVFB* N129C was amplified from pJV1 using primers pFB15 and SO-P318. Vector pSO282 was digested with BamHI. The spoIVFB N129C fragment was added to digested pSO282 using GA.	This study
pSO284	Km^R; T7-single Cys F18C Pro-σ^K(1-127)-His_6/T7-single-Cys P132C cytTM-SpoIVFB E44Q-$FLAG_2$	Fragment of *spoIVFB* P132C was amplified from pJV8 using primers pFB15 and SO-P318. Vector pSO282 was digested with BamHI. The *spoIVFB* P132C fragment was added to pSO282 using GA.	This study
pSO285	Km^R; T7-single Cys F18C Pro-σ^K(1-127)-His_6/T7-single-Cys I133C cytTM-SpoIVFB E44Q-$FLAG_2$	Fragment of *spoIVFB* I133C with no His6 epitope tag and a BamHI cut site was made by OEPCR. Fragment #1 (5' end of *spoIVFB* I133C) was amplified from pYZ107 and made with primers pFB15 and pFB30. Fragment #2 (3' end of *spoIVFB* I133C) was amplified from pYZ107 and made with primers pFB29 and SO-P318. Fragments #1 and #2 were used as template for OEPCR using primers pFB15 and SO-P318. Vector pSO282 was digested with BamHI. Product from OEPCR was joined to digested pSO282 using GA.	This study

Table S3.1 (cont'd)

pSO286	Km^R; T7-single Cys F18C Pro-σ^K(1-127)-His_6/T7-single-Cys W134C cytTM-SpoIVFB E44Q-$FLAG_2$	Fragment of *spoIVFB* W134C with no His6 epitope tag and a BamHI cut site was made by OEPCR. Fragment #1 (5' end of *spoIVFB* W134C) was amplified from pYZ107 and made with primers pFB15 and pFB26. Fragment #2 (3' end of *spoIVFB* W134C) was amplified from pYZ107 and made with primers pFB25 and SO-P318. Fragments #1 and #2 were used as template for OEPCR using primers pFB15 and SO-P318. Vector pSO282 was digested with BamHI. Product from OEPCR was joined to digested pSO282 using GA.	This study
pSO287	Km^R; T7-single-Cys F18C Pro-σ^K(1-127)-His_6/T7-single-Cys P135C cytTM-SpoIVFB E44Q-$FLAG_2$	Fragment of *spoIVFB* P135C was amplified from pJV5 using primers pFB15 and SO-P318. Vector pSO282 was digested with BamHI. The *spoIVFB* P135C fragment was added to pSO282 using GA.	This study
pSO288	Km^R; T7-Pro-σ^K(1-127)-His_6/T7-cytTM-SpoIVFB P135A-$FLAG_2$	pFB9 was subjected to SDM PCR using primers pFB7 and pFB8, substituting P135A in SpoIVFB	This study
pSO291	Km^R; T7-Pro-σ^K(1-127)-His_6/T7-cytTM-P135A SpoIVFB E44Q-$FLAG_2$	pSO288 was subjected to SDM PCR using primers LK2691 and YZ11, substituting E44Q in SpoIVFB	This study
pSO292	Km^R; T7-Pro-σ^K(1-127)/T7-cytTM-SpoIVFB E44Q-$FLAG_2$	pJV26 was subjected to SDM PCR using primers SO-P148 and SO-P149, removing the His_6 epitope tag from Pro-σ^K(1-127)	This study
pSO295	Km^R; T7-Cys-less Pro-σ^K(1-127)-His_6/T7-single-Cys I133C cytTM-SpoIVFB E44Q-$FLAG_2$	Fragment of *spoIVFB* I133C with no His_6 epitope tag and a BamHI cut site was made by OEPCR. Fragment #1 (5' end of *spoIVFB* I133C) was amplified from pYZ107 and made with primers pFB15 and pFB30. Fragment #2 (3' end of *spoIVFB* I133C) was amplified from pYZ107 and made with primers pFB29 and SO-P318. Fragments #1 and #2 were used as template for OEPCR using primers pFB15 and SO-P318. Vector pDP81 was digested with BamHI. Product from OEPCR was joined to digested pDP81 using GA.	This study
pSO296	Km^R; T7-single-Cys N25C Pro-σ^K(1-127)-His_6/T7-single-Cys I133C N129A cytTM-SpoIVFB E44Q-$FLAG_2$	pSO279 was subjected to SDM PCR using primers SO-P326 and SO-P327, substituting N129A in single-Cys I133C SpoIVFB E44Q.	This study

Table S3.1 (cont'd)

pSO297	Km^R; T7-single-Cys N25C Pro-σ^K(1-127)-His_6/T7-single-Cys I133C P132A cytTM-SpoIVFB E44Q-$FLAG_2$	pSO279 was subjected to SDM PCR using primers SO-P328 and SO-P329, substituting P132A in single-Cys I133C SpoIVFB E44Q.	This study
pSO298	Km^R; T7-single-Cys N25C Pro-σ^K(1-127)-His_6/T7-single-Cys I133C P135A cytTM-SpoIVFB E44Q-$FLAG_2$	pSO279 was subjected to SDM PCR using primers SO-P330 and SO-P331, substituting P135A in single-Cys I133C SpoIVFB E44Q.	This study
pSO299	Km^R; T7-single-Cys N25C Pro-σ^K(1-127)-His_6/T7-single-Cys W134C N129A cytTM-SpoIVFB E44Q-$FLAG_2$	pSO280 was subjected to SDM PCR using primers SO-P332 and SO-P333, substituting N129A in single-Cys I133C SpoIVFB E44Q.	This study
pSO300	Km^R; T7-single-Cys N25C Pro-σ^K(1-127)-His_6/T7-single-Cys W134C P132A cytTM-SpoIVFB E44Q-$FLAG_2$	pSO280 was subjected to SDM PCR using primers SO-P334 and SO-P335, substituting P132A in single-Cys I133C SpoIVFB E44Q.	This study
pSO301	Km^R; T7-single-Cys N25C Pro-σ^K(1-127)-His_6/T7-single-Cys W134C P135A cytTM-SpoIVFB E44Q-$FLAG_2$	pSO280 was subjected to SDM PCR using primers SO-P336 and SO-P337, substituting P135A in single-Cys I133C SpoIVFB E44Q.	This study
pSO302	Ap^R Sp^R; amyE::spoIVF N129A	pDR18a was subjected to SDM PCR using primers pFB9 and pFB10, substituting N129A in SpoIVFB	This study
pSO303	Ap^R Sp^R; amyE::spoIVF P132A	pDR18a was subjected to SDM PCR using primers pFB34 and pFB35, substituting P132A in SpoIVFB	This study
pSO304	Ap^R Sp^R; amyE::spoIVF I133A	pDR18a was subjected to SDM PCR using primers LK2517 and LK2518, substituting I133A in SpoIVFB	This study
pSO305	Ap^R Sp^R; amyE::spoIVF W134A	pDR18a was subjected to SDM PCR using primers W134A F and W134A R, substituting W134A in SpoIVFB	This study
pSO306	Ap^R Sp^R; amyE::spoIVF P135A	pDR18a was subjected to SDM PCR using primers pFB7 and pFB8, substituting P135A in SpoIVFB	This study
pYZ2	Km^R; T7-Pro-σ^K(1-127)-His_6/T7-cytTM-SpoIVFB-$FLAG_2$-His_6		Chapter 2
pYZ107	Ap^R; T7-Cys-less cytTM-SpoIVFB E44Q-$FLAG_2$-His_6		[67]

[a]Plasmids with pEN1 backbone did not induce properly with IPTG. Plasmids pSO282 and pSO283 were engineered to replace pEN1 and pEN6 respectively.
[b]Site-directed mutagenesis using the QuikChange kit (Stratagene).
[c]Overlap extension polymerase chain reaction.
[d]Gibson assembly.

Table S3.2 Primers used in this study

Primer	Sequence
LK1123	GTATGCAGCGAGATCTATTGAAAATG
LK1124	CATTTTCAATAGATCTCGCTGCATAC
LK1481	GTCTTTTTAGTATGTTACGTGAAAAAC
LK1482	GTTTTTCACGTAACATACTAAAAAGAC
LK2062	GTATCTTACGTGAAATGTAATGCCTTTGCAC
LK2063	GTGGAAAGGGATTACATTTCACGTAAGATAC
LK2465	AAAGAGCTTGTCTGTTTAGTATCTTAC
LK2466	GTAAGATACTAAACAGACAAGCTCTTT
LK2469	TTTTTAGTATCTTGCGTGAAAAACAAT
LK2470	ATTGTTTTTCACGCAAGATACTAAAAA
LK2473	GTATCTTACGTGTGTAACAATGCCTTT
LK2474	AAAGGCATTGTTACACACGTAAGATAC
LK2517	AATTTACTGCCGGCCTGGCCGCTGGAT
LK2518	ATCCAGCGGCCAGGCCGGCAGTAAATT
LK2691	GCAGCATGCCCCAGCTGATGAATCAATACAATC
pFB7	CAATTTACTGCCGATCTGGGCGCTGGATGGAGGAAAACTG
pFB8	CAGTTTTCCTCCATCCAGCGCCCAGATCGGCAGTAAATTG
pFB9	CTTTCTATCTTATTTGTCGCTTTACTGCCGATCTGGCCG
pFB10	CGGCCAGATCGGCAGTAAAGCGACAAATAAGATAGAAAG
pFB11	CGAAAACCTGTACTTCCAGGGCGGATCCGATCCGGCTGCTAACAAAG
pFB12	TTAGTGGTGGTGGTGGTGGTGGGAGCCTTTTTTTGTTTTTTTCAATGCG
pFB13	CGCATTGAAAAAAACAAAAAAAGGCTCCCACCACCACCACCACCACTAAGAT
pFB14	CTTTGTTAGCAGCCGGATCGGATCCGCCCTGGAAGTACAGGTTTTCG
pFB15	CGAAAACCTGTACTTCCAGGG
pFB16	AGCGGCCAGATCGGCAGTAAACAGACAAATAAGATAGAAAGATTATAAAAGGTG
pFB17	ATCTTTCTATCTTATTTGTCTGTTTACTGCCGATCTGGCCG
pFB18	CTTTGTTAGCAGCCGGATCGGATCCTTACTTGTCATCGTCATCCTTGTAATCC
pFB19	CTTTGTTAGCAGCCGGATCC
pFB23	ATTTGTCAATTTACTGCCGATCTGGTGCCTGGATGGAGGAAAACTGTTATTTTTG
pFB24	AAAATAACAGTTTTCCTCCATCCAGGCACCAGATCGGCAGTAAATTGACAAATA
pFB25	CTTATTTGTCAATTTACTGCCGATCTGCCCGCTGGATGGAGGAAAA
pFB26	ATAACAGTTTTCCTCCATCCAGCGGGCAGATCGGCAGTAAATTGACAAATAAGATAG
pFB27	TTCTATCTTATTTGTCAATTTACTGTGCATCTGGCCGCTGGATGGA
pFB28	GTTTTCCTCCATCCAGCGGCCAGATGCACAGTAAATTGACAAATAAGATAGAAAGAT
pFB29	TATCTTATTTGTCAATTTACTGCCGTGCTGGCCGCTGGATGGAGG
pFB30	CAGTTTTCCTCCATCCAGCGGCCAGCACGGCAGTAAATTGACAAATAAGATAGAA
pFB34	TTCTATCTTATTTGTCAATTTACTGGCGATCTGGCCGCTGGATGGA
pFB35	GTTTTCCTCCATCCAGCGGCCAGATCGCCAGTAAATTGACAAATAAGATAGAAAGAT
SO-P138	ATGAATAAATGGCTCGACCTTATCTTAAAG
SO-P139	GTAGGGCAGAAGCAGTTCC
SO-P140	CTTCCATGGAGGAACTGCTTC
SO-P141	GATAAGGTCGAGCCATTTATTCATGG
SO-P148	CGCATTGAAAAAAACAAAAAAATAAGATCCATGAGTAAAGGAGAAGATCT
SO-P149	AGATCTTCTCCTTTACTCATGGATCTTATTTTTTTGTTTTTTTCAATGCG
SO-P316	TTTAGTATCTTACGTGAAATGTAATGCCTTTCCACAACCGCTCTCAAGCA
SO-P317	TGCTTGAGAGCGGTTGTGGAAAGGCATTACATTTCACGTAAGATACTAAA

Table S3.2 (cont'd)

SO-P318	CTTTGTTAGCAGCCGGATCGGATCCTTACTTGTCATCGTCATCCTTGTAATCCTTGTCA T
SO-P326	CTTTCTATCTTATTTGTCGCTTTACTGCCGTGCTGGCCG
SO-P327	CGGCCAGCACGGCAGTAAAGCGACAAATAAGATAGAAAG
SO-P328	CTTATTTGTCAATTTACTGGCGTGCTGGCCGCTGGATGGAG
SO-P329	CTCCATCCAGCGGCCAGCACGCCAGTAAATTGACAAATAAG
SO-P330	CAATTTACTGCCGTGCTGGGCGCTGGATGGAGGAAAACTG
SO-P331	CAGTTTTCCTCCATCCAGCGCCCAGCACGGCAGTAAATTG
SO-P332	CTTTCTATCTTATTTGTCGCTTTACTGCCGATCTGCCCG
SO-P333	CGGGCAGATCGGCAGTAAAGCGACAAATAAGATAGAAAG
SO-P334	CTTATTTGTCAATTTACTGGCGATCTGCCCGCTGGATGGAG
SO-P335	CTCCATCCAGCGGGCAGATCGCCAGTAAATTGACAAATAAG
SO-P336	CAATTTACTGCCGATCTGCGCGCTGGATGGAGGAAAACTG
SO-P337	CAGTTTTCCTCCATCCAGCGCGCAGATCGGCAGTAAATTG
W134A F	GTCAATTTACTGCCGATCGCGCCGCTGG
W134A R	GTTTTCCTCCATCCAGCGGCGCGATCGG
YZ11	GATTGTATTGATTCATCAGCTGGGGCATGCTGC

Table S3.3 Sequencing primers used in this study

Primer	Sequence	Notes
SO-P84	CATACCCACGCCGAAACAAG	Forward primer. Binds upstream of the T7 promoter in pET29b.
SO-P86	GAGTAAAGGAGAAGATCTCGATCC	Forward primer. Binds in Pro-σ^K.
SO-P161	ACTGACGGGTCCAATGTTTG	Reverse primer. Binds in SpoIVFA.
SO-P338	GCTTGCTCACAGGCCATATG	Forward primer. Binds in SpoIVFB.
DP18	GCTAGTTATTGCTCAGCGG	Reverse primer. Binds T7 terminator
DP89	TAATACGACTCACTATAGGG	Forward primer. Binds T7 promoter.

Table S3.4 *B. subtilis* strains used in this study

Strain	Genotype	Construction	Citation
PY79	Prototrophic wild-type strain		[68]
BSL51	*spoIVFΔAB::cat*		[69]
BDP59	*spoIVFΔAB::cat amyE::spoIVF*	BSL51 was transformed with pDR18a	[70]
SO12	*spoIVFΔAB::cat amyE::spoIVF N129A*	BSL51 was transformed with pSO302	This study
SO14	*spoIVFΔAB::cat amyE::spoIVF P132A*	BSL51 was transformed with pSO303	This study
SO16	*spoIVFΔAB::cat amyE::spoIVF I133A*	BSL51 was transformed with pSO304	This study
SO18	*spoIVFΔAB::cat amyE::spoIVF W134A*	BSL51 was transformed with pSO305	This study
SO20	*spoIVFΔAB::cat amyE::spoIVF P135A*	BSL51 was transformed with pSO306	This study

REFERENCES

REFERENCES

1. Brown, M.S., et al., *Regulated intramembrane proteolysis: a control mechanism conserved from bacteria to humans.* Cell, 2000. **100**(4): p. 391-398.

2. Urban, S., *Mechanisms and cellular functions of intramembrane proteases.* Biochim. Biophys. Acta - Biomembr., 2013. **1828**: p. 2797-2800.

3. Manolaridis, I., et al., *Mechanism of farnesylated CAAX protein processing by the intramembrane protease Rce1.* Nature, 2013. **504**(7479): p. 301-305.

4. Hu, J., et al., *The crystal structure of GXGD membrane protease FlaK.* Nature, 2011. **475**(7357): p. 528-531.

5. Li, X., et al., *Structure of a presenilin family intramembrane aspartate protease.* Nature, 2013. **493**(7430): p. 56-61.

6. Feng, L., et al., *Structure of a site-2 protease family intramembrane metalloprotease.* Science, 2007. **318**(5856): p. 1608-1612.

7. Wang, Y., Y. Zhang, and Y. Ha, *Crystal structure of a rhomboid family intramembrane protease.* Nature, 2006. **444**(7116): p. 179-183.

8. Wu, Z., et al., *Structural analysis of a rhomboid family intramembrane protease reveals a gating mechanism for substrate entry.* Nat. Struct. Mol. Biol., 2006. **13**(12): p. 1084-1091.

9. Cho, S., S.W. Dickey, and S. Urban, *Crystal structures and inhibition kinetics reveal a two-stage catalytic mechanism with drug design implications for rhomboid proteolysis.* Mol. Cell, 2016. **61**(3): p. 329-340.

10. Zoll, S., et al., *Substrate binding and specificity of rhomboid intramembrane protease revealed by substrate-peptide complex structures.* EMBO J., 2014. **33**(20): p. 2408-2421.

11. Yang, G., et al., *Structural basis of Notch recognition by human γ-secretase.* Nature, 2019. **565**(7738): p. 192-197.

12. Zhou, R., et al., *Recognition of the amyloid precursor protein by human γ-secretase.* Science, 2019. **363**(6428): p. eaaw0930.

13. Rawson, R.B., *The site-2 protease.* Biochim. Biophys. Acta - Biomembr., 2013. **1828**(12): p. 2801-2807.

14. Ye, J., *Roles of regulated intramembrane proteolysis in virus infection and antiviral immunity.* Biochim. Biophys. Acta - Biomembr., 2013. **1828**(12): p. 2926-2932.

15. Urban, S., *Making the cut: central roles of intramembrane proteolysis in pathogenic microorganisms.* Nat. Rev. Microbiol., 2009. **7**: p. 411-423.

16. Kroos, L. and Y. Akiyama, *Biochemical and structural insights into intramembrane metalloprotease mechanisms.* Biochim. Biophys. Acta - Biomembr., 2013. **1828**(12): p. 2873-2885.

17. Schneider, J.S. and M.S. Glickman, *Function of site-2 proteases in bacteria and bacterial pathogens.* Biochim. Biophys. Acta - Biomembr., 2013. **1828**(12): p. 2808-2814.

18. Hastie, J.L. and C.D. Ellermeier, *Proteolytic activation of extra cytoplasmic function (ECF) σ factors*, in *Stress and Environmental Regulation of Gene Expression and Adaptation in Bacteria*, F.J. de Bruijn, Editor. 2016, John Wiley & Sons. p. 344-351.

19. Sineva, E., M. Savkina, and S.E. Ades, *Themes and variations in gene regulation by extracytoplasmic function (ECF) sigma factors.* Curr. Opin. Microbiol., 2017. **36**: p. 128-137.

20. Galperin, M.Y., et al., *Genomic determinants of sporulation in Bacilli and Clostridia: towards the minimal set of sporulation-specific genes.* Environ. Microbiol., 2012. **14**(11): p. 2870-2890.

21. McKenney, P.T., A. Driks, and P. Eichenberger, *The Bacillus subtilis endospore: assembly and functions of the multilayered coat.* Nat. Rev. Microbiol., 2013. **11**(1): p. 33-44.

22. Al-Hinai, M.A., S.W. Jones, and E.T. Papoutsakis, *The Clostridium sporulation programs: diversity and preservation of endospore differentiation.* Microbiol. Mol. Biol. Rev., 2015. **79**(1): p. 19-37.

23. Checinska, A., A. Paszczynski, and M. Burbank, *Bacillus and other spore-forming genera: variations in responses and mechanisms for survival.* Annu. Rev. Food Sci. Technol., 2015. **6**: p. 351-369.

24. Tan, I.S. and K.S. Ramamurthi, *Spore formation in Bacillus subtilis.* Environ. Microbiol. Rep., 2014. **6**(3): p. 212-225.

25. Cutting, S., et al., *A forespore checkpoint for mother-cell gene expression during development in Bacillus subtilis.* Cell, 1990. **62**: p. 239-250.

26. Resnekov, O., S. Alper, and R. Losick, *Subcellular localization of proteins governing the proteolytic activation of a developmental transcription factor in Bacillus subtilis.* Genes Cells, 1996. **1**(6): p. 529-542.

27. Rudner, D.Z., Q. Pan, and R.M. Losick, *Evidence that subcellular localization of a bacterial membrane protein is achieved by diffusion and capture.* Proc. Natl. Acad. Sci. USA, 2002. **99**(13): p. 8701-8706.

28. Rudner, D.Z. and R. Losick, *A sporulation membrane protein tethers the pro-σ^K processing enzyme to its inhibitor and dictates its subcellular localization.* Genes Dev., 2002. **16**(8): p. 1007-1018.

29. Zhou, R. and L. Kroos, *BofA protein inhibits intramembrane proteolysis of pro-σ^K in an intercompartmental signaling pathway during Bacillus subtilis sporulation.* Proc. Natl. Acad. Sci. USA, 2004. **101**(17): p. 6385-6390.

30. Cutting, S., et al., *Forespore-specific transcription of a gene in the signal transduction pathway that governs pro-σ^K processing in Bacillus subtilis.* Genes Dev., 1991. **5**: p. 456-466.

31. Pan, Q., R. Losick, and D.Z. Rudner, *A second PDZ-containing serine protease contributes to activation of the sporulation transcription factor σ^K in Bacillus subtilis.* J. Bacteriol., 2003. **185**(20): p. 6051-6056.

32. Campo, N. and D.Z. Rudner, *SpoIVB and CtpB are both forespore signals in the activation of the sporulation transcription factor σ^K in Bacillus subtilis.* J. Bacteriol., 2007. **189**(16): p. 6021-6027.

33. Dong, T.C. and S.M. Cutting, *SpoIVB-mediated cleavage of SpoIVFA could provide the intercellular signal to activate processing of Pro-σ^K in Bacillus subtilis.* Mol. Microbiol., 2003. **49**(5): p. 1425-1434.

34. Campo, N. and D.Z. Rudner, *A branched pathway governing the activation of a developmental transcription factor by regulated intramembrane proteolysis.* Mol. Cell, 2006. **23**(1): p. 25-35.

35. Zhou, R. and L. Kroos, *Serine proteases from two cell types target different components of a complex that governs regulated intramembrane proteolysis of pro-σ^K during Bacillus subtilis development.* Mol. Microbiol., 2005. **58**(3): p. 835-846.

36. Mastny, M., et al., *CtpB assembles a gated protease tunnel regulating cell-cell signaling during spore formation in Bacillus subtilis.* Cell, 2013. **155**(3): p. 647-658.

37. Rudner, D., P. Fawcett, and R. Losick, *A family of membrane-embedded metalloproteases involved in regulated proteolysis of membrane-associated transcription factors.* Proc. Natl. Acad. Sci. USA, 1999. **96**: p. 14765-14770.

38. Yu, Y.-T.N. and L. Kroos, *Evidence that SpoIVFB is a novel type of membrane metalloprotease governing intercompartmental communication during Bacillus subtilis sporulation.* J. Bacteriol., 2000. **182**: p. 3305-3309.

39. Zhou, R., et al., *Intramembrane proteolytic cleavage of a membrane-tethered transcription factor by a metalloprotease depends on ATP.* Proc. Natl. Acad. Sci. USA, 2009. **106**: p. 16174-16179.

40. Kroos, L., B. Kunkel, and R. Losick, *Switch protein alters specificity of RNA polymerase containing a compartment-specific sigma factor.* Science, 1989. **243**: p. 526-529.

41. Eichenberger, P., et al., *The program of gene transcription for a single differentiating cell type during sporulation in Bacillus subtilis.* PLoS Biol., 2004. **2**(10): p. e328.

42. Zhang, Y., et al., *Residues in conserved loops of intramembrane metalloprotease SpoIVFB interact with residues near the cleavage site in Pro-σ^K.* J. Bacteriol., 2013. **195**(21): p. 4936-4946.

43. Halder, S., et al., *Interaction of intramembrane metalloprotease SpoIVFB with substrate Pro-σ^K.* Proc. Natl. Acad. Sci. USA, 2017. **114**: p. E10677-E10686.

44. Olenic, S., et al., *Inhibitory proteins block substrate access to the active site of Bacillus subtilis intramembrane metalloprotease SpoIVFB.* bioRxiv, 2021.

45. Cutting, S., S. Roels, and R. Losick, *Sporulation operon spoIVF and the characterization of mutations that uncouple mother-cell from forespore gene expression in Bacillus subtilis.* J. Mol. Biol., 1991. **221**: p. 1237-1256.

46. Green, D. and S. Cutting, *Membrane topology of the Bacillus subtilis Pro-σ^K processing complex.* J. Bacteriol., 2000. **182**: p. 278-285.

47. Kinch, L.N., K. Ginalski, and N.V. Grishin, *Site-2 protease regulated intramembrane proteolysis: sequence homologs suggest an ancient signaling cascade.* Protein Sci., 2006. **15**(1): p. 84-93.

48. Lu, S., S. Cutting, and L. Kroos, *Sporulation protein SpoIVFB from Bacillus subtilis enhances processing of the sigma factor precursor pro-σ^K in the absence of other sporulation gene products.* J. Bacteriol., 1995. **177**: p. 1082-1085.

49. Lewis, A. and P. Thomas, *A novel clan of zinc metallopeptidases with possible intramembrane cleavage properties.* Protein Sci., 1999. **8**: p. 439-442.

50. Koide, K., K. Ito, and Y. Akiyama, *Substrate recognition and binding by RseP, an Escherichia coli intramembrane protease.* J. Biol. Chem., 2008. **283**(15): p. 9562-9570.

51. Saribas, A.S., L. Gruenke, and L. Waskell, *Overexpression and purification of the membrane-bound cytochrome P450 2B4.* Protein Expr. Purif., 2001. **21**(2): p. 303-309.

52. Prince, H., R. Zhou, and L. Kroos, *Substrate requirements for regulated intramembrane proteolysis of Bacillus subtilis pro-σ^K.* J. Bacteriol., 2005. **187**: p. 961-971.

53. Lu, S. and L. Kroos, *Overproducing the Bacillus subtilis mother-cell sigma factor precursor, pro-σ^K, uncouples σ^K-dependent gene expression from dependence on intercompartmental communication.* J. Bacteriol., 1994. **176**(13): p. 3936-3943.

54. Butcher, B.G., Y.P. Lin, and J.D. Helmann, *The yydFGHIJ operon of Bacillus subtilis encodes a peptide that induces the LiaRS two-component system.* J. Bacteriol., 2007. **189**(23): p. 8616-8625.

55. Hizukuri, Y., et al., *A structure-based model of substrate discrimination by a noncanonical PDZ tandem in the intramembrane-cleaving protease RseP.* Structure, 2014. **22**(2): p. 326-336.

56. Akiyama, K., Y. Hizukuri, and Y. Akiyama, *Involvement of a conserved GFG motif region in substrate binding by RseP, an Escherichia coli S2P protease.* Mol. Microbiol., 2017. **104**: p. 737-751.

57. Akiyama, K., et al., *Roles of the membrane-reentrant β-hairpin-like loop of RseP protease in selective substrate cleavage.* eLife, 2015. **4**: p. e08928

58. Miyake, T., Y. Hizukuri, and Y. Akiyama, *Involvement of a membrane-bound amphiphilic helix in substrate discrimination and binding by an Escherichia coli S2P peptidase RseP.* Front. Microbiol., 2020. **11**: p. 607381.

59. Zhang, Y., et al., *Complex formed between intramembrane metalloprotease SpoIVFB and its substrate, Pro-σ^K.* J. Biol. Chem., 2016. **291**: p. 10347-10362.

60. Zhou, R., et al., *Features of Pro-σ^K important for cleavage by SpoIVFB, an intramembrane metalloprotease.* J. Bacteriol., 2013. **195**: p. 2793-2806.

61. Parrell, D., et al., *Bacillus subtilis intramembrane protease RasP activity in Escherichia coli and in vitro.* J. Bacteriol., 2017. **199**: p. e00381-17.

62. Hanahan, D., *Studies on transformation of Escherichia coli with plasmids.* J. Mol. Biol., 1983. **166**: p. 557-580.

63. Notredame, C., D.G. Higgins, and J. Heringa, *T-Coffee: A novel method for fast and accurate multiple sequence alignment.* J. Mol. Biol., 2000. **302**(1): p. 205-217.

64. Kroos, L., et al., *Forespore signaling is necessary for pro-σ^K processing during Bacillus subtilis sporulation despite the loss of SpoIVFA upon translational arrest.* J. Bacteriol., 2002. **184**(19): p. 5393-5401.

65. Lu, S., R. Halberg, and L. Kroos, *Processing of the mother-cell σ factor, σ^K, may depend on events occurring in the forespore during Bacillus subtilis development.* Proc. Natl. Acad. Sci. USA, 1990. **87**: p. 9722-9726.

66. Harwood, C.R. and S.M. Cutting, *Molecular Biological Methods for Bacillus*. 1990, Chichester, England: John Wiley & Sons. 581.

67. Zhang, Y., et al., *Residues in conserved loops of intramembrane metalloprotease SpoIVFB interact with residues near the cleavage site in Pro-σ^K.* J. Bacteriol., 2013. **195**(21): p. 4936-4946.

68. Youngman, P., J.B. Perkins, and R. Losick, *Construction of a cloning site near one end of Tn917 into which foreign DNA may be inserted without affecting transposition in Bacillus subtilis or expression of the transposon-borne erm gene.* Plasmid, 1984. **12**: p. 1-9.

69. Lu, S. and L. Kroos, *Overproducing the Bacillus subtilis mother-cell sigma factor precursor, pro-σ^K, uncouples σ^K-dependent gene expression from dependence on intercompartmental communication.* J. Bacteriol., 1994. **176**(13): p. 3936-3943.

70. Halder, S., et al., *Interaction of intramembrane metalloprotease SpoIVFB with substrate Pro-σ^K.* Proc. Natl. Acad. Sci. USA, 2017. **114**: p. E10677-E10686.

CHAPTER 4: Examining Interactions Between SpoIVFA, SpoIVFB and BofA

Introduction

BofA and SpoIVFA are necessary to prevent SpoIVFB cleavage of Pro-σ^K [1-3]. Both inhibitory proteins form a stabilizing trimeric complex with SpoIVFB in *B. subtilis* and when produced in *E. coli* [2, 4]. Our work supports that BofA acts as the direct inhibitor of SpoIVFB [5], while SpoIVFA may act as a stabilizing scaffold for the trimeric complex [2, 6]. Membrane topology assays involving *phoA* and *lacZ* fusions have predicted that the C-terminal ends of SpoIVFA and BofA are located in the inter-membrane space surrounding the forespore (FS) [7, 8]. Additionally, small truncations in either the C-terminal end of SpoIVFA or BofA relieve inhibition of SpoIVFB, allowing cleavage of Pro-σ^K in *B. subtilis* [8-10]. These findings have led researchers to propose that a C-terminal interaction between the inhibitory proteins holds BofA in a specific conformation, allowing for direct inhibition of SpoIVFB [11].

Results

Efforts to Determine if SpoIVFA and BofA Interact in a Stable Complex. We first wanted to determine if BofA and SpoIVFA could form a stable complex without the presence of SpoIVFB. Using the GFPΔ27BofA variant co-produced with N-terminally tagged His_6-SpoIVFA we performed pull-down assays with cobalt resin, which binds to the His_6 tag (Figure 4.1). The SpoIVFA variant was detected in the concentrated bound sample (lane 7) and when the bound sample was diluted (lane 6) to match the input concentration sample (lane 1). However, little GFPΔ27BofA was observed in the concentrated bound sample (lane 7), indicating inefficient co-purification and/or recovery from the resin. A negative control with the

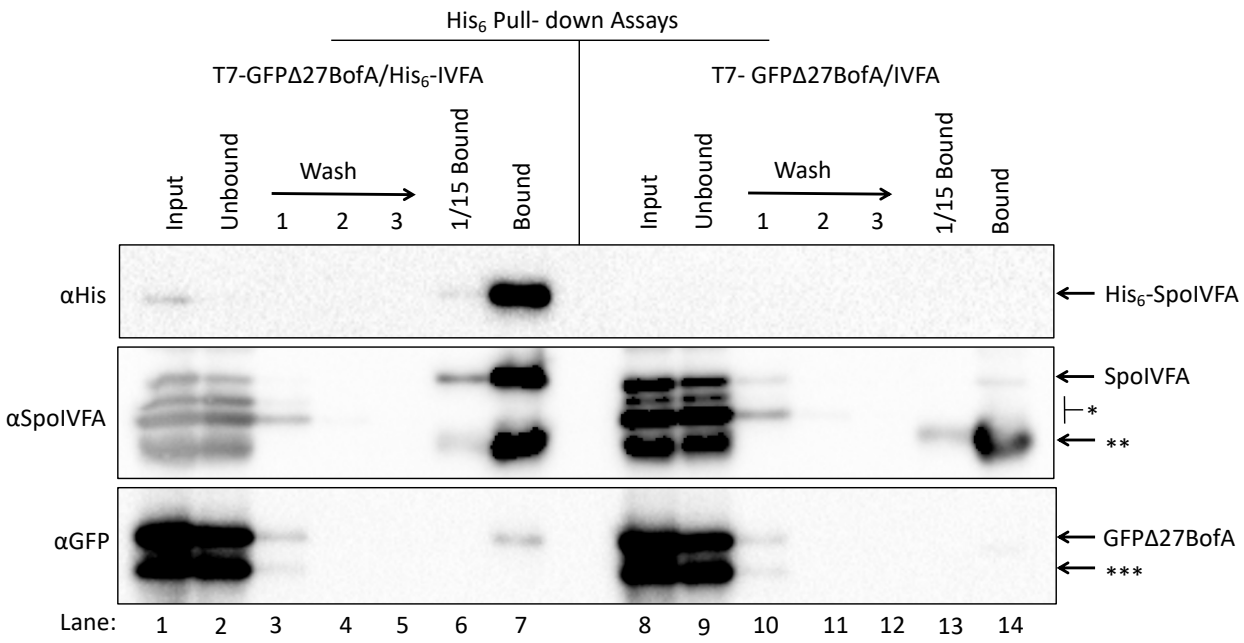

Figure 4.1 His_6-tagged SpoIVFA does not interact with GFPΔ27BofA. Plasmids were used to produce GFPΔ27BofA and N-terminally tagged His6-SpoIVFA (pSO162), or a variant lacking His_6 as a negative control (pYZ46) in *E. coli*. Samples collected after 2 h of IPTG induction were subjected to co-purification with cobalt resin. Input, unbound, wash, 1/15 bound (diluted to match input), and (undiluted) bound samples were subjected to immunoblot analysis with penta-His, SpoIVFA, and GFP antibodies as indicated. The single star (*) indicates cross-reacting proteins below SpoIVFA that fail to co-purify. The double star (**) indicates a putative breakdown species of SpoIVFA that appears to co-purify, but also binds non-specifically. The triple star (***) indicates a cross-reacting protein or breakdown species of GFPΔ27BofA that fails to co-purify. A representative result from two biological replicates is shown.

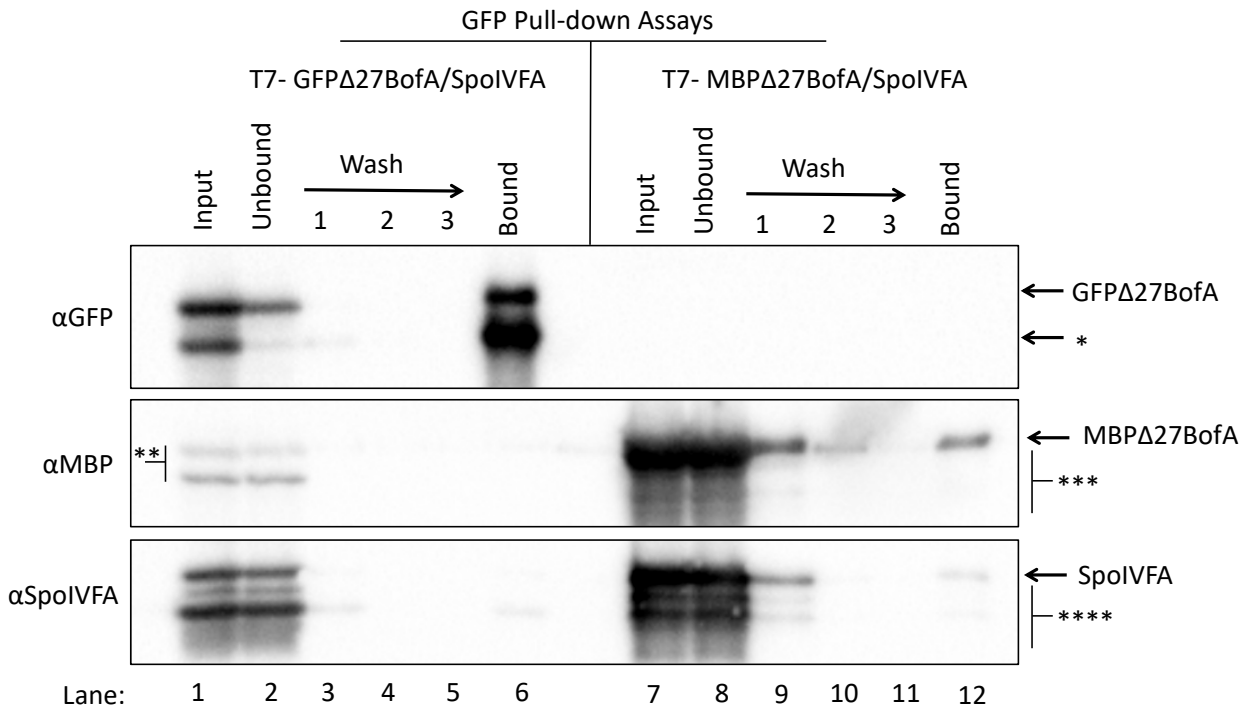

Figure 4.2 GFPΔ27BofA does not interact with SpoIVFA. Plasmids were used to produce SpoIVFA and GFPΔ27BofA (pYZ46), or MBPΔ27BofA as a negative control (pSO161) in *E. coli*. Samples collected after 2 h of IPTG induction were subjected to co-purification with GFP antibody beads. Input, unbound, wash, and bound samples were subjected to immunoblot analysis with GFP, MBP and SpoIVFA antibodies as indicated. The single star (*) indicates a cross-reacting protein or breakdown species of GFPΔ27BofA that fails to co-purify. The double star (**) indicates a cross-reacting protein with MBP antibodies that fails to co-purify. The triple star (***) indicates cross-reacting protein or breakdown species of MBPΔ27BofA that fails to co-purify. The quadruple star (****) indicates cross-reacting proteins and a putative breakdown species of SpoIVFA that fail to co-purify. A representative result from two biological replicates is shown.

SpoIVFA variant lacking the His_6 epitope tag showed very little GFPΔ27BofA in the bound sample (lane 14), indicative of weak, nonspecific binding to the cobalt resin. We also performed pull-down assays with anti-GFP antibody beads (Figure 4.2). GFPΔ27BofA was detected in the concentrated bound sample, but little SpoIVFA was observed (lane 6). As a negative control to determine if there was nonspecific binding to the beads, MBPΔ27BofA was produced with SpoIVFA. A small amount of SpoIVFA and MBPΔ27BofA was detected in the bound sample (lane 12), indicating nonspecific binding to the beads. We concluded that both pull-downs showed little interaction between SpoIVFA and GFPΔ27BofA, suggesting that they do not form a stable dimeric complex without SpoIVFB.

Efforts to Determine if the C-terminal Ends of SpoIVFA and BofA Interact. We also examined whether the C-terminal end of BofA was in proximity to the C-terminal end of SpoIVFA, using disulfide cross-linking assays. Undergraduate students Elizabeth Lyons and Maura Barrett engineered plasmids containing single-Cys MBPΔ27BofA and SpoIVFA with Cys-less variants of catalytically-inactive cytTM-SpoIVFB E44Q and Pro-σ^K(1-127), and performed the following disulfide cross-linking experiments. Cells were treated with the oxidant Cu^{2+}(phenanthroline)$_3$ to promote disulfide bond formation. Disulfide cross-linking of cells producing single-Cys Q84C MBPΔ27BofA in combination with single-Cys SpoIVFA (I258C, Q259C, I261C, S262C or F263C) variants did not result in a species of the expected size for a cross-linked complex, upon immunoblotting with anti-SpoIVFA antibodies (Figure 4.3A, lanes 2, 5, 8, 11 & 14). Additionally, no complex of the expected size was visible upon cross-linking of cells producing single-Cys MBPΔ27BofA (I82C, K83C, or F85C) in combination with single-Cys SpoIVFA (I258C or Q259C) variants (Figure 4.3B, lanes 2, 4**,** 7, 10, 13 & 16).

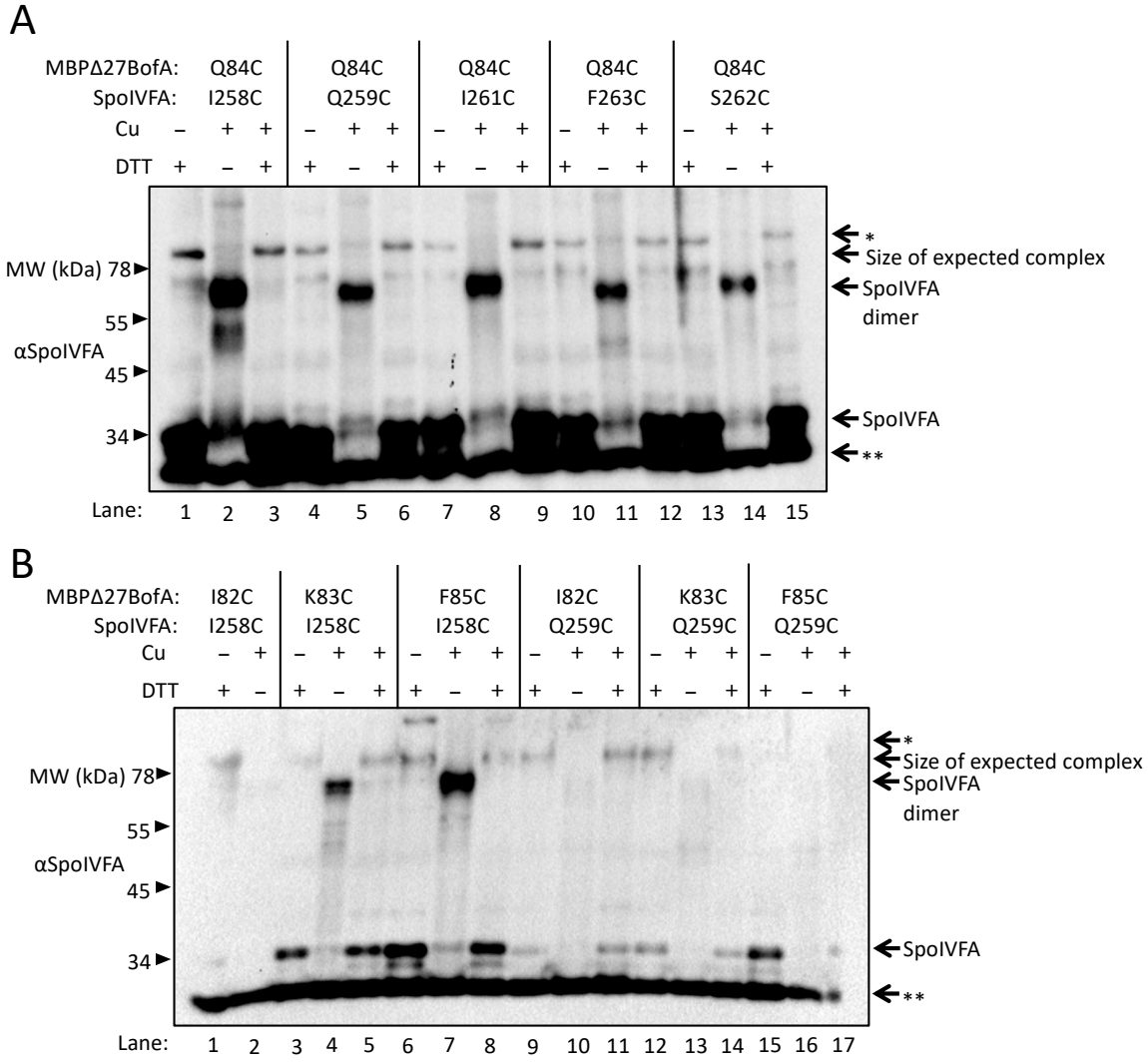

Figure 4.3 Disulfide cross-linking of single-Cys SpoIVFA with single-Cys MBPΔ27BofA in *E. coli*. (*A*) Disulfide cross-linking of single-Cys SpoIVFA (I258C, Q259C, I261C, S262C, F263C) to single-Cys MBPΔ27BofA (Q84C). Plasmids (pMB1-4, pEL6) were used to produce single-Cys SpoIVFA in combination with single-Cys MBPΔ27BofA and Cys-less variants of inactive cytTM-SpoIVFB E44Q and Pro-σ^K(1-127) in *E. coli*. Samples collected after 2 h of IPTG induction were treated with Cu^{2+}(phenanthroline)$_3$ (Cu +) for 60 min or with 2-phenanthroline (Cu –) as a control. Samples were treated with TCA to precipitate proteins and resuspended in sample buffer with DTT (+) or without (–) and subjected to immunoblot analysis with SpoIVFA antibodies to visualize SpoIVFA monomer, dimer, and complex with MBPΔ27BofA. (*B*) Disulfide cross-linking of single-Cys SpoIVFA (I258C, Q259C) to single-Cys MBPΔ27BofA (I82C, K83C, F85C). Plasmids (pMB12-17) were used to produce single-Cys SpoIVFA in combination with single-Cys MBPΔ27BofA and Cys-less variants of inactive cytTM-SpoIVFB E44Q and Pro-σ^K(1-127) in *E. coli*. Samples collected after 2 h of IPTG induction were treated and subjected to immunoblot analysis as in *A*. A representative result from at least two biological replicates is shown in *A* and *B*. The single star (*) indicates a cross-reacting protein that appears to be cross-linked to high molecular weight species and double star (**) indicates a cross-reacting protein or breakdown species of SpoIVFA.

Interestingly, a species of the expected size for cross-linked SpoIVFA dimer was observed in some samples, suggesting that the C-terminal ends of SpoIVFA monomers interact. Formation of dimer varies by construct, which implies that some single-Cys BofA variants prevent proximity between monomers of SpoIVFA. In any case, our disulfide cross-linking results provide no evidence that the C-terminal ends of BofA and SpoIVFA are in proximity to one another. Additionally, the structural model of complex containing SpoIVFB, BofA, and parts of SpoIVFA and Pro-σ^K shows that the C-terminal end of BofA is predicted to be near the membrane surface, perhaps hindering accessibility for interaction. Thus, it is unlikely that these two inhibitory proteins interact as previously predicted [11].

Efforts to Determine if the SpoIVFA TMS Is in Proximity to Either BofA C46 or the SpoIVFB Active Site. SpoIVFA contains two native Cys residues (C82, C77) within its TMS. We wanted to examine if SpoIVFA C82 is in proximity to either BofA or SpoIVFB using disulfide cross-linking assays. SpoIVFA C82 was chosen as a candidate for disulfide cross-linking experiments since we predicted that it was at a similar depth within the membrane as BofA C46 and the SpoIVFB active site.

In order to examine the proximity between SpoIVFA and MBPΔ27BofA, we engineered plasmids to produce single-Cys C82 SpoIVFA and MBPΔ27BofA (C46, I76C) with Cys-less variants of Pro-σ^K(1-127) and inactive cytTM-SpoIVFB E44Q. Cys-less variants of Pro-σ^K(1-127) C110S and cytTM-SpoIVFB E44Q were created previously [12]. We included single-Cys I76C MBPΔ27BofA in this analysis because Dr. Michael Feig suggested that BofA I76 follows a turn formed by a conserved GXPG motif, which is bordered by hydrophobic residues that may embed this region of BofA in the membrane. As a negative control, we engineered a plasmid to

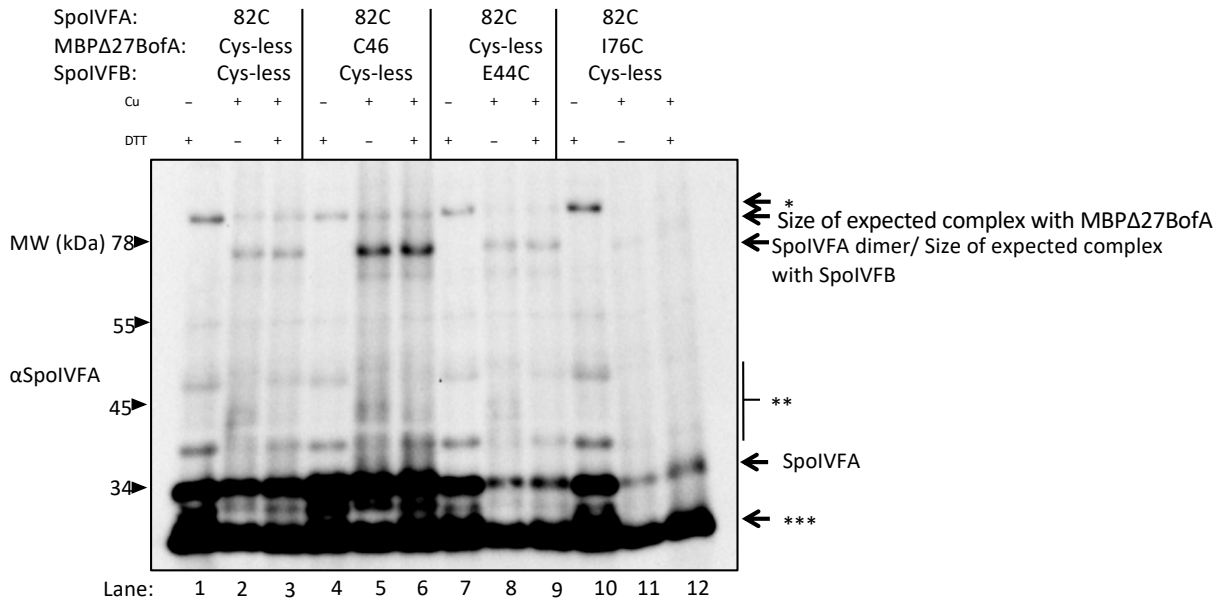

Figure 4.4 Disulfide cross-linking of single-Cys SpoIVFA with single-Cys variants of MBPΔ27BofA or cytTM-SpoIVFB in *E. coli*. Disulfide cross-linking of single-Cys SpoIVFA (C82) to single-Cys variants of MBPΔ27BofA (C46, I76C) or inactive cytTM-SpoIVFB (E44C). Plasmids (pSO140, pSO145 pSO151, pSO155) were used to produce single-Cys SpoIVFA in combination with single-Cys MBPΔ27BofA or single-Cys cytTM-SpoIVFB and Cys-less Pro-σ^K(1-127) in *E. coli*. Samples collected after 2 h of IPTG induction were treated with Cu^{2+}(phenanthroline)$_3$ (Cu +) for 60 min or with 2-phenanthroline (Cu –) as a control. Samples were treated with TCA to precipitate proteins and resuspended in sample buffer with DTT (+) or without (–) and subjected to immunoblot analysis with SpoIVFA antibodies to visualize SpoIVFA monomer, dimer, and complex with MBPΔ27BofA or cytTM-SpoIVFB. A representative result from at least two biological replicates is shown in *A* and *B*. The single star (*), double star (**), and triple star (***) indicate cross-reacting protein.

produce single-Cys 82C SpoIVFA and a Cys-less variants of MBPΔ27BofA, Pro-σ^K(1-127), and cytTM-SpoIVFB E44Q. Cells were treated with the oxidant Cu^{2+}(phenanthroline)$_3$ to promote disulfide bond formation. Disulfide cross-linking did not result in a species of the expected size for a cross-linked complex of SpoIVFA and MBPΔ27BofA (Figure 4.4, lanes 5 & 11), a result similar to the negative control (lane 2).

To determine proximity between SpoIVFA and SpoIVFB, we engineered a plasmid to produce single-Cys SpoIVFA C82, single-Cys E44C cytTM-SpoIVFB, and Cys-less variants of Pro-σ^K(1-127) and MBPΔ27BofA. The inactive single-Cys E44C variant of cytTM-SpoIVFB and Cys-less Pro-σ^K(1-127) were created previously [12], and Cys-less MBPΔ27BofA was made in our previous studies (Chapter 2). Our results show that disulfide cross-linking did not result in a species of the expected size for a cross-linked complex of SpoIVFA and cytTM-SpoIVFB (Figure 4.4, lane 8).

Thus, we were unable to find proximity between SpoIVFA C82 with either BofA or SpoIVFB. These results are consistent with the structural model presented in Chapter 2. It is worth noting that the model predicts, as Dr. Feig suggested, that BofA I76 follows a turn formed by GIPG and this region is predicted to be in the membrane, but the model predicts a distance of 11.8 angstroms between the alpha carbons of BofA I76 and SpoIVFA C82, so it is not surprising that a complex of the expected size was not observed in our disulfide cross-linking experiment (Figure 4.4, lane 11).

Materials and Methods

Immunoblot Analysis. Samples were subjected to immunoblot analysis as described [6]. Briefly, proteins were separated by SDS-PAGE using either 14% or 10% Prosieve (Lonza)

polyacrylamide gels and electroblotted to Immobilon-P membranes (Millipore). Protein migration was monitored using SeeBlue Plus2 Prestained Standard (Invitrogen) and blots were blocked with 5% nonfat dry milk (Meijer) in TBST (20 mM Tris-HCl pH 7.5, 0.5 M NaCl, 0.1% Tween 20) for 1 h at 25°C with shaking. Blots were probed with antibodies against His_6 (penta-His Qiagen 34460; 1:10,000), GFP [6] (1:10,000), SpoIVFA [6] (1:3,000), and/or MBP (NEB catalog #E8030S; 1:10,000) diluted in TBST with 2% milk, overnight at 4°C with shaking. Since the GFP, SpoIVFA and MBP antibodies were not HRP-conjugated, they were detected with goat anti-rabbit-HRP antibody (Bio-Rad catalog #170-6515; 1:10,000) diluted in TBST with 2% milk, 1 h at 25°C with shaking. Signals were generated using the Western Lightning Plus ECL reagent (PerkinElmer) and detected using a ChemiDoc MP imaging system (Bio-Rad).

Colbalt Affinity Purification. Strain BL21(DE3) (Novagen) was used to produce proteins in *E. coli*. Plasmids were transformed, with selection on Luria-Bertani (LB) agar supplemented with ampicillin (100 μg/mL). Transformants (4-5 colonies) were grown in LB medium with 200 μg/mL ampicillin at 37°C with shaking (200 rpm). Overnight culture (10 mL) was transferred to 1 L of LB medium with antibiotics, cultures were grown at 37°C with shaking (250 rpm) to an optical density of 0.6-0.8 Klett units, and isopropyl β-D-thiogalactopyranoside (IPTG) (0.5 mM) was added to induce protein production for 2 h. The culture was split, cells were harvested, and cell pellets were stored at -80°C. Cell lysates were prepared as described [13] and each cell pellet was resuspended in 20 mL of lysis buffer lysis buffer containing 50 mM Tris-HCl pH 7.1 rather than PBS. Cell lysates were centrifuged (15,000 × *g* for 15 min at 4 °C) to sediment cell debris and protein inclusion bodies. The supernatant was treated with 1% *n*-dodecyl-β-D-maltoside (DDM) (Anatrace) for 1 h at 4 °C to solubilize membrane proteins, then

centrifuged at 150,000 × *g* for 1 h at 4 °C. The supernatant was designated the input sample and 15 mL was mixed with imidazole (5 mM) and 0.5 mL of Talon superflow metal affinity resin (Clontech) that had been equilibrated with buffer (50 mM Tris-HCl pH 7.1, 0.1% DDM, 5 mM 2-mercaptoethanol, 10% glycerol). The mixture was rotated for 1 h at 4°C. The cobalt resin was sedimented by centrifugation at 708 × *g* for 2 min at 4 °C and the supernatant was saved (unbound sample). The resin was washed three times with 5 mL wash buffer (PBS pH 7.4, 150 mM NaCl, 10% glycerol, 0.1% DDM, 20 mM imidazole), each time gently vortexing the mixture for 1 min and sedimenting the resin as above. The resin was mixed with 0.5 mL 2× sample buffer and boiled for 3 min (bound sample). A portion of the bound sample was diluted fifteen-fold (1/15 bound sample) with 1× sample buffer to match the concentration of the input sample. Samples were subjected to immunoblot analysis using 14% Prosieve (Lonza) polyacrylamide gels.

GFP Affinity Purification. Input sample (1 mL) prepared as described above was mixed with 25 uL GFP-Trap magnetic agarose (ChromoTek) that had been equilibrated with buffer (50 mM Tris-HCl pH 7.1, 0.1% DDM, 5 mM 2-mercaptoethanol, 10% glycerol) and the mixture was rotated for 1 h at 4°C. The magnetic agarose was localized in the tube with a DynaMag-2 magnet (Invitrogen) and the supernatant was saved (unbound sample). The magnetic agarose was washed three times by gently vortexing with 500 µL wash buffer (50 mM Tris-HCl pH 7.1, 150 mM NaCl, 10% glycerol, 0.1% DDM), localizing the magnetic agarose with the magnet, and collecting the supernatant (wash). The magnetic agarose was mixed with 80 µL of 2× sample buffer (50 mM Tris·HCl pH 6.8, 4% SDS, 20% glycerol, 200 mM DTT

0.03% bromophenol blue) and boiled for 5 min (bound sample). Samples were subjected to immunoblot analysis using 14% Prosieve (Lonza) polyacrylamide gels.

Disulfide Cross-Linking. As described for Pro-σ^K(1-127) cleavage (Chapter 2), *E. coli* BL21(DE3) was transformed with a plasmid, grown in LB (10 mL), induced with IPTG, and equivalent amounts of cells (based on optical density in Klett units) were collected. Cells were mixed with chloramphenicol (200 μg/mL) and 2-phenanthroline (3 mM), collected by centrifugation (12,000 × *g* for 1 min), washed with 10 mM Tris-HCl pH 8.1 containing 3 mM 2-phenanthroline, and suspended in 10 mM Tris-HCl pH 8.1. Samples were treated with 1 mM Cu^{2+}(phenanthroline)$_3$ or 3 mM 2-phenanthroline (as a negative control) for 60 min at 37°C, followed by incubation with neocuproine (12.5 mM) for 5 min at 37°C. Cells were lysed and proteins were precipitated by addition of trichloroacetic acid (5%) and inversion every 5 min for 30 min on ice. Proteins were sedimented by centrifugation (12,000 × *g*) for 15 min at 4°C, the supernatant was removed, and the pellet was washed with cold acetone. The pellets were sedimented by centrifugation (12,000 × *g*) for 5 min at 4°C and the supernatants were discarded. The pellets were dried for 5 min at 25°C and resuspended in buffer (100 mM Tris-HCl pH 7.5, 1.5% SDS, 5 mM EDTA, 25 mM *N*-ethylmaleimide) for 30 min at 25°C. Portions were mixed with an equal volume of sample buffer (25 mM Tris-HCl pH 6.8, 2% SDS, 10% glycerol, 0.015% bromophenol blue) with or without 100 mM DTT, and were typically incubated at 37°C for 10 min, prior to immunoblot analysis using 10% Prosieve (Lonza) polyacrylamide gels.

APPENDICES

APPENDIX A

Supplemental Information

Table 4.1 Plasmids used in this study

Name	Description	Construction	Reference
pEL2	Km^R; T7- Pro-σ^K(1-127)-His_6/T7-cytTM-SpoIVFB-$FLAG_2$-His_6/T7-MBPΔ27BofA/single-Cys 262C SpoIVFA	pSO90 was subjected to SDM[a] using primers ELP20 and ELP21, substituting S262C in SpoIVFA.	This study
pEL3	Km^R; T7- Pro-σ^K(1-127)-His_6/T7-cytTM-SpoIVFB-$FLAG_2$-His_6/T7-Q84C MBPΔ27BofA/single-Cys 262C SpoIVFA	pEL2 was subjected to SDM using primers ELP22 and ELP23, substituting Q84C in MBPΔ27BofA.	This study
pEL4	Km^R; T7- Pro-σ^K(1-127)-His_6/T7-cytTM-SpoIVFB-$FLAG_2$-His_6/T7-single-Cys Q84C MBPΔ27BofA/single-Cys 262C SpoIVFA	pEL3 was subjected to SDM using primers SO-P152 and SO-P153, substituting C46S in MBPΔ27BofA.	This study
pEL5	Km^R; T7-Cys-less Pro-σ^K(1-127)-His_6/T7-Cys-less cytTM-SpoIVFB E44Q-$FLAG_2$-His_6/T7-single-Cys Q84C MBPΔ27BofA/Cys-less SpoIVFA	Fragment *T7-mbpΔ27bofA/spoIVFA* (single-Cys Q84C MBPΔ27BofA/Cys-less SpoIVFA) was amplified from pEL4 using primers SO-P82 and SO-P90 (S262C SpoIVFA variant was changed back to S262 by SO-P82 primer). Vector pSO96 was amplified using primers SO-P80 and SO-P89. Fragment was joined to pSO96 using GA[b].	This study
pEL6	Km^R; T7-Cys-less Pro-σ^K(1-127)-His_6/T7-Cys-less cytTM-SpoIVFB E44Q-$FLAG_2$-His_6/T7-single-Cys Q84C MBPΔ27BofA/single-Cys S262C SpoIVFA	pEL5 was subjected to SDM using primers ELP20 and ELP21, substituting S262C in SpoIVFA.	This study
pMB1	Km^R; T7-Cys-less Pro-σ^K(1-127)-His_6/T7-Cys-less cytTM-SpoIVFB E44Q-$FLAG_2$-His_6/T7-single-Cys Q84C MBPΔ27BofA/single-Cys I1258C SpoIVFA	pEL5 was subjected to SDM using primers ELP24 and ELP25, substituting I258C in SpoIVFA.	This study
pMB2	Km^R; T7-Cys-less Pro-σ^K(1-127)-His_6/T7-Cys-less cytTM-SpoIVFB E44Q-$FLAG_2$-His_6/T7-single-Cys Q84C MBPΔ27BofA/single-Cys Q259C SpoIVFA	pEL5 was subjected to SDM using primers ELP26 and ELP27, substituting Q259C in SpoIVFA.	This study
pMB3	Km^R; T7-Cys-less Pro-σ^K(1-127)-His_6/T7-Cys-less cytTM-SpoIVFB E44Q-$FLAG_2$-His_6/T7-single-Cys Q84C MBPΔ27BofA/single-Cys I261C SpoIVFA	pEL5 was subjected to SDM using primers ELP28 and ELP29, substituting I261C in SpoIVFA.	This study

Table 4.1 (cont'd)

pMB4	Km^R; T7-Cys-less Pro-σ^K(1-127)-His_6/T7-Cys-less cytTM-SpoIVFB E44Q-$FLAG_2$-His_6/T7-single-Cys Q84C MBPΔ27BofA/single-Cys F263C SpoIVFA	pEL5 was subjected to SDM using primers ELP30 and ELP31, substituting F263C in SpoIVFA.	This study
pMB9	Km^R; T7-Cys-less Pro-σ^K(1-127)-His_6/T7-Cys-less cytTM-SpoIVFB E44Q-$FLAG_2$-His_6/T7-single-Cys I82C MBPΔ27BofA/Cys-less SpoIVFA	pSO139 was subjected to SDM using primers MB-P1 and MB-P2, substituting I82C in MBPΔ27BofA.	This study
pMB10	Km^R; T7-Cys-less Pro-σ^K(1-127)-His_6/T7-Cys-less cytTM-SpoIVFB E44Q-$FLAG_2$-His_6/T7-single-Cys K83C MBPΔ27BofA/Cys-less SpoIVFA	pSO139 was subjected to SDM using primers MB-P3 and MB-P4, substituting K83C in MBPΔ27BofA.	This study
pMB11	Km^R; T7-Cys-less Pro-σ^K(1-127)-His_6/T7-Cys-less cytTM-SpoIVFB E44Q-$FLAG_2$-His_6/T7-single-Cys F85C MBPΔ27BofA/Cys-less SpoIVFA	pSO139 was subjected to SDM using primers MB-P5 and MB-P6, substituting F85C in MBPΔ27BofA.	This study
pMB12	Km^R; T7-Cys-less Pro-σ^K(1-127)-His_6/T7-Cys-less cytTM-SpoIVFB E44Q-$FLAG_2$-His_6/T7-single-Cys I82C MBPΔ27BofA/single-Cys I258C SpoIVFA	pMB9 was subjected to SDM using primers ELP24 and ELP25, substituting I258C in SpoIVFA.	This study
pMB13	Km^R; T7-Cys-less Pro-σ^K(1-127)-His_6/T7-Cys-less cytTM-SpoIVFB E44Q-$FLAG_2$-His_6/T7-single-Cys K83C MBPΔ27BofA/single-Cys I258C SpoIVFA	pMB10 was subjected to SDM using primers ELP24 and ELP25, substituting I258C in SpoIVFA.	This study
pMB14	Km^R; T7-Cys-less Pro-σ^K(1-127)-His_6/T7-Cys-less cytTM-SpoIVFB E44Q-$FLAG_2$-His_6/T7-single-Cys F85C MBPΔ27BofA/single-Cys I258C SpoIVFA	pMB11 was subjected to SDM using primers ELP24 and ELP25, substituting I258C in SpoIVFA.	This study
pMB15	Km^R; T7-Cys-less Pro-σ^K(1-127)-His_6/T7-Cys-less cytTM-SpoIVFB E44Q-$FLAG_2$-His_6/T7-single-Cys I82C MBPΔ27BofA/single-Cys Q259C SpoIVFA	pMB9 was subjected to SDM using primers ELP26 and ELP27, substituting Q259C in SpoIVFA.	This study
pMB16	Km^R; T7-Cys-less Pro-σ^K(1-127)-His_6/T7-Cys-less cytTM-SpoIVFB E44Q-$FLAG_2$-His_6/T7-single-Cys K83C MBPΔ27BofA/single-Cys Q259C SpoIVFA	pMB10 was subjected to SDM using primers ELP26 and ELP27, substituting Q259C in SpoIVFA.	This study

Table 4.1 (cont'd)

pMB17	Km^R; T7-Cys-less Pro-σ^K(1-127)-His_6/T7-Cys-less cytTM-SpoIVFB E44Q-$FLAG_2$-His_6/T7-single-Cys F85C MBPΔ27BofA/single-Cys Q259C SpoIVFA	pMB11 was subjected to SDM using primers ELP26 and ELP27, substituting Q259C in SpoIVFA.	This study
pSO90	Km^R; T7-Pro-σ^K(1-127)-His_6/T7-cytTM-SpoIVFB-$FLAG_2$-His_6/T7-MBPΔ27BofA/Cys-less SpoIVFA	Fragment of *mbp* was amplified from pYZ112 using primers SO-P156 and SO-P157. Vector pSO72 was amplified using primers SO-P158 and SO-P159. Fragment was joined to pSO72 using GA.	Chapter 2
pSO91	Km^R; T7-Cys-less Pro-σ^K(1-127)-His_6/T7- single-Cys E44C cytTM-SpoIVFB-$FLAG_2$-His_6/T7-MBPΔ27BofA/Cys-less SpoIVFA	Fragment *T7-mbpΔ27bofA/spoIVFA* (single-Cys MBPΔ27BofA/Cys-less SpoIVFA) was amplified from pSO90 using primers SO-P82 and SO-P90. Vector pSO80 was amplified using primers SO-P89 and SO-P80. Fragment was joined to pSO80 using GA.	Chapter 2
pSO94	Km^R; T7-Cys-less Pro-σ^K(1-127)-His_6/T7-Cys-less cytTM-SpoIVFB E44Q-$FLAG_2$-His_6/T7-MBPΔ27BofA/ Cys-less SpoIVFA	pSO91 was subjected to SDM using primers LK2691 and YZ11, substituting E44Q in cytTM-SpoIVFB.	Chapter 2
pSO96	Km^R; T7-Cys-less Pro-σ^K(1-127)-His_6/T7-Cys-less cytTM-SpoIVFB E44Q-$FLAG_2$-His_6	pSO79 was subjected to SDM using primers LK2691 and YZ11, substituting E44Q in cytTM-SpoIVFB.	Chapter 2
pSO110	Km^R; T7-Cys-less Pro-σ^K(1-127)-His_6/T7-single-Cys E44C cytTM-SpoIVFB-$FLAG_2$-His_6/T7-Cys-less MBPΔ27BofA/Cys-less SpoIVFA	Fragment *T7-mbpΔ27bofA/spoIVFA* (Cys-less MBPΔ27BofA/Cys-less SpoIVFA) was amplified from pSO97 using primers SO-P82 and SO-P90. Vector pSO80 was amplified using primers SO-P89 and SO-P80. Fragment was joined to pSO80 using GA.	Chapter 2
pSO139	Km^R; T7-Cys-less Pro-σ^K(1-127)-His_6/T7-Cys-less cytTM-SpoIVFB E44Q-$FLAG_2$-His_6/T7-Cys-less MBPΔ27BofA/Cys-less SpoIVFA	pSO94 was subjected to SDM using primers SO-P152 and SO-P153, substituting C46S in MBPΔ27BofA.	Chapter 2
pSO140	Km^R; T7-Cys-less Pro-σ^K(1-127)-His_6/T7-Cys-less cytTM-SpoIVFB E44Q-$FLAG_2$-His_6/T7-MBPΔ27BofA/ single-Cys C82 SpoIVFA	pSO94 was subjected to SDM using primers SO-P200 and SO-P201, changing C82L back to C82 in SpoIVFA.	This study

Table 4.1 (cont'd)

pSO145	Km^R; T7-Cys-less Pro-σ^K(1-127)-His_6/T7-single-Cys E44C cytTM-SpoIVFB-$FLAG_2$-His_6/T7-Cys-less MBPΔ27BofA/single-Cys C82 SpoIVFA	pSO110 was subjected to SDM using primers SO-P200 and SO-P201, changing C82L back to C82 in SpoIVFA.	This study
pSO151	Km^R; T7-Cys-less Pro-σ^K(1-127)-His_6/T7-Cys-less cytTM-SpoIVFB E44Q-$FLAG_2$-His_6/T7-Cys-less MBPΔ27BofA/single-Cys C82 SpoIVFA	pSO139 was subjected to SDM using primers SO-P200 and SO-P201, changing C82L back to C82 in SpoIVFA.	This study
pSO155	Km^R; T7-Cys-less Pro-σ^K(1-127)-His_6/T7-Cys-less cytTM-SpoIVFB E44Q-$FLAG_2$-His_6/T7-single-Cys I176C MBPΔ27BofA/single-Cys C82 SpoIVFA	pSO151 was subjected to SDM using primers SO-P213 and SO-P214, substituting I76C in MBPΔ27BofA.	This study
pSO161	Ap^R; T7-MBPΔ27BofA/SpoIVFA	Fragment of *mbp* was amplified from pSO91 and made from primers SO-P156 and SO-P157. Vector pYZ46 was amplified using primers SO-P158 and SO-P159. Fragment was joined to pYZ46 using GA.	This study
pSO162	Ap^R; T7-GFPΔ27BofA/His_6-SpoIVFA	pYZ46 was subjected to SDM using primers SO-P216 and SO-P217, adding an N-terminal His_6 epitope tag to SpoIVFA.	This study
pYZ46	Ap^R; T7-GFPΔ27BofA/SpoIVFA	pZR33 was digested with BamHI and NotI, and fragment *spoIVFA* was ligated with BamHI-NotI-digested pZR62.	Chapter 2

[a]Site-directed mutagenesis using the QuikChange kit (Stratagene).
[b]Gibson assembly [14].

Table 4.2 Primers used in this study

Primer	Sequence
ELP20	TCCGATCCGATTCAGGTGATTTGTTTTGAATAAGCGGCCGCT
ELP21	AGCGGCCGCTTATTCAAAGCAAATCACCTGAATCGG
ELP22	GCGTTAGTCGTCATTAAGTGTTTTATCATTTAAGGATCC
ELP23	GGATCCTTAAATGATAAAACACTTAATGACGACTAACGC
ELP24	AATTTATTGATCCGTGTCAGGTGATTTCATTTGAAT
ELP25	ATTCAAATGAAATCACCTGACACGGATCAATAAATT
ELP26	AATTTATTGATCCGATTTGTGTGATTTCATTTGAATAAG
ELP27	CTTATTCAAATGAAATCACACAAATCGGATCAATAAATT
ELP28	TCCGATCCGATTCAGGTGTGTTCATTTGAATAAGCGG
ELP29	CCGCTTATTCAAATGAACACACCTGAATCGGATCGGA
ELP30	GATCCGATTCAGGTGATTTCATGTGAATAAGCGGCC
ELP31	GGCCGCTTATTCACATGAAATCACCTGAATCGGATC
LK2691	GCAGCATGCCCCAGCTGATGAATCAATACAATC
MB-P1	GAATAGCTGCGTTAGTCGTCTGTAAGCAATTTATCATTTAA
MB-P2	TTAAATGATAAATTGCTTACAGACGACTAACGCAGCTATTC
MB-P3	GCTGCGTTAGTCGTCATTTGTCAATTTATCATTTAAGGATC
MB-P4	GATCCTTAAATGATAAATTGACAAATGACGACTAACGCAGC
MB-P5	GCGTTAGTCGTCATTAAGCAATGTATCATTTAAGGATCCGAAG
MB-P6	CTTCGGATCCTTAAATGATACATTGCTTAATGACGACTAACGC
SO-P80	TGAGATCCGGCTGCTAACAAAGCCC
SO-P82	GGCTTTGTTAGCAGCCGGATCTCAGCGGCCGCTTATTCAAATGAAATC
SO-P89	CTTTAAGAAGGAGATATACATATGGCTAGCATGA
SO-P90	ATGACAAGCTCGAGCACCACCACCACCACCACTGAGATCTCGATCCCGCGAAATTAAT A
SO-P152	GGTGCTTTGCTGCTGGTTAGTGTAAATATGTTTGGCG
SO-P153	CGCCAAACATATTTACACTAACCAGCAGCAAAGCACC
SO-P156	GAGATATACATATGGCTAGCATGGAAACTGAAGAAGGTAAACTGGTAATCTGGATTA ACG
SO-P157	CTGATGCCAATCCACTTCTCGAGGGCCGCCGCGTCTTT
SO-P158	CTCGAGAAGTGGATTGGC
SO-P159	CATGCTAGCCATATGTATATCTCC
SO-P200	GAAATTACTTCTGTCGGCCTGCCTTGTTCTCGTTTCAGCT
SO-P201	AGCTGAAACGAGAACAAGGCAGGCCGACAGAAGTAATTTC
SO-P213	ATTTTAGGAATACCCGGATGTGCTGCGTTAGTCGTCATT
SO-P214	AATGACGACTAACGCAGCACATCCGGGTATTCCTAAAAT
SO-P216	TCCGAAGGAGATATACATATGCACCACCACCACCACCACAGTCACAGAGCAGATGAA
SO-P217	TTCATCTGCTCTGTGACTGTGGTGGTGGTGGTGGTGCATATGTATATCTCCTTCGGA
YZ11	GATTGTATTGATTCATCAGCTGGGGCATGCTGC

Table 4.3 Sequencing primers used in this study

Primer	Sequence	Notes
SO-P23	CATTACCTGTCCACACAATCTGC	Forward primer. Binds in GFP.
SO-P84	CATACCCACGCCGAAACAAG	Forward primer. Binds upstream of the T7 promoter in pET29b.
SO-P86	GAGTAAAGGAGAAGATCTCGATCC	Forward primer. Binds in Pro-σ^K.
SO-P104	CATGGAGGAACTGCTTCTGC	Forward primer. Binds in SpoIVFB.
SO-P157	CTGATGCCAATCCACTTCTCGAGGGCCGCCGCGTCTTT	Reverse primer. Binds in MBP.
SO-P160	CTTCAGCGAGACCGTTATAGC	Reverse primer. Binds in MBP.
SO-P161	ACTGACGGGTCCAATGTTTG	Reverse primer. Binds in SpoIVFA.
DP18	GCTAGTTATTGCTCAGCGG	Reverse primer. Binds T7 terminator
DP89	TAATACGACTCACTATAGGG	Forward primer. Binds T7 promoter.

APPENDIX B

Contributions to Another Publication

I have contributed to the following publication during my dissertation work.

> Parrell D, Zhang Y., **Olenic S**. and Kroos L. *Bacillus subtilis* Intramembrane Protease RasP Activity in *Escherichia coli* and *In Vitro*. 2017. *J. Bacteriol* 199(19):e00381-17. doi: 10.1128/JB.00381-17.

My contributions to this work included performing cleavage assays in a *clpP* mutant of *E. coli* BL21(DE3) to examine activity of RasP on two substrates: FtsL and RsiW. Samples were collected and immunoblot analysis with antibodies against His_6-tagged substrate and FLAG-tagged RasP were performed. I contributed to the manuscript by performing the experiments of Figure 4 and helped with editing.

REFERENCES

REFERENCES

1. Cutting, S., et al., *A forespore checkpoint for mother-cell gene expression during development in Bacillus subtilis.* Cell, 1990. **62**: p. 239-250.

2. Rudner, D.Z. and R. Losick, *A sporulation membrane protein tethers the pro-σ^K processing enzyme to its inhibitor and dictates its subcellular localization.* Genes Dev., 2002. **16**(8): p. 1007-1018.

3. Ramirez-Guadiana, F.H., et al., *Evidence that regulation of intramembrane proteolysis is mediated by substrate gating during sporulation in Bacillus subtilis.* PLoS Genet., 2018. **14**(11): p. e1007753.

4. Zhou, R. and L. Kroos, *Serine proteases from two cell types target different components of a complex that governs regulated intramembrane proteolysis of pro-σ^K during Bacillus subtilis development.* Mol. Microbiol., 2005. **58**(3): p. 835-846.

5. Zhou, R. and L. Kroos, *BofA protein inhibits intramembrane proteolysis of pro-σ^K in an intercompartmental signaling pathway during Bacillus subtilis sporulation.* Proc. Natl. Acad. Sci. USA, 2004. **101**(17): p. 6385-6390.

6. Kroos, L., et al., *Forespore signaling is necessary for pro-σ^K processing during Bacillus subtilis sporulation despite the loss of SpoIVFA upon translational arrest.* J. Bacteriol., 2002. **184**(19): p. 5393-5401.

7. Green, D. and S. Cutting, *Membrane topology of the Bacillus subtilis Pro-σ^K processing complex.* J. Bacteriol., 2000. **182**: p. 278-285.

8. Varcamonti, M., et al., *Membrane topology analysis of the Bacillus subtilis BofA protein involved in pro-σ^K processing.* Microbiol., 1997. **143**(Pt 4): p. 1053-1058.

9. Cutting, S., S. Roels, and R. Losick, *Sporulation operon spoIVF and the characterization of mutations that uncouple mother-cell from forespore gene expression in Bacillus subtilis.* J. Mol. Biol., 1991. **221**: p. 1237-1256.

10. Ricca, E., S. Cutting, and R. Losick, *Characterization of bofA, a gene involved in intercompartmental regulation of pro-σ^K processing during sporulation in Bacillus subtilis.* J. Bacteriol., 1992. **174**: p. 3177-3184.

11. Dong, T.C. and S.M. Cutting, *SpoIVB-mediated cleavage of SpoIVFA could provide the intercellular signal to activate processing of Pro-σ^K in Bacillus subtilis.* Mol. Microbiol., 2003. **49**(5): p. 1425-1434.

12. Zhang, Y., et al., *Residues in conserved loops of intramembrane metalloprotease SpoIVFB interact with residues near the cleavage site in Pro-σ^K.* J. Bacteriol., 2013. **195**(21): p. 4936-4946.

13. Zhang, Y., et al., *Complex formed between intramembrane metalloprotease SpoIVFB and its substrate, Pro-σ^K.* J. Biol. Chem., 2016. **291**: p. 10347-10362.

14. Gibson, D.G., et al., *Enzymatic assembly of DNA molecules up to several hundred kilobases.* Nat. Methods, 2009. **6**(5): p. 343-345.

CHAPTER 5: Conclusions and Future Directions

Introduction

Knowledge of IPs has grown significantly over the last decade, including advances on IMMPs like SpoIVFB and RseP (Chapter 1). IMMPs function in numerous, diverse signaling processes that impact health. For example, IMMPs regulate microbial pathogenesis [1-3] and cholesterol biosynthesis in humans [4]. Thus, knowledge of IMMP substrate recognition or inhibition in model organisms, like SpoIVFB in *B. subtilis* or RseP in *E. coli*, could inform design of therapeutics or guide efforts to develop inhibitors of IMMPs in pathogens. We have expanded the study of SpoIVFB to reveal its inhibition by BofA and SpoIVFA (Chapter 2), and its substrate interaction (Chapter 3), increasing fundamental knowledge of IMMP function. In this final chapter, key findings will be summarized and future directions will be discussed.

Inhibition of SpoIVFB Provides Potential Insights into Inhibition of Other IMMPs. A major finding was the discovery that BofA interacts with the SpoIVFB active site (Chapter 2). Disulfide cross-linking assays using single-Cys variants of SpoIVFB and MBPΔ27BofA with Cys-less variants of SpoIVFA and Pro-σ^K showed proximity between BofA C46 in TMS2 and the active site region of SpoIVFB (E44C, P135C). Additional disulfide cross-linking experiments with single-Cys variants of SpoIVFB and MBPΔ27BofA were extensive, allowing for modeling to predict the orientation of BofA TMS2 within the SpoIVFB active site (Chapter 2). To expand on these results, further disulfide cross-linking experiments could be performed to determine the position of BofA TMS1. Previous cross-linking results show that the membrane re-entrant loop of SpoIVFB is in proximity to the substrate [5], but our results show that native

BofA inhibits this interaction more strongly than MBPΔ27BofA, which lacks TMS1 (Chapter 2). Hence, TMS1 appears to sterically hinder the N-terminal Proregion of Pro-σ^K from interacting with the membrane re-entrant loop in the SpoIVFB active site region. Unfortunately, our new structural model does not include the N-terminal Proregion of Pro-σ^K (Chapter 2). Further disulfide cross-linking experiments could be performed to determine the position of the Proregion, particularly in relation to BofA TMS1.

Another important result was the discovery that three conserved residues (N48, N61, T64) in BofA are important for inhibition of Pro-σ^K cleavage. Ala substitutions to these residues in GFPΔ27BofA impacted inhibition upon heterologous expression in *E. coli* and during *B. subtilis* sporulation, impaired the assembly of the inhibitory complex, and caused partial or complete mislocalization during sporulation (Chapter 2). Interestingly, our structural model predicts proximity between the N48 side chain with the loop containing N61 and T64. Thus, the three conserved residues may help to stabilize and position the BofA structure, promoting interactions with both SpoIVFB and SpoIVFA. Pull-down assays using Ala-substituted variants (N48A, N61A, T64A) might elucidate how these residue changes impact the complex. Howeever, in order to confirm the roles of N48, N61 and T64, a structure of the hetertotrimeric complex of SpoIVFA, SpoIVFB, and BofA is needed.

Another potentially interesting interaction involves F66 in SpoIVFB. Mutational analysis using SpoIVFB F66A results in constitutively active SpoIVFB in sporulating *B. subtilis* [6] and in *E. coli* (Chapter 2). It was previously proposed that SpoIVFB adopts open and closed conformations [6, 7], based on the mjS2P structures [8], which may be facilitated by interactions between Phe residues. F66 resides at the top of the membrane re-entrant loop, and is predicted to interact with F188 located in TMS6 of SpoIVFB, and with several other hydrophobic residues

when in the closed state. These interactions are predicted to occlude substrate in the closed state [6]. The SpoIVFB F66A variant was predicted to destabilize those hydrophobic contacts, displacing the loop and destabilizing the closed state relative to the open, active state. Since our new structural model shows that BofA occupies the SpoIVFB active site, the SpoIVFB F66A variant may impact this interaction, preventing inhibition. Future pull-down assays using the SpoIVFB F66A variant would help to determine whether this Ala substitution impacts interactions with BofA. However, in sporulating *B. subtilis*, SpoIVFB F66A tagged with yellow fluorescence protein (YFP) localizes properly to the forespore in a manner that depends on both SpoIVFA and BofA, supporting the idea that the F66A substitution does not disrupt interactions between SpoIVFB and its inhibitors [6]. Thus, SpoIVFB F66A may still interact with BofA, but may disrupt the correct alignment of BofA TMS2 and prevent the steric hindrance mechanism of SpoIVFB inhibition. Instead, disulfide cross-linking assays comparing e.g., single-Cys E44C variants of SpoIVFB and SpoIVFB F66A in combination with BofA C46 may be a better approach to elucidate this potential change in interaction.

Our results suggest that BofA interacts with the SpoIVFB active site and may form several important contacts with SpoIVFA and SpoIVFB to maintain inhibition. We predict that small peptides, analogous to TMS2 of BofA, have the potential to inhibit other IMMPs by blocking the IMMP active site through interactions with the membrane reentrant loop.

Heterotrimeric Complex of SpoIVFA, SpoIVFB, and BofA. Previous studies suggest that SpoIVFA, SpoIVFB, and BofA form a trimeric complex in *B. subtilis* and when expressed in *E. coli* [9, 10]. Our results show that BofA and SpoIVFA do not form a stable complex without SpoIVFB and we were unable to find points of proximity between the SpoIVFA C-terminal end

or TMS and either BofA or SpoIVFB by disulfide cross-linking assays (Chapter 4). However, our new structural model shows a prediction of SpoIVFA within the complex based on coevolutionary analyses (Chapter 2). This new model leads to several new questions: 1) does the C-terminal end of BofA interact with the TMS of SpoIVFA; 2) how does SpoIVFA interact with SpoIVFB; and 3) after inhibition is removed by SpoIVB and CtpB cleavage, does BofA leave the SpoIVFB active site?

Our new model predicts that the hydrophobic C-terminal end of BofA resides in the membrane environment and may interact with the TMS of SpoIVFA (Chapter 2). Previous membrane topology assays using *phoA* and *lacZ* fusions to BofA predicted that the C-terminal end was located in the inter-membrane space surrounding the forespore [11]. Our new model agrees with these results since the C-terminal end of BofA contains a highly conserved GXPG motif, which would function as a turn, breaking up the putative C-terminal α-helix and preventing it from crossing through the membrane to the mother cell cytoplasm. Additionally, our model shows areas of proximity and potential interactions between the C-terminal end of BofA and SpoIVFA (e.g., C82 in the TMS). In order to confirm this prediction, disulfide cross-linking assays using single-Cys BofA and single-Cys SpoIVFA need to be performed. Plasmids containing either single-Cys MBPΔ27BofA (I82C, K83C, F85C) or single-Cys C82 SpoIVFA were created (Chapter 4) and are being re-engineered for future disulfide cross-linking between the C-terminal end of BofA and the TMS of SpoIVFA.

Another interesting prediction from our model includes potential points of proximity between SpoIVFA and SpoIVFB (Chapter 2). This area includes I101-T111 of SpoIVFA and F120-F127 in TMS4 of SpoIVFB. Interestingly, F109 in SpoIVFA appears to be in proximity to F127 SpoIVFB. If either SpoIVFA F109A or SpoIVFB F127A show impaired inhibition by

cleavage assays or fail to co-purify in pull-down assays, this would provide indirect evidence for an important interaction. However, we note that F127 is not conserved in SpoIVFB and is present in some *Clostridium* orthologs, which do not contain *spoIVFA* in their genome (Chapter 3), so this potential interaction is only speculative.

While disulfide cross-linking and pull-down assays can give us insights into potential interactions and the proximity of residues, obtaining a structure of this heterotrimeric complex is also a future goal. Improvements in cryo-electron microscopy (cryo-EM) have enabled researchers to obtain protein structures and complexes at better resolutions. For instance, the structures of human γ-secretase were solved using cryo-EM, with resolutions between 3.4 and 4.5 angstroms [12-14]. However, much more work is needed to determine the best methods for protein expression and purification for structure determination of the SpoIVFA:SpoIVFB:BofA complex with cryo-EM.

Finally, the last major question to address is how SpoIVB and CtpB signaling relieves inhibition of SpoIVFB. Our work shows that BofA occupies the SpoIVFB active site and our model predicts that SpoIVFA makes additional contacts with BofA and SpoIVFB, potentially holding BofA in the right conformation to bind the active site zinc ion (Chapter 2). Since our model predicts that all three proteins interact extensively, how does cleavage by SpoIVB and CtpB disrupt inhibition of SpoIVFB? During sporulation, SpoIVB first cleaves the C-terminal end of SpoIVFA [15-17], then CtpB cleaves both the C-terminal end of SpoIVFA and the C-terminal end of BofA [10, 16-18]. The initial cleavage event by SpoIVB may disrupt the interaction between SpoIVFA and BofA, causing a conformational change that moves these proteins away from the SpoIVFB active site. This conformational change might also move the C-terminal end of BofA out of the membrane environment, allowing for cleavage by CtpB.

However, this is all speculative and much more work is needed to determine how SpoIVB/CtpB cleavage impacts the inhibitors. Our disulfide cross-linking work shows that Pro-σ^K can still interact with the linker and CBS domain of SpoIVFB when both BofA and SpoIVFA are produced (Chapter 2). Thus, a conformational change that moves BofA TMS2 away from the active site may be sufficient for the cleavage of the Prodomain. There are many challenges in trying to determine the impact of SpoIVB/CtpB cleavage: 1) small C-terminal truncations in SpoIVFA and BofA, not at the site of SpoIVB and CtpB cleavage, impair inhibition in *B. subtilis* [11, 19, 20] and *E. coli* (Chapter 2); 2) production of SpoIVB is toxic to *E. coli* cells (Chapter 2); and 3) we do not have a structure of the inhibited heterotrimeric complex, so much more work is needed to determine how SpoIVFB, BofA, and SpoIVFA interact before we consider how inhibition is removed.

The Predicted Short Loop of IMMPs Is Important for Substrate Interaction and Cleavage. The work in this dissertation also examined the functions of conserved residues in the predicted short loop of SpoIVFB. We found that both conserved Pro residues (P132, P135) in the predicted short loop of SpoIVFB play an important role in substrate interaction and cleavage. Ala substitutions for both Pro residues impacted co-purification with the substrate and substrate cleavage in *E. coli* and sporulating *B. subtilis* (Chapter 3). However, disulfide cross-linking assays showed that SpoIVFB P132A and P135A variants impact substrate interactions differently. The SpoIVFB P132A variant prevents the majority of cross-linking between the predicted short loop and the substrate, while SpoIVFB P135A does not (Chapter 3). These results suggest that P132A, which belongs in the conserved NPDG motif, changes the loop structure, disrupting interactions with the substrate, while P135A does not impact loop proximity

to the substrate, but impairs other interactions with substrate, preventing cleavage. We predicted that SpoIVFB P135A may prevent D137 from acting as a zinc ligand, due to the proximity of the residues and the strongly impaired substrate cleavage observed for both the SpoIVFB P135A and D137A variants during sporulation of *B. subtilis* [21] (Chapter 3). It would be interesting to compare the zinc content of the variants with wild-type SpoIVFB. Structures of SpoIVFB and SpoIVFB variants (P132A, P135A) in complex with substrate are needed to assess our predictions about the interactions.

In SpoIVFB orthologs, P135 is highly conserved, however not all IMMPs contain two Pro residues in their predicted short loop. For instance, human S2P and *B. subtilis* YydH contain only one Pro residue while IMMPs from hyperthermophilic archaea, *Aeropyrum pernix* and *Pyrococcus abyssi*, and the hyperthermophilic bacterium *Aquifex aeolicus* have three Pro residues [21]. Are there differences in how these IMMPs interact with their substrates? Do differences in Pro residues impact loop flexibility and/or positioning of the conserved Asp residue that acts a zinc ligand? Unlike the other divergent IMMPs, extensive work has been done on S2P and its substrate, TMS1 of SREBP [22, 23], so future experiments examining interactions between the predicted S2P short loop and its substrate would be the best starting point.

Better understanding of the predicted short loop function in IMMPs could contribute new knowledge about how substrates bind and orient within the active site. Since IMMPs play roles in pathogenesis and can impact human health, understanding this interaction could also aid in developing therapeutics and IMMP inhibitors.

Closing Remarks

The work described in this dissertation benefited from extensive prior work on *B. subtilis* endosporulation. I thank all of those who provided me with strains, antibodies, methodologies, and advice. Our work with SpoIVFB contributes to the understanding of IMMP inhibition and substrate recognition/binding. I look forward to the future of this field and the development of new techniques. A great amount of work lies ahead in pursuit of the structures of SpoIVFB and other IMMPs.

REFERENCES

REFERENCES

1. Makinoshima, H. and M.S. Glickman, *Site-2 proteases in prokaryotes: regulated intramembrane proteolysis expands to microbial pathogenesis.* Microbes Infect., 2006. **8**(7): p. 1882-1888.

2. Urban, S., *Making the cut: central roles of intramembrane proteolysis in pathogenic microorganisms.* Nat. Rev. Microbiol., 2009. **7**: p. 411-423.

3. Schneider, J.S. and M.S. Glickman, *Function of site-2 proteases in bacteria and bacterial pathogens.* Biochim. Biophys. Acta - Biomembr., 2013. **1828**(12): p. 2808-2814.

4. Rawson, R., et al., *Complementation cloning of SP2, a gene encoding a putative metalloprotease required for intramembrane cleavage of SREBPs.* Mol. Cell, 1997. **1**: p. 47-57.

5. Zhang, Y., et al., *Residues in conserved loops of intramembrane metalloprotease SpoIVFB interact with residues near the cleavage site in Pro-σ^K.* J. Bacteriol., 2013. **195**(21): p. 4936-4946.

6. Ramirez-Guadiana, F.H., et al., *Evidence that regulation of intramembrane proteolysis is mediated by substrate gating during sporulation in Bacillus subtilis.* PLoS Genet., 2018. **14**(11): p. e1007753.

7. Zhou, R., et al., *Intramembrane proteolytic cleavage of a membrane-tethered transcription factor by a metalloprotease depends on ATP.* Proc. Natl. Acad. Sci. USA, 2009. **106**: p. 16174-16179.

8. Feng, L., et al., *Structure of a site-2 protease family intramembrane metalloprotease.* Science, 2007. **318**(5856): p. 1608-1612.

9. Rudner, D.Z. and R. Losick, *A sporulation membrane protein tethers the pro-σ^K processing enzyme to its inhibitor and dictates its subcellular localization.* Genes Dev., 2002. **16**(8): p. 1007-1018.

10. Zhou, R. and L. Kroos, *Serine proteases from two cell types target different components of a complex that governs regulated intramembrane proteolysis of pro-σ^K during Bacillus subtilis development.* Mol. Microbiol., 2005. **58**(3): p. 835-846.

11. Varcamonti, M., et al., *Membrane topology analysis of the Bacillus subtilis BofA protein involved in pro-σ^K processing.* Microbiol., 1997. **143**(Pt 4): p. 1053-1058.

12. Lu, P., et al., *Three-dimensional structure of human gamma-secretase.* Nature, 2014. **512**(7513): p. 166-170.

13. Sun, L., et al., *Structural basis of human gamma-secretase assembly.* Proc Natl Acad Sci U S A, 2015. **112**(19): p. 6003-8.

14. Bai, X.C., et al., *An atomic structure of human gamma-secretase.* Nature, 2015. **525**(7568): p. 212-217.

15. Dong, T.C. and S.M. Cutting, *SpoIVB-mediated cleavage of SpoIVFA could provide the intercellular signal to activate processing of Pro-σ^K in Bacillus subtilis.* Mol. Microbiol., 2003. **49**(5): p. 1425-1434.

16. Campo, N. and D.Z. Rudner, *A branched pathway governing the activation of a developmental transcription factor by regulated intramembrane proteolysis.* Mol. Cell, 2006. **23**(1): p. 25-35.

17. Campo, N. and D.Z. Rudner, *SpoIVB and CtpB are both forespore signals in the activation of the sporulation transcription factor σ^K in Bacillus subtilis.* J. Bacteriol., 2007. **189**(16): p. 6021-6027.

18. Mastny, M., et al., *CtpB assembles a gated protease tunnel regulating cell-cell signaling during spore formation in Bacillus subtilis.* Cell, 2013. **155**(3): p. 647-658.

19. Cutting, S., S. Roels, and R. Losick, *Sporulation operon spoIVF and the characterization of mutations that uncouple mother-cell from forespore gene expression in Bacillus subtilis.* J. Mol. Biol., 1991. **221**: p. 1237-1256.

20. Ricca, E., S. Cutting, and R. Losick, *Characterization of bofA, a gene involved in intercompartmental regulation of pro-σ^K processing during sporulation in Bacillus subtilis.* J. Bacteriol., 1992. **174**: p. 3177-3184.

21. Rudner, D., P. Fawcett, and R. Losick, *A family of membrane-embedded metalloproteases involved in regulated proteolysis of membrane-associated transcription factors.* Proc. Natl. Acad. Sci. USA, 1999. **96**: p. 14765-14770.

22. Sakai, J., et al., *Sterol-regulated release of SREBP-2 from cell membrane requires two sequential cleavages, one within a transmembrane domain.* Cell, 1996. **85**: p. 1037-1048.

23. Kroos, L. and Y. Akiyama, *Biochemical and structural insights into intramembrane metalloprotease mechanisms.* Biochim. Biophys. Acta - Biomembr., 2013. **1828**(12): p. 2873-2885.